Understanding and improving the reactivity of low loaded noble metal three-way catalysts

Thesis

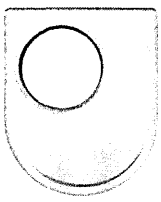

The Open University

JM
Johnson Matthey

Understanding and Improving the Reactivity of Low Loaded Noble Metal Three-Way Catalysts

A dissertation submitted in accordance with the requirements for the degree of Doctor of Philosophy

Noelia Cortes Felix*

*felixn@matthey.com

The Open University
Department of Life, Health and Chemical Sciences

June 2014

Supervisors:

Dr. Eleanor Crabb[a]
Dr. Anthony Stephen Cohen[a]
Dr. Paul Millington[b]

[a]The Open University; [b]Johnson Matthey

DATE OF SUBMISSION: 16 JUNE 2014

DATE OF AWARD: 24 NOVEMBER 2014

Abstract

Three-Way Catalysts (TWC) were created to control pollutants emissions from gasoline engines by performing simultaneous oxidation of CO and HC and reduction of NO_x. Over the last 20 years, the main focus on their development has been the optimisation of the oxygen storage capacity (OSC) component, which is based on CeO_2 materials. Improved thermal stability of these materials, in addition to improvements in fuel quality, has enabled the noble metal (NM) content of these catalysts to be reduced. As a result, the metal dispersion has improved and the interactions within the support become more important, making significant changes to the character of the noble metal, sometimes even leaving it fixed in a less reactive state.

Conventional preparative routes to disperse low NM amounts (< 1wt %) have been successful in the past but this is reaching its limit. The proposed approach to disperse low NM contents on CeO_2 materials is based on the precipitation method to create a more intimate contact between the NM and the ceria, and improve in this way the oxygen mobility.

The effect of the Ce-precursor was firstly evaluated. The co-precipitation of Pd^{2+} and Ce^{3+} led to a catalyst with a similar Pd surface area to the material prepared by impregnation but with an improved Pd-Ce interaction, due to the partial ceria decoration of Pd particles. The co-precipitation of Pd^{2+} and Ce^{4+} led to a catalyst with low Pd surface area content, partly due to some Pd leaching during the preparation, but also likely to be due to higher encapsulation with the ceria.

0.5Pt-CeO_2 and 0.5Rh-CeO_2 catalysts were also studied. The co-precipitation of these NM with Ce^{3+} also led to products with an improved NM-Ce interaction. However, in this case, the co-precipitated catalysts contained a lower NM surface area compared to their reference catalysts prepared by impregnation. The improved NM-Ce contact improved their OSC and pollutants conversions, but the lower surface metal content did not allow an improvement in their light-off temperatures.

Overall, the catalysts prepared by the co-precipitation method have increased the number of NM and Ce atoms in contact leading to higher OSC and pollutants conversions. This leads to a more efficient usage of noble metals and potentially cheaper catalyst.

Acknowledgements

I gratefully thank Johnson Matthey and the Open University for this opportunity, especially my supervisors Eleanor Crabb, Paul Millington and Anthony Cohen for their help and support, as well as David Thompsett who has been like an extra supervisor to me.

I would also like to express my gratitude to all my colleagues from Johnson Matthey, but especially those from the Emissions Control Research department for all the support they have shown in all these last years, and all my colleagues working in the Analytical department for all the work.

There are lots more people to thank. Those who have made life easier through the PhD, those that have been supportive and have tried to help in whatever way possible, those who have calmed me down in the most stressful moments... To all my friends and family (you all know who you are), a big thank you! Gracias! Gràcies!

A les meves companyes de doctorat, Cristina i Silvia, també us volia donar les gràcies. Tot sembla mes fàcil quan les experiències es poden compartir. Molta sort amb els vostres doctorats!

A mi familia, quien sin ellos esto no habría sido posible. Os agradezco todo el apoyo que siempre habéis mostrado, siempre me habéis ayudado a llegar donde me lo he planteado sin cuestionarme.

And finally I would like to thank my husband. You are the one who taught me to be a fighter to achieve my objectives. Thanks a lot for all your help and support!

Contents

Chapter 3: Probe reactions for the surface characterisation of Pd, Pt and Rh

Chapter 4: Pd-CeO_2 samples prepared by co-precipitation

Chapter 5: Co-precipitation of [Pd+Ce+Zr]

Chapter 6: Impact of the noble metal on NM-CeO_2 co-precipitation (NM = Pd, Pt, Rh)

Chapter 7: Bimetallic catalysts based on 0.5Pd-0.1Rh-CeO_2

Chapter 8: Conclusions

Appendix

List of symbols and abbreviations

(ads)	Adsorbed
(g)	Gas
[A+B]	Sample prepared by co-precipitation of A and B
A/F	Air/Fuel ratio
a.u.	Arbitrary units
BET	Brunauer, Emmett, Teller
BET-SSA	BET-specific surface area
CeZr	Ceria-Zirconia mixed oxide
DRIFTS	Diffuse Reflectance Infrared Fourier Transform Spectroscopy
E_a	Activation energy
EGO	Exhaust gas oxygen sensor
EHC	Electrically heated catalyst
EPA	Environmental protection agency
EtOH-TPSR	Ethanol temperature programmed surface reaction
eV	Electronvolt
F650	Calcination in air at the indicated temperature
FTP	Federal test procedure
g	gram
H	Enthalpy
HC	Hydrocarbons
ICP-ES	Inductively Coupled Plasma Emission Spectroscopy
k	Rate constant
K_{sp}	Solubility product
min	Minute
ml	Millilitre
MS	Mass spectrometer
NM	Noble metal
NMHC	Non-methane hydrocarbons
NO_x	Nitrogen oxides
OSC	Oxygen storage capacity

PM	Particulate matter
r	Rate
R	Ideal gas constant
RDS	Relative standard error
s	Second
SE	Standard error
SSITKA or ITK	Steady state isotopic transient kinetic analysis
T	Temperature
T50	Necessary temperature for 50% conversion
TCD	Thermal conductivity detector
TEL	Tetraethyl lead
TEM	Transmission electron microscope
TOF	Turn over frequency
TPR	Temperature programmed reduction
TWC	Three-way catalyst
μ	Micro
V_o^-	Oxygen vacancy
WGS	Water gas shift
wt%	Weight percent
XPS	X-ray photoelectron spectroscopy
XRD	X-ray diffraction
λ	Lambda or equivalence ratio (related to air/fuel ratio)

List of tables

List of figures

1. Introduction

Contents

1.1. Introduction to Three-Way catalysts

Human activity has led to the contamination of key resources such as soil, water and air. The effect of pollutants on people's health is a concern, especially those related to mobile sources, as their contribution is significantly higher compared to the other sectors (Figure 1-1) [1, 2].

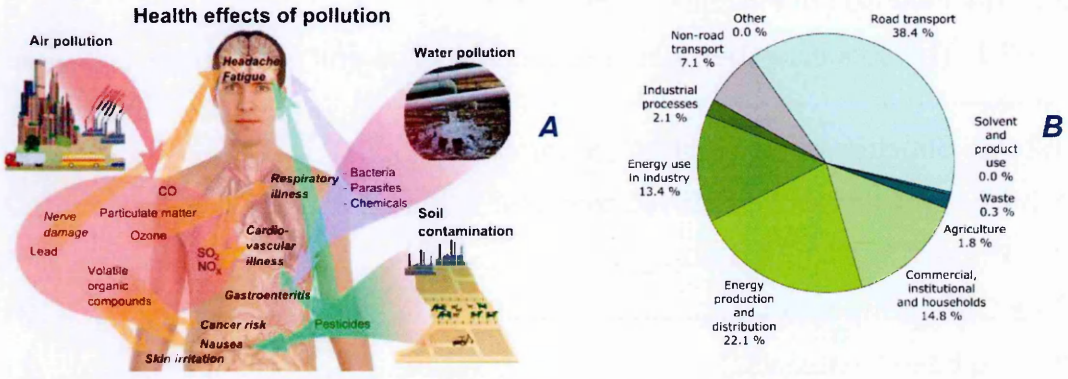

Figure 1-1: A) Effect of Environmental pollutants on human health (from [3]). B) Sector share of nitrogen oxides emissions (EEA member countries) (from [4]).

By the mid-20th century, air quality problems became a real issue due to the increasing number of cars on the roads [2, 5]. At that time, the car engine was relatively inefficient and complete oxidation of petrol to CO_2 and H_2O was not achieved. The exhaust gas therefore contained high amounts of unburned hydrocarbons (HC[1]) and CO, in addition to nitrogen oxides (NO_x[2]) created during the explosive combustion in the cylinder between N_2 and O_2 [5, 6].

CO can act as a poison by binding to haemoglobin decreasing the oxygen carrying capacity of the blood leading to headaches, dizziness, disorientation, nausea and fatigue. NO_x and unburnt hydrocarbons can undergo a photochemical reaction with sunlight, forming ground-level ozone. This phenomenon is known as smog[3]

[1] HC (= hydrocarbons) is referred to as unburned fuel and other hydrocarbons formed by pyrolysis, and various oxygenated species.
[2] NO_x (= Nitrogen oxides) is referred to as the combination of NO and NO_2.
[3] The word "smog" is the combination of "smoke" and "fog".

and is extremely dangerous for human health, causing effects from minor irritation to eyes to severe respiratory illnesses (Figure 1-2) [2, 7, 8].

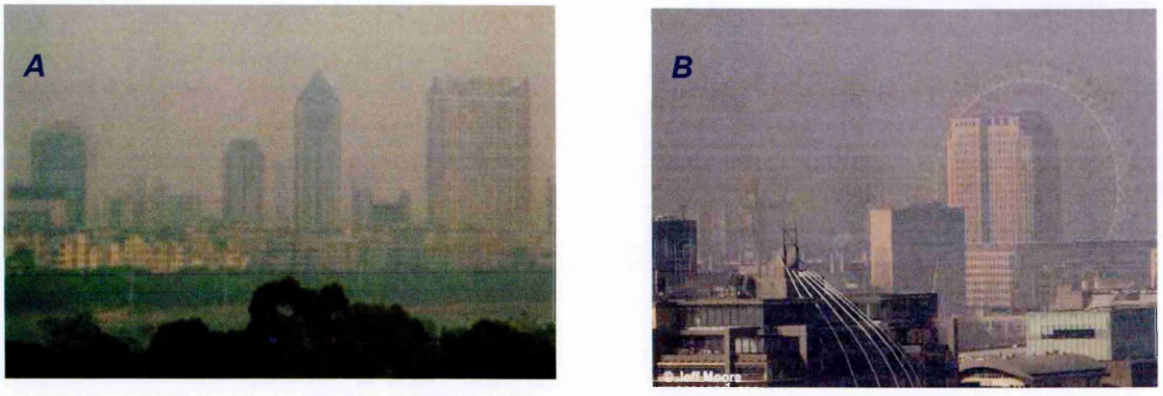

Figure 1-2: Examples of smog phenomenon at Beijing (A) (from [9]), and London (B) (from [10]).

Catalytic converters were first introduced in the mid-1970s with the objective of reducing the level of pollutants emitted in the exhaust gas of vehicles [11]. Initial models contained just oxidation catalysts; this was followed by the development of a "Three-Way Catalyst" (TWC) technology, which was able to simultaneously perform three reactions: 1) oxidation of carbon monoxide, 2) oxidation of unburned hydrocarbons, and 3) reduction of nitrogen oxides. [12, 13].

The Three-Way catalyst is a multicomponent material, which is typically comprised of precious metals (mostly Rh with Pt and/or Pd) distributed across a thermally stable support (typically alumina) and a material with high oxygen storage capacity (such as ceria-based supports) [5, 14, 15]. Rh is used to promote NO_x reduction, while Pt and/or Pd primarily perform CO & HC oxidation [5, 16-18].

The mechanisms of reactions with a TWC is complicated, as the simultaneous reduction and oxidations of NO_x, CO and HC depend highly on the conditions experienced by the catalyst. The following reactions are simplifications of the real process (1-1 to 1-7) [6, 13, 19]:

a) Removal of CO

CO oxidation:

$$2CO + O_2 \rightarrow 2CO_2 \quad (1\text{-}1)$$

Water-gas shift (WGS) reaction:

$$CO + H_2O \rightarrow CO_2 + H_2 \quad (1\text{-}2)$$

b) Removal of HC

Hydrocarbon oxidation:

$$C_yH_n + (y+n/4)O_2 \rightarrow (n/2)H_2O + yCO_2 \quad (1\text{-}3)$$

Steam reforming:

$$C_yH_n + yH_2O \rightarrow yCO + (y+n/2)H_2 \quad (1\text{-}4)$$

c) Removal of NO_x

CO + NO redox reaction:

$$2NO + 2CO \rightarrow 2CO_2 + N_2 \quad (1\text{-}5)$$

H_2 + NO redox reaction:

$$2NO + 2H_2 \rightarrow 2H_2O + N_2 \quad (1\text{-}6)$$

HC + NO redox reaction:

$$(2y+n/2)NO + C_yH_n \rightarrow (y+n/4)N_2 + yCO_2 + n/2H_2O \quad (1\text{-}7)$$

The exhaust gas that flows through the catalyst contains a mixture of paraffin (C_nH_{2n+2}) and aromatic hydrocarbons, which are combusted with controlled amounts of air producing CO_2 and H_2O. The mass ratio of air to fuel in the exhaust is known as the Air/Fuel (A/F) ratio. Considering the mix of hydrocarbons and all the components in air, for gasoline an A/F ratio of 14.7:1 would be needed for the complete combustion of the pollutants [6, 19]. This is known as the stoichiometric ratio, and represents the conditions where it is theoretically possible to completely convert the three pollutants CO, NO_x and HC, to CO_2, N_2 and H_2O. The A/F ratio

can be also expressed as lambda (λ) or equivalence ratio, which is the ratio between the actual A/F ratio and the stoichiometric A/F ratio:

$$\lambda = \frac{A/F}{Stoich.\ A/F}$$

At A/F ratios above the stoichiometric value (fuel lean or simply lean) there is an excess of oxygen, thus the conversion of CO and HC is facilitated; however, due to the lower concentration of reductant, the NO_x conversion will be low. In contrast, below the stoichiometric ratio (rich conditions) there is a deficit of O_2; the insufficient amount of oxidant will not allow the complete combustion of carbon monoxide and hydrocarbons, but NO_x conversion increases [6, 14, 19]. This is represented in Figure 1-3:

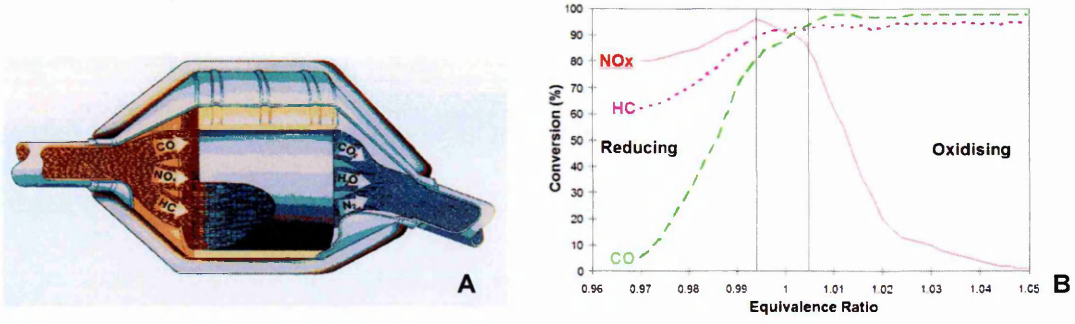

Figure 1-3: A) Representation of a Three-Way catalyst; B) Example of an engine bench performance of a TWC. In the vicinity of the stoichiometric point all three pollutants are efficiently converted to CO_2, H_2O and N_2.

As the working window for an efficient conversion is very narrow, many of the developments in TWCs have been focused on optimising the sensors that control the A/F ratio. Nowadays, these sensors measure oscillations around 1±0.03 about the stoichiometric ratio at a typical frequency of 1 cycle per second [14, 19]. Figure 1-4 shows a schematic representation of the gasoline catalytic system.

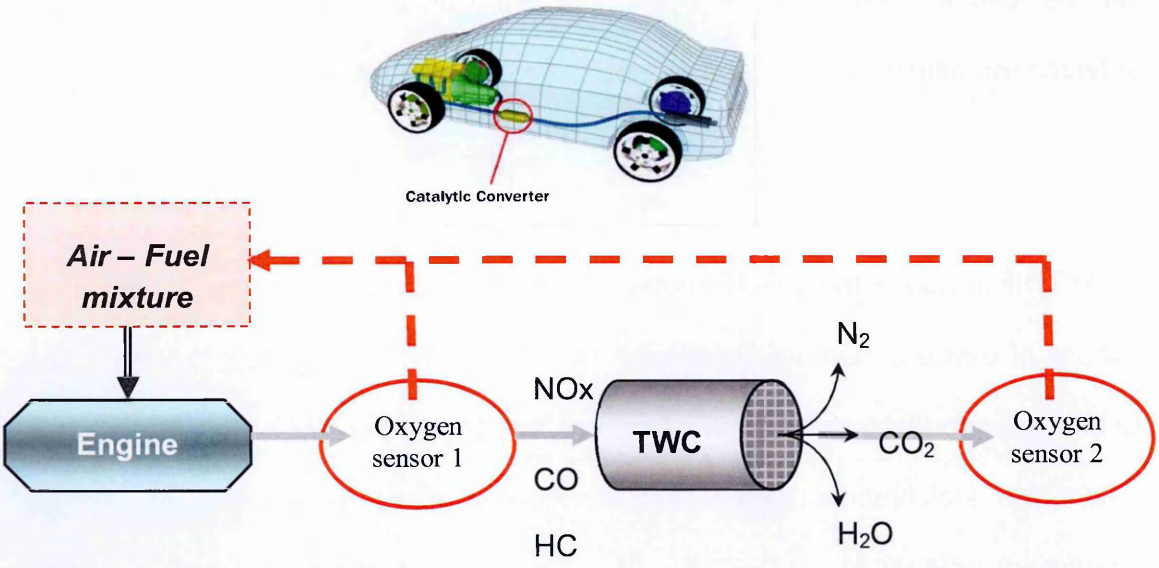

Figure 1-4: schematic representation of the gasoline catalytic system using a Three-Way Catalyst. The first oxygen sensor is used for A/F control (closed loop control); the second sensor is used for diagnostics of catalyst activity.

In addition to this, the use of materials with a high oxygen storage capacity (OSC) have also helped to minimise the fluctuation of the A/F ratio around this point (see reactions 1-8 to 1-13) [6, 20, 21]. Ceria (CeO_2) was recognised as a key material for this role in the mid-1970s, and is able to store or release oxygen depending on the A/F ratio due to its redox properties. Its use is so important that most of the world production of ceria is destined for the automotive sector, where usage has doubled over the last 15 years [14, 22, 23]. More information about the OSC component can be found in *section 3*.

Ceria releasing oxygen:

$$CeO_2 + xCO \rightarrow CeO_{2-x} + xCO_2 \quad (1\text{-}8)$$

$$CeO_2 + C_xH_y \rightarrow CeO_{2-(2x+0.5y)} + xCO_2 + 0.5yH_2O \quad (1\text{-}9)$$

$$CeO_2 + xH_2 \rightarrow CeO_{2-x} + xH_2O \quad (1\text{-}10)$$

Ceria uptaking oxygen:

$$CeO_{2-x} + xNO \rightarrow CeO_2 + 0.5xN_2 \quad (1\text{-}11)$$

$$CeO_{2-x} + xH_2O \rightarrow CeO_2 + xH_2 \quad (1\text{-}12)$$

$$CeO_{2-x} + 0.5xO_2 \rightarrow CeO_2 \quad (1\text{-}13)$$

1.2. Historical background

1.2.1. Evolution of emissions regulations

USA became the first country to introduce regulations for the control of harmful emissions. This was in the form of the Clean Air Act, which was approved by the U.S. Congress in 1970 [6, 16, 17, 24].

The Clean Air Act established the limits allowed for some pollutants, mostly emitted from automobiles: CO, HC, NO_x and Particulate Matter (PM). Europe and Japan soon followed the example set by the USA [25, 26], with the rest of the world subsequently bringing in their own legislations [17]. These limits have become increasingly stringent over time (see Figure 1-5).

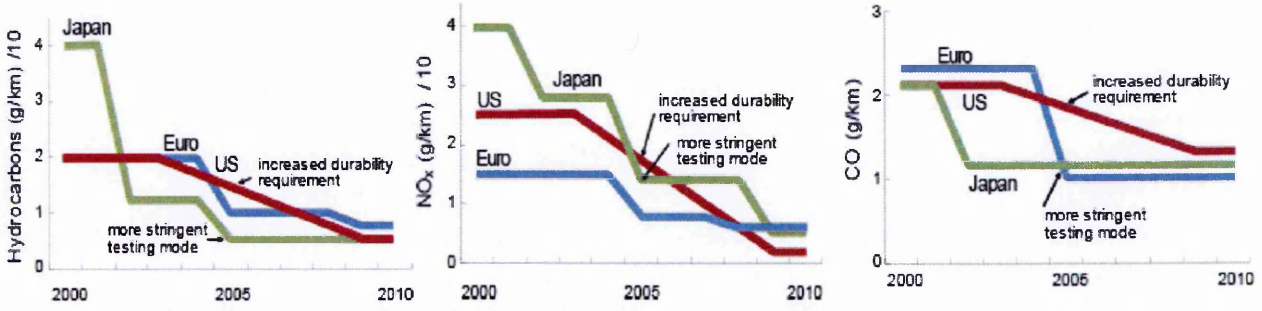

Figure 1-5: Benchmark emissions for gasoline engines. Evolution limits for HC, NOx and CO between the years 2000 and 2010 for legislations at Europe, Japan and United States. (from [27])

To test engine-out emissions, the Environmental Protection Agency (EPA) established the Federal Test Procedure (FTP) (Figure 1-6), which consisted of measuring CO, HC and NO_x concentrations simulating the average driving conditions in the United States. In this test three different conditions were measured:

1. Cold start
2. Hot start
3. Combination of urban and highway driving conditions

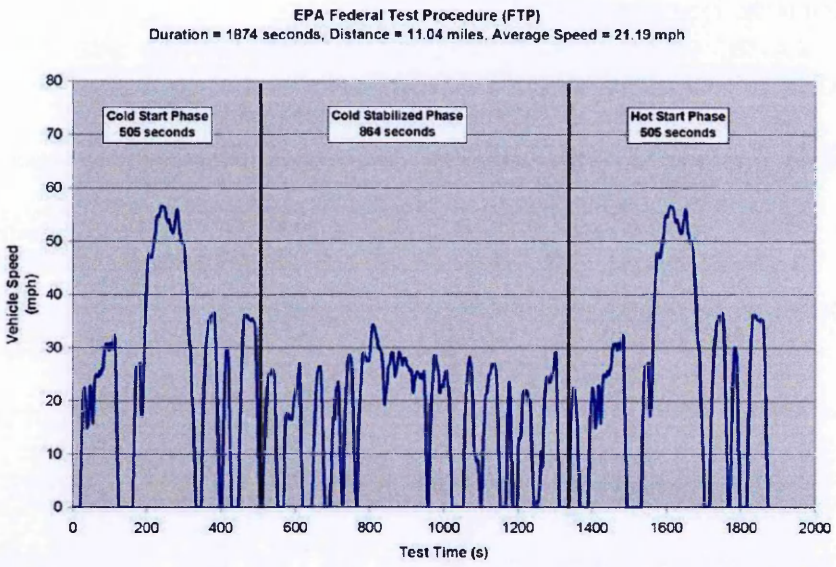

Figure 1-6: Example of EPA Federal Test Procedure for light-duty vehicles under urban driving, in which a vehicle is started with the engine cold and driven in stop-and-go rush hour traffic (from [28])

By 1976 the catalyst was required to achieve >90% CO and HC conversion and to maintain its activity for at least 50,000 miles [6]. Thanks to improvements in the catalytic converter technology, this and further tighter standards were achieved, and a significant decrease of pollutant emissions was soon observed. An example of the tightening of the European emissions legislation can be seen in Figure 1-7, which shows the maximum limit for the different emissions.

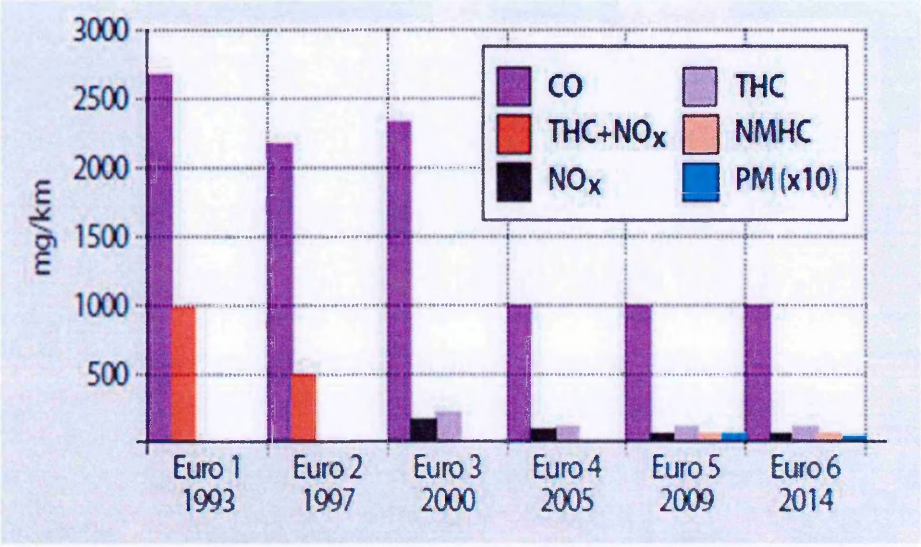

Figure 1-7: Development of Gasoline European legislation (Johnson Matthey Plc, 2008). (CO = carbon monoxide, THC = total hydrocarbons, NO_x = nitrogen oxides, NMHC = non-methane hydrocarbons, PM = particulate matter)

1.2.2. The invention of the catalytic converter

Practically all the published literature reports that the catalytic converter was invented by workers at the Engelhard Corporation in the United States in the mid-1960s [29]. However, in 1909 two patents applications, one in France (FR 402173) and another in United Kingdom (GB 9364/1909) were filed with an extremely similar technology by Michael Frenkel [30]. The principle of his invention was to use a high content of noble metal, mainly platinum, supported onto a solid to be used into the main exhaust stream. His invention even included a mechanism for diluting the exhaust stream by a secondary air blast before passing through the catalytic converter. His patent was published in the United Kingdom, but for unknown reasons, the final stage of acceptance (payment of the sealing fee) was never completed. It was not until 1950 that Eugene Houdry was then granted with a patent on an invention called a "Catalytic Converter" (US2742437), based on similar principles to Michel Frenkel's technology [31-33] . A few years later, this idea was further developed by John J. Mooney and Carl D. Keith at the Engelhard Corporation, creating the first production catalytic converter in 1973 [29, 34].

1.2.2.1. The connection between unleaded gasoline and the catalytic converter

One of the biggest changes in the composition of gasoline occurred as a consequence of the catalytic converter. Previous to the creation of the catalytic converter, gasoline contained tetraethyl lead (TEL), which was an additive used to increase the octane rating of gasoline and to avoid premature ignition (known as "knocking") [35-38]. The effect of TEL was discovered by Thomas Midgley of General Motors (US) in 1921 [39], and was quickly commercialised worldwide.

Unfortunately, TEL is a neurotoxin that can irreparably damage the brain and central nervous system, and can even cause death [36, 37]. Because of these effects, leaded fuel was known as "loony gas". At first, the dangers of TEL were not known, and soon after it started being produced at several refineries in New Jersey and Ohio (in 1924) some of the workers fell mysteriously ill and died [35-37].

In 1925, the Surgeon General temporarily suspended the production and sale of leaded gasoline, and started an investigation to clarify the health concerns [35-37]. After seven months it was concluded that there were no detectable symptoms of lead poisoning and its commercialisation was restored. Some published articles suggested that this decision was political influenced [36]. In fact, between 1950 and 1960, the Surgeon General allowed an increase of TEL content in gasoline [35, 36]. In 1970 vehicle emissions started to be controlled under the Clean Air Act created by the EPA, and the catalytic converter was added to the engines. It was soon noticed that the lead was irreversibly poisoning the active metal of the oxidation catalyst, significantly decreasing its activity to convert the pollutants [35-38]. This was an important issue, as the catalyst was needed to achieve the new emissions legislation. The EPA responded to this issue by limiting the lead content in gasoline, with further decreasing limits in the following years.

Currently, lead is not added to gasoline, instead highly branched isomers are used. In addition, oxygenated fuels are also being produced by blending ethanol with gasoline, which burn more efficiently and thus produces less air pollutants [38].

1.2.2.2. Structure of the catalytic converter

The major developments in catalyst design have come about through an observational/empirical approach based on numerous trials. Since the invention of the catalytic converter, only two different structures have been commercialised: beaded (or particulate) and monolithic [16] shown in Figure 1-8. The original beaded catalysts were based on γ-Al_2O_3 spheres (1/8-1/4 inch. in diameter), which contain the active catalytic component impregnated onto their surface. These beads were loaded in a flat radial flow-like reactor and placed before the muffler in the exhaust. Monolithic catalysts use a ceramic honeycomb monolith that has parallel open channels. Because of the relatively low porosity, this ceramic material cannot be used as a catalyst support. For this reason the catalyst is washcoated and impregnated onto the walls of the honeycomb.

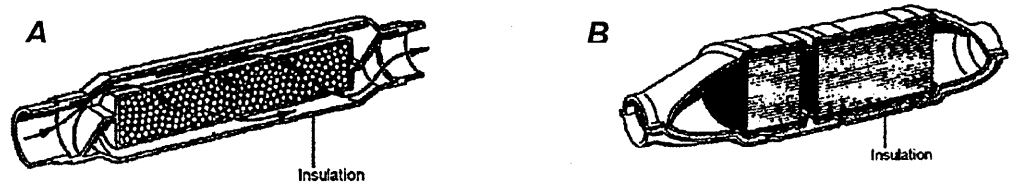

Figure 1-8: Representation of a beaded catalytic converter (A), and a monolithic catalytic converter (B) (After ref. [40]).

Monolithic catalysts quickly replaced the beaded system, due to their longer durability and flexibility, but mainly due to their lower backpressure [16]. However, one disadvantage they presented initially was the expansion of the ceramic material when thermally stressed (as the catalyst can see temperatures of up to 1200 °C), creating cracks in the washcoat on the walls. This problem was soon solved by the use of a new low-thermal-expansion ceramic material: cordierite. This material has a composition of $(Mg,Fe)_2Al_3(Si_5AlO_{18})$ and is still in use today. Metallic honeycomb can also be used as a washcoat-support, although its use is

not as wide as the ceramic substrates, due to expense and temperature limitations [6, 16, 17].

The formulation of the catalytic converter has been largely dependent on the legislation at that time, with regulation driving the innovation and invention of new materials. At the beginning, the primary target for autocatalysts[4] was the oxidation of HC and CO, where maximum conversion of these pollutants was required. After a short time, the legislation included NO_x as regulations tightened, forcing significant changes in the design of the entire catalytic system [6, 16, 17, 41].

1.2.2.3. Evolution of the catalytic converter

First generation: from base metals to Pt-Pd

The first oxidation catalysts were based on beaded systems where base metals (i.e. Cu, Ni, Co, Mn) were supported on alumina. These were found to be good active catalytic components, but due to their high sensitivity to poisoning by compounds present in the fuel (lead, halide, sulphur dioxide) and their low thermal durability it was necessary to find alternatives [6] [16-18].

Platinum group metals were found to be extremely active, but their high cost and availability was an issue of concern. However, it quickly became obvious that base metals were not able to fulfil the requirements for automotive applications. Noble metals showed an excellent reactivity, thermal durability and high (compared to base metals) resistance to poisoning [16, 17].

Within the platinum group, ruthenium, iridium and osmium all formed volatile oxides at high temperature, thus leading to metal losses [16, 17, 42]. However, palladium and platinum showed higher stability under most operating conditions

[4] The catalysts used in the automotive sector are referred as autocatalysts.

and met all the requirements to be used as catalysts for emission control [13, 16, 18]. In this first generation of autocatalysts rhodium was not used as this metal showed very poor activity for CO and HC oxidation [17].

Issues were also seen when using Pd-only and Pt-only catalysts. Pd-only TWC were found to be more affected by fuel poisoning, and Pt-only catalysts showed less thermal resistance under oxidising environments than Pd [6, 11, 16]. The combination of Pt and Pd on a high surface area support (i.e. ~ 200 m^2 g^{-1}), like alumina, did however lead to a reasonable performance. The typical formulation of the first generation catalysts, as stated by Ronald M. Heck & Robert J. Farrauto, was 2.5:1 weight ratio of Pt:Pd with a total precious metal of 0.05% for beads, and 0.12% for honeycombs (1976-1979) [6].

Second generation: Rh (bed 1) & Pt-Pd (bed 2)

In 1979 the requirement to control NO_x emissions forced a change in the design of the catalytic system. The first approach to control the three pollutants (NO_x, CO, HC) at the same time was the creation of a dual bed system. The first bed was run in the absence of oxygen to promote the reduction reaction of NO_x to N_2; this was followed by an air injection before the second bed to perform the oxidation of CO and HC in the second bed [6, 17, 18] (Figure 1-9B).

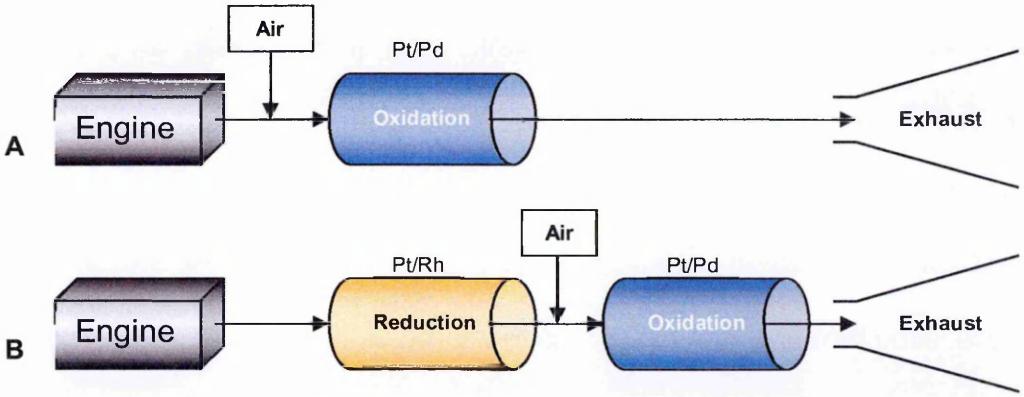

Figure 1-9: Schematic representation of A) first catalytic oxidation system for HC and CO removal, and B) later modification of the catalytic system, which included NO_x reduction.

Several authors studied Ru as a possible reductant catalyst due to its high selectivity to reduce NO_x to N_2, however Ru volatilises at temperatures higher than 300 °C, which made it unsuitable for commercialisation [11, 17, 18, 41, 43]. H.S. Gandhi from the Ford Motor Company explained in his review "Automotive Exhaust Catalysis" how they tried to stabilise Ru forming ruthenate compounds, but the additional cost and the reduced activity could not compete with the most expensive noble metal: Rh [17]. Pt and Pd were also considered for this role, but they showed higher selectivity towards NH_3 instead of N_2. Therefore, a dual-bed system was introduced; the first bed was a Rh containing catalyst which performed NO_x reduction, whilst the second bed was still based on a typical oxidation catalyst of Pt and Pd.

Third generation: three-way catalysts

The earliest car engines were fuelled via carburettors that could not precisely control the A/F mix which subsequently affects the performance of the catalyst. It was observed that when the exhaust gas was close to an A/F mass ratio of 14.7:1, it was possible to obtain high conversion of all the three pollutants at the same time [5, 16]. This was the starting point for the design of a new technology: the Three-Way Catalyst [44].

The idea was to control the A/F ratio thanks to a sensor called an exhaust gas oxygen (EGO) or lambda sensor, which could control the air-fuel mix going through the catalyst. This allowed a single catalyst to be used (instead of two) in a controlled narrow window around the stoichiometric point of the exhaust gas to assure the simultaneous conversion of the three pollutants (Figure 1-9). By the early 1980s, the single catalyst system was used worldwide. [6, 21].

In order to buffer the impact of the small oscillations around the stoichiometric point, a material that could release oxygen when operating under rich conditions (to remove the excess of HC and CO), and then adsorb the excess of oxygen during the lean conditions was required. This necessity led to the use of high oxygen storage materials, which due to their redox properties could adsorb or release oxygen during the lean-rich oscillations. Oxides such as NiO/Ni or Fe_2O_3/FeO were used in the past, but the material found with the highest capacity was CeO_2/Ce_2O_3 [14, 17]. Ceria not only presented good redox properties but it was also highly active for the water-gas shift reaction [44]. This reaction between CO, HC and H_2O is performed under rich conditions and forms H_2 which can be used to reduce NO_x to N_2 (reactions 1-14 to 1-16).

$$CO + H_2O \rightarrow H_2 + CO_2 \quad (1\text{-}14)$$

$$C_yH_n + 2yH_2O \rightarrow (2y + n/2)H_2 + yCO_2 \quad (1\text{-}15)$$

$$NO_x + xH_2 \rightarrow 1/2N_2 + xH_2O \quad (1\text{-}16)$$

The first generation of TWC were based on Pt and Rh supported on Al_2O_3 with a weight ratio of 5:1 (Pt:Rh) and some added ceria [17]. Despite its relatively low cost, in this early formulation Pd was not considered for this role due to its lower resistance, in comparison to Pt, to sulphur poisoning [17]. It was not until the mid-1990s that Pd started to be included in TWC formulations [17, 45], due to the development of fuels with lower sulphur content [5]. Due to its higher demand for this application, Pd cost suddenly increased, and its market price quickly reached similar values to Pt (Figure 1-10) [5, 13]. In later years legislation forced petrol and oil suppliers to further lower the content of sulphur and phosphorus in their fuels [17]. For example, in the US from 2003 the sulphur content could not exceed 50 ppm; nowadays it is possible to find petrol with less than 10 ppm of sulphur, in what is referred to as ultra-clean fuels [46, 47]. The improvement can be

appreciated when this value is compared with the maximum sulphur allowed in 1995, which was more than 300 ppm [21, 48].

Figure 1-10: Evolution of Platinum, Palladium and Rhodium prices from 1994 to 2014. (Source - Johnson Matthey)

One disadvantage found for Pd-Rh catalysts was that under oxidising conditions at high temperature (~800 ºC) Pd segregated as PdO, covering the Pd-Rh alloy, which resulted in the suppression of Rh activity to reduce NO_x [17]. Therefore, the separation of the noble metals to avoid these Pd-Rh interactions became a necessity, which significantly increased the complexity of the catalyst design process [45]. About the same time, Pd-only catalysts were studied as potential TWCs, where NO_x conversion was increased by modifying Pd properties with the addition of promoters, particularly alkaline-earth and lanthanide oxides, which can change the electronegativity around the Pd [16, 17]. Despite some of them

showing very good activity for NO_x conversion and selectivity to N_2, the majority had poor thermal stability [49] or were highly efficient but in a narrower A/F window [50, 51].

Durability and fast light-off performance (high pollutants conversions at low temperature) for cold starts[5] were added as two extra requirements from the 1990s and onwards [5, 17, 44]. In order to increase the durability, stabilised cerias started to be developed. The best results were found using ceria-zirconia mixed oxides, which provided higher surface area after high temperature ageing and a significant improvement in the OSC compared to simple cerium oxides [17, 44].

To improve cold-start emissions, initial attempts increased the noble metal loading. However, this also increased the level of metal sintering at high temperature in addition to adding a significant extra cost [5]. Development then focussed on modifying the catalytic system, incorporating extra components such as hydrocarbon adsorbers, electrically heated catalysts or close-coupled converters (also known as start-up converters) to increase the initial temperature (Figure 1-11). At the present time durability and fast light-off performance are still a matter of on-going investigation.

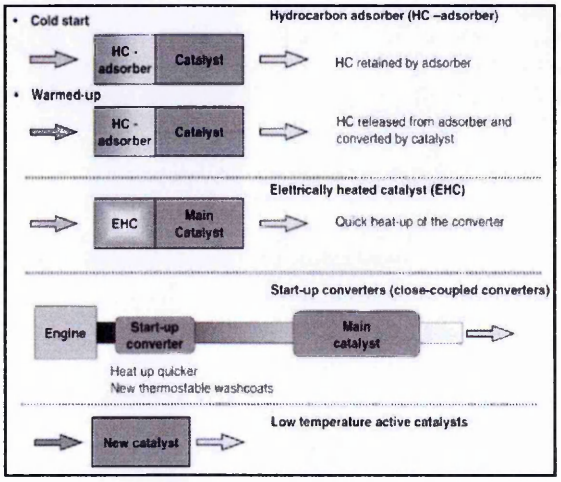

Figure 1-11: Main strategies developed for the control of the emission during cold-starts (from [5]).

[5] First 10-20 seconds during the start-up of the engine.

1.2.3. Present and future challenges

More than 30 years after its creation, TWCs are still being used. The basic composition of the catalyst has not changed much; current formulations are still mainly based on precious metals (principally Pd and Rh) on stabilised aluminas and ceria-based mixed oxides [12]. However, considerable development has been performed on improving the catalyst preparation process. In most commercialised catalysts Rh is separated from Pt and/or Pd on different washcoat layers, but it is also possible to find single layer catalysts where the noble metals have been selectively deposited onto certain supports to avoid detrimental interactions [16]. Another important improvement has been achieved around fuel economy, due to more efficient oxygen sensors, which have further minimised the oscillations of A/F ratio around the stoichiometric point (Figure 1-12) [5].

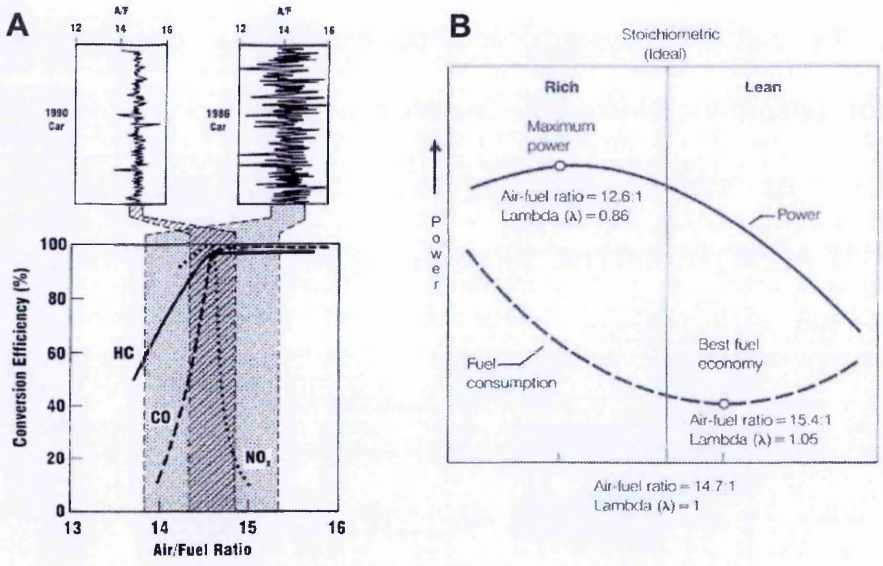

Figure 1-12: A) Conversion efficiency vs air-fuel ratio, showing typical air-fuel oscillations of 1986 and 1990 cars (from [5]). B) Relation between lambda and fuel & power (from [52]).

Durability and fast light-off performance are some of the main requirements that have not yet been completely solved, for example, where emissions typically exceed regulations for the first 15 seconds after engine ignition [5]. Therefore,

most of the worldwide on-going investigations are currently focussing on these issues. In addition, current economic pressure is forcing researchers to find cheaper alternatives which will still meet all technical requirements. Predictions for future emissions legislation discuss including new standards for specific pollutants that until now were either not measured or were included within a group (CO_2, CH_4, NO_2, N_2O, NH_3), in addition to more stringent regulations [53, 54]. Between the US and the EU legislation there are already a few differences regarding the way some of these pollutants are measured. For example, in the US CH_4 is specifically controlled separately from the rest of the hydrocarbons; this last group known as non-methane hydrocarbons (NMHC), whilst the EU had not performed this differentiation until now. In the upcoming EU legislation CH_4 will be looked at separately as a green-house gas. A scheme of the predicted future changes in the emissions legislations can be found in Figure 1-13. These future measures will certainly create new challenges for those working in the automotive sector.

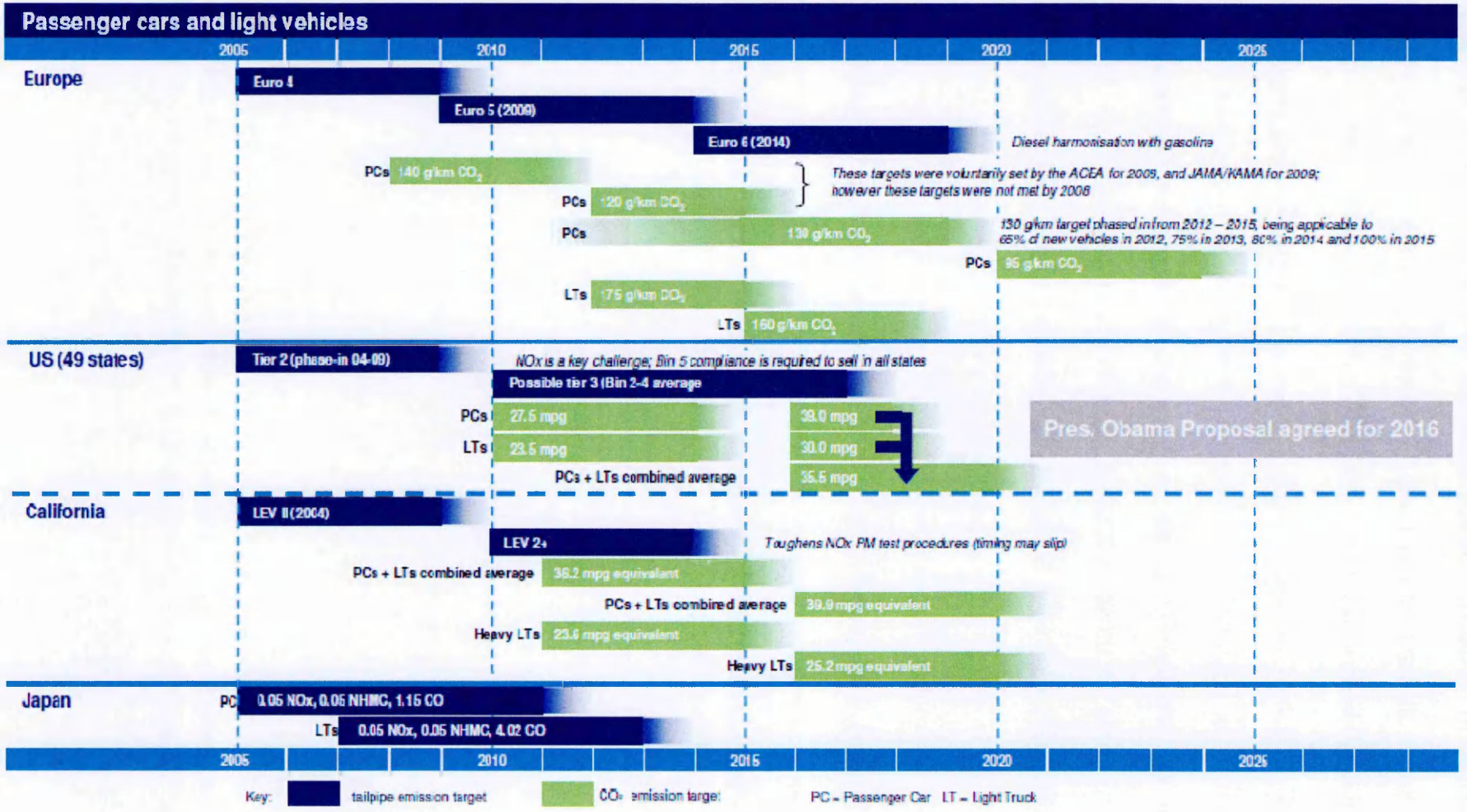

Figure 1-13: Predictions of the emissions control legislations' evolution. Source: Ricardo, National government sources, Arbuthnot securities estimates (from [53]).

1.3. The OSC component

1.3.1. Ce-based materials

As previously mentioned, the oxygen storage capacity (OSC) is one of the most important properties that any TWC needs to have. The most common materials known to have high OSC are the rare-earth metals oxides; ceria and ceria-zirconia mixed oxides are typically used for this application.

The most stable form of cerium under oxygen is CeO_2, which has a fluorite structure (Figure 1-14). Mass transport in fluorite-type materials is faster for anions than for cations. In this structure O^{2-} ions are removed from the CeO_2 lattice during the reduction to Ce_2O_3, leaving a number of anion vacancies [21]:

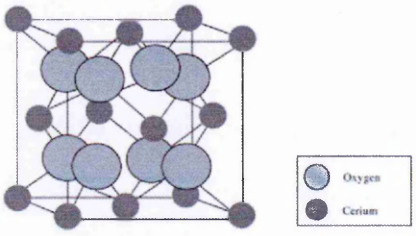

$$Ce^{4+} - O^{2-} \rightarrow Ce^{3+} - V_o^{\cdot} + \tfrac{1}{2}O_2 \qquad (1\text{-}17)$$

$V_o^{\cdot}$ = *oxygen vacancy*

Figure 1-14: Representation of the fluorite structure of CeO_2 (from [55]).

Whilst CeO_2 presents a high OSC, the low thermal stability makes it inadequate for practical use. This material was soon replaced by Ce-Zr mixed oxides, which showed better durability due to Zr higher thermal stability, and improved OSC [17, 44, 56].

The structure formed after Zr addition plays an important role in the performance of the material. The OSC appears to be 3-5 times higher if Ce and Zr are homogeneously distributed as a result of a mixed oxide formation [5, 57-60]. During the oxygen release process the structure of the ceria component is exposed to a stress, due to the increase of Ce size when Ce^{4+} is converted to Ce^{3+} [60, 61]. The stress produced further restricts changes of the Ce. However, the

incorporation of Zr ions, which are smaller than Ce ions, compensates the volume increment facilitating the valence change from Ce^{4+} to Ce^{3+}, as a consequence the OSC improves (Ionic radius: Zr^{4+} = 0.84 Å; Ce^{4+} = 0.97 Å, Ce^{3+} = 1.14 Å) [60].

Opinions are divided over the effect of the oxygen coordination around Zr. Nagai *et al.* found that a more centrosymmetric coordination of oxygen around Zr (same length for all Zr-O bonds) improved the oxygen mobility [60], whilst other authors concluded that a Zr-O coordination of the type 4+2 (short + long) further enhanced the OSC [62, 63].

It is well known that the OSC results from a combination of surface and bulk phenomena for Ce-Zr solid solutions; however, it is mainly a surface process for CeO_2 alone [5, 17, 44, 56, 57]. Figure 1-15 shows a H_2 temperature programmed reduction (H_2-TPR) comparison of ceria samples with different surface areas. Here it is possible to see how the first reduction peak (~775 K), associated to the surface reduction of ceria, is dependent on the surface area, being almost non-existent for the sample with the lowest value. Instead, the second peak (~1100 K) associated to the bulk ceria reduction increases when the surface area decreases. The reason for this behaviour is that pure Ce samples nanocrystals and bulk Ce^{4+} possess different kinetic and thermodynamic properties. This is contrary to what is seen for Ce-Zr, where the electron conductivity and activation energy for oxygen diffusion is similar in both nanocrystalline and sintered bulk material [5, 15]. Therefore, even CeZr systems with low surface area can have a good OSC [5, 58].

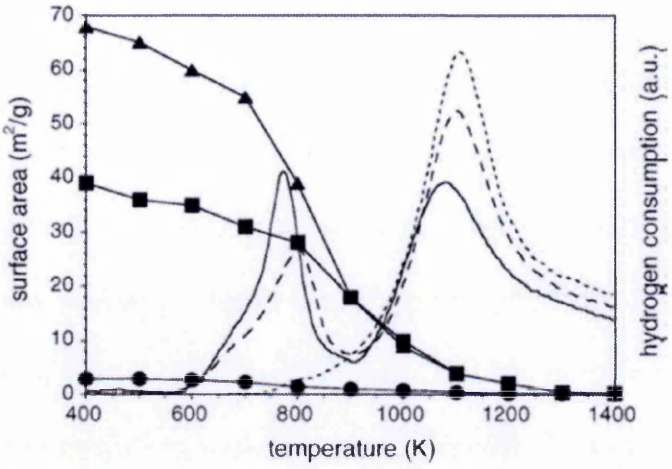

Figure 1-15: Evaluation of simultaneous changes on TPR profile (right) and surface area (left) of different samples of ceria: high-surface area (▲, —), medium surface area (■, - - -), low surface area (●, · · ·) (from [15]).

1.3.2. Noble metal-ceria interaction

Two different possibilities for the OSC rate-determining step have been proposed in the literature: i) the surface reaction between the oxygen acceptor (i.e. CO, HC) and the oxygen of the mixed oxide [57, 61], or ii) oxygen diffusion from the bulk of the support [5, 59]. This discussion is ongoing with no universally agreed OSC mechanism for CeO_2 and Ce-Zr solid solutions.

To promote the OSC reaction a noble metal can be added, either on the support or as a dopant, acting as a link to facilitate the adsorption of the oxygen-donor and consequent oxygen migration to the support vacancies (and vice versa) [56]. Thus, this metal-support interface is a key factor for a good OSC. Ir and Ru were found to be the most active noble metals for this reaction, however, as mentioned previously, the formation of volatile oxides make their use impractical [64]. Focusing on the OSC activity seen on noble metals supported on CeO_2 the following activity order has been reported: Ir > Ru > Rh > Pt > Pd [56, 57].

According to Bedrane *et al.* the noble metal particle size needed for an optimum OSC will depend on each of the metals [64]. Bedrane and co-workers found that small particles enhanced the OSC when using Rh, but decreased it when using Ru or Ir. The Pt particle size however, does not show any influence when Ce-Zr is used as the support; but when Pt was supported onto CeO_2 the particle size was dependent on the operating temperature: small particles were more active at temperatures lower than 400 ºC, but above this temperature larger particles demonstrated better OSC. This peculiar behaviour of Pt was believed to be related to changes in the metal particle phase with temperature: (111), (110) and (100), with Pt(111) phase the most active for oxygen desorption [64]. Fan *et al.* found similar results with Pt on Ce-Zr mixed oxides; in this case the study was based on Ce/Zr/La catalysts with different Pt loadings, where the best catalyst for propane conversion was the one with the lowest Pt dispersion [65].

Several studies revealed that noble metals deposited on Ce-based supports were interacting with the ceria forming a NM-O-Ce bond (NM = noble metal) [66-69]. S.J. Tauster *et al.* were first in reporting this metal-support interaction, nowadays known as SMSI (Strong Metal Support Interaction) [70]. One of the benefits seen was that this interaction helped to stabilise the metal dispersion and therefore reduced the level of metal sintering [55, 67-69]. In addition, the NM-O-Ce interaction enabled the noble metal particle to be reduced under reductive conditions at high temperature leaving it in a metallic state that was more active than the oxidised state [68].

It was found that the electron density of the oxygen from the support mainly controlled the strength of the metal-support interaction [68]. Thus, different CeZr materials will show different NM-O-Ce strengths for each particular noble metal. In

the same way, any other metal added to the support will also modify the electron density around the oxygen.

1.4. Deactivation of the catalyst

The severe conditions to which the catalyst is exposed during realistic driving times causes some catalyst deactivation. As the catalyst is placed close to the engine the main cause of deactivation is usually associated with thermo-chemical degradation, especially under oxidising conditions at temperatures higher than 900 ºC [5, 14, 21, 46]. The main deactivation processes are summarised in Table 1-1:

Table 1-1: Deactivation mechanism on Three-Way Catalysts

Thermal	Chemical
• Sintering of support and/or metals • Noble metals alloying • Support phase separation • Noble metal-base metal interactions • Oxidation • Encapsulation of the noble metal by the support • Metal volatilization	• Poisoning: irreversible adsorption • Inhibition: reversible adsorption • Physical/chemical blockage of support pore structure

Chemical poisoning is produced by the chemisorption of unwanted and harmful species from gasoline and lubricant oils on the active sites of the catalysts. The impurities block the sites leaving them inaccessible to the reactants. This deactivation is mainly due to sulphur from gasoline, and phosphorus from lubricant oils among others [6, 46]. The A/F ratio affects the behaviour of sulphur. Under lean conditions sulphur is stored as SO_2, SO_3, and SO_4^{2-}, and under rich conditions it is released as H_2S. The deactivation by sulphur is also more

significant at low temperatures (T < 650 °C), whereas at high temperatures (T > 1000 °C) sulphur adsorption is almost non-existent [6, 46].

Lubricants oils also contain several other harmful species, for example P, Zn, Ca, and Mg. Over time, these impurities are deposited on the surface of the catalyst forming a thin layer, covering the precious metals in the porous washcoat. For example, phosphorus contamination can be seen as adsorbed phosphates with the other impurities (pore blockage) or with the support (pore collapse); when this happens with Ce, the Ce remains in the Ce^{3+} oxidation state, which is detrimental for the OSC [46]. Unlike sulphur, phosphorus species are not believed to poison noble metals [6].

Generally, precious metals in metallic form show more resistance to poisoning than the respective metal oxides, however each of them present different resistance levels. For example, Pd is highly sensitive to sulphur and lead poisoning, whereas Rh and Pt are more resistant to such species [21, 46].

Thermal sintering of noble metals and supports is an on-going problem. As noble metal particle size increases the dispersion decreases, which means there are a lower number of active sites to create the noble metal-support interaction. This in addition to the sintering of the CeZr support will further decrease the number of interactions. The presence of additives in the support, such as La, Nd, Pr, Sm, and Y, among others, is known to reduce the level of sintering of the support [5, 12, 21, 46].

For each noble metal, degradation by sintering occurs to different extents. If Pt, Pd and Rh are compared, metallic Pt is fairly stable to sintering, but under oxidising conditions at high temperatures forms PtO_2, which is the most mobile of the oxides compared here (PtO_2, PdO, Rh_2O_3). Pd usually exists as a more stable oxide that

is highly active for oxidation reactions [16, 46]. Rh degradation is often associated with interactions between Rh_2O_3 and the support, forming inactive Rh-support species (i.e. Rh aluminates). As metallic Rh is needed for NO_x reduction, these reactions are highly undesirable [16, 71].

At the same time, the sintering rate is also dependent on the exhaust gas mixture (Figure 1-16). Oxidative atmospheres at high temperature (T > 900 ºC) are especially detrimental for the support and the noble metal [5, 46, 71].

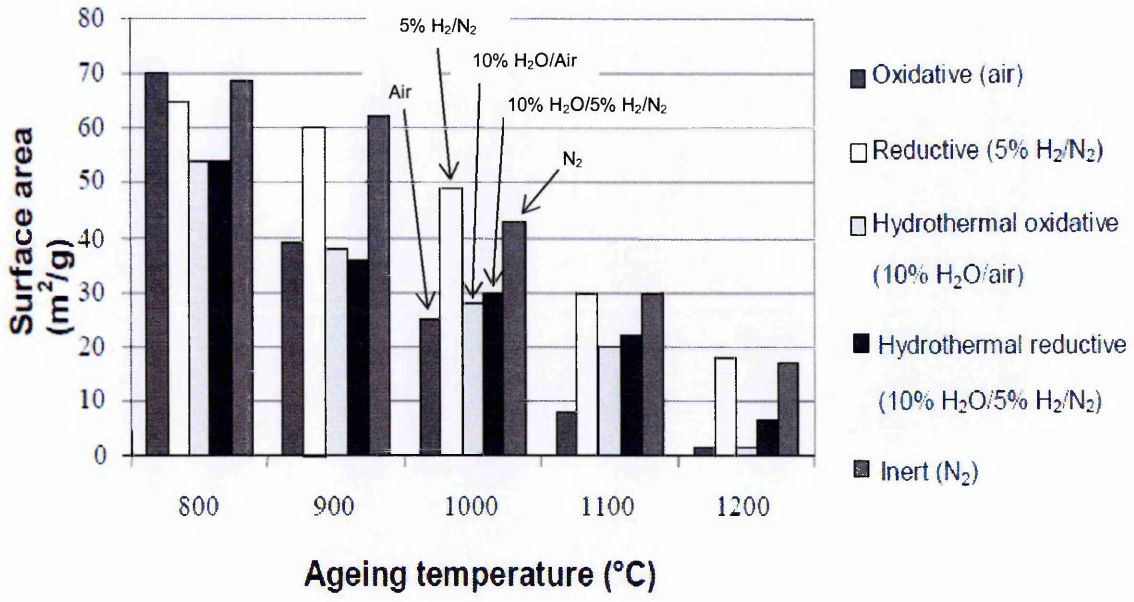

Figure 1-16: Comparison of surface areas in different ageing gas atmospheres after 3 hours of ageing on a commercial Pd-Rh based TWC (from [46])

Precious metals can also suffer deactivation by alloying. Due to the high TWC operation temperatures, when the metals are all placed on the same support this is practically impossible to avoid. The surface composition of the alloys is also sensitive to the gas mixture. In Pt-Rh alloys O_2 and NO induce Rh segregation due to a stronger Rh-O bond strength compared to Pt-O [72], whereas H_2 promotes Pt segregation on the surface of the alloy [13].

Encapsulation of the noble metal by the support is also a serious type of deactivation as this can be an irreversible process [5, 6, 46]. The noble metal can be lost by deep encapsulation as the oxygen-storage material sinters and is therefore not accessible for the adsorption of gas phase molecules. The extent of encapsulation depends on additional factors, including metal loading and CeZr composition. Noble metals can also be found to be covered by the support without being trapped inside the bulk, this phenomenon is known as decoration and, unlike encapsulation, it can be a reversible process [67] (Figure 1-17).

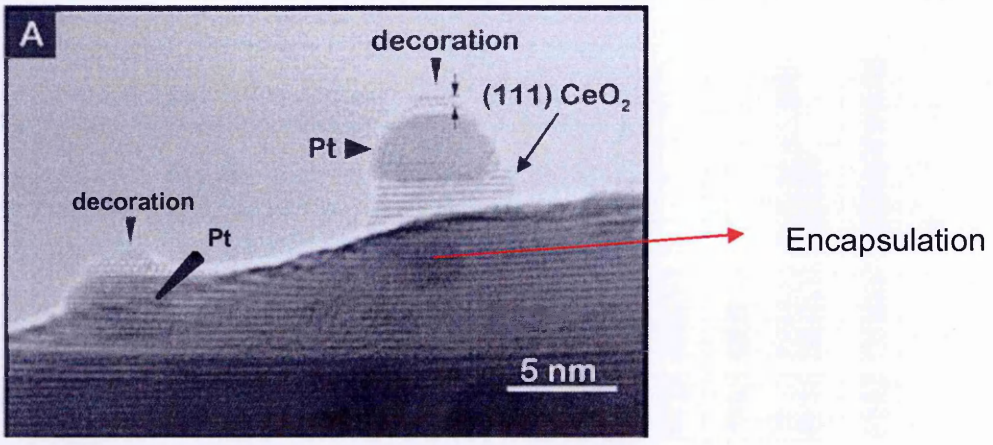

Figure 1-17: HREM study of the metal decoration and encapsulation effects occurring in Pt(4%)/CeO_2 reduced at 973 K (from [67]).

1.5. Preparation methods for $Ce_xZr_{1-x}O_2$ and NM-$Ce_xZr_{1-x}O_2$ materials (NM = noble metal)

Textural properties such as surface area, pore volume, and crystallite phase play an important role in the activity of the catalyst. Therefore, the control of the preparation parameters is critical to achieve the most optimised product.

Over the years, a range of different preparation methods have been studied for the synthesis of CeO_2 and CeZr solid solutions, such as co-precipitation [73-80],

hydrothermal synthesis [73, 76, 78], high energy mechanical milling [21], sol-gel preparation [75, 78-81], solution combustion [75], surfactant-assisted approach [21], or microemulsion [73, 75, 77, 78], among others. The final properties of the Ce-Zr material, such as structure, texture and surface, were found to be highly dependent on the preparation method chosen [5, 44, 73, 75, 80]. Overall, co-precipitation, sol-gel and microemulsion preparation methods have been the most used techniques, where products are highly homogeneous and so are more stable structures after high temperature ageing [73]. Table 1-2 shows the main advantages and disadvantages of each of these three methods. The next sections focus exclusively in the co-precipitation synthesis as this was the method chosen for this research.

Table 1-2: Advantages and disadvantages of the main techniques used for mixed oxides preparations. For a description of each process refer to the Appendix.

Method	Advantages	Disadvantages
Co-precipitation	- No organic solvents - Low temperature - Inexpensive - Easy process	- Formation of aggregates - Similar precipitation rates required (for good homogeneity) - Small changes during preparation lead to different products
Sol-gel	- Final product on the nm scale - Low temperature - Easy process	- Need alkoxides solutions as precursors (expensive) - Difficult to find a solvent that can dissolve all the metal alkoxides required
Microemulsion	- Final product on the nm scale - Easy to control the final particle size	- Precursor is a mixture of water, surfactant, and oil. - The nuclei must form at the same time and rate to form monodispersed particles

1.5.1. Co-precipitation

Co-precipitation was considered a promising method to prepare mixed oxides, due to its minimal use of reactants and simple procedure to synthesise powders with moderate surface area (~100 $m^2 g^{-1}$) [44, 82]. In this method a solution containing the precursors in the desired stoichiometric ratio is mixed with a second solution containing the precipitant agent. This leads to the precipitation of a mixed solid powder. The product is then filtered, dried and calcined.

However, tiny modifications of the different parameters of this preparation can have an impact on the final structure of the solid solution as discussed below [5]. As an example, the impacts of some of the preparation parameters during the synthesis of $Ce_xZr_{1-x}O_2$ materials are discussed:

Ce precursor:

Most authors agree that the Ce precursor is the important factor controlling the final structure of the Ce-Zr mixed oxide [74, 76, 83]. It has been reported that the use of a Ce^{3+} precursor leads to a heterogeneous structure with a Ce-enrichment at the surface of the particles [76], whereas a homogeneous CeZr mixed oxide is obtained when a Ce^{4+} precursor is used [74, 83]. Some authors state that this behaviour is due to the different precipitation rate of Ce^{3+} and Ce^{4+}, the precipitation of $Ce(OH)_4$ (using Ce^{4+} precursor) being closer to that of $Zr(OH)_4$ (or $ZrO(OH)_2$ depending on the case). Contrary to these findings, Duprez *et al.* did not see any changes when using Ce^{3+} or Ce^{4+}; however, in their preparation the base was added to the precursors' solution with no control of the pH [80], which could have led to different results than those obtained by the authors above.

Base addition and pH:

Mixed opinions are found in the literature regarding the impact of the way the precipitant base is added. Some authors prefer to control the pH between 9-9.5 during the precipitation, which is believed to help form more homogeneous structures [74, 75]. Contrary results are also found in the literature, as seen in the study performed by Letichevsky *et al.* comparing co-precipitations with or without control of the pH, where they conclude that no significant differences exist in the final structure regarding the base addition[6] [83].

Carter *et al.* found that the pH determines the type of hydrous zirconium in the solution, existing as $Zr(OH)_4$ at pH 3 and as $ZrO(OH)_2$ at pH 12 [84]. In their studies this had a significant impact on the final particle size of the product, obtaining smaller particles at pH 12 than at pH 3; unfortunately no experiments were performed with other pH values between this range. Zhao *et al.* confirmed that the pH in which the co-precipitation is performed affects the final pore volume, and consequently the surface area. In these experiments, samples precipitated at pH 10 showed smaller pore volume than samples precipitated at pH 8.6-9 [82].

Other factors

Agitation levels and starting solution concentration have also been reported to affect the particle size of the final solid, however their impact was not that significant when compared to the impact of the factors discussed above [84].

The ability to obtain a specific phase in the final product is however difficult to control with the preparation method as the formation of a cubic or tetragonal phase is mainly dependent on the Ce:Zr molar ratio ($Ce_xZr_{1-x}O_2$ with $x > 0.5$ will mainly

[6] References [65-66] used NH_3 and reference [74] used NH_4OH.

contain cubic phase, whereas with x < 0.5 the tetragonal phase will be formed) [44, 80, 81]. In terms of reactivity Thammachart *et al.* reported that CO conversion was considerably higher with cubic-phase samples due to its more reducible character compared to tetragonal-phase catalysts; however in their article it is not clear if the improvement could also be related to a higher content of the active element Ce in the structure [81]. Duprez *et al.* were able to create a fluorite-type structure (tetrahedral), which is more stable, for mixed oxides with high content of cerium (x up to 0.9) using a modified sol-gel preparation [80]. It was not however possible to achieve this structure when using a co-precipitation method. In agreement with Thammachart *et al.*, this group also found higher oxygen mobility in the samples with cubic-phase.

1.5.1.1. Co-precipitation of NM-$Ce_xZr_{1-x}O_2$

In most cases the aim is to dope the support with the NM (NM-$Ce_xZr_{1-x}O_2$) in order to decrease the level of sintering of ceria during the high temperature ageing, as well as to enhance its reducibility at low temperatures (< 200 °C) due to a higher contact between the NM and the ceria [85-87]. The majority of the NM-$Ce_xZr_{1-x}O_2$ catalysts are prepared by the microemulsion [85], combustion [88, 89], or the co-precipitation methods [86, 90].

Focusing on the co-precipitation method, similarly to the preparation of $Ce_xZr_{1-x}O_2$ materials, the parameters of the synthesis need to be chosen carefully as they can have a significant impact in the final product [86]. As an example, Huang *et al.* studied the impact of the precipitant base and the temperature during the co-precipitation of H_2IrCl_6 and $Ce(NO_3)_3$. In terms of the precipitant base, from Na_2CO_3, urea, and NaOH (adding the precursors to the base solution and without

controlling the pH), they found NaOH to be the most suitable precipitant base to achieve the highest activity for the CO oxidation reaction; once they had chosen the precipitant base, they also tried the co-precipitation at 20, 80 and 100 ºC, and found that the optimum temperature was 80 ºC for their application [86].

In the literature only a few studies focus on the impact of the preparation factors during the co-precipitation of the NM and the Ce or CeZr, contrary to the co-precipitation of $Ce_xZr_{1-x}O_2$ which has been extensively studied.

1.6. Project Motivation

The current approach to create a good metal-ceria interaction has been achieved by using common preparation techniques, such as the impregnation method. However, due to the continuous drifting towards lower noble metal loadings, this is reaching a limit and new techniques to prepare catalysts with extremely low noble metal contents (≤ 0.5 wt% Pd, or Pt, and ≤ 0.1 wt% Rh) are necessary. Based on this, the objective of this work has been to develop an alternative preparation method to disperse low metal loadings on ceria, mostly focusing on Pd-ceria catalysts.

References Chapter 1

[1] D. R. Middleton, in R. M. Harrison and R. E. Hester (Editors), *Air Quality Management*, Vol. 8, 1997, p. 1-18.

[2] R. F. Gould, *Photochemical Smog and Ozone Reactions*, American Chemical Society, Washington, 1972.

[3] K. Saini, *Effect of environmental pollutants on human health*, Environment About: The Encyclopedia of Environment, 2011, http://www.environmentabout.com/723/effect-of-environmental-pollutants-on-human-health [20-09-2011].

[4] EEA, *Sector share of nitrogen oxides emissions (EEA member countries)*, 2011, http://www.eea.europa.eu/data-and-maps/figures/sector-share-of-nitrogen-oxides-emissions-eea-member-countries-2 [[22-12-2011]].

[5] J. Kašpar, P. Fornasiero and N. Hickey, Catalysis Today, 77 (2003) 419-449.

[6] R. M. Heck and R. J. Farrauto, *Catalytic air pollution control - Commercial Technology*, Willey-Interscience, 2002.

[7] R. P. Wayne, *Chemistry of Atmospheres*, Oxford University Press, 2000.

[8] R. Wayne, in J.D. Coyle, R.R. Hill and D.R. Roberts (Editors), *Light, chemical change and life: a source book in photochemistry*, The Open University press, UK, 1982.

[9] Y.-G. Zhu, J. P. A. Ioannidis, H. Li, K. C. Jones and F. L. Martin, *Understanding and Harnessing the Health Effects of Rapid Urbanization in China*, Environmental Science and Technology, American Chemical Society, 2011, http://dx.doi.org/10.1021/es2004254 [20-09-2011].

[10] J. Wheldon, *Who stole Big Ben?*, MailOnline, Associated Newspapers Ltd, 2007, http://www.dailymail.co.uk/news/article-445046/Who-stole-Big-Ben.html [14-07-2011].

[11] J. E. McEvoy, *Catalysts for the Control of Automotive Pollutants*, American Chemical Society, Allentown, 1975.

[12] Q. Wang, B. Zhao, G. Li and R. Zhou, Environmental Science and Technology, 44 (2010) 3870–3875.

[13] B. E. Nieuwenhuys, *Advances in Catalysis*, in Academic Press Inc (Editor), The Surface Science Approach Toward Understanding Automotive Exhaust Conversion Catalysis at the Atomic Level, Vol. 44, Elsevier Inc, 1999, p. 259-328.

[14] A. Trovarelli, C. d. Leitenburg, M. Boaro and G. Dolcetti, Catalysis Today, 50 (1999) 353-367.

[15] A. Trovarelli, E. Aneggi, M. Boaro, C. d. Leitenburg and G. Dolcetti, Journal of Alloys and Compounds, 408-412 (2006) 1096-1102.

[16] M. V. Twigg, Applied Catalysis B: Environmental, (2007) 2-15.

[17] H. S. Gandhi, G. W. Graham and R. W. McCabe, Journal of Catalysis, (2003) 433-442.

[18] M. V. Twigg, Catalysis Today, 117 (2006) 407-418.

[19] T. O. University, *The Three-Way Catalytic Converter*, OpenLearn, http://openlearn.open.ac.uk/course/view.php?id=2440 [10-05-2010].

[20] M. Zhao, M. Shen and J. Wang, Journal of Catalysis, 248 (2007) 258-267.

[21] A. Trovarelli, *Catalysis by Ceria and Related Materials*, Imperial College Press, 2002.

[22] B. G. Survey, *Rare earth elements: a beginner's guide from the BGS*, 2011, http://www.bgs.ac.uk/research/highlights/rare_earth_elements.html [25-07-2011].

[23] A. Pappacena, K. Schermanz, A. Sagar, E. Aneggi and A. Trovarelli, *10th International Symposium "Scientific Bases for the Preparation of Heterogeneous Catalysts"* 2010.

[24] S. Adams, World Patent Information, (2009) 323-326.

[25] Defra, *EU Emission standards for petrol vehicles*, in Department of Environment Food and Rural Affairs (Editor), Crown.

[26] DieselNet, *Emission Standards. European Union: Cars and Light Trucks*, DieselNet, http://www.dieselnet.com/standards/eu/ld.php [01-08-2011].

[27] I. D. Platinum, *Emission Standards*, http://www.implats.co.za/implats/Emission-standards.asp [01-08-2011].

[28] U. S. E. P. Agency, *EPA Federal Test Procedure (FTP)*, 2009, http://www.epa.gov/oms/standards/light-duty/ftp.htm [20-11-2011].

[29] S. Adams, World Patent Information, 31 (2009) 323-326.

[30] M. Frenkel, *Procédé et appareil pour la désodorisation des gaz déchappement des moteurs dautomobiles et autres*, FRD402173 1909.

[31] E. J. Houdry, *Catalytic Structure and Composition*, in United States Patent Office (Editor), Vol. US2742437, 1952.

[32] E. J. Houdry, *Catalytic apparatus and method for treating exhaust gases*, US 2664340, 1953.

[33] E. J. Houdry, *Catalytic structure and composition*, US2742437 A, 1956.

[34] C. D. Keith, T. Schreuders and C. E. Cunningham, *Apparatus for purifying exhaust gases of an internal combustion engine*, US3441381 A, 1969.

[35] J. Lewis, *Lead Poisoning: A Historical Perspective*, United States Environmental Protection Agency, 1985, http://www2.epa.gov/aboutepa/lead-poisoning-historical-perspective [30-05-2014].

[36] I. McDowell, *Societal Pressures and Action on Scientific Evidence: the Story of Leaded Gasoline*, University of Ottawa, 2011, http://www.med.uottawa.ca/SIM/Data/Lead_in_Gasoline.htm [30-05-2014].

[37] M. Beychok, *Tetraethyl lead (TEL)*, The Encyclopedia of Earth, 2012, http://www.eoearth.org/view/article/173640/ [30-05-2014].

[38] J. H. Wong, C. Lim and G. L. Nolen, *Design of Remediation Systems*, CRC Press, 1997.

[39] T. Midgley, *Motor Fuel*, Vol. US1592955 1926.

[40] M. Sideris, *Methods for monitoring and diagnosing the efficiency of catalytic converters*, Elsevier Science B.V., 1998.

[41] M. Shelef and R. W. McCabe, Catalysis Today, (2000) 35-50.

[42] A. G.Graham and S. E. Wanke, Journal of Catalysis, 68 (1981) 1-8.

[43] M. Shelef and H. S. Gandhi, Platinum Metals review, 18 (1974) 2-14.

[44] M. Ozawa, Journal of Alloys and Compounds, 275-277 (1998) 886-890.

[45] C.-H. Wu and R. H. Hammerle, Industrial And Engineering Chemistry, Product Research And Development, 22 (1983) 559-565.

[46] U. Lassi, *Deactivation correlations of Pd/Rh Three-Way catalysts designed for Euro IV emission limits: Effect of Ageing Atmosphere, Temperature and Time*, Department of Process and Environmental Engineering, University of Oulu, Oulu, 2003.

[47] C. European Parliament, *Amending Directive 98/70/EC relating to the quality of petrol and diesel fuels*, Vol. 76, Official Journal of the European Union, 2003, p. 10-19.

[48] S. Chunshan, Catalysis Today, 86 (2003) 211-263.

[49] K. M. Adams and H. S. Gandhi, Industrial & Engineering Chemistry Product Research and Development, 22 (1983) 207-212.

[50] H. Muraki, H. Shinjoh and Y. Fujitani, Applied Catalysis, 22 (1986) 325-335.

[51] H. Muraki, K. Yokota and Y. Fujitani, Applied Catalysis, 48 (1989) 93-105.

[52] Wikipedia, *Air-Fuel ratio ideal stoichiometry*, Wikipedia, Wikipedia, 2011, http://en.wikipedia.org/wiki/Air%E2%80%93fuel_ratio [22-08-2011].

[53] R. plc, *Interims presentation FY 09/10*, 2010.

[54] ACEA, *European Automobile Manufacturers' Association*, Air Quality, 2011, http://www.acea.be/collection/environmental_track_record_air_quality_background/ [20-07-2011].

[55] K. C. Patil, M. S. Hegde, T. Rattan and S. T. Aruna, *Chemistry of nanocrystalline oxide materials: Combustion synthesis, Properties and applications.*, World Scientific Publishing Co. Pte. Ltd., 2008.

[56] C. Descorme, S. Bedrane and D. Duprez, Catalysis Today, 75 (2002) 401-405.

[57] D. Belton, C. E. Hori, H. Permana, K. Y. S. Ng, A. Brenner, K. More and K. M. Rahmoeller, Applied Catalysis B: Environmental, 16 (1998) 105-117.

[58] J. Wang, M. Zhao and M. Shen, Journal of Catalysis, 248 (2007) 258-267.

[59] F. Dong, A. Suda, T. Tanabe, Y. Nagai, H. Sobukawa, H. Shinjoh, M. Sugiura, C. Descorme and D. Duprez, Catalysis Today, 93-95 (2004) 827-832.

[60] Y. Nagai, T. Yamamoto, T. Tanaka, S. Yoshida, T. Nonaka, T. Okamoto, A. Suda and M. Sugiura, Catalysis Today, 74 (2002) 225-234.

[61] A. Martorana, G. Deganello, A. Longo, A. Prestianni, L. Liotta, A. Macaluso, G. Pantaleo, A. Balerna and S. Mobilioc, Journal of Solid State Chemistry, 117 (2004) 1268-1275.

[62] G. Vlaic, P. Fornasiero, S. Geremia, J. Kašpar and M. Graziani, Journal of Catalysis, 168 (1997) 386-392.

[63] Y. Nagai, *Physicochemical Study of Automotive Catalysts for Emission Control*, Kyoto University, 2007.

[64] S. Bedrane, C. Descorme and D. Duprez, Applied Catalysis A: General, 289 (2005) 90-96.

[65] Y. Guo, G. Lu, Z. Zhang, S. Zhang, Y. Qi and Y. Liu, Catalysis Today, 126 (2007) 296-302.

[66] P. J. Schmitz, K. Otto and J. E. deVries, Applied Catalysis A: General, 92 (1992) 59-72.

[67] S. Bernal, J. J. Calvino, M. A. Cauqui, J. M. Gatica, C. Larese, J. A. P. Omil and J. M. Pintado, Catalysis Today, 50 (1999) 175-206.

[68] Y. Nagai, T. Hirabayashi, K. Dohmae, N. Takagi, T. Minami, H. Shinjoh and S. i. Matsumoto, Journal of Catalysis, 242 (2006) 103-109.

[69] M. Hatanaka, N. Takahashi, T. Tanabe, Y. Nagai, K. Dohmae, Y. Aoki, T. Yoshida and H. Shinjoha, Applied Catalysis B: Environmental, 99 (2010) 336-342.

[70] S. J. Tauster, S. C. Fung and R. L. Garten, Journal of American Chemical Society, 4 (1978) 170-175.

[71] D. M. Fernandes, C. F. Scofield, A. A. Neto, M. J. B. Cardoso and F. M. Z. Zotin, Chemical Engineering Journal, 160 (2010) 85-92.

[72] T. Li, E.A.Marquis, P.A.J.Bagot, S.C.Tsang and G.D.W.Smith, Catalysis Today, 175 (2011) 552-557.

[73] R. Zhou, B. Zhao, G. Li, C. Ge and Q. Wanga, Applied Catalysis B: Environmental, 96 (2010) 338-349.

[74] A. García-García, N. Guillén-Hurtado, I. Atribak and A. Bueno-López, Journal of Molecular Catalysis A: Chemical, 323 (2010) 52-58.

[75] S. Wang, L. Cao, L. Pan, C. Ni and Z. Yuan, Fuel Processing Technology, 91 (2010) 306-312.

[76] S.-K. Ihm, J.-R. Kim and W.-J. Myeong, Journal of Catalysis, 263 (2009) 123-133.

[77] A. Glisenti, J. Rebellato and M. M. Natile, Applied Catalysis A: General, 339 (2008) 108-120.

[78] X. Wu, J. Fan, R. Ran, J. Yang and D. Weng, Journal of Alloys and Compounds, 395 (2005) 135-140.

[79] S. Rossignol, Y. Madier and D. Duprez, Catalysis Today, 50 (1999) 261-270.

[80] D. Duprez, S. Rossignol and F. Gerard, Journal of Materials: Chemistry, 9 (1999) 1615-1620.

[81] M. Thammachart, V. Meeyoo, T. Risksomboon and S. Osuwan, Catalysis Today, 68 (2001) 53-61.

[82] B. Zhao, Q. Wang, G. Li and R. Zhou, Journal of Alloys and Compounds, 508 (2010) 500-506.

[83] S. Letichevsky, C. A. Tellez, R. R. d. Avillez, M. I. P. d. Silva, M. A. Fraga and L. G. Appel, Applied Catalysis B: Environmental, 58 (2005) 203-210.

[84] G. A. Carter, R. D. Hart, M. R. Rowles, C. E. Buckley and M. I. Ogden, Powder Technology, 191 (2009) 218-226.

[85] M. Kurnatowska, L. Kepinski and W. Mista, Applied Catalysis B: Environmental, 117–118 (2012) 135-147.

[86] Y. Huang, A. Wang, L. Li, X. Wang, D. Su and T. Zhang, Journal of Catalysis, 255 (2008) 144-152.

[87] Y. Zhao, B.-T. Teng, X.-D. Wen, Y. Zhao, L.-H. Zhao and M.-F. Luo, Catalysis Communications, 27 (2012) 63-68.

[88] R. V. Gulyaev, A. I. Stadnichenko, E. M. Slavinskaya, A. S. Ivanova, S. V. Koscheev and A. I. Boronin, Applied Catalysis A: General, 439–440 (2012) 41-50.

[89] S. Roy, A. Marimuthu, M. S. Hegde and G. Madras, Applied Catalysis B: Environmental, 71 (2007) 23-31.

[90] J.-Y. Luo, M. Meng, J.-S. Yao, X.-G. Li, Y.-Q. Zha, X. Wang and T.-Y. Zhang, Applied Catalysis B: Environmental, 87 (2009) 92-103.

2. Experimental Techniques

Contents

2.1. Catalysis preparation

TWC are traditionally prepared by the impregnation method. However, the economic pressure to lower the noble metal content is directing research into different preparation techniques, as the common impregnation methods used to prepare low noble metal loadings catalysts (<0.5 wt%) can leave the noble metal particles so highly dispersed that they can finish fixed in a ionic state which can be less reactive due to an over-strong interaction with the ceria [1].

In order to attempt to optimise the metal-CeO_2 interaction, the co-precipitation method was chosen to prepare noble metal-CeO_2, and -CeZr catalysts, with a special focus on Pd-CeO_2 catalysts. The effect of the ceria precursors (Ce^{3+} vs Ce^{4+}) during the preparation of these catalysts was also studied, using in all cases a Pd^{2+} precursor. In addition, platinum and rhodium catalysts were prepared in a similar way using Pt^{2+} and Rh^{3+} precursors with the Ce^{3+} precursor, to study the impact of the noble metal.

Table 2-1 summarises the main catalysts prepared for this work. Reference catalysts for all samples (not listed here) were also prepared by the wet impregnation method.

Table 2-1: Summary of the type of catalysts prepared by the co-precipitation method for this work.

Pd-catalysts	[Pd^{2+}+Ce^{3+}]
	[Pd^{2+}+Ce^{4+}]
	[Pd+Ce^{3+}+ZrO_2]
Pt-catalysts	[Pt^{2+}+Ce^{3+}]
Rh-catalysts	[Rh^{3+}+Ce^{3+}]

2.1.1. Co-precipitation of the noble metal and cerium

Co-precipitation is considered an inexpensive method, due to its minimal use of reactants and simple procedure to synthesise powders with moderate surface area [2, 3]. In this method a solution containing the precursors in the desired stoichiometric ratio is mixed with a second solution containing the precipitating agent. This leads to the precipitation of a mixed solid powder. The product is then filtered, dried and calcined.

The main factor that controls the co-precipitation is the inter-particle force, meaning that the agglomeration of the particles (thus, precipitation of a solid) will be subjected to the rate of particle collision per unit time [4]. One of the main causes of collision is the shear force caused by the stirring; if there is a net attractive force, commonly due to Van der Waals forces, the particles will bond to form agglomerates [4].

Through the years, several authors have studied how the different parameters of this preparation can impact the final structure (particle size and distribution, shape, and stoichiometry, among others) of the solid solution, such as the type of precursors, pH, temperature, cation concentration... [2, 4-6]. From all the conditions studied, pH appeared to have the biggest effect on the precipitate particle size, with higher pH values leading to lower particle sizes [2, 4, 6]. Agitation levels and the initial starting solution concentration have also been seen to affect the particle size of the final solid, however their impact was not as significant [6]. It is therefore necessary to choose the co-precipitation parameters carefully.

2.1.1.1. Parameters used in this project for the co-precipitation

For complete precipitation of the precursors 725 ml of a basic solution of demineralised water with 20% excess of NaOH (4M), based on the necessary amount for complete precipitation, was added to a 1 L round bottomed flask. A condenser was then connected and the solution was refluxed (~102 °C) under continuous stirring using a magnetic stirrer at a rate of 700 rpm. Separately, a solution was prepared by mixing the desired amounts of precursors [Ce precursor + NM precursor] in 150 ml of demineralised water. Once the basic solution was boiling the precursor mixture was added using a peristaltic pump (10 ml min^{-1}). A schematic representation of the set up can be found in Figure 2-1. Upon complete precipitation the solution was then allowed to cool down to room temperature (under stirring), filtered under vacuum, and then washed with warm demineralised water (60 °C) until the conductivity was less than 40 µS, to ensure that most of the nitrates and Na^+ ions were removed. The materials were then dried at 105 °C overnight, followed by a calcination at 650 °C for 2 hours.

The majority of the catalysts were prepared using a Ce^{3+} precursor ($Ce(NO_3)_3 \cdot 6H_2O$). In addition, in order to study the impact of the cerium-precursor, a Ce^{4+} precursor was also used to prepare a Pd-CeO_2 catalyst:

a) Precipitation with Ce(III) precursor – $Ce(NO_3)_3 \cdot 6H_2O$ + $Pd(NO_3)_2$
b) Precipitation with Ce(IV) precursor – $Ce(NH_4)_2(NO_3)_6$ + $Pd(NO_3)_2$

The $Ce(NO_3)_3 \cdot 6H_2O$ and $Ce(NH_4)_2(NO_3)_6$ salts were supplied by Alfa Aesar and the noble metal solutions $Pd(NO_3)_2$ (14.95% Pd assay), $Pt(NO_3)_4$ (15.71% Pt assay), and $Rh(NO_3)_3$ (12.85% Rh assay) by Johnson Matthey.

Zirconium was also co-precipitated with Ce^{3+} and Pd^{2+} using the same procedure. For these preparations, in addition to $Ce(NO_3)_3 \cdot 6H_2O$ and $Pd(NO_3)_2$ precursors, a

$ZrO(NO_3)_2$ solution supplied by Aldrich was used. The Ce:Zr molar ratio for these samples was 1:1.

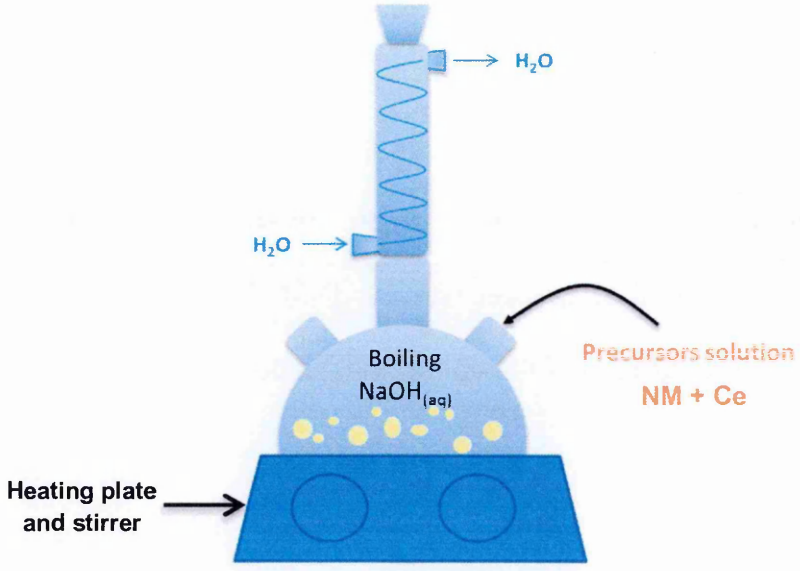

Figure 2-1: Schematic representation of the set up for the co-precipitation synthesis.

2.1.2. Wet impregnation

The impregnation method is the most commonly used technique to prepare catalysts due to its simplicity and low cost; however, it is difficult to control the metal particle size and distribution. This method simply consists of soaking a porous material with the dissolved precursor, followed by a drying-step and a calcination.

The most common precursors used are based on nitrate/nitrite salts, and carbonyl complexes; metal chloride salts are normally avoided, as the chloride can be left on the support poisoning the catalytic activity [7].

There are two main impregnation methods: incipient wetness or wet impregnation. For the incipient wetness impregnation, the precursor's solution contains enough liquid to just fill all the pores of the support without leaving the outside wet. For the wet impregnation, there is an excess of liquid which will be eventually removed by

drying the sample [8]. For the control preparations in this project, the wet impregnation method was used.

For this preparation, CeO_2 and $Ce_{0.5}Zr_{0.5}O_2$ supports were made 'in house' by the precipitation method and the NM was added by the wet impregnation technique. The conditions used were the same as described above in order to have the closest materials to the co-precipitated [NM+Ce^{3+}] samples for a better comparison. The preparation of these supports is described below.

2.1.2.1. CeO_2 and $Ce_{0.5}Zr_{0.5}O_2$ preparation

The CeO_2 and $Ce_{0.5}Zr_{0.5}O_2$ support materials were prepared using the same method described in *section 2.1.1.1.* but using a larger reactor in order to prepare larger amounts of sample. For this preparation the reactor capacity was 10 L, and the precursor solution ([$Ce(NO_3)_3$] or [$Ce(NO_3)_3$ + $ZrO(NO_3)_2$] depending on the preparation) was added at a rate of 25 ml min^{-1}. The solution was stirred using an electric head stirrer (300 rpm). Filtration, drying, and calcination steps remained the same.

2.1.2.2. Noble metal (NM) impregnation

The required amount of the NM precursor solution was diluted with enough demineralised water in order to have a small excess of solution volume (~20% excess) to fully fill the pore volume of the support[1]. The solution was then added slowly to the support with the help of a pipette and stirred to achieve maximum

[1] The pore volume of the support is calculated by wetting ***y*** grams of the support with ***x*** ml of demineralised water, until a point where it cannot accept more liquid. The pore volume is then calculated by dividing ***x*** by ***y*** (PV = x/y).

homogeneity. The material was then dried at 105 °C overnight followed by a calcination in air at 650 °C for 2 hours.

2.2. Characterisation

2.2.1. Bulk characterisation

The bulk characterisation performed in this project refers to that which studies the structure and composition of the catalyst overall. For this, X-ray diffraction (XRD) and inductively coupled plasma emission spectroscopy (ICP-ES) analyses were performed.

The ICP analysis gave information about the composition of the sample, in order to determine if the preparation used leads to the required catalyst; whilst XRD, gave information about the catalytic structure and presence of dopants. This is important, as different structures have different stabilities, and the presence of dopants can create a certain level of distortion that can affect the oxygen mobility.

2.2.1.1. X-Ray Diffraction (XRD)[2]

X-Ray diffraction (XRD) was used to investigate the bulk phases present in the sample as X-rays have enough energy to penetrate into the material. The crystal structure of a material can be described in terms of its unit cell. The unit cells describe the bulk arrangement of atoms of the crystal. This unit cell is given by its lattice parameters, which are the length of the cell edges and the angles between them. Depending on the symmetry of the crystal, this is classified using the seven lattice systems: triclinic, monoclinic, orthorhombic, rhombohedral, tetragonal, hexagonal, or cubic (Figure 2-2A).

[2] Analyses performed by Dr Hoi Jobson (jobsoh@matthey.com) and Dr Edward Bilbe (BilbeE01@matthey.com)

X-rays are elastically scattered by electrons. When an X-ray beam hits an atom, the electrons around the atom start to oscillate with the same frequency as the incoming beam. As the atoms in a crystal are arranged in a regular pattern, the waves will be in phase and there will be well defined X-ray beams leaving the sample at various directions (Figure 2-3). Hence, a diffracted beam may be described as a beam composed of a large number of scattered rays mutually reinforcing one another.

Due to the complexity of the model this is considered as X-ray reflections from a series of parallel planes inside the crystal. The orientation and interplanar spacings of these planes are defined by *h, k, l* called Miller indices. A given set of planes with indices *h, k, l* cut the *a* axis of the unit cell in *h* sections, the *b* axis in *k* sections and the *c* axis in *l* sections. A zero indicates that the planes are parallel to the corresponding axis (Figure 2-2B).

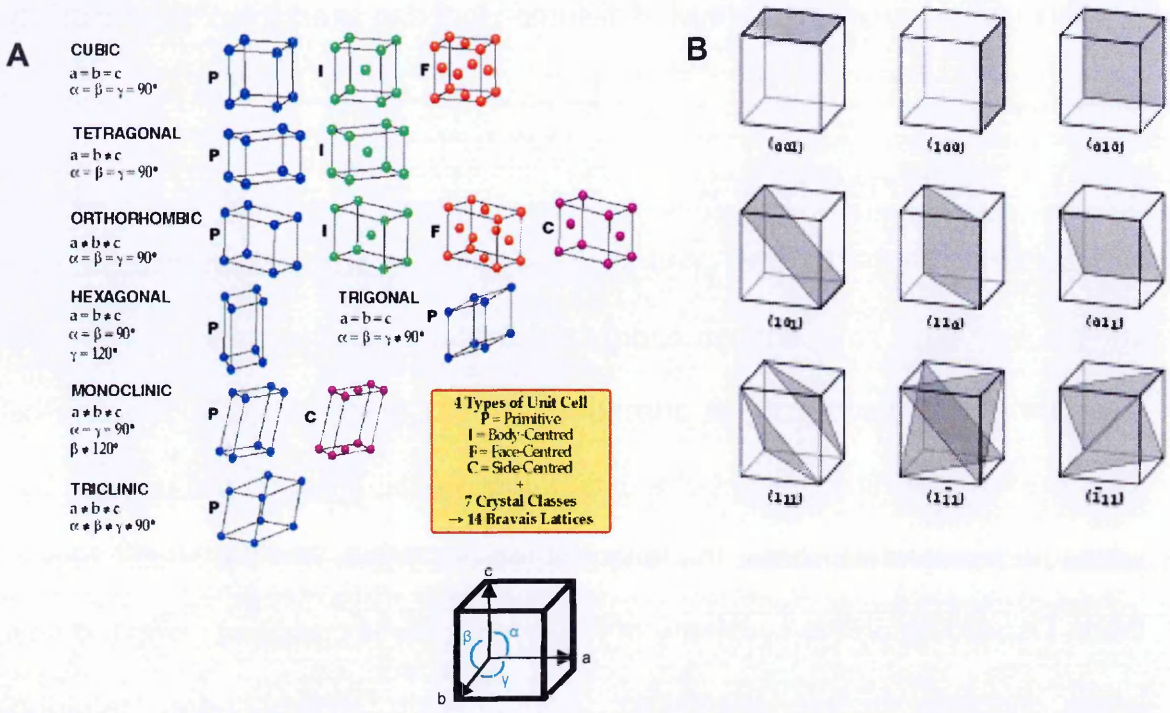

Figure 2-2: A) Summary of the lattice systems (from [9]). B) Graphical representation of the planes inside a crystal.

The angle that the X-rays form with the crystal planes when leaving the sample allows the lattice parameter to be calculated using Bragg's law (2-1) (see Figure 2-3 for a graphical representation):

$$n\lambda = 2d \sin\theta \tag{2-1}$$

where
- λ wavelength of the X-rays (nm)
- d distance between two atomic planes in the crystalline phase (nm)
- n order of the diffraction.
- θ incoming diffraction angle.

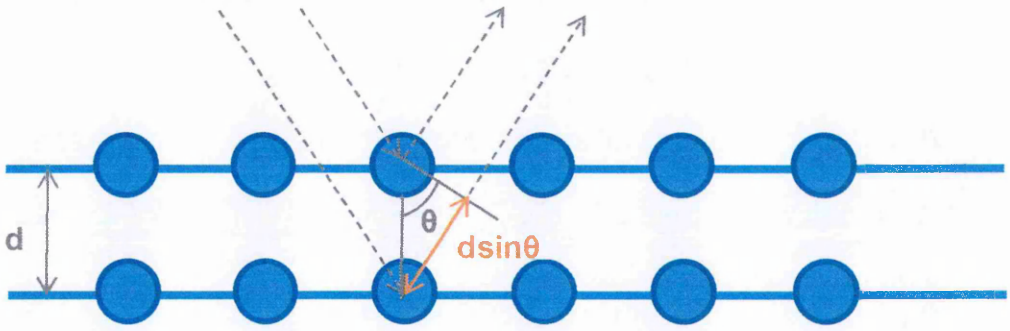

Figure 2-3: Schematic representation of Bragg's diffraction. Two X-rays with identical wavelength (λ) hit two different atoms in a crystal and are then scattered off. The lower beam traverses an extra length of 2dsinθ. When this length is equal to an integer multiple of the wavelength of the radiation (nλ), constructive interference occurs.

The diffraction pattern obtained can be matched against a library of standards to identify the phases present [10].

The crystallite size was calculated using the Rietveld method [11]. This technique consists in minimising the function M (2-2), which analyses the difference between the calculated diffraction pattern and the observed data:

$$M = \sum W_i \left\{ y_i^{obs} - \frac{1}{c} y_i^{calc} \right\}^2 \tag{2-2}$$

Where	y_i^{obs}	observed peak profiles
	y_i^{calc}	calculated peak profiles
	W_i	statistical weight
	c	scale factor such as $y^{cal} = cy^{obs}$

By combining mathematical methods and chemical data a model of the examined molecules was then elaborated, which allowed obtaining information about their atomic connectivity, bond distances and angles. Using these parameters it was then possible to calculate the crystallite size.

The powder XRD experiments were performed on a Bruker AXS D8 diffractometer employing Ni filtered Cu Kα radiation (40 kV, 40 mA) and a Lynxeye PSD detector. The X-ray powder diffractogram was recorded at 0.02 ° intervals in the range of 10 ° ≤ 2θ ≤ 130 °. The crystallite size was calculated by Rietveld analysis fitting technique (nm, LVol-IB method). ICDD (International Centre for Diffraction Data) PDF diffraction patterns were used to assign phase identification (PDF2-Diffraction Database File, 2003).

2.2.1.2. Inductively Coupled Plasma Emission Spectroscopy (ICP-ES)[3]

Inductively Coupled Plasma Emission Spectroscopy was used to measure element concentrations, as well as any Na residue possibly present from the preparation. In ICP-ES experiments the sample is sprayed into the inductively coupled plasma where it interacts with the charged ions that compose the plasma. The sample is then ionised into excited ions that radiate at specific wavelengths for each element involved, which allows their quantification.

The sample was prepared by dissolving 50 mg in a solution containing 6 ml H_2SO_4, 2 ml HNO_3, and 2 ml of HCl in a microwave digestion system (Anton Paar

[3] Analyses performed by Matt Gregory (gregom@matthey.com), Ian Briggs (briggi@matthey.com), and Paul Fisher (pafisher@matthey.com)

Multiwave 3000). The mixture was then heated at ~ 200 ºC in a sealed system. The ICP-ES analyses were performed in Argon plasma (temperature up to 10000 ºC), which was maintained by passing 1 kW of radiofrequency energy through a coil wrapped round a torch carrying argon gas.

2.2.2. BET-Specific Surface Area[4]

The specific surface area was calculated by the BET method, based on the physisorption of nitrogen at sub-ambient temperature (at 77 K, the boiling temperature of liquid nitrogen).

Stephen Brunauer, Paul Hugh Emmett, and Edward Teller (BET) developed this theory using Langmuir's theory as a base. Langmuir's theory is based on monolayer molecular adsorption, while the BET theory is based on a multilayer gas adsorption. For the BET theory the following hypothesis need to be assumed [12, 13]:

- The adsorbent surface is homogeneous.
- There are no lateral interactions between the adsorbant molecules.
- Gas molecules physically adsorb infinitely as layers on a solid.
- At equilibrium the rate of adsorption is equal to the rate of desorption.

The resulting equation from this theory can be found below (2-3) [12, 13]. This equation can be represented as a linear regression (y = c + mx) (Figure 2-4):

$$\frac{1}{V\left[\frac{P}{P_0}-1\right]} = \frac{1}{V_m C} + \frac{C-1}{V_m C}\left(\frac{P}{P_0}\right) \qquad (2\text{-}3)$$

$$y = c + m \cdot x$$

[4] For more details about BET see Appendix 1.

where
- V amount of gas adsorbed (volume units)
- V_m amount of gas adsorbed on the monolayer (volume units)
- P equilibrium pressure of adsorbate at the temperature of adsorption (pressure units)
- P_0 saturation pressure of adsorbate at the temperature of adsorption (pressure units)
- C BET constant

Using the slope (**m**) and y-interception (**c**) values it is possible to calculate the monolayer adsorbed gas quantity (V_m) and the BET constant (C). With this, is then possible to calculate the total surface area (S_{total}) and the specific surface area (SSA or S_{BET}) using the following equations (2-4 and 2-5):

$$S_{total} = \frac{V_m N_A s}{MV} \tag{2-4}$$

$$S_{BET} = \frac{S_{total}}{a} \tag{2-5}$$

where
- S_{total} total surface area (m^2)
- S_{BET} specific surface area ($m^2\ g^{-1}$)
- V_m amount of gas adsorbed on the monolayer (m^3)
- N_A Avogadro's number ($6.022\times10^{23}\ mol^{-1}$)
- s adsorption cross section of the adsorbing species (for $N_2 = 16.2\times10^{-20}\ m^2$ molecule)
- MV molar volume of adsorbate gas (for $N_2 = 22.4\times10^{-3}\ m^3\ mol^{-1}$)
- a mass of adsorbent (g)

The N_2 adsorption was performed at 77 K using an Autosorb-1 analyser from Quantachrome. Prior to the analysis the samples were outgassed at 350 °C to remove any moisture or unwanted adsorbed species that may have been present on the surface.

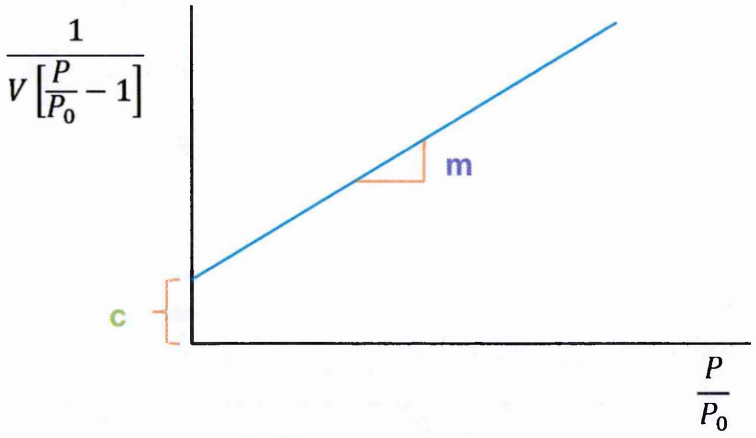

Figure 2-4: Example of BET plot.

2.2.3. Surface characterisation

Surface characterisation is performed in order to quantify the number of active sites, as well as to understand their nature and any possible interaction with the support, as this will affect their reactivity.

For the quantification of active sites CO chemisorption, EtOH-TPSR and ethane hydrogenolysis (these last two described in Chapter 3, as they involved development work as part of the research project) were performed. XPS was also performed to study the level of interaction of the noble metal with the ceria.

2.2.3.1. X-ray Photoelectron Spectroscopy (XPS)[5]

XPS was used to characterise the surface of the sample, as this technique provides information on the elemental composition, and on the oxidation state of the elements.

[5] Analysis performed by Dr Richard Smith (rsmith@matthey.com) and Dr Tugce Eralp (eralpt@matthey.com).

The theory of XPS is based on the photoelectric effect; when an atom absorbs energy ($h\upsilon$) from electromagnetic radiation from a light of sufficiently small wavelength and high frequency (in XPS this is X-rays) it emits electrons (Figure 2-5).

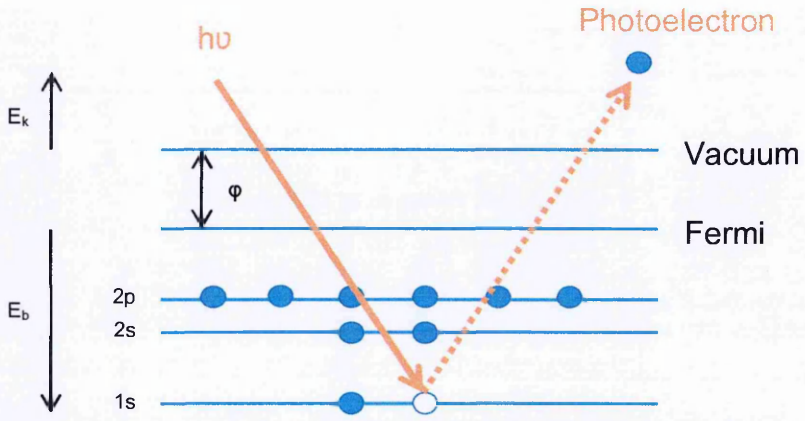

Figure 2-5: Schematic representation of the photoelectric effect.

The electrons emitted are known as photoelectrons, and their energy is calculated using equation 2-6 [10]. The depth of the XPS analysis varies between 1.5 and 6 nm, depending on the kinetic energy of these photoelectrons.

$$E_k = h\upsilon - E_b - \varphi \qquad (2\text{-}6)$$

Where
- E_k kinetic energy of the photoelectron (eV)
- h Planck's constant (4.136×10^{-15} eV s)
- υ frequency of the exciting radiation (Hz)
- E_b binding energy of the photoelectron with respect to the Fermi level of the sample (eV)
- φ work function[6] of the spectrometer (eV)

In addition, when the vacancy is filled with an electron from a higher orbital, there is a release of energy. This can be in the form of an emitted photon or this energy

[6] Work function is the minimum energy needed to remove an electron from a solid to a point immediately outside the solid surface (or energy needed to move an electron from the Fermi level into vacuum).

can be transferred to another electron which will be then ejected from the atom. This second electron is known as an Auger electron and carries the energy equal to the difference in the orbitals. Auger electrons are independent of the X-ray photon energy, but their peak positions depend on the X-ray source [10].

The measurements taken from XPS are the intensity of photoelectrons *N(E)* as a function of their kinetic energy (E_k). However, the spectrum is usually a plot of *N(E)* versus the binding energy (E_b), as the binding energy is element-specific. The peaks are labelled according to the quantum numbers of the level from which the electron originates. An electron with orbital momentum *l* (0 - *s*, 1 - *p*, 2 - *d*, 3 - *f*) and spin momentum *s* (+1/2 or -1/2) has a total momentum $j = l + s$ [10]. This is represented in Table 2-2:

The position of the binding energy peaks provides information about the oxidation state. In general, the binding energy increases with increasing oxidation state (due to a higher attractive force from the nucleus as a consequence of the valence electrons), and for a fixed oxidation state this increases with the electronegativity of the ligands. However, there are exceptions to this rule as in the case of alkali metals [10].

Table 2-2: Nomenclature used in XPS.

n	*l*	*j*	X-ray level	Electron level
1	0	1/2	K	1s
2	0	1/2	L1	2s
2	1	1/2	L2	$2p_{1/2}$
2	1	3/2	L3	$2p_{3/2}$
3	0	1/2	M1	3s
3	1	1/2	M2	$3p_{1/2}$
3	1	3/2	M3	$3p_{3/2}$
3	2	3/2	M4	$3d_{3/2}$
3	2	5/2	M5	$3d_{5/2}$
4	3	5/2	N6	$4f_{5/2}$
4	3	7/2	N7	$4f_{7/2}$

XPS analyses were performed in an ESCALAB 250. The samples were dusted onto carbon tape and thereby attached to a sample stub. The exciting radiation used in the studies was monochromatised aluminium Kα radiation in a 650 μm spot at 170 W power. Charge compensation was activated, provided by (i) the in-lens flood gun at a 2 eV setting and (ii) the 401 argon ion flood source at a "zero energy" setting. Energy scales were corrected to the carbon 1*s* binding energy (284.8 eV). Because of the overlapping signals of carbon 1*s* and cerium 4*s*, qualification and the quantification of the carbon signal was subject to error. The data was processed using the Thermo Avantage v5.52 software. The photoelectron peaks were analysed by the Gaussian/Lorentzian peak fitting, introducing parameter constrains to restrict the full width at half maximum (FWHM) and relative intensities of the peaks.

2.2.3.2. CO-chemisorption

CO pulse chemisorption is one of the most used techniques to measure metal dispersion[7] and metal surface area. A molecule or atom is said to be chemisorbed when the binding forces created between the adsorbed species and the surface species are as strong as those corresponding to covalent, ionic or polar bonds (ΔH_{ads} = 50-200 kJ mol^{-1}) [14, 15]. This occurs as a monolayer and it is assumed that it adsorbs non-reversibly. It is important not to confuse chemisorption with physisorption; for the latter, the species are bonded by Van der Waals forces, which are significantly weaker (ΔH_{ads} < 40 kJ mol^{-1}). The physisorption process can occur as multilayers and it is a reversible isothermic process [15]. CO chemisorption is selective to the metallic sites and does not adsorb on the support

[7] Metal dispersion = number of surface atoms/total number of atoms.

when this is a non-reducible oxide (i.e. silica or alumina), as CO adsorption energy is not high enough on these materials for it to chemisorb [16, 17].

To measure metal dispersion using this method, a probe molecule (e.g. CO) is added to a pre-reduced sample and the adsorption of this probe molecule is quantified. There are typically three different chemisorption conformations: linear, bridge, and twin type (see Figure 2-6) [18]. Linear adsorption occurs when one CO molecule adsorbs on one metal site (CO/M stoichiometry 1), bridge type when one CO molecule adsorbs on two metal sites (CO/M stoichiometry 0.5), and twin type when two CO molecules adsorb on one metal site (CO/M stoichiometry 2). The type of adsorption depends on the gas, the metal, and its surface. The CO adsorption stoichiometry is still not completely defined, but work reported in the literature have suggested an average CO/Pd stoichiometry[8] of 0.5 [19], CO/Pt of 0.5-1 [20], and CO/Rh of 2 [21].

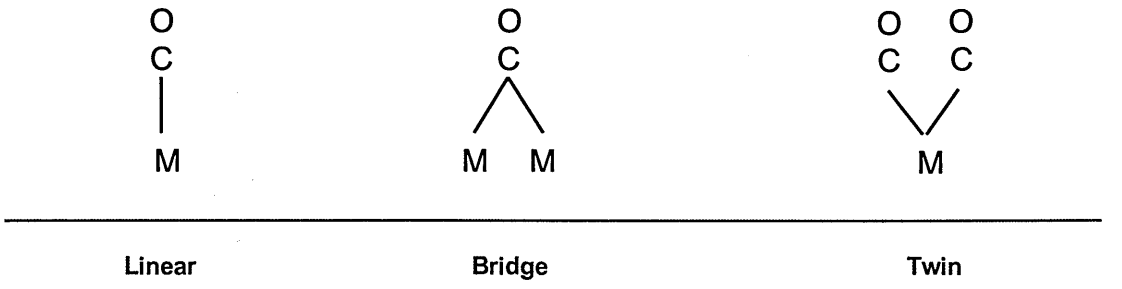

Figure 2-6: Typical chemisorption conformations.

When performing this measurement on a ceria-based material some CO adsorption can also occur at the interface of the metal-ceria, giving higher dispersion values [22]. In this work all the materials were ceria-based; for this reason this measurement has only been taken for comparative purposes.

[8] Stoichiometry calculated when the metals were supported on Al_2O_3.

The metal dispersion was measured using a Micromeritics Autochem II instrument. Approximately 0.3 g of powder sample was placed in a quartz reactor. The sample was then pre-treated at 300 °C for 30 min under a flow of hydrogen in order to clean the surface of any undesired adsorbed species (i.e. atmospheric H_2O or CO_2), and to reduce the surface metallic species. After the pre-treatment the sample was cooled to room temperature under a flow of He and then dosed with pulses of CO. The CO signal was monitored using a thermal conductivity detector (TCD). Initial CO pulses lead to small peaks as CO is chemisorbed on the metallic sites; the following peaks gradually increase with each dose until the pulse area becomes stable due to the saturation of all the available metallic sites. The peak area under the last peak corresponds to the total volume of the loop (V_{loop}), as no further gas is being adsorbed. With this and the integration of the peaks from the pulses (V_{pulse}) it will be then possible to calculate the total volume of gas adsorbed ($\sum V_{adsorbed\ in\ each\ pulse}$) (equation 2-7).

$$\sum V_{adsorbed\ in\ each\ pulse} = \sum (V_{loop} - V_{pulse}) \qquad (2\text{-}7)$$

The pulses are repeated until the volume of gas adsorbed is zero (saturation). The sum of the volume adsorbed from each of the pulses will correspond to the total amount of gas adsorbed. If the CO/M stoichiometry is known, then it is possible to calculate the number of surface metal atoms (2-8) [23].

$$N_{ads} = \frac{N_{CO\ ads}}{SF} \qquad (2\text{-}8)$$

where

N_{ads}	number of exposed metal atoms found by adsorption
$N_{CO\ ads}$	number of adsorbed CO atoms
SF	CO/M stoichiometry factor

The dispersion (δ) is calculated from (2-9):

$$\delta\,(\%) = MW \cdot \left(\frac{V_s \cdot SF}{Wt \cdot V_{mole}}\right) \cdot 100 \qquad (2\text{-}9)$$

Where
- δ percent dispersion
- MW molecular weight (g mole^{-1})
- V_s volume adsorbed at standard temperature and pressure (cm^3)
- SF CO/M stoichiometry factor
- Wt mass of sample (g)
- V_{mole} volume of a mole at standard temperature and pressure (22414 cm^3 mole^{-1})

To calculate the metal surface area (m^2 g^{-1} sample) equation 2-10 is used:

$$Metal\ surface\ area = \frac{N_{ads} \cdot A_{metal}}{Wt} \qquad (2\text{-}10)$$

where
- N_{ads} number of exposed metal atoms found by adsorption
- A_{metal} area of metal atom in sample (m^2)
- Wt mass of sample (g)

An average metal particle size can also be calculated using the equation below (2-11). For simplification it has been assumed that the metallic particles are spherical and that the adsorption stoichiometry obtained for all the metals is CO/M = 1 [24].

$$d = \frac{6M\rho_{surf}}{\rho_{metal} N_A \delta} \qquad (2\text{-}11)$$

Where
- d average metal particle size (nm)
- δ metal dispersion
- M atomic weight (g mol^{-1})
- ρ_{surf} metal surface site density (atoms nm^{-2})
- ρ_{metal} metal density (g nm^{-3})
- N_A Avogadro's number (6.022×10^{23} mol^{-1})

2.2.4. Redox characterisation

The redox properties of ceria are what make its use so important. Therefore the study of these is of great importance.

In order to study the reducibility of the catalyst, H_2-TPR and CO-TPR were performed. In addition, oxygen-storage capacity tests were undertaken to study the total capacity of the catalysts to uptake and release oxygen.

2.2.4.1. Temperature Programmed Reduction (H_2-TPR and CO-TPR)

TPR experiments were performed to study the reducibility of the samples. In temperature-programmed reaction methods a reductant is used to reduce oxide in the sample. This reduction reaction is monitored while the temperature is increased linearly over time.

H_2-TPR

The reduction of a metal oxide by H_2 is described below:

$$2CeO_2 + H_2 \rightarrow Ce_2O_3 + H_2O \qquad (2\text{-}12)$$

H_2-TPR analyses were carried out on an instrument equipped with a thermal conductivity detector (TCD). 30 ml min^{-1} of 10%H_2/N_2 were passed through 0.2 g of sample at ambient temperature until the baseline remained unchanged. The sample was then heated at a rate of 10 °C min^{-1} from ambient temperature to 900 °C.

CO-TPR

CO is a better probe molecule to study the surface reactions due to a lower spillover[9] effect than H_2 [25]. During this process CO is consumed to form CO_2 and H_2. H_2 is formed due to the water gas-shift reaction between CO and hydroxyls on

[9] Spillover occurs for example when H_2 dissociates on a catalytic active site (i.e. noble metal) and some of these dissociated H-atoms diffuse onto the support.

the support (reaction 2-13). CO_2 can also be formed from the water gas-shift reaction (reaction 2-14), from the reduction of reducible species (reactions 2-15, 2-16), or from the disproportionation[10] of CO (reaction 2-17).

$$CO_{(ads)} + 2OH^-_{(support)} \rightarrow CO_{2(g)} + H_{2(g)} + O_2^-{}_{(support)} \quad (2\text{-}13)$$

$$CO + H_2O \rightarrow CO_2 + H_2 \quad (2\text{-}14)$$

$$CO + 2CeO_2 \rightarrow CO_2 + Ce_2O_3 \quad (2\text{-}15)$$

$$CO + PdO \rightarrow CO_2 + Pd \quad (2\text{-}16)$$

$$2CO \rightarrow CO_2 + C \quad (2\text{-}17)$$

CO-TPR analyses were performed in a Micromeritics Autochem II. Approximately 0.2 g of powder sample was placed in a quartz reactor. In order to clean the surface of any undesired adsorbed species (i.e. atmospheric H_2O or CO_2) that could interact with the results of the reaction, the sample was first pre-treated under continuous flow of He ramping from room temperature to 500 °C at 10 °C min^{-1}. The sample was then cooled down under 5%O_2/He to 30 °C to ensure complete oxidation of the species. Following this, the sample was exposed to 10%CO/He; when a stable baseline was achieved, the sample was then heated at a rate of 10 °C min^{-1} from 30 °C to 800 °C. The reaction was monitored using a TCD and a mass spectrometer.

2.2.4.2. Oxygen Storage Capacity (OSC)

Oxygen Storage Capacity (OSC) is a key property of TWCs. Under fuel rich condition (excess of reductants) the stored oxygen can be used for oxidation of

[10] Disproportionation reaction occurs as a consequence of the reorganisation of the atoms of a molecule that leads to two different products, typically involving two redox processes (same molecule reducing and oxidising simultaneously). The re-organisation of atoms can occur upon heating or changing pressure.

CO and HC while under lean conditions (excess of oxidants) re-oxidation of the OSC component allows reduction of NO_x.

$$CO + 2CeO_2 \rightleftharpoons CO_2 + Ce_2O_3 \quad (2\text{-}18)$$

$$\tfrac{1}{2} O_2 + 2Ce_2O_3 \rightleftharpoons CeO_2 \quad (2\text{-}19)$$

$$NO + 2Ce_2O_3 \rightleftharpoons \tfrac{1}{2} N_2 + CeO_2 \quad (2\text{-}20)$$

$$CO + NO \rightleftharpoons CO_2 + \tfrac{1}{2} N_2 \quad (2\text{-}21)$$

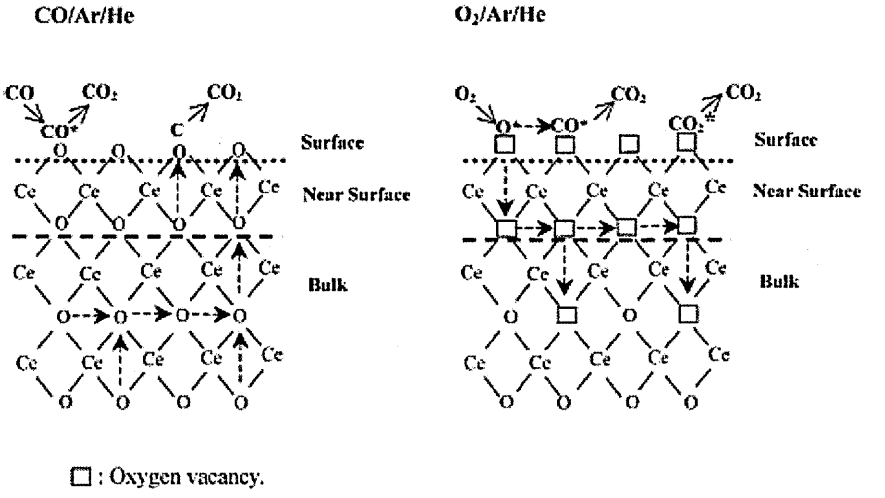

Figure 2-7: Oxygen migration process during rich treatment (CO/Ar/He), and reoxidation during lean treatment (O_2/Ar/He) after O_2 depletion (from [26]). The CO reacts with CeO_2 reducing it to Ce_2O_3 and using the oxygen to form CO_2; then, O_2 fills the vacancies created during the rich treatment by reoxidising the Ce_2O_3 again to CeO_2.

OSC is promoted by NM especially Pd and Rh. At low temperatures (100 – 300 °C) oxygen is typically removed from the surface but at higher temperatures (> 300 °C) oxygen migration through the bulk ceria-zirconia becomes important. Figure 2-7 shows a mechanism of this oxygen migration.

OSC is determined by exposing the sample to alternate lean and rich gas mixtures and measuring the time taken between the CO_2 formation and the time where the CO signal appears, following a switch from oxidising to reducing conditions.

A test was designed to study the total oxygen that the samples could store during oxidative conditions and release during reducing conditions. Approximately 0.1-0.2 g (accurately weighed, amount dependent on expected OSC of sample) of 250-355 µm pelletised sample was placed in the centre of a quartz tube, held in position with quartz wool. The tube was introduced into the micro reactor connected to a mass spectrometer. The sample was then programmed to be cycled between oxidising (10 ml min^{-1} of 5 $\%O_2$/He) and reducing conditions (10 ml min^{-1} of 10 %CO/He), using He as a carrier gas 90 ml min^{-1}. The cycling was performed at a rate of two redox cycles per 1000 seconds (shown in Figure 2-8) and the mass spectrometer data was collected over three completed cycles (25 minutes). The data from the final cycle was analysed (Excel spreadsheet) in order to determine the OSC.

The OSC was determined from the time between CO_2 and CO breakthroughs and expressed in µmol O g $sample^{-1}$.

$$A = \frac{Q_{CO}}{V_{RT}} \tag{2-22}$$

$$\mathrm{OSC} = \mathrm{A} \cdot \frac{\mathrm{t}}{\mathrm{Wt}} \tag{2-23}$$

where
- t time for the CO to breakthrough (s)
- Wt sample weight (g)
- A conversion factor (µmol O s^{-1})
- Q_{CO} CO flow (ml s^{-1})
- V_{RT} Molar volume of an ideal gas at RT ($24 \cdot 10^{+3}$ ml mol^{-1})

Variable temperature OSC measurements have been carried out on experimental samples within the range 200-500 °C.

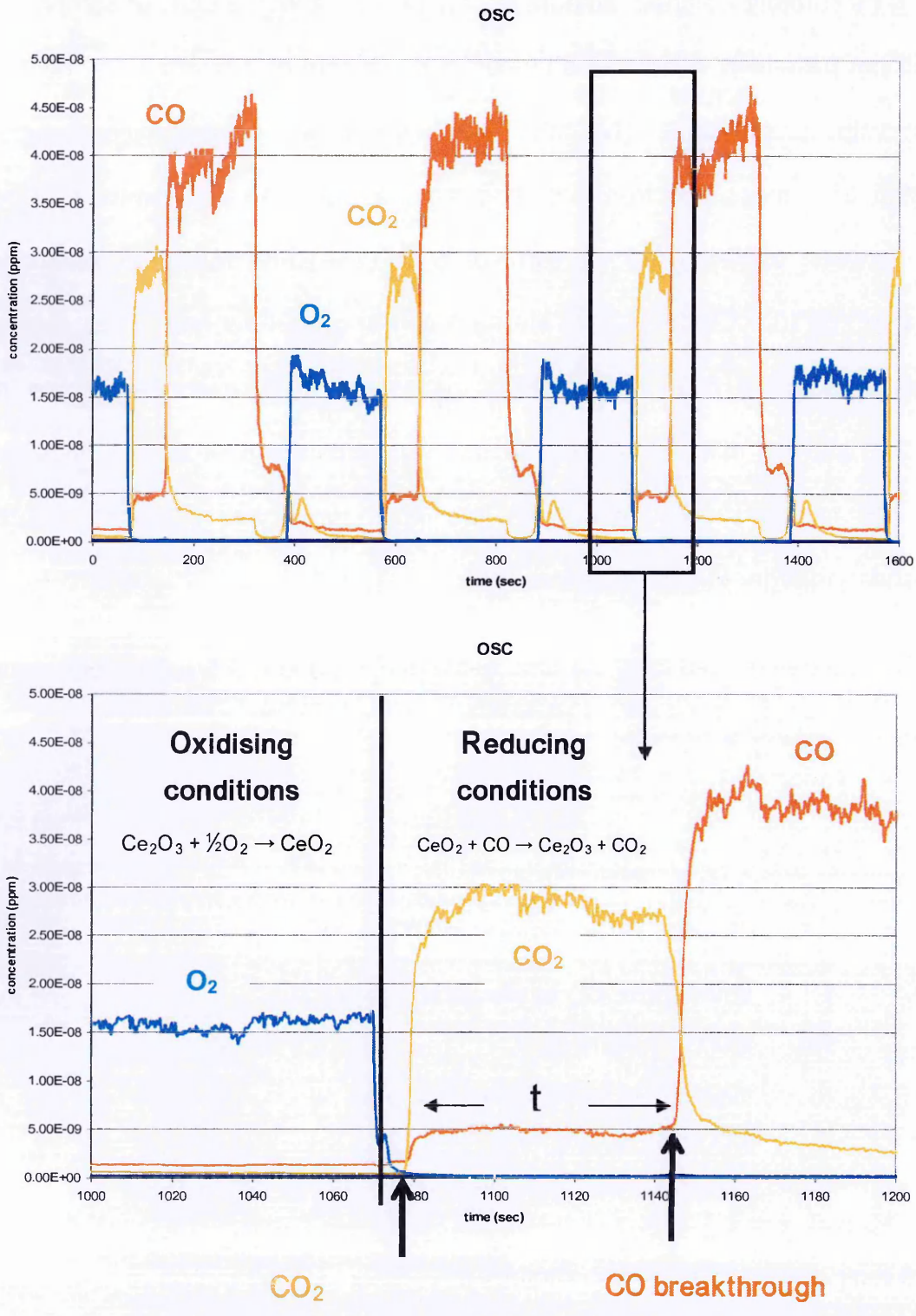

Figure 2-8: Signals from the mass-spectrometer corresponding to the concentration of CO, CO_2, O_2 and H_2O during the OSC test. The time between CO_2 and CO breakthroughs of the 3rd cycle is used for the calculation of the OSC.

2.2.5. Kinetic characterisation

TWC typically perform under rapidly fast oscillations between rich and lean conditions. Therefore, under rich conditions the catalyst is required to release oxygen, and under lean conditions to uptake oxygen. Thus, the oxygen capacity is of great importance, but as the oscillations occur very fast, high reaction rates are also required.

For this project, the CO oxidation reaction was studied using the steady-state isotopic transient kinetics analysis (SSITKA) described below.

2.2.5.1. Steady-State Isotopic Transient Kinetics Analysis (SSITKA)

SSITKA was used to study the kinetics of the CO oxidation reaction (CO-SSITKA) over the different catalysts. This technique enables the simultaneous quantification of the number of active catalytic sites on the catalyst and the activity of these catalytic sites under *in-situ* conditions.

This method is based on the monitoring of the reactant species in the reactor feed during a switch in which one of the reactants is switched to its isotopic labelled equivalent (i.e. ^{12}CO is switched to ^{13}CO). To maintain isothermal and isobaric reaction conditions, all the gas concentrations and flows need to remain undisturbed during the step change. As the gas reactants will be the same, the intermediates formed will not change, and this allows the steady-state kinetic behaviour of the surface of the catalyst to be studied [27]. See Figure 2-9 for a graphical representation of this process:

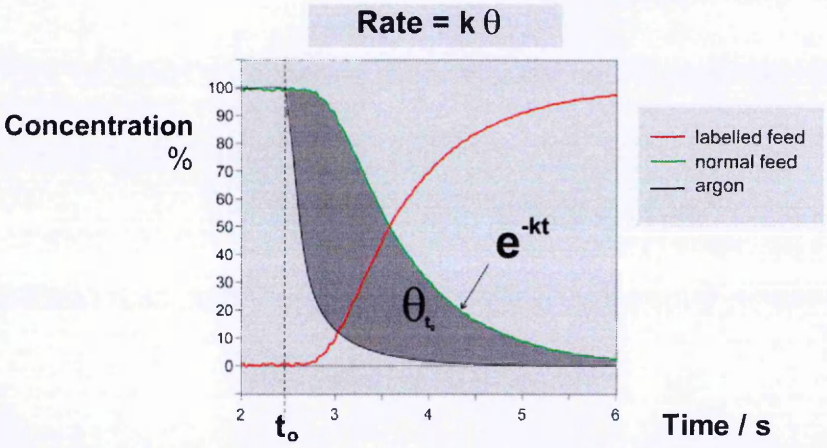

Figure 2-9: Graphical example of the profiles obtained during SSITKA experiments.

Consider CO oxidation where CO is reversibly adsorbed on the catalyst and no re-adsorption of CO_2 occurs:

$$CO_{(g)} \rightleftharpoons CO_{(ads)} \quad (2\text{-}24)$$

$$O_{2(g)} \rightarrow 2O_{(ads)} \quad (2\text{-}25)$$

$$CO_{(ads)} + O_{(ads)} \longrightarrow CO_{2(ads)} \quad (2\text{-}26)$$

$$CO_{2(ads)} \rightarrow CO_{2(g)} \quad (2\text{-}27)$$

To monitor the kinetics of this reaction the gas feed will contain ^{12}CO, O_2, an Ar tracer, and He carrier gas. The reactant concentrations and temperature are set to generate $^{12}CO_2$ at a known rate. After a certain period ^{12}CO will be switched for ^{13}CO. This switch will lead to a decay in the concentration of ^{12}CO and an increase in the concentration of ^{13}CO, with similar changes also observed for $^{12}CO_2$ and $^{13}CO_2$.

During this switch, the decay of the ^{12}CO concentration will give information about the rate of CO desorption, and the decay of the $^{12}CO_2$ concentration about the rate of reaction. Similarly, the area under the CO_2 curve (less the area under the Ar curve) gives the number of intermediates on the catalyst surface going to products

(in the absence of readsorption of CO_2), while the area under the CO curve (less the area under the Ar curve) gives the number of CO molecules adsorbed on the surface (which may or may not be on active sites capable of turning them into product).

The reaction rate (r) gives information on how fast the sample can perform the reaction under the specific conditions (reactants concentration, temperature...); the turnover frequency (TOF) gives information about the generation rate of product (CO_2 in this case) per catalyst-surface site. Ideally, these measurements should be run at a temperature where the CO conversion is less than 10% to ensure that the reaction is kinetically and not diffusion controlled.

Reaction order and rate constant (k)

For the calculation of the reaction order experimentally, CO-SSITKA experiments were run at constant temperature using different [CO]:[O_2] ratios. To calculate the reaction order with respect to [CO], the [O_2] was left constant and the [CO] was varied; the opposite was done to calculate the reaction order with respect to the [O_2].

Assuming A + B → C, the equation to calculate the reaction rate can be written as (2-28):

$$r = k[\mathrm{A}]^a[\mathrm{B}]^b \qquad (2\text{-}28)$$

where

r	reaction rate (mols s^{-1})
k	the rate constant (units depending on reaction order)
[A] and [B]	concentration of the reactants (M)
a and b	the respective reaction orders

As the reaction rate is proportional to $[A]^a[B]^b$, if one of the concentrations is kept constant (i.e. [B]) then r is proportional to $[A]^a$ and therefore $\ln(r)$ will be proportional to $a\ln([A])$. A straight line (y = c + mx) is obtained when representing $\ln(r)$ against $\ln([A])$, the slope of which will correspond to the reaction order ($a = \ln(r)/\ln([A])$) (equation 2-29). Once all the reaction orders have been determined, it is then possible to calculate k, the units of which will depend on the order of reaction.

$$\ln(r) = \ln(k) + b \cdot \ln([B]) + a \cdot \ln([A]) \qquad (2\text{-}29)$$

$$y = c + m \cdot x$$

Activation Energy (E_a)

The activation energy is calculated by the Arrhenius equation (2-30):

$$k = Ae^{\frac{-E_a}{RT}} \qquad (2\text{-}30)$$

where
- k rate constant (units depend on order of reaction)
- A pre-exponential factor (same units as the rate constant)
- E_a activation Energy (J mol^{-1})
- R universal gas constant (8.314 J mol^{-1} K^{-1})
- T temperature (K)

Similarly, to calculate E_a experimentally, it is necessary to plot a graphical representation of this equation in the naperian logarithmic form to obtain a straight line (y = c + mx) (equation 2-30):

$$\ln(k) = \ln(A) - \frac{Ea}{R} \cdot \frac{1}{T} \qquad (2\text{-}31)$$

$$y = c + m \cdot x$$

In this case, the slope (m) of the line corresponds to ($-E_a/R$). As R is a constant, the value of E_a can then be calculated.

2.3. Activity testing

The activity of these catalysts was measured under two different conditions: cold-start, and perturbed conditions. Cold-start conditions represent those seen by the catalyst during an engine start up, whilst the perturbed conditions represent those to which the catalyst is exposed during driving conditions.

2.3.1. Cold-start light-off performance

The test used was designed based on the first few seconds of the start of a gasoline engine. During this time, the catalyst is exposed to low temperatures, as it has to warm up from ambient temperature to 400 – 500 ºC. During this period of time, higher levels of pollutants are emitted due to the poor conversion that TWC show in this range of temperature.

The gas mix used in this test is shown below and is based on the conditions used at the 30 seconds point of an engine test performed at Johnson Matthey (Table 2-3). In those 30 seconds, the catalyst is heated from 0 to 350 ºC.

Table 2-3: gas composition during cold-start conditions.

Gas	Concentration
N_2	carrier
C_3H_8	833 ppm
C_3H_6	1666 ppm
CO	1 %
CO_2	14 %
NO	300 ppm
O_2	0.95 %
H_2O	5 %
H_2	0.33 %

The sample taken was 0.4 g (0.2 g sample + 0.2 g cordierite[11]) and the gas flow rate 2 L min^{-1}. The catalyst was heated using a ramp rate of 10 °C min^{-1} from 100 to 400 °C. The composition of the gas mixture was monitored using FTIR (MKS2030). Two ramps using identical conditions were tested to follow any type of activation. The results are typically represented as conversion of CO, hydrocarbons (C_3H_8 + C_3H_6), and NO_x (NO + NO_2) against temperature.

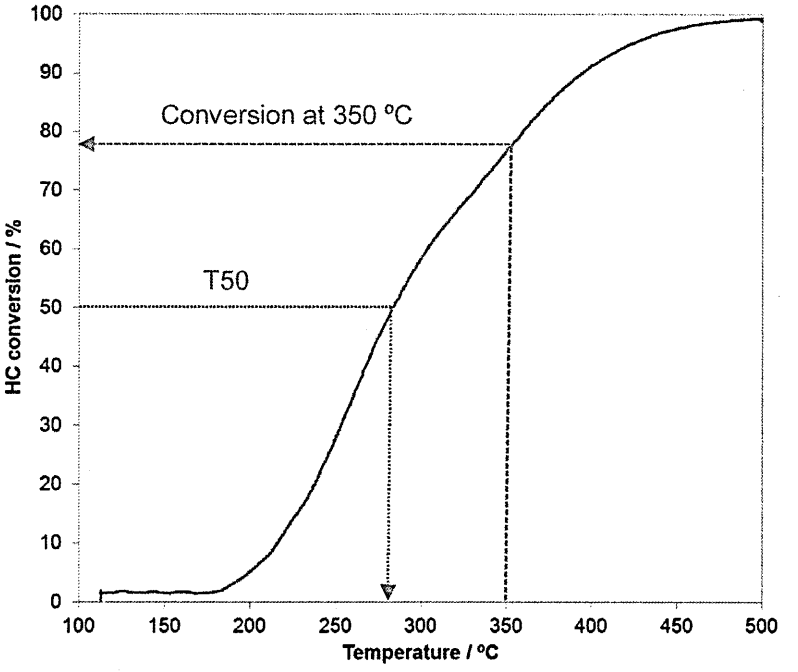

Figure 2-10: Example of the profile obtained for hydrocarbon (HC) conversion against temperature, during a light-off test. Typically, the data is represented as T50 values (temperature for 50 % conversion) or conversion at 350 °C.

2.3.2. Perturbed activity test

This test is designed to mimic the real conditions to which the catalyst is exposed during driving cycles. Under realistic conditions lambda[12] is not always constant, and usually fluctuates around the stoichiometric point (λ = 1). It is at this point that the OSC of the catalyst is used, helping to minimise the fluctuations around λ = 1 and to increase the conversion of the pollutants.

[11] Low-thermal-expansion ceramic material that is used as washcoat support. This material has a composition of $(Mg,Fe)_2Al_3(Si_5AlO_{18})$.

[12] The A/F ratio can be also expressed as lambda (λ), which is the ratio between the actual A/F ratio and the stoichiometric A/F ratio. Therefore, at stoichiometric conditions λ = 1.

The test was performed switching between rich (excess of reductant) and lean (excess of oxidant) lambdas during a temperature ramp. Two different light-off conditions were used at a) rich average lambda λ_{rich} = 0.99 ± 0.05, and b) lean average lambda λ_{lean} = 1.01 ± 0.05, at a frequency of 3 seconds between gas perturbations (3 s rich – 3 s lean):

The gas composition at each λ value is given in Table 2-4:

Table 2-4: Gas composition used in the perturbed activity test. During the temperature ramp the gas mixture is switching between lean and rich conditions.

Gas	Lean	Rich
N_2	balance	balance
C_3H_8	333 ppm	333 ppm
C_3H_6	666 ppm	666 ppm
CO	0.73 %	2.2 %
CO_2	14 %	14 %
NO	2200 ppm	2200 ppm
O_2	a) 0.65 % b)1.04 %	a) 1.56 % b) 1.92 %
H_2O	5 %	5 %
H_2	0.24 %	0.73 %

The sample size taken was 0.4 g (0.2 g sample + 0.2 g cordierite) and the gas flow rate 5 L min^{-1}. The catalyst was heated using a ramp rate of 10 °C min^{-1} from 110 to 500 ºC. The composition of the gas mixture was monitored using FTIR. The results were represented as conversion of CO, THC (C_3H_8 + C_3H_6), and NO_x (NO + NO_2) against temperature.

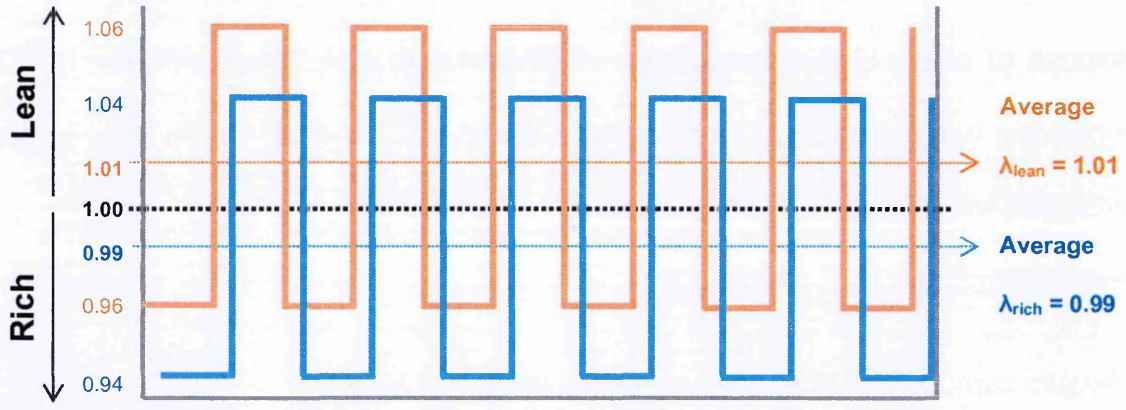

Figure 2-11: Schematic representation of the lambda variations during a perturbed light-off. For the first light-off at average rich lambda 0.99 (blue) the switches occur between 0.94 and 1.04 lambdas; for the second light-off at average lean lambda 1.01 (orange) the switches occur between lambdas 0.96 and 1.06. Each switch happens every 3 seconds while the catalyst is ramp from 110 °C to 500 °C at 10 °C min^{-1}.

References Chapter 2

[1] A. Satsuma, R. Sato, K. Osaki and K. Shimizu, Catalysis Today, 185 (2012) 61-65.

[2] B. Zhao, Q. Wang, G. Li and R. Zhou, Journal of Alloys and Compounds, 508 (2010) 500-506.

[3] M. Ozawa, Journal of Alloys and Compounds, 275-277 (1998) 886-890.

[4] Z. L. Wang, Y. Liu and Z. Zhang, *Handbook of Nanophase and Nanostructured Materials: Synthesis*, Kluwer Academic/Plenum Publishers, 2002.

[5] J. Kašpar, P. Fornasiero and N. Hickey, Catalysis Today, 77 (2003) 419-449.

[6] G. A. Carter, R. D. Hart, M. R. Rowles, C. E. Buckley and M. I. Ogden, Powder Technology, 191 (2009) 218-226.

[7] G. Wilde, *Nanostructured materials*, Elsevier, 2009.

[8] D. A. Martin, *Trends in Nanotubes Research*, Nova Publishers, 2006.

[9] *Basic crystal concepts*, 2005, http://home.iitk.ac.in/~sangals/crystosim/crystaltut.html [07/01/2013].

[10] J. W. Niemantsverdriet, *Spectroscopy in Catalysis*, WILEY-VCH, 2007.

[11] H. Rietveld, Acta Crystallographica, 22 (1967) 151-152.

[12] S. Lowel, J. E. Shields, M. A. Thomas and M. Thommes, *Characterisation of porous solids and powders: surface area, pore size and density*, Kluwer Academic Publisher, The Netherlands, 2004.

[13] S. Brunauer, P. H. Emmett and E. Teller, Journal of the American Chemical Society, 60 (1938) 309-319.

[14] J. B. Hudson, *Surface Science: An Introduction*, John Wiley & Sons, USA, 1998.

[15] Q. Corporation, *Chemisorption*, Quantachrome Corporation, 2004.

[16] R. M. Lambert and G. Pacchioni, *Chemisorption and Reactivity on Supported Clusters and Thin Films: Towards an Understanding of Microscopic Processes in Catalysis*, Kluwer Academic Publishers, 1997.

[17] O. Maresca, A. Ionescu, A. Allouche, J. P. Aycard, M. Rajzmann and F. Hutschka, Journal of Molecular Structure, 620 (2003) 119-128.

[18] K. Nakai and K. Nakamura, *Pulse Chemisorption Method: Metal Dispersion Measurement*, 2003, http://www.tdno.ru/files/file/CAT-APP-002%28E%29.pdf [13-12-2013].

[19] P. Canton, G. Fagherazzi, M. Battagliarin, F. Menegazzo, F. Pinna and N. Pernicone, Langmuir, 18 (2002) 6530-6535.

[20] J. Freel, Journal of Catalysis, 25 (1972) 149-160.

[21] H. F. J. V. t. Blik, J. B. A. D. V. Zon, D. C. Koningsberger and R. Prins, Journal of Molecular Catalysis, 25 (1984) 379-396.

[22] M. Cargnello, V. V. T. Doan-Nguyen, T. R. Gordon, R. E. Diaz, E. A. Stach, R. J. Gorte, P. Fornasiero and C. B. Murray, Science, 341 (2013) 771-773.

[23] T. E. Whyte, Catalysis Reviews, 8 (1974) 117-134.

[24] P. Chen, L. M. Chew, A. Kostka, M. Muhler and W. Xia, Catalysis Science & Technology, 3 (2013) 1964-1971.

[25] M. Kurnatowska, L. Kepinski and W. Mista, Applied Catalysis B: Environmental, 117–118 (2012) 135-147.

[26] M. Zhao, M. Shen and J. Wang, Journal of Catalysis, 248 (2007) 258-267.

[27] S. L. Shannon and J. G. Goodwin, Chemical Reviews, 95 (1995) 677-695.

3. Probe reactions for the surface characterisation of Pd, Pt and Rh

Contents

3. Probe reactions for the surface characterisation of Pd, Pt and Rh

The basic composition of the TWC catalyst has evolved over the last 25 years. The improvements achieved have allowed researchers to lower the loading of the precious metals significantly while improving the thermal stability of the catalyst. Whilst this is cost beneficial, the low loadings used can make them undetectable for many of the common analytical techniques in use, such as XPS or XRD.

In addition, TWC are composed of multiple metals, and the selective characterisation of each of these metals also adds an extra complication. For example, CO chemisorption can be used for samples with very low noble metal loadings, but it cannot differentiate between them. Moreover, this technique is unsuitable to measure metal surface areas and metal dispersions of ceria containing catalysts (such as TWC), as CO also adsorbs at the interface between the metal and the ceria [1, 2]. Ceria is also a problem when using TEM; due to similar atomic masses of Ce and some of the noble metals (i.e. Pd and Rh) there is not enough contrast to detect the noble metal particles [3].

Figure 3-1 summarises the issues found for the characterisation of low Pd loadings on ceria-based supports when using some of the common characterisation techniques.

As a consequence probe reactions are starting to be more commonly used for the characterisation of surface active sites. For example, ethane hydrogenolysis has been used to study Rh surface area [4, 5], methanol oxidation has been used to study structural and chemical properties of mixed oxides [6], and chloromethane has been used for zeolites to study their Brönsted acidity [7].

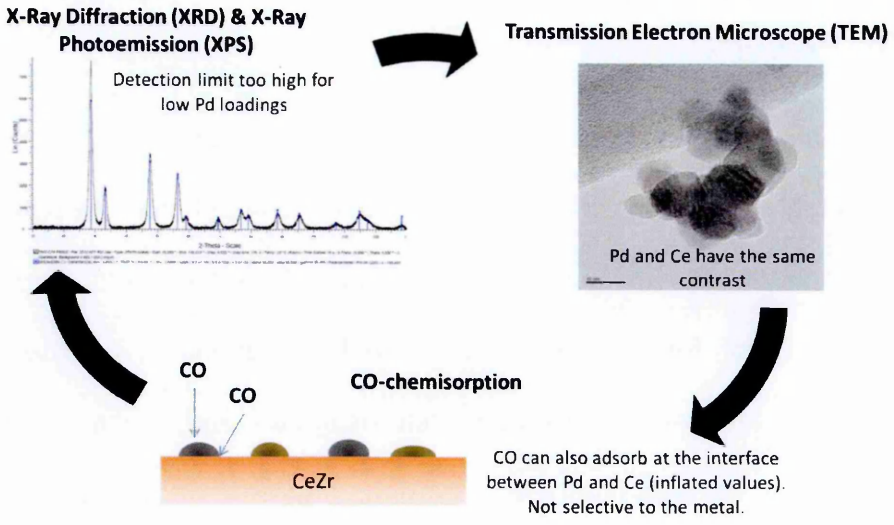

Figure 3-1: Examples of issues found during the characterisation of low Pd loadings supported on ceria-based materials when using common characterisation techniques, such as XRD, TEM or CO chemisorption.

As an example, TEM is one of the most common techniques to obtain particle sizes. However, TEM cannot be used to obtain an average Pd particle size for Pd supported on Ce-based materials, as the contrast obtained between Pd and Ce in TEM images is highly similar and the metal particles cannot be detected (Figure 3-2 – A). In contrast, Pd supported on Al_2O_3 can be easily detected in TEM images (Figure 3-2 – B).

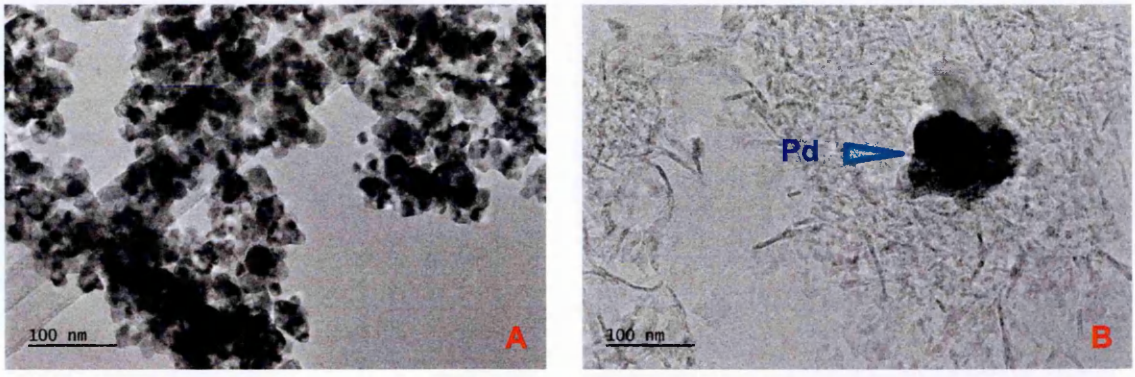

Figure 3-2: TEM images of 2Pd/CeZr (A) and 2Pd/Al_2O_3 (B) samples, calcined at 950 °C for 4 h.

3.1. Ethanol Temperature Programmed Surface Reaction (EtOH-TPSR) for Pd surface characterisation

In this project an ethanol temperature programmed surface reaction (EtOH-TPSR) has been evaluated as a possible tool to selectively characterise the palladium in the prepared catalysts. EtOH is commonly used in steam reforming for the production of H_2 for fuel cell applications [8-12]. Depending on the reaction conditions and metals used, EtOH steam reforming can lead to a wide number of by-products, such as acetaldehyde, methane, ethylene or CO among others [13-15]. In the literature it is reported that the formation of these by-products is strongly related to the nature of the metal and the support [16, 17]. For example, for a series of ceria-supported catalysts, Mattos *et al.* found that at 300 °C a Pd/CeO_2 catalyst had greater selectivity to form CH_4 in comparison to a Pt/CeO_2 and a Co/CeO_2 catalyst, which both mostly formed acetaldehyde [14]. Similarly Silva *et al.* studied the product selectivity of a Rh/CeO_2 catalyst at 500 °C, showing in this case that there was no significant CH_4 formation [18].

Based on these studies, the aim of this work was to perform EtOH-TPSR to monitor the product selectivity of EtOH on Pd/CeZr, Rh/CeZr and Pd-Rh/CeZr catalysts, to develop a new characterisation tool for the selective surface quantification of Pd.

3.1.1. Experimental

3.1.1.1. Catalysis preparation for the development of this technique

Two different sets of catalysts were prepared:

a) The first set was based on Pd/CeZr and Pd-Rh/CeZr catalysts for the development of the EtOH-TPSR technique.

b) The second set was based on Pd/Al_2O_3 catalysts used to build a calibration curve that correlates the EtOH-TPSR results with Pd surface area. Al_2O_3-based catalysts were needed in order to quantify Pd surface area using CO chemisorption without any risk of having extra CO chemisorbed at the interface between the metal and the support, as this does not occur in alumina-supported catalysts (contrary to ceria-supported) [1].

For the first set of catalysts the support used was a stabilised Zr-rich CeZr mixed oxide supplied by Rhodia, and for the second set γ-Al_2O_3 supplied by Sasol. $Pd(NO_3)_2$ (assay 14.95%) and $Rh(NO_3)_3$ (assay 12.85%) solutions, supplied by Johnson Matthey, were used for Pd and Rh impregnations.

a) Catalysts for the EtOH-TPSR development

A series of xPd/CeZr and xPd-0.2wt%Rh/CeZr catalysts with several Pd loadings (x = 0, 0.2, 0.5, 0.75, 1 wt%) were prepared to evaluate if Pd-surface area could be directly correlated with the amount of CH_4 being formed during the EtOH-TPSR method. These catalysts were prepared by wet impregnation using aqueous solutions of $Pd(NO_3)_2$ and $Rh(NO_3)_3$ on a CeZr support. For the bimetallic preparations, Rh was impregnated first and Pd second with a drying step in between additions. The catalysts were then dried in air at 105 ºC and calcined at 500 ºC for 2h. Following this, the catalysts were submitted to a high temperature ageing at 1100 ºC in air for 24 hours.

b) Catalysts for the calibration curve

In order to build a calibration curve to correlate the Pd-surface area with the CH_4 formed during the EtOH-TPSR, it was necessary to prepare a series of Pd-Al_2O_3 catalysts. For this work, xPd/Al_2O_3 catalysts with different Pd loadings (x = 0.5, 0.8, 0.9, 1, 2 wt%) were prepared by the wet impregnation technique described above. After calcination at 500 ºC, half of the catalysts was submitted to an

additional calcination at higher temperature (900 °C/40 h) with the aim of obtaining further Pd-surface areas.

3.1.1.2. Ethanol temperature programmed surface reaction (EtOH-TPSR)

To perform this test the sample was first pre-treated under oxygen at 300 °C for 30 min using 1.2% O_2 in N_2 (total gas flow rate of 2 L min^{-1}) in order to clean the surface of adsorbed atmospheric H_2O and carbonates, as well as to assure the complete oxidation of the metal. The sample was then cooled to 70 °C under the same oxidative gas mixture. After the pre-treatment the sample was exposed to a constant flow of 2 L min^{-1} containing 700 ppm of EtOH in N_2, followed by a temperature ramp to 450 °C at 10 °C min^{-1}. The reaction was monitored using FTIR spectroscopy. All products were quantified by integrating the area under the curve only up to 300 °C to avoid any interference from any possible thermal decomposition of the hydrocarbons at temperatures above 300 °C. The sample size used was 0.4 g (0.2 g sample + 0.2 g cordierite) of powder sample.

3.1.2. Results

3.1.2.1. Initial screening

The EtOH-TPSR experiment was initially performed on samples 1Pd/CeZr, 0.2Rh/CeZr[1] and on the CeZr support by itself, all aged at 1100 °C for 24 h. The main products obtained in the range of 70 °C to 450 °C were CH_4 and CH_3CHO for Pd samples. For the Rh-only and CeZr samples only CH_3CHO was formed over the temperature range studied here (Figure 3-3).

[1] 1 wt% Pd and 0.2 wt% Rh are close loadings and Pd:Rh ratios to those used in TWC.

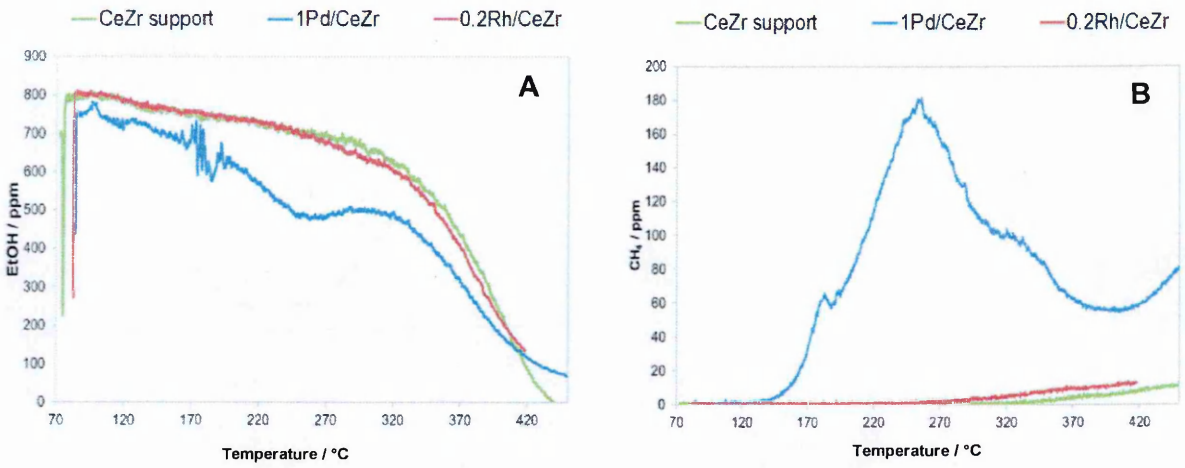

Figure 3-3: EtOH trends (A) and CH_4 formed (B) during EtOH-TPSR for 1Pd/CeZr, 0.2Rh/CeZr, and CeZr aged at 1100 °C for 24 h (F1100/24h). The sample size taken was 0.4 g (0.2 g sample + 0.2 g cordierite) and was previously pre-treated under 1.2% O_2 in N_2 at 300 °C for 30 min; for the EtOH-TPSR test the gas flow rate used was 2 L min^{-1} containing 700 ppm of EtOH in N_2. The catalyst was heated using a ramp rate of 10 °C min^{-1} from 70 to 450 °C while recording the trends using an FTIR spectrometer.

Based on the mechanistic studies in the literature the adsorption of EtOH on Pd/CeO_2 samples produces ethoxy species, which are dehydrogenated, producing acetaldehyde [14, 19]. Acetaldehyde is further dehydrogenated over the Pd producing acetyl species which can then decompose forming CH_4, H_2 and CO. The acetyl species can also be oxidised with the oxygen from the ceria support to form acetates, which can then decompose to CH_4 and CO and/or oxidise to CO_2 via carbonate species [14, 18]. In the case of Rh/CeO_2 catalysts the initial ethoxy species are dehydrogenated to adsorbed acetaldehydes, which will further be desorbed from the surface of the catalyst as they do not continue reacting over Rh [16-18].

A range of xPd-0.2Rh/CeZr catalysts were also tested. For 1Pd-0.2Rh/CeZr CH_4 was also obtained; the CH_4 peak overlapped that obtained from the 1Pd/CeZr sample (Figure 3-4). Similar experiments were performed with different Pd loadings leading to similar results.

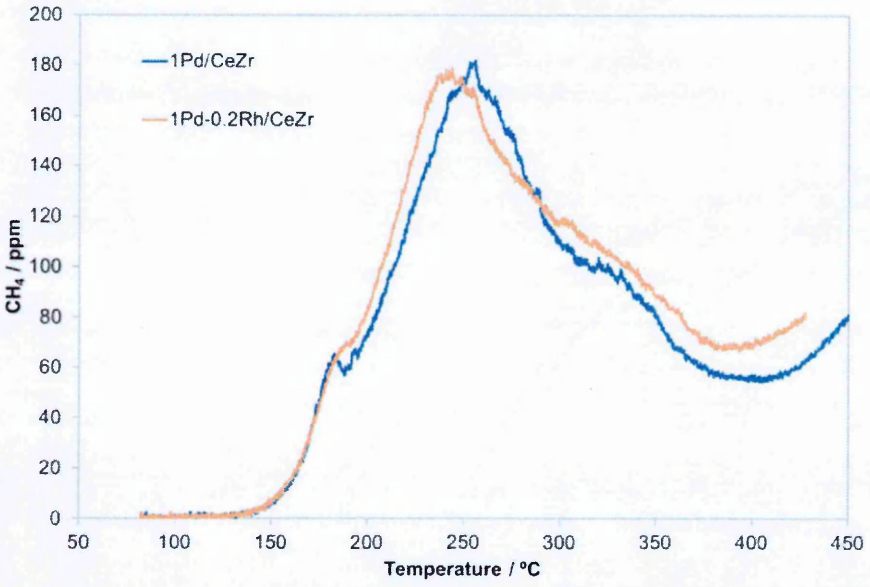

Figure 3-4: CH_4 formed during EtOH-TPSR on 1 wt% Pd/CeZr samples with and without 0.2 wt% Rh. Both catalysts were aged at 1100 °C for 24 h (F1100/24h). The sample size taken was 0.4 g (0.2 g sample + 0.2 g cordierite) and was previously pre-treated under 1.2% O_2 in N_2 at 300 °C for 30 min; for the EtOH-TPSR test the gas flow rate used was 2 L min^{-1} containing 700 ppm of EtOH in N_2. The catalyst was heated using a ramp rate of 10 °C min^{-1} from 70 to 450 °C.

Therefore the presence of Rh does not appear to significantly affect the CH_4 formation by changing the amount formed or by shifting the formation peak to different temperature (~20 °C), indicating that CH_4 formation is only selective to surface Pd.

3.1.2.2. Impact of Pd oxidation state

It was mentioned that prior to the EtOH-TPSR a pre-oxidation was performed on the sample at 300 ºC using O_2 in N_2, with the aim of cleaning the catalyst surface and oxidising the metal. Therefore, all the Pd should exist as PdO.

In order to study if metallic Pd was also active for the formation of CH_4, a pre-reduction was used instead to clean the surface of $1Pd/Al_2O_3$[2] [20]. The reduction was also performed at 300 ºC for 30 min using 1% H_2 in N_2 to ensure

[2] An alumina-based catalyst was used to avoid ceria-decoration on the metal if a Pd/CeO_2 catalyst was used, due to the reductive pre-treatment.

complete reduction of the palladium species [21]. In Figure 3-5 it is possible to see that after this pre-reduction no CH_4 was formed, suggesting that only PdO is active for this reaction.

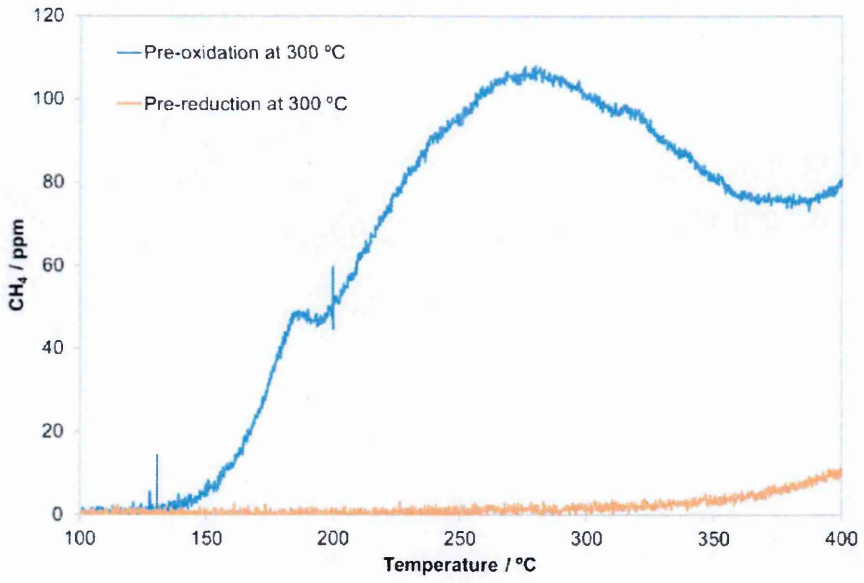

Figure 3-5: CH_4 formed during EtOH-TPRS for $1Pd/Al_2O_3$ F1100/24h, after the sample was exposed to a pre-oxidation (1.2% O_2) or a pre-reduction (1% H_2). The shoulder obtained in the CH_4 formation profile (~190 °C) after the pre-oxidation could indicate the existence of multiple Pd species. The sample size taken was 0.4 g (0.2 g sample + 0.2 g cordierite); for the EtOH-TPSR test the gas flow rate used was 2 L min^{-1} containing 700 ppm of EtOH in N_2. The catalyst was heated using a ramp rate of 10 °C min^{-1} from 70 to 450 °C.

3.1.2.3. Effect of Pd loading

The CH_4 formation was seen to increase with increasing Pd loading. Samples with loadings from 0 to 1 wt% Pd were tested. The maximum concentration of CH_4 obtained divided by the grams of sample and ppm of EtOH in the flow (max ppm CH_4 g $sample^{-1}$ ppm $EtOH^{-1}$) was then represented against Pd loading to monitor any possible trend between Pd total loading and the CH_4 formed (Figure 3-6). The amount of CH_4 formed with Pd weight % is not linear. This is likely to be related to a change in particle size. At low Pd loadings Pd particle size is expected to be smaller than at high Pd loadings, as at higher Pd loadings the particles will tend to agglomerate more (less Pd exposed on the surface). Unfortunately, Pd particle

size cannot be measured using any of the common techniques due to the low Pd loadings used (as the levels are below their detection limit) or due to errors that can be caused by the interaction with CeO_2 (such as peaks overlapping, or chemical adsorption at the Pd-Ce interface).

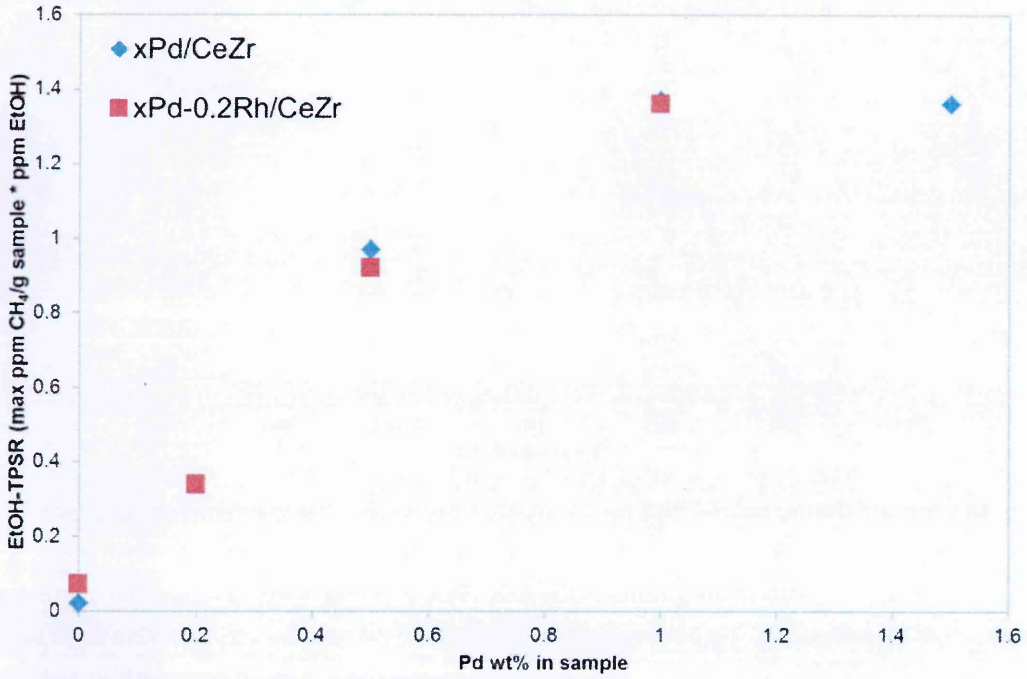

Figure 3-6: CH_4 formed during EtOH-TPSR as a function of Pd weight %. Comparison between Pd-CeZr samples with and without Rh. All catalysts were aged at 1100 °C for 24 h.

3.1.2.4. Calibration curve

In order to create a calibration curve that could allow us to quantify Pd surface area, samples with different Pd loadings supported on Al_2O_3 were evaluated both by CO-chemisorption[3] and by the EtOH-TPSR method. The samples were tested after calcination at 500 °C for 2 h (fresh) and after calcination at 900 °C for 40 h (aged). By doing this, the sensitivity of this technique to the particle size (and therefore the Pd-surface content) could be also demonstrated. The Pd surface content calculated by CO-chemisorption can be found in Table 3-1:

[3] Pd/Al_2O_3 samples can be evaluated by CO-chemisorption to quantify Pd-surface area, as there is no CO-adsorption at the interface of the metal and the support.

Table 3-1: Pd surface area and dispersion of xPd/Al_2O_3 samples calcined at 500 °C for 2 h (F500/2h) and at 900 °C for 40 h (F900/40h) calculated by CO-chemisorption.

	Pd surface area calculated by CO-chemisorption / m^2 g sample^{-1}		Pd dispersion calculated by CO chemisorption / %	
Sample	**F500 °C/2 h**	**F900 °C/40 h**	**F500 °C/2 h**	**F900 °C/40 h**
$0.5Pd/Al_2O_3$	0.48	0.34	21	15
$0.8Pd/Al_2O_3$	0.92	0.46	27	13
$0.9Pd/Al_2O_3$	0.98	0.48	23	11
$1Pd/Al_2O_3$	1.13	0.49	25	10

The maximum ppm of CH_4 formed (up to 300 °C) during the EtOH-TPSR divided by the grams of sample and ppm of EtOH in the flow (max ppm CH_4 g sample^{-1} ppm $EtOH^{-1}$) was then represented against Pd surface area obtained from the CO-chemisorption analyses (Figure 3-7). In this way it was then possible to obtain a straight line to correlate CH_4 formed with an actual quantification of Pd surface exposed, which can be used as a calibration curve when testing any other Pd-sample.

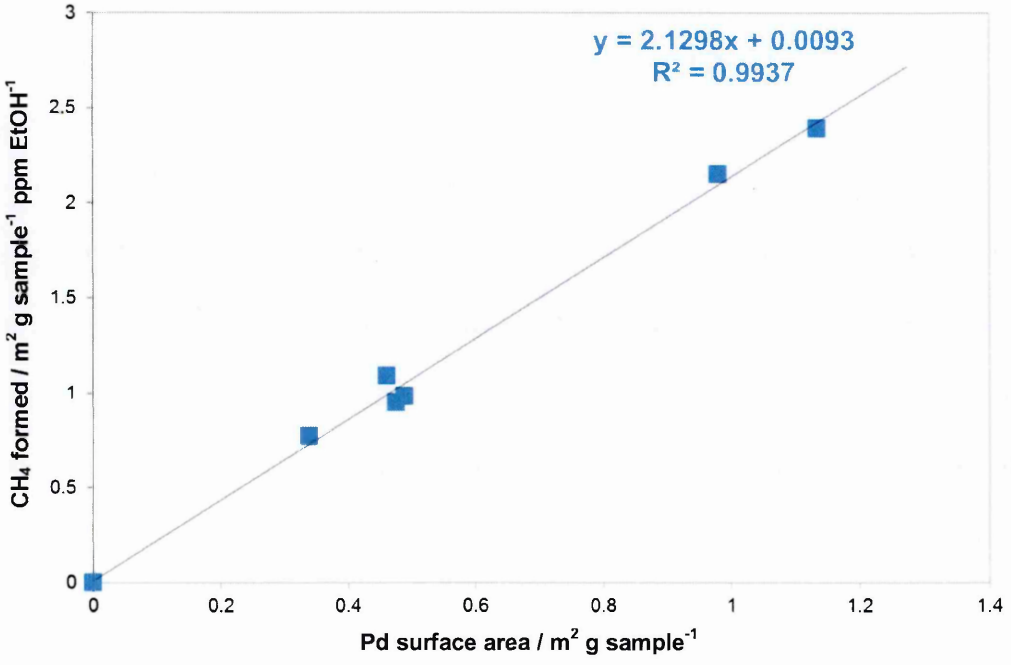

Figure 3-7: Calibration curve to quantify Pd surface area based on the amount of CH_4 formed during EtOH-TPSR.

To demonstrate some of the changes in Pd surface area mentioned above, two of the samples used to build the calibration curve (1Pd/Al_2O_3 calcined at 500 ºC and at 900 ºC, with Pd surface areas of 1.13 and 0.49 m^2 g^{-1}, respectively) were analysed by TEM. In the following Figure 3-8 it can be observed that the sample calcined at 500 ºC contained Pd particles with an average size of 10 nm, whilst the same sample calcined at 900 ºC contained Pd particles with an average size of 80 nm. The increase of Pd particle size occurred due to thermal sintering.

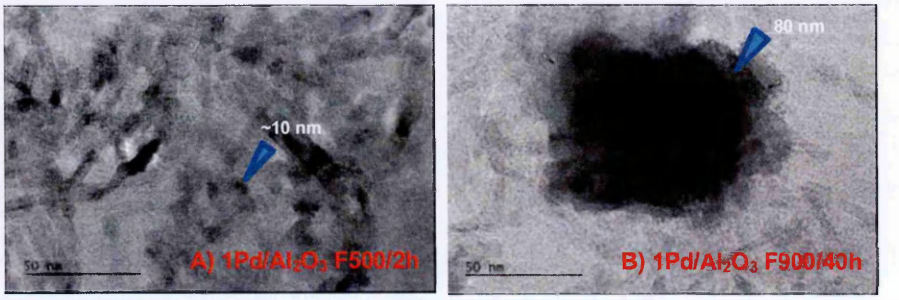

Figure 3-8: TEM images of 1 wt% Pd/Al_2O_3 fired at 500 ºC for 2 h and at 900 ºC for 40 h. The images showed the different Pd particles sizes obtained depending on the calcination temperature (500 vs 900 ºC).

3.1.3. Remarks

The EtOH-TPSR technique has been used for the work of this thesis as a complementary measurement to characterise Pd surface area, together with CO-chemisorption and XPS. It has been especially useful to compare the Pd surface area on those samples where Pd and Rh co-existed, as CO chemisorption could not give selective measurements for each of the metals and XPS could not be used due to the low Pd and Rh loadings used. In addition to this, this technique can give realistic Pd surface areas, as the reaction occurs exclusively on the metal and not on the interface between the metal and the ceria (contrary to chemisorption techniques), and it is sensitive to palladium oxide only.

As a practical example, the metal surface area of a $0.5Pd/CeO_2$ catalyst was analysed by CO chemisorption and by EtOH-TPSR. The metal surface area obtained from CO chemisorption was significantly higher than that obtained from the EtOH-TPSR method (using the calibration curve) due to the extra contribution of the Pd-Ce interface sites (see Figure 3-9).

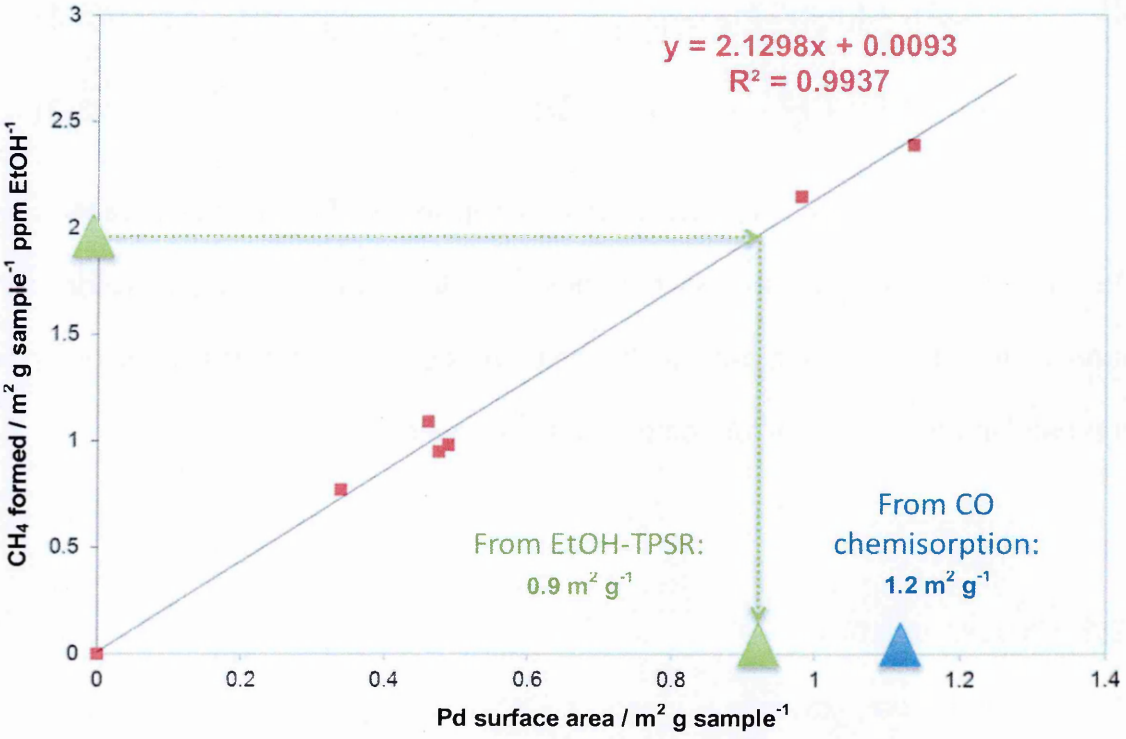

Figure 3-9: Example of Pd surface area calculated by the EtOH-TPSR method using the calibration curve, and compared to the value obtained from CO chemisorption analyses on the same sample.

3.2. Ethane Hydrogenolysis for Rh surface characterisation

The ethane hydrogenolysis reaction was used to obtain qualitative information related to the concentration of rhodium active sites in a catalyst. This reaction allowed us to separate the effect of the Rh active sites from the Pd active sites (in case of co-existence), as Rh is significantly more active than Pd for this reaction (Ru > Rh > Ir >> Pd = Pt) [4, 5, 22].

According to the mechanism proposed by Cimio, Boudart and Taylor [23], the initial step in the reaction sequence is the dehydrogenation of the ethane to form an unsaturated surface residue (reaction 3-1). This step is followed by rupture of the carbon-carbon bond, with subsequent hydrogenation of the cracked fragments to produce methane (reactions 3-2):

$$C_2H_6 \rightleftharpoons C_2H_x + [(6-x)/2]H_2 \qquad (3\text{-}1)$$

$$C_2H_x \xrightarrow{H_2} CH_y + CH_z \xrightarrow{H_2} CH_4 \qquad (3\text{-}2)$$

This technique is highly sensitive to changes in the surface of the catalyst and different slopes can be obtained depending on the support used, therefore the quantification of Rh surface area is challenging. Because of this, the technique has been used in this work only for comparative purposes.

3.2.1. Experimental

3.2.1.1. Catalysis preparation

A series of xRh/CeZr catalysts with several Rh loadings (x = 0.02, 0.05, 0.1, 0.2, and 0.3 wt%) were prepared by incipient wetness impregnation using aqueous solution of $Rh(NO_3)_3$ on a CeZr support. Following the impregnation the catalysts were dried in air at 105 ºC and calcined at 500 ºC for 2h.

The support used was a stabilised Zr-rich CeZr mixed oxide supplied by Rhodia, and $Rh(NO_3)_3$ (assay 12.85%) solution, supplied by Johnson Matthey, was used for Rh impregnations.

3.2.1.2. Ethane hydrogenolysis

0.1 g of 250-355 µm pelletised sample was placed in the centre of a quartz tube, held in position with quartz wool. The quartz tube was then introduced into the micro reactor.

The sample was first submitted to a pre-treatment under He (50 ml min^{-1}) at 300 °C for 30 minutes to clean the surface of the catalyst of adsorbed atmospheric water and carbonates.

Following this pre-treatment, the temperature was then set at 150 °C and a gas mixture of 8.3% H_2 and 1.7% C_2H_6 in N_2 (50 ml min^{-1} 10%H_2/N_2 + 10 ml min^{-1} 10%C_2H_6/N_2) was flowed through the sample, and the gas composition monitored using a mass spectrometer (MS). Once a stable signal was obtained, a temperature ramp of 10 °C min^{-1} was applied up to 500 °C. The CH_4 MS signal was then represented against the temperature; this is known as the light-off curve.

3.2.2. Results

Figure 3-10 shows the evolution of the C_2H_6 and CH_4 signals during a temperature ramp between 150 and 350 °C. It is possible to appreciate how C_2H_6 is progressively consumed, reacting to form CH_4.

The activity of the catalyst correlates with the specific surface area of rhodium metal. The lower the temperature of the light-off, the more surface Rh it contains. If Rh surface area quantification is needed, a calibration curve could be obtained. For example, Stoyanovskii *et al.* generated calibration light-off curves for a series of Rh/Al_2O_3 samples at different Rh loadings [5].

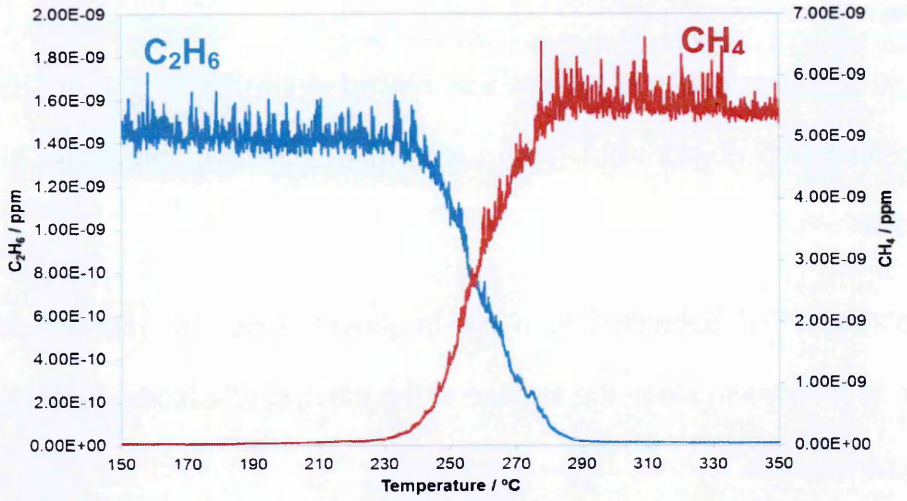

Figure 3-10: Ethane hydrogenolysis performed over a 0.3wt %Rh/CeZr sample calcined at 650 °C for 2 h. The sample was firstly pre-treated under He at 300 °C for 30 minutes. Following this, the sample was cooled down to 150 °C and the gas flows set to 50 ml min^{-1} 10%H_2/N_2 and 10 ml min^{-1} 10%C_2H_6/N_2. Once a stable signal was obtained, a temperature ramp of 10 °C min^{-1} was applied up to 450 °C.

A similar experiment was performed here by testing Rh/CeZr samples with different Rh loadings. These samples were also compared with two Pd/CeZr samples to demonstrate the significant higher activity that Rh presents compared to Pd (Figure 3-11).

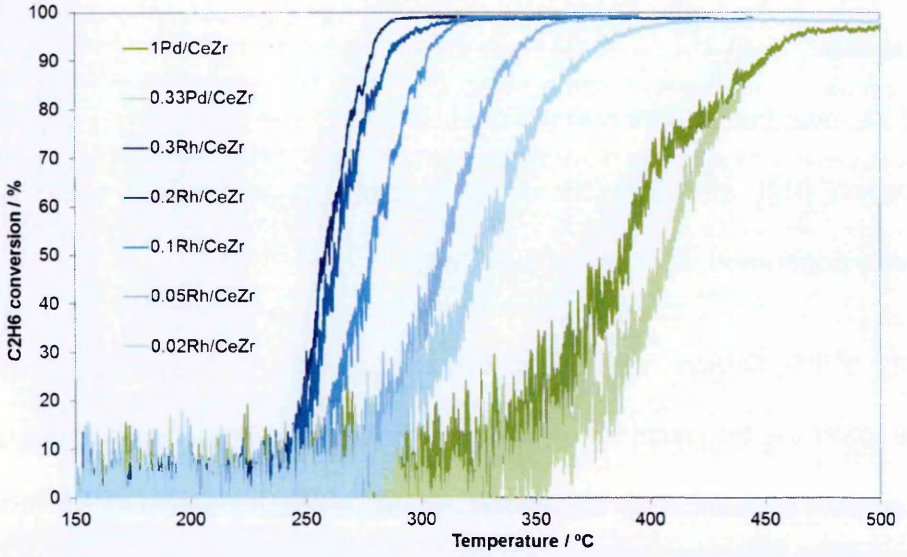

Figure 3-11: Light-off curves for samples with different Rh loadings. Two Pd/CeZr catalysts were also evaluated for comparison. Each sample was firstly pre-treated under He at 300 °C for 30 minutes. Following this, the sample was cooled down to 150 °C and the gas flows set to 50 ml min^{-1} 10%H_2/N_2 and 10 ml min^{-1} 10%C_2H_6/N_2. Once a stable signal was obtained, a temperature ramp of 10 °C min^{-1} was applied up to 450 °C.

It is possible to observe that the light-off temperature decreases with increasing the Rh content. In addition, changes in the slope were noticeable, due to changes in the reaction rate. This has already been reported in literature, where it was found that the type of support, Rh particle size and morphology could have an impact on the gradient of the slope [24].Figure 3-12 shows an example of how the type of support and particle size can affect the slope of C_2H_6 conversion:

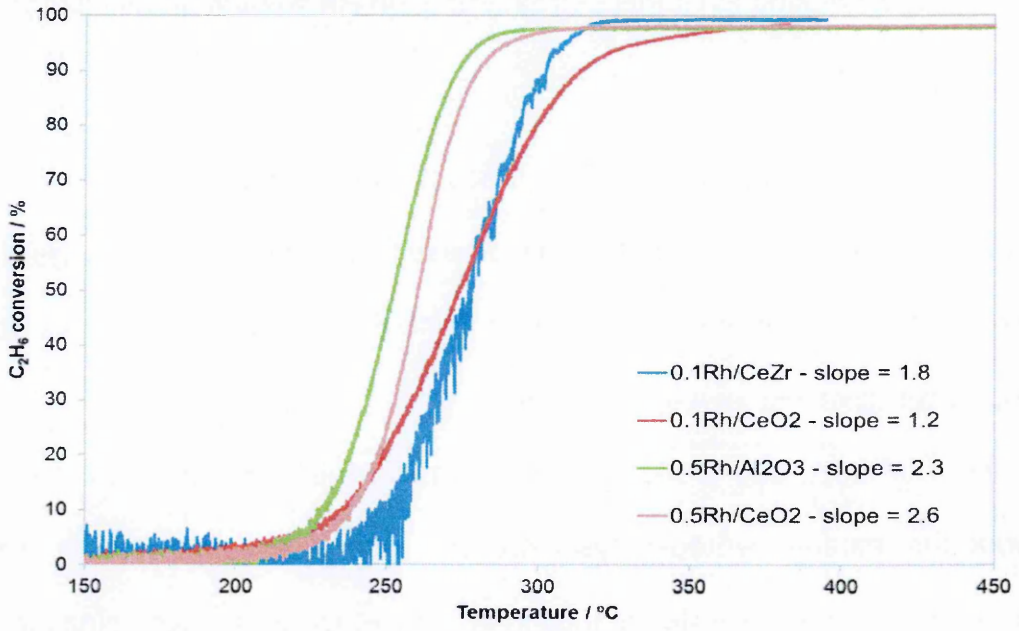

Figure 3-12: Light-off curves of Rh-samples calcined at 500 °C for 2h, where 0.1wt% Rh or 0.5 wt% Rh was supported on different commercial supports (CeZr, CeO_2 or Al_2O_3). The slope of each curve was calculated and can be found in the figure's legend. Each sample was firstly pre-treated under He at 300 °C for 30 minutes. Following this, the sample was cooled down to 150 °C and the gas flows set to 50 ml min^{-1} 10%H_2/N_2 and 10 ml min^{-1} 10%C_2H_6/N_2. Once a stable signal was obtained, a temperature ramp of 10 °C min^{-1} was applied up to 450 °C.

A calibration curve could not be obtained for Rh/CeZr samples, as there was no alternative method to quantify Rh surface area (CO chemisorption would also adsorb at the interface of Rh-Ce giving higher values). Al_2O_3-based samples could not be used for this, as the slope of the C_2H_6 conversion could suffer changes due to the different type of support [24]. Thus, due to these issues, the ethane hydrogenolysis method was used in this thesis only for comparative purposes.

3.2.3. Remarks

Ethane hydrogenolysis reaction has been reported as a method to quantify Rh surface area [4, 5, 22]. This method is based on the conversion of C_2H_6 to CH_4, and its light-off temperature greatly depends on the metal used, Rh being significantly more active than Pd (lower light-off temperature). Moreover, Rh surface area greatly affects the light-off temperature and due to this it is possible to qualitatively determine Rh surface area, with high Rh surface areas giving lower light-off temperatures.

For a quantitative determination of Rh surface area a calibration curve is needed, however in the case of Rh supported on Ce-based materials this is not possible as there is no other method to realistically determine Rh surface area (chemisorption techniques will give higher values due to the Rh-Ce interface contribution, and TEM cannot be used due to the lack of contrast between Rh and Ce). Thus, for this work the ethane hydrogenolysis reaction was used as a complimentary technique for the qualitative determination of Rh surface area in combination with CO chemisorption and XPS analyses.

References Chapter 3

[1] R. M. Lambert and G. Pacchioni, *Chemisorption and Reactivity on Supported Clusters and Thin Films: Towards an Understanding of Microscopic Processes in Catalysis*, Kluwer Academic Publishers, 1997.

[2] M. Cargnello, V. V. T. Doan-Nguyen, T. R. Gordon, R. E. Diaz, E. A. Stach, R. J. Gorte, P. Fornasiero and C. B. Murray, Science, 341 (2013) 771-773.

[3] J. W. Niemantsverdriet, *Spectroscopy in Catalysis*, WILEY-VCH, 2007.

[4] J. H. Sinfelt and D. J. C. Yates, Journal of Catalysis, 8 (1967) 82-90.

[5] V. O. Stoyanovskii, A. A. Vedyagin, G. I. Aleshina, A. M. Volodin and A. S. Noskov, Applied Catalysis B: Environmental, 90 (2009) 141-146.

[6] J. M. Tatibouët, Applied Catalysis A: General, 148 (1997) 213-252.

[7] D. Jaumain and B.-L. Su, Catalysis Today, 73 (2002) 187-196.

[8] J. Y. Z. Chiou, J.-Y. Siang, S.-Y. Yang, K.-F. Ho, C.-L. Lee, C.-T. Yeh and C.-B. Wang, International Journal of Hydrogen Energy, 37 (2012) 13667-13673.

[9] S. Cavallaro, V. Chiodo, S. Freni, N. Mondello and F. Frusteri, Applied Catalysis A: General, 249 (2003) 119-128.

[10] M. A. Goula, S. K. Kontou and P. E. Tsiakaras, Applied Catalysis B: Environmental, 49 (2004) 135-144.

[11] J.-L. Bi, Y.-Y. Hong, C.-C. Lee, C.-T. Yeh and C.-B. Wang, Catalysis Today, 129 (2007) 322-329.

[12] A. Perna, International Journal of Hydrogen Energy, 32 (2007) 1811-1819.

[13] W. Wang and Y. Wang, International Journal of Hydrogen Energy, 33 (2008) 5035-5044.

[14] L. V. Mattos and F. B. Noronha, Journal of Power Sources, 152 (2005) 50-59.

[15] A. Gutierrez, R. Karinen, S. Airaksinen, R. Kaila and A. O. I. Krause, International Journal of Hydrogen Energy, 36 (2011) 8967-8977.

[16] M. Mavrikakis and M. A. Barteau, Journal of Molecular Catalysis A: Chemical, 131 (1998) 135-147.

[17] P. Y. Sheng, A. Yee, G. A. Bowmaker and H. Idriss, Journal of Catalysis, 208 (2002) 393-403.

[18] A. M. Silva, L. O. O. Costa, A. P. M. G. Barandas, L. E. P. Borges, L. V. Mattos and F. B. Noronha, Catalysis Today, 133–135 (2008) 755-761.

[19] A. Yee, S. J. Morrison and H. Idriss, Journal of Catalysis, 186 (1999) 279-295.

[20] Y. Zhang, J. Zhou, Z. Wang, J. Liu and K. Cen, International Journal of Hydrogen Energy, 33 (2008) 2211-2217.

[21] H. W. Jen, G. W. Graham, W. Chun, R. W. McCabe, J. P. Cuif, S. E. Deutsch and O. Touret, Catalysis Today, 50 (1999) 309-328.

[22] J. H. Sinfelt, Catal Lett, 9 (1991) 159-171.

[23] A. Cimino, M. Boudart and H. S. Taylor, Journal of Physical Chemistry, 58 (1954) 796.

[24] B. Coq, R. Dutartre, F. Figueras and T. Tazi, Journal of Catalysis, 122 (1990) 438-447.

4. Pd-CeO_2 samples prepared by co-precipitation

Contents

4. Pd-CeO_2 samples prepared by co-precipitation

Wet impregnation[1] is a widely used method to prepare catalysts as it leads to products with high metal dispersion and metal surface areas. However, when impregnating extremely low metal loadings, this can lead to too small particles that get locked in a less reactive state [1-3]. This occurs as a consequence of the formation of $M^{\gamma+}$-O-Ce bonds[2], which makes the metal interact too strongly with the Ce [1]. Thus, a certain level of M-Ce interaction is desired in order to achieve good oxygen mobility between the metal and the support, and *vice versa*, but without dispersing the metal as ionic $M^{\gamma+}$ species.

Here, co-precipitation was evaluated as an alternative method to prepare Pd-CeO_2 catalysts. Co-precipitation was chosen with the aim of increasing the contact between Pd and ceria atoms in order to promote a larger number of Ce atoms by the Pd, yet not to prepare Pd in a too dispersed state [4].

In this chapter the effect of the ceria precursor (Ce^{3+} vs Ce^{4+}) and the effect of Pd loading in the structure and catalytic performance of the final product, were evaluated.

4.1 Pd-CeO_2 based catalysts: impact of the Ce-precursor

To study the impact that the Ce-precursor has in the final structure and the catalytic performance of Pd-CeO_2 catalysts, [0.5Pd+Ce] samples were prepared by co-precipitation using $Ce(NO_3)\cdot 6H_2O$ (as Ce^{3+} precursor) and $Ce(NH_4)_2(NO_3)_6$ (as Ce^{4+} precursor). All the other conditions during the preparation were kept the same, as detailed in Chapter 2.

---

[1] For a description of the wet impregnation technique refer to *Chapter 2*.

[2] $M^{\gamma+}$ refers to a positively charged metal. The value of γ depends on the type of metal, oxidation state and electronic interactions.

4.1.1. Observations during the catalysts preparation

When Ce^{3+} and Pd^{2+} precursors were added to boiling NaOH, a dark grey solid was obtained, suggesting the reduction of Pd^{2+} to metallic palladium through a redox reaction with Ce^{3+} (Figure 4-1 – A1) [5, 6]. In contrast, when Ce^{4+} and Pd^{2+} precursors were used, a redox reaction did not occur and a yellow precipitate was obtained, suggesting in this case no metallic palladium formed, only PdO_x (Figure 4-1 – B1).

After calcination at 650 °C for 2h the [0.5Pd+Ce^{3+}] sample became significantly lighter in colour (Figure 4-1 – A2), while no change in colour was seen for the catalyst prepared with Ce^{4+} precursor, which remained yellow during the whole process (Figure 4-1 – B2). The change in colour from dark grey to yellow for the Ce^{3+} preparation, suggests that the metallic palladium was re-oxidised to PdO_x during the calcination process.

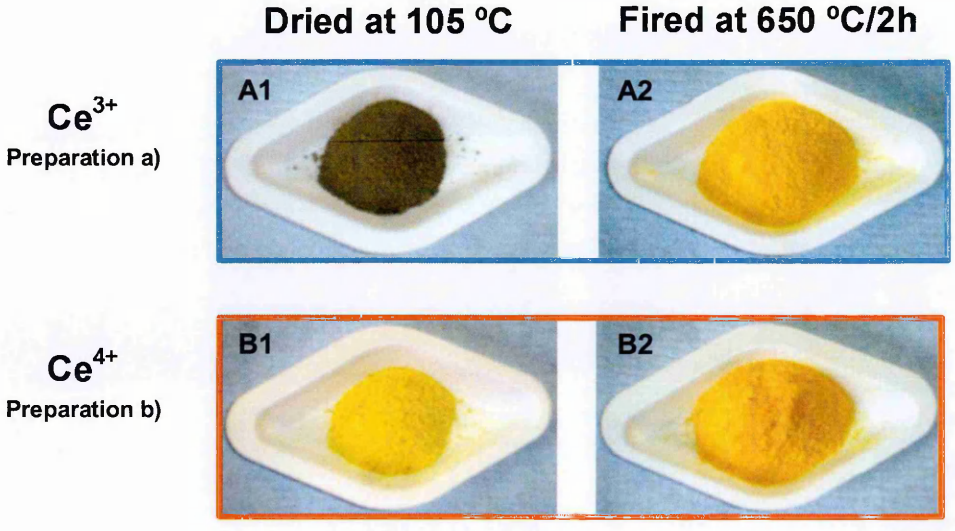

Figure 4-1: Comparison of the colour obtained after the co-precipitation using a Ce^{3+} precursor (A1 and A2) or a Ce^{4+} precursor (B1 and B2) before (dried at 105 °C) and after the calcination at 650 °C for 2 hours (F650 °C/2h).

4.1.2. Structural characterisation

It is important to understand the structure of the catalyst, especially to determine the presence of dopants, as these can create a distortion in the structure changing the oxygen mobility of the ceria.

With the aim of understanding if Pd is deposited within the lattice of the ceria or separately, the samples were analysed by XRD.

4.1.2.1. X-Ray Diffraction (XRD)

XRD analyses showed that all the 0.5Pd-CeO_2 samples had a cubic CeO_2 structure [7]. Due to the low Pd loadings used (0.5 wt%), it was not possible to extract any information regarding the noble metal using the X-ray diffraction technique.

The XRD patterns for the 0.5Pd-CeO_2 samples can be found in Figure 4-2, and the lattice parameter *a* and the ceria crystallite sizes in Table 4-1.

Table 4-1: Lattice parameter and ceria crystallite size analysed by XRD, and specific surface area calculated by BET, of Pd-CeO_2 samples prepared by impregnation (0.5Pd/CeO_2) and by co-precipitation with Ce^{3+} ([0.5Pd+Ce^{3+}]) and Ce^{4+} ([0.5Pd+Ce^{4+}]) precursors. Calculated errors for ceria crystallite size are reported in brackets; BET-SSA instrument standard error = ± 4 m^2 g^{-1}.

	a lattice parameter / Å	Crystallite size / nm	BET-SSA / m^2 g^{-1}	ICP / Pd wt%
CeO_2 XRD Reference [7]	5.411	-	-	-
0.5Pd/CeO_2	5.410	5.83 (± 0.07)	138	0.51
[0.5Pd+Ce^{3+}]	5.409	5.51 (± 0.05)	114	0.50
[0.5Pd+Ce^{4+}]	5.412	6.83 (± 0.08)	54	0.38

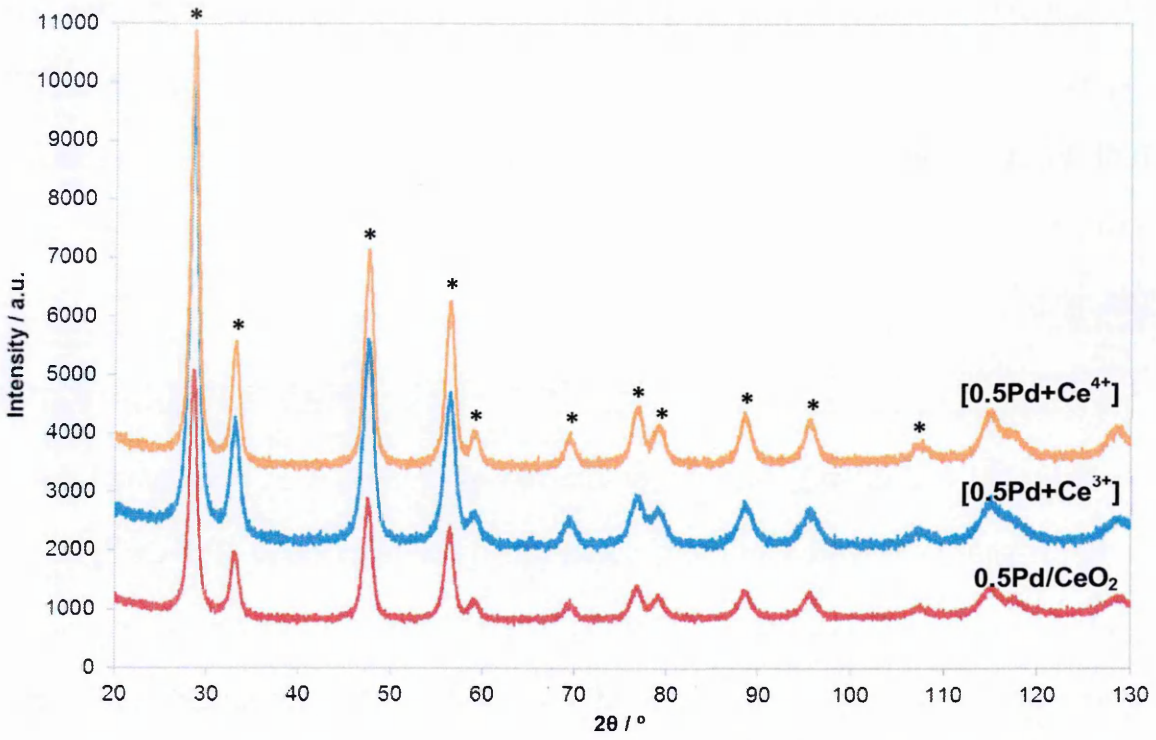

Figure 4-2: XRD profiles for 0.5Pd-CeO_2 samples prepared by impregnation (0.5Pd/CeO_2) and by co-precipitation with Ce^{3+} ([0.5Pd+Ce^{3+}]) and Ce^{4+} ([0.5Pd+Ce^{4+}]) precursors. The peaks corresponding to the cubic CeO_2 phase are indicated as (*).

The lattice parameter of all the catalysts prepared did not show any significant cell contraction compared to the reference value, thus there was no indication of Pd ions being added to the ceria structure[3].

In terms of ceria crystallite size, the sample prepared with Ce^{3+} had the smallest value (5.51 nm) and the sample with Ce^{4+} the largest (6.83 nm); the larger crystallite size obtained with Ce^{4+} is likely to be due to higher particle agglomeration during the synthesis. The agglomeration is strongly related to supersaturation, the higher this is the more agglomeration occurs [8]. Considering that the starting Ce-concentration for both preparations was the same and that the K_{sp} value (at 25 ºC) of $Ce(OH)_4$ is significantly lower than that of $Ce(OH)_3$ ($2 \cdot 10^{-48}$ M^5 and $1.6 \cdot 10^{-20}$ M^4 respectively)[4], it can be observed that Ce^{4+}

[3] Ionic radius: Pd^{+2} =0.86 Å; Ce^{4+} = 0.97 Å, Ce^{3+} = 1.14 Å

[4] Values obtained at 25 ºC. The lower the K_{sp} value, the less concentration is needed to start the precipitation.

precipitation was exposed to a higher supersaturation during the preparation. This hypothesis also agrees with the specific surface areas obtained, where the 0.5Pd/CeO_2 and [0.5Pd+Ce^{3+}] samples had similar surface areas (138 and 114 m^2 g^{-1}, respectively), whilst [0.5Pd+Ce^{4+}] presented a significantly lower value (54 m^2 g^{-1}).

The Pd content was analysed by ICP. The results in Table 4-1 shows that the impregnated 0.5Pd/CeO_2 and the co-precipitated [0.5Pd+Ce^{3+}] contained the Pd content initially calculated for these catalysts; in contrast, the [0.5Pd+Ce^{4+}] sample contained a lower Pd content (0.38 wt%). The filtrates obtained during the vacuum filtration and following washes were not analysed, but it is suspected that some of the $Pd(OH)_2$ formed during the precipitation of [0.5Pd+Ce^{4+}] could have dissolved and leached out. Most of the available published information determined that $Pd(OH)_2$ is largely insoluble in H_2O, however a few studies have revealed that small amounts of aqueous Pd complexes could be dissolved in water under certain conditions [9-11]. It is believed that Pd did not leach during the preparation of [0.5Pd+Ce^{3+}] due to the formation of different palladium species (metallic Pd), as described in section 4.1.1., which are considered highly insoluble.

4.1.3. Surface characterisation

In addition to understanding the bulk properties of the catalysts, surface characterisation is needed to quantify the number of available active sites on the surface, as this is important to determine the level of adsorption of the pollutants. Due to the low noble metal loadings, as well as the presence of ceria, the results obtained from XPS, CO chemisorption and EtOH-TPSR analyses were combined to provide a more accurate understanding of the catalysts surface.

4.1.3.1. X-Ray Photoelectron Spectroscopy (XPS)

The surface composition of the samples obtained with the different preparation methods was analysed by XPS, which has a depth of analysis of ~5 nm [12]. Figure 4-3 shows the signals obtained for the Ce3d spectra, which typically contains bands at 883.3 eV, 886.0 eV, 890.0 eV and 899.3 eV, denoted as v, v', v'', and v''', respectively, as well as bands at 901.8 eV, 904.1 eV, 908.4 eV and 917.5 eV, denoted as u, u', u'', and u'''. The peaks denoted as *v* and *u* refer to $3d_{5/2}$ and $3d_{3/2}$ spin-orbitals, respectively. In terms of oxidation state identification, the bands u, v, u'', v'', u''' and v''' are related to Ce^{4+} species, whilst u' and v' can be assigned to Ce^{3+} [13, 14].

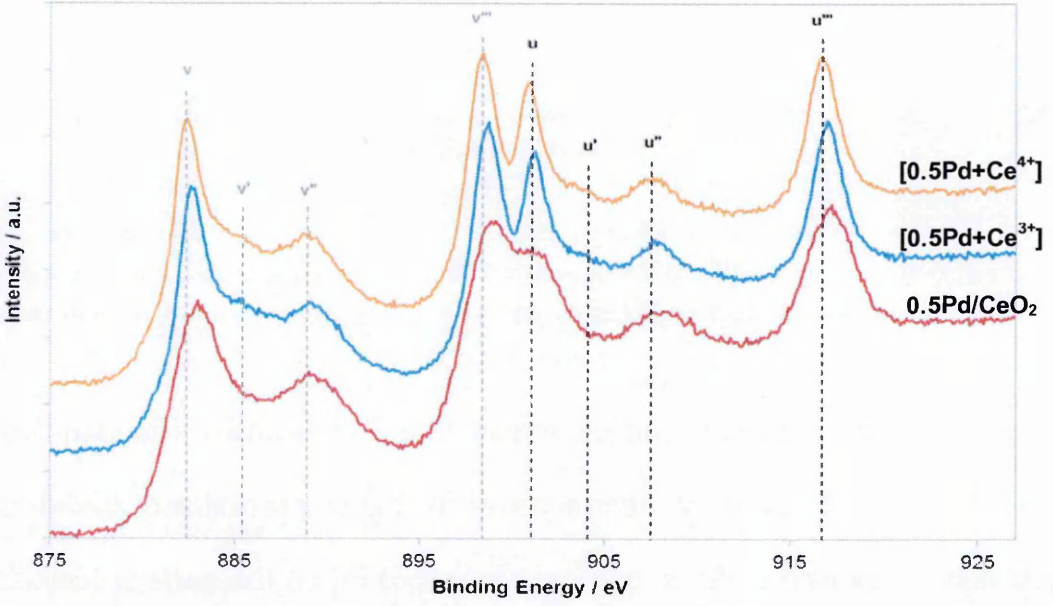

Figure 4-3: Ce3d XPS spectra for the 0.5Pd-CeO_2 samples prepared by co-precipitation using Ce^{3+} ([0.5Pd+Ce^{3+}]) and Ce^{4+} ([0.5Pd+Ce^{4+}]) precursors, and the sample prepared by impregnation on CeO_2 (0.5Pd/CeO_2). The bands u, v, u'', v'', u''' and v''' are related to Ce^{4+} species, whilst u' and v' are assigned to Ce^{3+}.

The Ce3d spectra indicated that CeO_2 can be identified as the main cerium species present in all these catalysts. In addition 15-20 % of Ce^{3+} was also present in all the samples, however, exact quantification is difficult as the X-ray beam can induce reduction of Ce^{4+} to Ce^{3+} [15]. The presence of Ce^{4+} as the main

species suggests that the majority of the cerium added during the preparation is oxidised during the calcination irrespective of the Ce-precursor used. This is consistent with the colour of the samples observed.

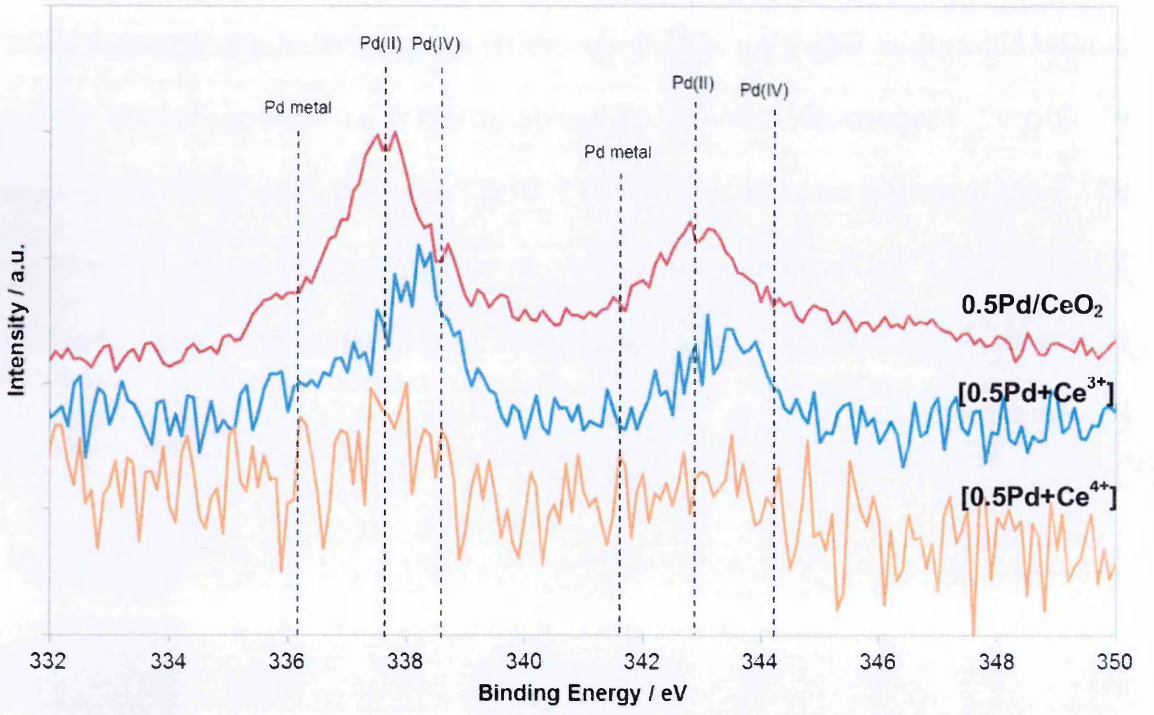

Figure 4-4: Pd3d spectra obtained by XPS comparing the Pd species found in the samples prepared by co-precipitation using Ce^{3+} ([0.5Pd+Ce^{3+}]) and Ce^{4+} ([0.5Pd+Ce^{4+}]) precursors, and the sample prepared by impregnation on CeO_2 (0.5Pd/CeO_2). The vertical lines point the position of the different Pd species detected.

Figure 4-4 compares the XPS profiles obtained for Pd3d signals. The identification and quantification of Pd on the near-surface[5] for the co-precipitated [0.5Pd+Ce^{4+}] sample was not possible due to the low amount of Pd on the surface (calculated Ce/Pd atomic ratio = 109). [0.5Pd+Ce^{3+}] also contained little surface Pd (calculated Ce/Pd atomic ratio 54), but the resolution and identification of its bands was possible. The doublet at 335.94 eV ($Pd3d_{5/2}$) and 341.20 eV ($Pd3d_{3/2}$) are believed to correspond to metallic clusters, whilst the bands at 337.61 eV ($Pd3d_{5/2}$) and 342.87 eV ($Pd3d_{3/2}$) to palladium species with higher oxidation state (Figure 4-5 - A) according to the literature [14]. For Pd^{2+}, these bands should

[5] The depth of XPS analysis is approximately 5 nm.

appear at 336.8 and 342.06 ± 0.2 eV, but for this catalyst ([0.5Pd+Ce^{3+}]) they were shifted towards higher binding energies indicating that palladium was interacting strongly with the support [13, 16]. Pd^{4+} bands should also appear at this region, however it is improbable that the sample contained these species, as PdO_2 is unstable at high calcination temperatures (T > 400 ºC), similar to those used in this study [13].

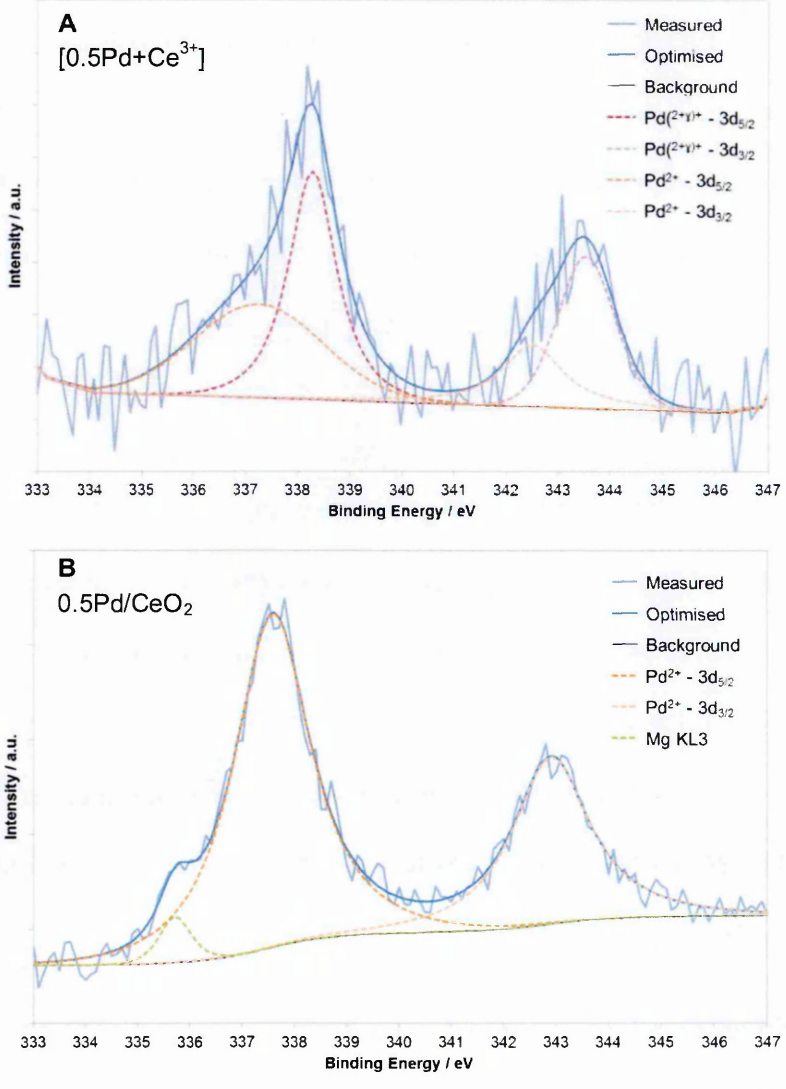

Figure 4-5: Deconvolution of Pd3d XPS peaks for [0.5Pd+Ce^{3+}] (A) and 0.5Pd/CeO_2 (B).

The impregnated 0.5Pd/CeO_2 had the highest Pd loading on the surface (calculated Ce/Pd atomic ratio = 34). The palladium species in this sample were

present as Pd^{2+} (Figure 4-5 - B). A shoulder at 335.7 eV was also observed which is believed to be due to traces of Mg contamination (Mg Auger peak from L to K shell).

The higher calculated Ce/Pd atomic ratio of 0.5Pd/CeO_2 compared to that found for [0.5Pd+Ce^{3+}] (34 and 54, respectively) can indicate either a higher Ce-decoration and/or the formation of larger Pd particles in the co-precipitated [0.5Pd+Ce^{3+}] sample. Further surface analyses (CO chemisorption, and EtOH-TPSR) will be required in order to establish this conclusively. In addition, the appearance of palladium peaks at higher binding energies for [0.5Pd+Ce^{3+}] indicated that Pd-Ce interaction is significantly stronger for this sample compared to 0.5Pd/CeO_2, which is suspected to be attributed to an improved contact between Pd and Ce atoms in the [0.5Pd+Ce^{3+}] sample.

4.1.3.2. Metal dispersion analyses: CO chemisorption & EtOH-TPSR

It has been discussed previously that the measurement of metal dispersion on CeO_2-based samples is a complicated parameter to measure by CO-chemisorption due to CO adsorption occurring at the interface of the metal and the ceria, as well as on the metal itself, giving higher dispersion and metal area values than the actual [2]. For this reason, the analyses performed here were only taken for comparative purposes.

A new technique, developed during the work of this thesis, was used in addition to the CO chemisorption to measure Pd surface area: ethanol temperature programmed surface reaction (EtOH-TPSR), as described in *Chapter 3*. During EtOH-TPSR Pd-catalysts form CH_4, the amount of which increases with Pd surface area, which can then be calculated using a calibration curve.

Table 4-2 compares the results obtained for the 0.5Pd-CeO_2 samples prepared using the different methods:

Table 4-2: Pd dispersion and surface area calculated using CO-chemisorption, and Pd surface area calculated by EtOH-TPSR for 0.5Pd-CeO_2 samples prepared by impregnation on CeO_2 (0.5Pd/CeO_2) and by co-precipitation using Ce^{3+} ([0.5Pd+Ce^{3+}]) and Ce^{4+} ([0.5Pd+Ce^{4+}]) precursors. CO chemisorption instrument standard error = ± 2% (for metal dispersion) and ± 0.04 m^2 g^{-1} (for metal surface area); EtOH-TPSR instrument standard error = ± 0.1 m^2 g^{-1}.

	CO chemisorption		EtOH-TPSR	
Sample	Pd dispersion / %	Pd surface area / m^2 g^{-1}	max ppm CH_4 g sample^{-1} ppm $EtOH^{-1}$	Pd surface area / m^2 g^{-1}
0.5Pd/CeO_2	52	1.2	1.9	0.9
[0.5Pd+Ce^{3+}]	51	1.1	1.1	0.5
[0.5Pd+Ce^{4+}]	14	0.2	0.1	0.1

**The dispersion has been calculated based on the real Pd loading (0.50 wt% Pd for 0.5Pd/CeO_2 and [0.5Pd+Ce^{3+}], and 0.38 wt% Pd for [0.5Pd+Ce^{4+}]).*

The values obtained from the CO chemisorption and the EtOH-TPSR techniques followed the same trend, and were in agreement with the trend observed using XPS. The results showed that the impregnated sample had the highest levels of Pd at the surface, followed by the co-precipitated [0.5Pd+Ce^{3+}] and by the co-precipitated [0.5Pd+Ce^{4+}], this last showing a significantly lower Pd surface area.

The lower Pd surface area of [0.5Pd+Ce^{4+}] is believed to be not only a consequence of the lower Pd content compared to the other two samples. If the Pd surface area of [0.5Pd+Ce^{4+}] is compared to a sample that contains 1.5 times less Pd than this sample[6], it was observed that [0.5Pd+Ce^{4+}] had about ⅓ of its Pd surface area[7]; therefore in this case the decrease of Pd surface area was not proportional to the Pd content in the sample. This suggested that other factors should be involved, such as the formation of larger Pd particles or a higher level of ceria encapsulation compared to 0.5Pd/CeO_2 and [0.5Pd+Ce^{3+}] samples.

---

[6] [0.5Pd+Ce^{4+}] contains 0.38 wt% Pd, and it is compared to a sample prepared by impregnation that contains 0.25 wt% Pd (0.25Pd/CeO_2).

[7] Pd surface area of 0.25Pd/CeO_2: from CO chemisorption = 0.6 m^2 g^{-1}; from EtOH-TPSR = 0.4 m^2 g^{-1}.

Compared to the values obtained from the CO chemisorption, those obtained from the EtOH-TPSR method were lower. This is believed to be due to the extra CO adsorption occurring at the interface of the metal and the ceria during CO chemisorption experiments [2, 17]. Therefore, the EtOH-TPSR method appears to be a better technique to obtain more realistic metal surface area values, as only the surface Pd sites are involved. This can be specially noticed when comparing [0.5Pd+Ce^{3+}] and 0.5Pd/CeO_2 samples. Based on the values obtained from the EtOH-TPSR method, [0.5Pd+Ce^{3+}] had a significantly lower surface Pd content than 0.5Pd/CeO_2, whilst they appeared to contain very similar Pd surface areas when comparing the values obtained using the CO chemisorption. This could suggest that there is a considerable amount of CO adsorbing at interface sites for this co-precipitated sample, and hence that the interaction between Pd and Ce is greater for the co-precipitated sample prepared using the Ce^{3+} precursor.

This agrees with the conclusions from the XPS studies in section 4.1.3.1., where it was suggested that the co-precipitated [0.5Pd+Ce^{3+}] sample could contain some Ce-decoration on the Pd particles. This is likely to result in a greater number of Pd-Ce interfacial sites for the co-precipitated sample where CO would adsorb during CO chemisorption experiments.

4.1.4. Redox characterisation

The samples were submitted to H_2- and CO-TPR experiments, with the aim to further determine how the Pd-Ce interaction depends on the preparation method. The samples were also submitted to oxygen storage capacity (OSC) tests as any changes in the Pd-Ce interaction should have an impact on the OSC of the catalyst.

4.1.4.1. H_2-TPR

The reducibility of the samples was analysed by H_2-TPR. All the samples showed three main peaks corresponding to the reduction of Pd and promoted surface ceria (70-250 ºC), the reduction of unpromoted surface ceria (270-500 ºC) and the reduction of bulk ceria (600-900 ºC) [18, 19] (Figure 4-6).

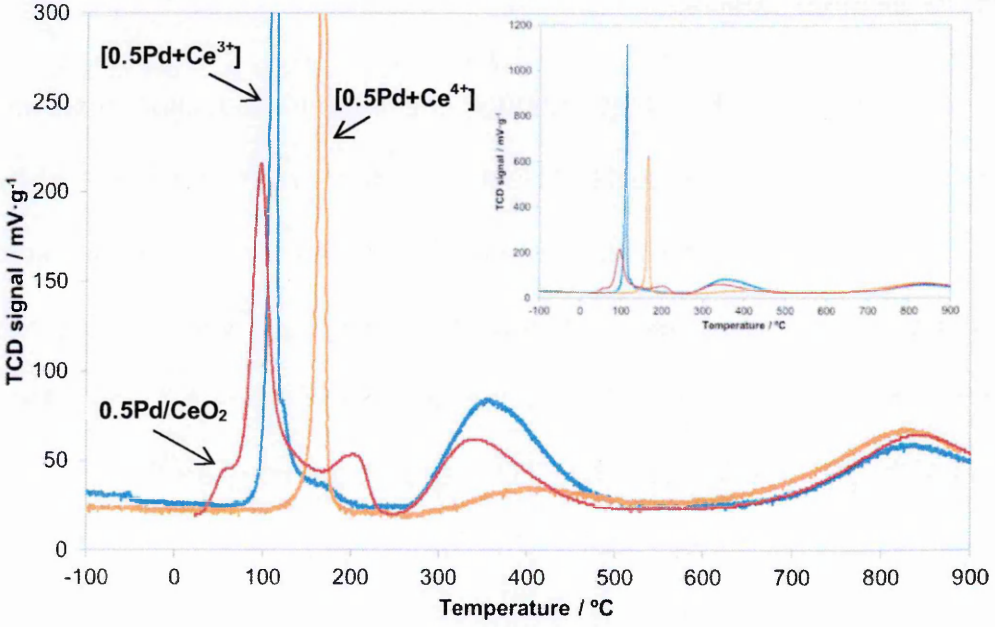

Figure 4-6: H_2-TPR profiles of 0.5Pd-CeO_2 samples prepared by impregnation (0.5Pd/CeO_2), and by co-precipitation with Ce^{3+} ([0.5Pd+Ce^{3+}]) and with Ce^{4+} ([0.5Pd+Ce^{4+}]) precursors. The sample taken was ~0.2 g, and the flow used was 30 ml min^{-1} of 10% H_2/N_2 using 30 ml min^{-1} of N_2 as carrier gas.

Comparing these three peaks it can be seen that the reduction of Pd was significantly different for the different samples. For the impregnated sample, a wide peak was observed centered at ~90 ºC with a small shoulder at 50 ºC and a second, more prominent one, at 205 ºC. In contrast, the Pd reduction appeared as a sharp peak for both co-precipitated samples, at ~110 ºC for [0.5Pd+Ce^{3+}] sample with two small shoulders at 120 and 160 ºC, and at 165 ºC for [0.5Pd+Ce^{4+}] catalyst. The presence of shoulders is an indication of the co-existence of Pd particles with different sizes [20]. Based on these results, the reduction of Pd occurs faster (sharp peak over a smaller temperature range) for the species created during the co-precipitation preparations than for the impregnated sample.

Surface ceria reduction was practically identical for the 0.5Pd/CeO_2 and [0.5Pd+Ce^{3+}] samples, and significantly lower for the [0.5Pd+Ce^{4+}] catalyst. This agrees with the specific surface area values, calculated by BET (0.5Pd/CeO_2 and [0.5Pd+Ce^{3+}] samples showed a SSA of 138 and 114 m^2 g^{-1}, respectively; whilst [0.5Pd+Ce^{4+}] sample showed a lower value of 54 m^2 g^{-1}). Ceria bulk reduction was similar for all three catalysts.

It is important to mention that although the second reduction peak is usually referred to as unpromoted ceria surface reduction, in the presence of the noble metal it appears at a lower temperature than when CeO_2-only is tested. Thus, technically the second peak is related to surface ceria which is promoted to a lower extent by the noble metal. This can be seen in Figure 4-7 where the H_2-TPR profiles of the 0.5Pd/CeO_2 and the CeO_2 samples are compared.

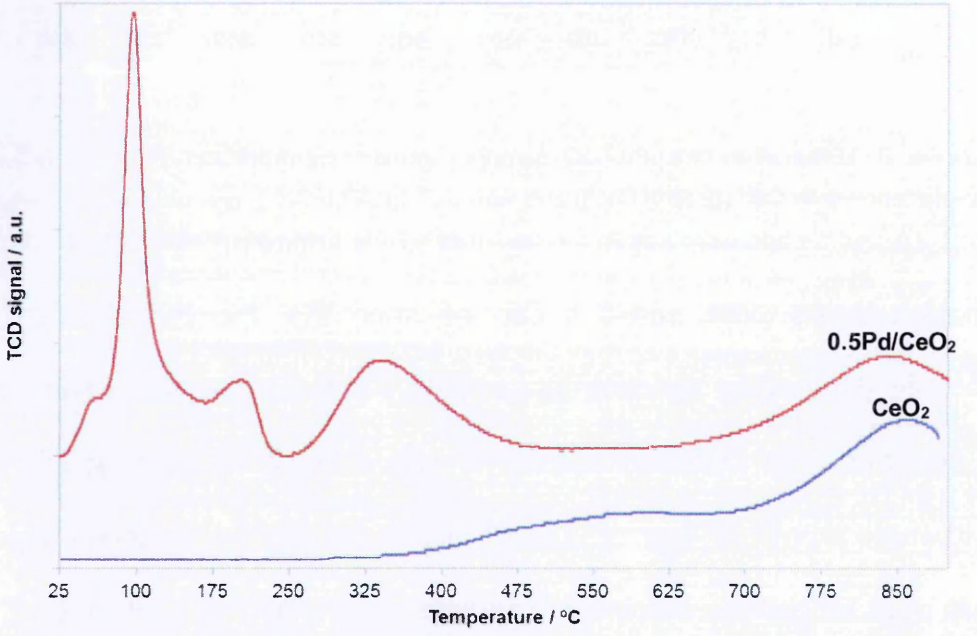

Figure 4-7: H_2-TPR profiles of 0.5Pd-CeO_2 samples prepared by impregnation (0.5Pd/CeO_2), and a CeO_2-only sample supplied by Rhodia. The sample taken was ~0.2 g, and the flow used was 30 ml min^{-1} of 10% H_2/N_2 using 30 ml min^{-1} of N_2 as carrier gas.

The only reduction peaks for CeO_2 were associated to surface (peak between 400 – 700 ºC) and bulk (700 – 900 ºC) reduction. For 0.5Pd/CeO_2, the bulk reduction

appeared at the same temperature, however the surface reduction appeared at lower temperature (250 – 500 ºC) due to the promotion caused by Pd.

Table 4-3 summarises the reduction temperatures of the peaks together with their hydrogen consumption for each sample:

Table 4-3: Summary of peak positions and H_2 consumption during the H_2-TPR experiments on 0.5Pd-CeO_2 samples prepared by impregnation (0.5Pd/CeO_2), and by co-precipitation with Ce^{3+} ([0.5Pd+Ce^{3+}]) and Ce^{4+} ([0.5Pd+Ce^{4+}]) precursors. Average instrument standard error ± 0.02 mmol g^{-1}.

	PdO_x reduction		Surface CeO_2 reduction		Bulk CeO_2 reduction	
Sample	Peak temperature / ºC	H_2 consumed / mmol g^{-1}	Peak temperature / ºC	H_2 consumed / mmol g^{-1}	Peak temperature / ºC	H_2 consumed / mmol g^{-1}
0.5Pd/CeO_2	90 ºC 50, 204 ºC (shoulders)	0.58	250-505 ºC	0.30	580-900 ºC	0.47
[0.5Pd+Ce^{3+}]	110 ºC 120, 160 ºC (shoulders)	0.64	260-535 ºC	0.40	580-900 ºC	0.38
[0.5Pd+Ce^{4+}]	165 ºC	0.41	260-530 ºC	0.10	580-900 ºC	0.39

The experimental H_2 consumption required to reduce 0.5 wt% Pd was much higher for all three catalysts than the calculated theoretical consumption (0.05 mmol g^{-1}); this is due to the extra contribution of the reduction of ceria in contact with palladium which occurs simultaneously, due to the spillover effect [3, 21]. It can be noticed that the H_2 consumption associated with the PdO_x reduction was the greatest for the co-precipitated [0.5Pd+Ce^{3+}] sample, again providing evidence for the highest Pd-Ce interaction for this catalyst.

4.1.4.2. CO-TPR

CO is a better probe molecule than H_2 to study surface reduction due to a lower spillover effect. This allows a more detailed study of the reducibility of Pd-species [21].

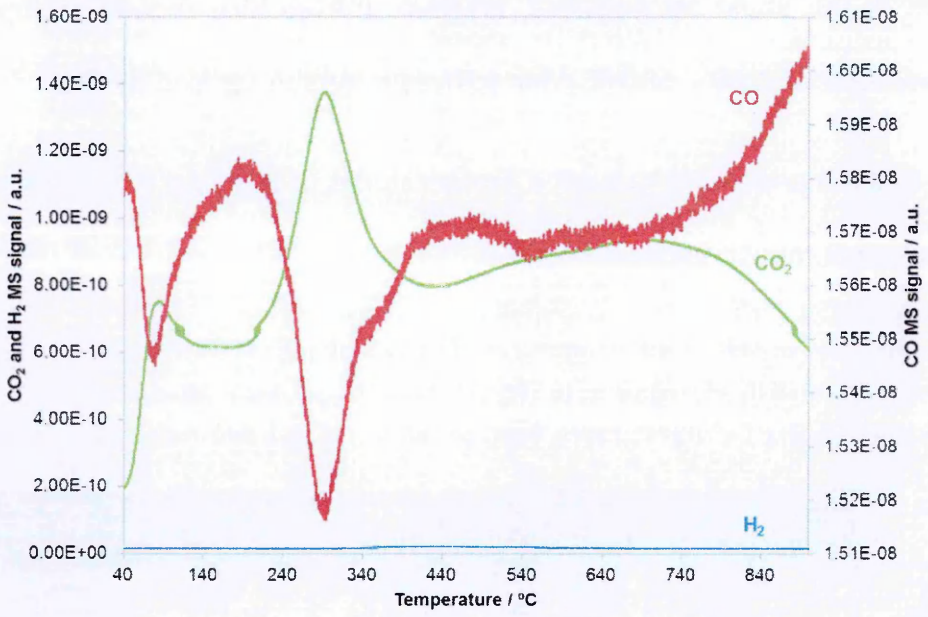

Figure 4-8: CO, CO_2 and H_2 mass spectrometer (MS) signals during a CO-TPR experiment on [0.5Pd+Ce^{3+}] sample, after the sample was previously pre-treated under 50 ml min^{-1} of He at 500 ºC. During the CO-TPR the flow consisted in 20 ml min^{-1} of 10%CO/He in 30 ml min^{-1} of He.

Figure 4-8 shows an example of the profiles obtained for CO, CO_2 and H_2 mass spectrometer (MS) signals during a CO-TPR experiment, in this case on the [0.5Pd+Ce^{3+}] sample. The main product obtained was CO_2; H_2 formation was not significant as there was no water in the flow, for this reason to compare the samples only CO consumption and CO_2 formation were overlaid.

The profiles obtained for the 0.5 wt% Pd samples prepared by impregnation, by co-precipitation with Ce^{3+}, and by co-precipitation with Ce^{4+} precursors can be found in Figure 4-9. Three main reductions could be identified in the CO_2 formation and CO conversion profiles and these were compared to values quoted in the literature [13, 21-23]. Peaks between 50-350 ºC are believed to relate to the reduction of surface PdO_x (multiple peaks or shoulders are related to PdO_x species with different strengths of interaction with the ceria support or different particle size) [21]. A wide peak between 400 and 600 ºC is associated with surface CeO_2 reduction, and the peak between 700 and 900 ºC due to bulk CeO_2

reduction [13, 21, 22]. Focusing on the CO consumption and CO_2 formation profiles it is possible to appreciate that the signals did not return to the baseline at high temperature, indicating that either the bulk ceria reduction was not completed or that the Boudouard reaction was possibly occurring [22]. The Boudouard reaction is the disproportionation reaction where carbon monoxide oxidises and reduces simultaneously producing carbon and carbon dioxide ($2CO \rightarrow C + CO_2$) [24].

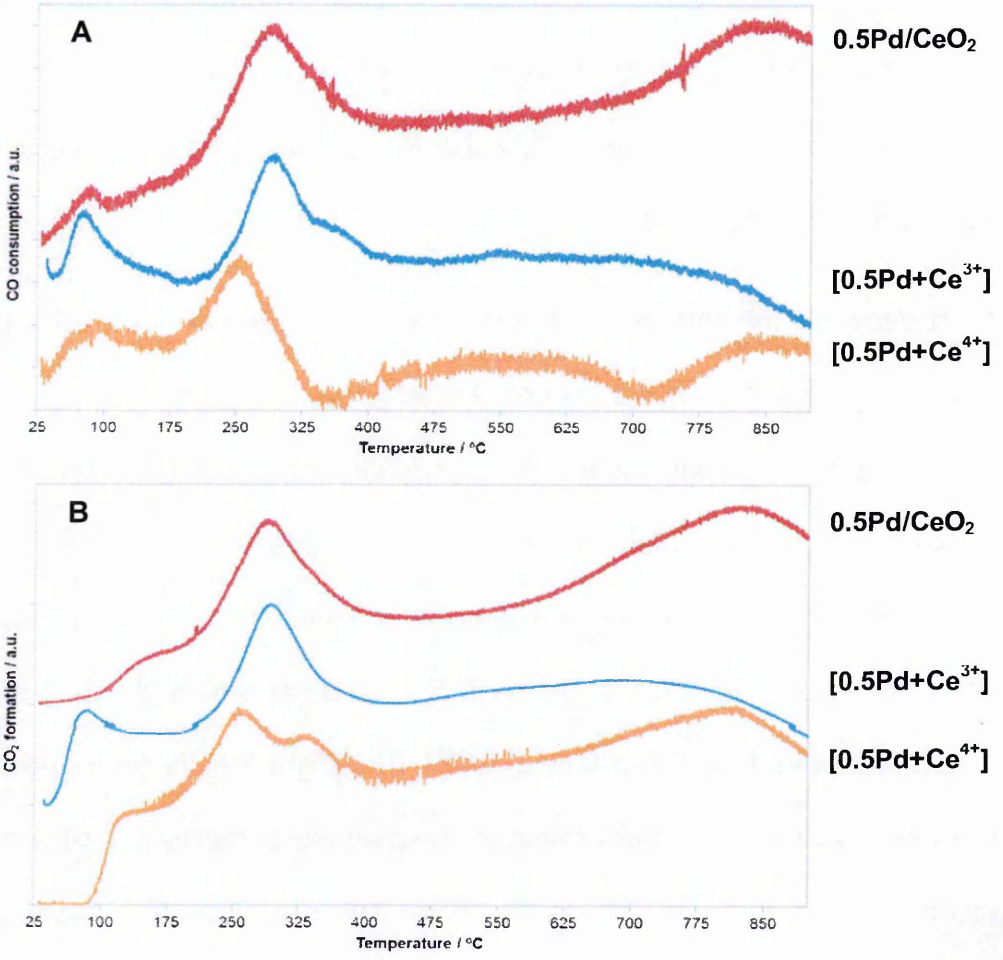

Figure 4-9: CO consumption (A) and CO_2 formation (B) during CO-TPR for 0.5Pd-CeO_2 samples prepared by impregnation (0.5Pd/CeO_2) and by co-precipitation using Ce^{3+} ([0.5Pd+Ce^{3+}]) and Ce^{4+} ([0.5Pd+Ce^{4+}]) precursors. The samples were previously pre-treated under 50 ml min^{-1} of He at 500 °C. During the CO-TPR the flow consisted in 20 ml min^{-1} of 10%CO/He in 30 ml min^{-1} of He.

Comparing the CO and CO_2 profiles, it is possible to see that initially at low temperature (< 125 °C) there was CO consumption without a consequent CO_2 formation for both 0.5Pd/CeO_2 and [0.5Pd+Ce^{4+}]. This could be due to CO

adsorption with CO remaining on the surface until the sample reached a high enough temperature for reaction. This was not the case for [0.5Pd+Ce^{3+}] which formed CO_2 simultaneously as CO was consumed.

Focusing on the CO_2 profiles, it is observed that an initial small peak at low temperature, related to PdO_x surface species, is more pronounced for [0.5Pd+Ce^{3+}] sample (at 80 ºC), indicating the presence of less stable (and therefore more reactive) PdO_x particles [21]. A similar peak appeared at higher temperature and was significantly less intense for the 0.5Pd/CeO_2 and [0.5Pd+Ce^{4+}] samples (at 120 ºC and 145 ºC, respectively). The higher the reduction temperature, the more stable the Pd-species, and therefore the more difficult they are to be reduced [13, 21].

The main peak for the reduction of surface PdO_x in contact with ceria (peak at 200-350 ºC), appeared as a single broad peak for the 0.5Pd/CeO_2 and [0.5Pd+Ce^{3+}] samples, suggesting that the particles are more homogeneous than on [0.5Pd+Ce^{4+}], which contained two overlapping peaks. The position of these peaks, based on the CO_2 profiles, appeared over a similar temperature range, with the maximum at around 290 ºC for the 0.5Pd/CeO_2 and [0.5Pd+Ce^{3+}] samples, and around 255 and 330 ºC for [0.5Pd+Ce^{4+}]. The higher temperature position for these peaks indicate either the presence of small Pd particles or/and a stronger interaction with the support [21]; in this case it is not possible to conclude the cause of the higher temperature position of the peak found for the [0.5Pd+Ce^{4+}] sample, as Pd particles could not be detected with any of the analysis performed to this point to further understand the Pd particle size and level of interaction with the ceria.

Surface ceria reduction was difficult to compare as no distinctive peaks were obtained between 400–600 ºC. In terms of bulk ceria reduction (700-900 ºC)

0.5Pd/CeO_2 and [0.5Pd+Ce^{4+}] catalysts followed a similar profile; however, [0.5Pd+Ce^{3+}] had a less well-defined peak and started at lower temperature than for the other two samples. This could suggest a better mobility of the oxygen atoms in the structure of this catalyst.

4.1.4.3. Oxygen Storage Capacity (OSC)

The total OSC for the catalysts prepared using the different methods is shown as a function of temperature in Figure 4-10.

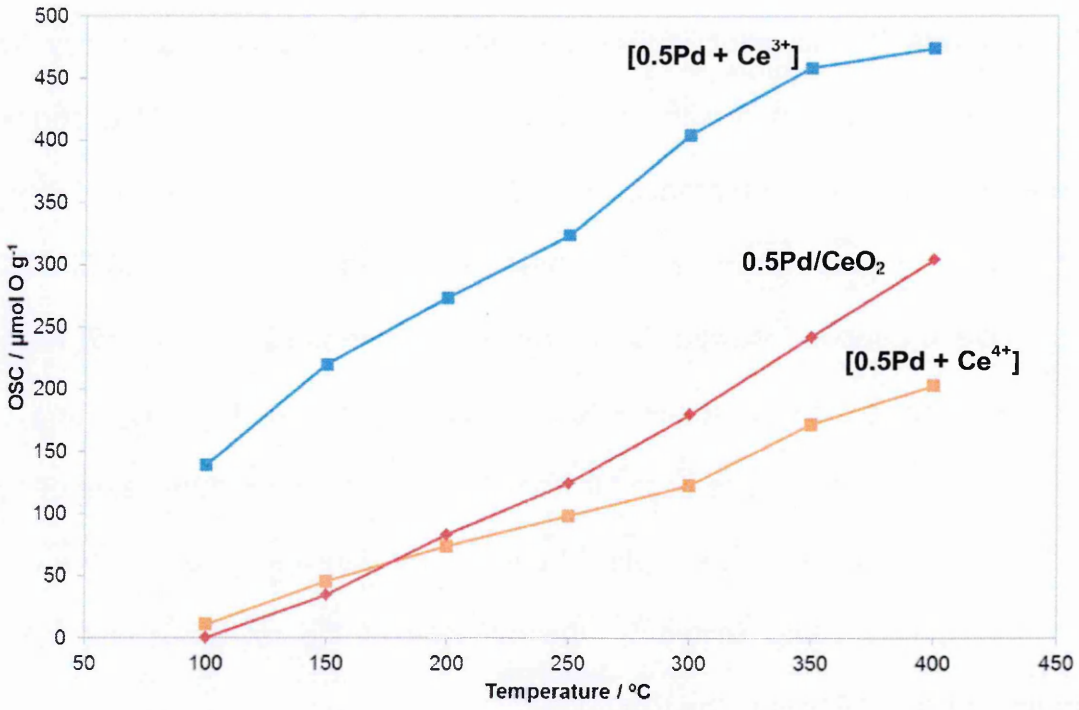

Figure 4-10: Comparison of the oxygen storage capacity of Pd-CeO_2 samples prepared by impregnation (0.5Pd/CeO_2), and by co-precipitation with Ce^{3+} ([0.5Pd+Ce^{3+}]) and Ce^{4+} ([0.5Pd+Ce^{4+}]) precursors. The OSC measurement was performed alternating switches between O_2 (10 ml min^{-1} of 5 %O_2/He) and CO (10 ml min^{-1} of 10 %CO/He) using He as a carrier gas (90 ml min^{-1}) at steady state temperatures. OSC instrument average standard error = ± 8 µmol O g^{-1}.

All the samples showed a similar curve with the OSC increasing with increasing temperature. The best performance was seen for the [0.5Pd+Ce^{3+}] preparation, and the worst for [0.5Pd+Ce^{4+}], although this last was not very different to the impregnated catalyst, especially at lower temperature. The improvement showed

by [0.5Pd+Ce^{3+}] was noticeable over the whole temperature range tested here (100-400 ºC).

Ceria efficiency, without the contribution of Pd, was calculated for each sample as described in *Appendix 2*. The values below 350 ºC should only be taken as qualitative information, as it was assumed that all palladium existed as PdO and that complete oxidation of PdO occurred in this range of temperature. The catalysts were also compared to a 0.5Pd/CeO_2 catalysts prepared by impregnation on a commercial CeO_2[8]. The results can be found in Table 4-4.

At 100 ºC, 0.5Pd/CeO_2 and [0.5Pd+Ce^{4+}] did not show any OSC, therefore their efficiency was 0%; however, [0.5Pd+Ce^{3+}] showed 3.4% of ceria efficiency. These values can be correlated with the results obtained from CO-TPR experiments, where it was seen that the production of CO_2 on the 0.5Pd/CeO_2 and [0.5Pd+Ce^{4+}] samples did not start until ~125 ºC, whilst this started at ~50 ºC for [0.5Pd+Ce^{3+}]. The efficiency trends followed those obtained for the OSC values, with the most efficient sample being [0.5Pd+Ce^{3+}], followed by 0.5Pd/CeO_2 and then [0.5Pd+Ce^{4+}]. These values were far from 100%, with a maximum value of 15.0% at 400 ºC for [0.5Pd+Ce^{3+}] sample. These low efficiencies are due to the oxygen storage capacity being limited by the diffusion of the oxygen either from the surface or from the bulk of the CeO_2 [25].

Compared to a commercial sample, which was based on 0.5 wt% Pd impregnated on a CeO_2 support supplied by Rhodia, the [0.5Pd+Ce^{3+}] sample still showed a higher ceria efficiency, giving proof of the advantages of this preparation technique over the commonly used impregnation method to obtain a better OSC.

[8] CeO_2 support supplied by Rhodia.

Table 4-4: Ceria efficiency (%) during the OSC test, comparing 0.5Pd-CeO_2 samples prepared by impregnation on a precipitated and on a commercial CeO_2 support (0.5Pd/CeO_2), and by co-precipitation using Ce^{3+} ([0.5Pd+Ce^{3+}]) and Ce^{4+} ([0.5Pd+Ce^{4+}]) precursors.

Temperature / °C	0.5Pd/CeO_2	[0.5Pd+Ce^{3+}]	[0.5Pd+Ce^{4+}]	0.5Pd/ CeO_2 (commercial support)
100	0	3	0	1
200	1	8	1	6
300	5	13	3	8
400	9	15	6	9

4.1.5. Kinetic characterisation: CO-SSITKA

Steady-state isotopic transient kinetic analyses (SSITKA) were performed in order to determine *in situ* kinetic information about the CO oxidation reaction in a simple gas mixture of CO and O_2. The comparison of the reaction rate (r) at different temperatures gives information on how fast the sample can perform the reaction. In addition, the results can also be represented as turnover frequency (TOF) which gives information about the generation rate of product (CO_2 in this case) per catalyst-surface site [26]. The number of surface-sites is usually calculated as μmol of CO per gram of sample using the CO chemisorption method. However, as this method is not suitable for Ce-based materials, due to the extra CO adsorption at the Pd-Ce interface, the TOF was not used here.

The CO oxidation over Pd/CeO_2 has been widely reported in literature [27-30]. On the materials studied here, the CO oxidation could have occurred through three different pathways [27, 28]:

1. CO and O_2 competing for their adsorption on Pd sites, and reacting once adsorbed, this last step being the rate determining step (rds) (Langmuir-Hinshelwood mechanism):

$CO_{(g)} \rightleftharpoons CO_{(ads)}$

$O_{2(g)} \rightleftharpoons 2O_{(ads)}$

$CO_{(ads)} + O_{(ads)} \xrightarrow{rds} CO_{2(ads)} \xrightarrow{fast} CO_{2(g)}$

2. CO in the gas phase reacting with an oxygen atom that had been previously adsorbed on Pd (Eley-Rideal mechanism):

$O_{2(g)} \rightleftharpoons 2O_{(ads)}$

$CO_{(g)} + O_{(ads)} \xrightarrow{rds} CO_{2(ads)} \xrightarrow{fast} CO_{2(g)}$

3. CO adsorbed on Pd reacting with the oxygen from CeO_2. In this case the rate determining step would be also determined by the oxygen diffusion from the support:

$CO_{(g)} \rightleftharpoons CO_{(ads)}$

$CO_{(ads)} + O_{(support)} \xrightarrow{rds} CO_{2(ads)} \xrightarrow{fast} CO_{2(g)}$

The rate coefficient of CO desorption from Pd sites has been reported to occur around 207 ºC [27]. Consequently, as the kinetic experiments were performed at a lower temperature, the oxygen adsorption rate on Pd sites (involved in *pathways 1 and 2*) could be lowered due to Pd sites being blocked by non-reacted CO [27, 28]. In the case of *pathway 3*, the reaction between CO adsorbed on Pd and the oxygen from the support mainly depends on oxygen diffusivity to the surface of the CeO_2, thus the diffusion of this oxygen will be the limiting step during this mechanism [27, 28].

Figure 4-11 compares the reaction rates of the co-precipitated and impregnated Pd samples. It can be seen that the [0.5Pd+Ce^{3+}] sample had the fastest reaction rate and [0.5Pd+Ce^{4+}] the slowest.

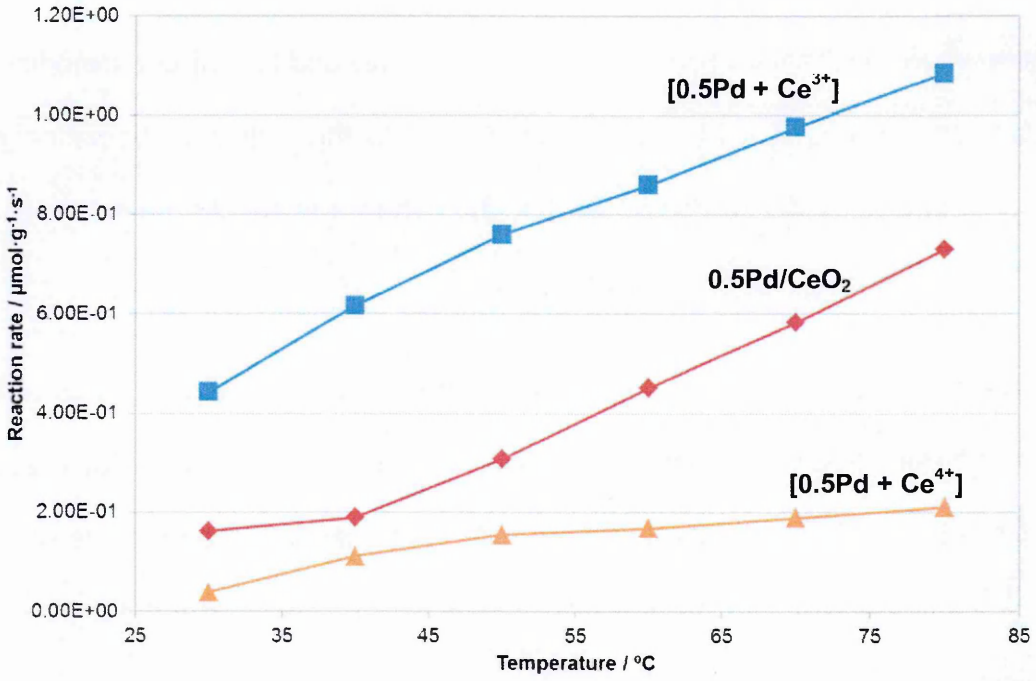

Figure 4-11: Comparison of the CO oxidation reaction rate measured at steady state temperatures for 0.5Pd-CeO_2 samples prepared by impregnation (0.5Pd/CeO_2) and by co-precipitation using Ce^{3+} ([0.5Pd+Ce^{3+}]) and Ce^{4+} ([0.5Pd+Ce^{4+}]) precursors. The gas flows used were 52.5 ml min^{-1} of 5% O_2/He, 5.5 ml min^{-1} of 1%CO/5%Ar/He (^{12}C) and 5.5 ml min^{-1} of 1%CO/He (^{13}C). The average reaction rate standard error was ±0.01 µmol g^{-1} s^{-1}.

Based on the characterisation results reported previously it was suggested that the oxygen diffusivity to the surface of the CeO_2 occurred faster for the [0.5Pd+Ce^{3+}] co-precipitated material than for the impregnated catalyst (sharp reduction peaks during H_2-TPR, CO_2 formation during CO-TPR at the lowest temperatures, higher OSC), thus *pathway 3* is likely to have been of greater importance for this sample. As samples 0.5Pd/CeO_2 and [0.5Pd+Ce^{3+}] had similar CO adsorption (based on CO chemisorption analyses), the better oxygen mobility in [0.5Pd+Ce^{3+}] will explain the faster reaction rate obtained for this co-precipitated sample. The lowest

reaction rate observed for [0.5Pd+Ce^{4+}] is suspected to be associated to a significantly lower Pd surface content than on the other two samples.

Previous reported studies on supported noble metals (Pd, Rh, and Pt) on Al_2O_3 have determined that the mechanism for CO oxidation with O_2 follows a Langmuir-Hinshelwood mechanism (*pathway 1*); however the addition of ceria modifies this mechanism making it a bi-modal system, due to the active participation of the oxygen from the ceria (*pathway 3*) [31, 32]. Thus, the results found here agree with previous studies reported in literature.

The reaction order was also calculated by running CO-ITK experiments at 80 °C using different [CO]:[O_2] ratios. To calculate the reaction order with respect to [CO], the [O_2] was left constant and the [CO] was modified; the opposite was done to calculate the reaction order with respect to [O_2]. For further details refer to *Appendix 3*.

The reaction orders for all the catalysts appeared to be 0 with respect to oxygen concentration, and between 0.8 – 1 with respect to CO (1 for the 0.5Pd/CeO_2 and [0.5Pd+Ce^{3+}] samples, and 0.8 for the [0.5Pd+Ce^{4+}] catalyst). The zero O_2 reaction order indicated that the concentration of O_2 did not have an impact on the reaction rate, which suggests that *pathways 1 and 2* occurred to a lower extent than *pathway 3*. This agrees with published studies, where it is explained that the active involvement of the oxygen from ceria has a greater participation and enhances the bi-modal mechanism (*pathway 3*) [27, 31, 32]. With respect to [CO], the lower reaction order found for the [Pd+Ce^{4+}] sample could be related to the lower availability of surface active sites in this sample.

Table 4-5: Estimated equation rates of CO oxidation reaction and activation energies for 0.5Pd-CeO_2 catalysts prepared by impregnation (0.5Pd/CeO_2) and by co-precipitation using Ce^{3+} ([0.5Pd+Ce^{3+}]) and Ce^{4+} ([0.5Pd+Ce^{4+}]) precursors. The standard errors for E_a are shown between brakets next to the values.

Sample	Equation rate	E_a / kJ mol^{-1}
0.5Pd/CeO_2	$r = k$ [CO]	27 (± 2)
[0.5Pd+Ce^{3+}]	$r = k$ [CO]	11 (± <1)
[0.5Pd+Ce^{4+}]	$r = k$ [CO]$^{0.8}$	9 (± <1)

The activation energies (E_a) calculated for the co-precipitated samples were similar (11 and 9 kJ mol^{-1} for [0.5Pd+Ce^{3+}] and [0.5Pd+Ce^{4+}], respectively), which were also significantly lower than the E_a calculated for the impregnated sample 0.5Pd/CeO_2 (27 kJ mol^{-1}). The lower E_a found for the co-precipitated materials could be associated with a higher Pd-Ce interaction which would allow faster oxygen transfer. The lower E_a also found for the [0.5Pd+Ce^{4+}] catalysts, besides the low Pd surface content on this catalyst, suggests that also here Pd and Ce atoms are in greater contact than for the impregnated sample, allowing an easier transfer of the reactants between the ceria and the Pd. Thus, based on these results it could be concluded that the co-precipitation method improves Pd and Ce contact, independently of the Ce-precursor used. However, the precursor seems to have an impact on the Pd surface area, and this will greatly affect the overall reaction rate (the lower Pd surface content, the lower the reaction rate).

It was noticed that the temperature coefficient[9] was below 2. This is due to the rate of the inversed reactions (desorption reactions) increasing with temperature, thus having a negative impact on the overall reaction rate.

[9] Increase of reaction rate with each 10 ºC increase. Typically the temperature coefficient is 2, which means that the reaction doubles with each 10 ºC increase.

4.1.6. Light-off performance

The aim of this work was to understand and improve the catalytic activity related to the ceria component of a TWC; therefore it was necessary to measure the activity of the samples prepared in this study. This was done by testing the catalysts under two different conditions. For the first test, the samples were tested under a continuous gas mix (constant $\lambda = 0.95$), reproducing the gas composition to which the catalyst is exposed during the start-up of some engines. For the second test, the samples were tested under perturbed conditions ($\lambda \pm 0.05$) to reproduce realistic driving conditions. For the first test the activity mainly depends on the number of active sites and the pollutant adsorption strength, whilst for the second test the OSC properties of the catalyst are also highly important.

4.1.6.1. Cold-start conditions

The light-off performance of these catalysts was measured under 'cold start' gas mix conditions from 100 to 400 °C. The HC, NO_x[10] and CO conversions can be seen in Figure 4-12 for all three catalysts. The sample prepared by the co-precipitation of [0.5Pd+Ce^{3+}] showed a small improvement in the CO light-off performance compared to that of the catalyst prepared by the impregnation method, reducing by 14 °C the necessary temperature for 50% CO conversion (T50). The NO_x and HC light-offs however showed little difference. The small improvement seen during the CO light-off agrees with the results seen in section 4.1.5. where it was shown that the CO oxidation rate was faster for the [0.5Pd+Ce^{3+}] than for 0.5Pd/CeO_2, despite having a lower Pd surface content (based on EtOH-TPSR results). The larger contribution of the interface Pd-Ce

[10] The products obtained from the NO_x conversion during this test and the following presented in this work were mainly N_2, NH_3 and N_2O.

sites apparent in the [0.5Pd+Ce^{3+}] sample allowed an easier oxygen transfer which improved CO oxidation kinetics, and therefore its light-off.

Contrary to this, the sample prepared by the co-precipitation of [0.5Pd+Ce^{4+}] showed a significantly lower performance (T50 > 400 °C) than the other catalysts. The lower performance of [0.5Pd+Ce^{4+}] was mainly due to the lower number of active sites, as shown by the characterisation [33, 34].

Table 4-6 shows a summary of the necessary temperatures to achieve 50% conversion for CO, NO_x, and HC, for the 0.5Pd-CeO_2 catalysts prepared by the different methods:

Table 4-6: Necessary temperature for 50% conversion of CO, NO_x and HC during a light-off test under constant lambda at 0.95, for 0.5Pd-CeO_2 catalysts prepared by impregnation (0.5Pd/CeO_2) and by co-precipitation using Ce^{3+} ([0.5Pd+Ce^{3+}]) and Ce^{4+} ([0.5Pd+Ce^{4+}]) precursors. Light-off instrument average standard error = ± 2 °C.

Sample	CO T50 / °C	NO_x T50 / °C	HC T50 / °C
0.5Pd/CeO_2	242	257	327
[0.5Pd+Ce^{3+}]	228	252	327
[0.5Pd+Ce^{4+}]	> 400	> 400	> 400

It was observed that CO conversion initially increased, but after ~280 °C this started to decrease. This is due to the lack of available oxygen to complete both CO and HC oxidation reactions which are in competition (see *Appendix 4*).

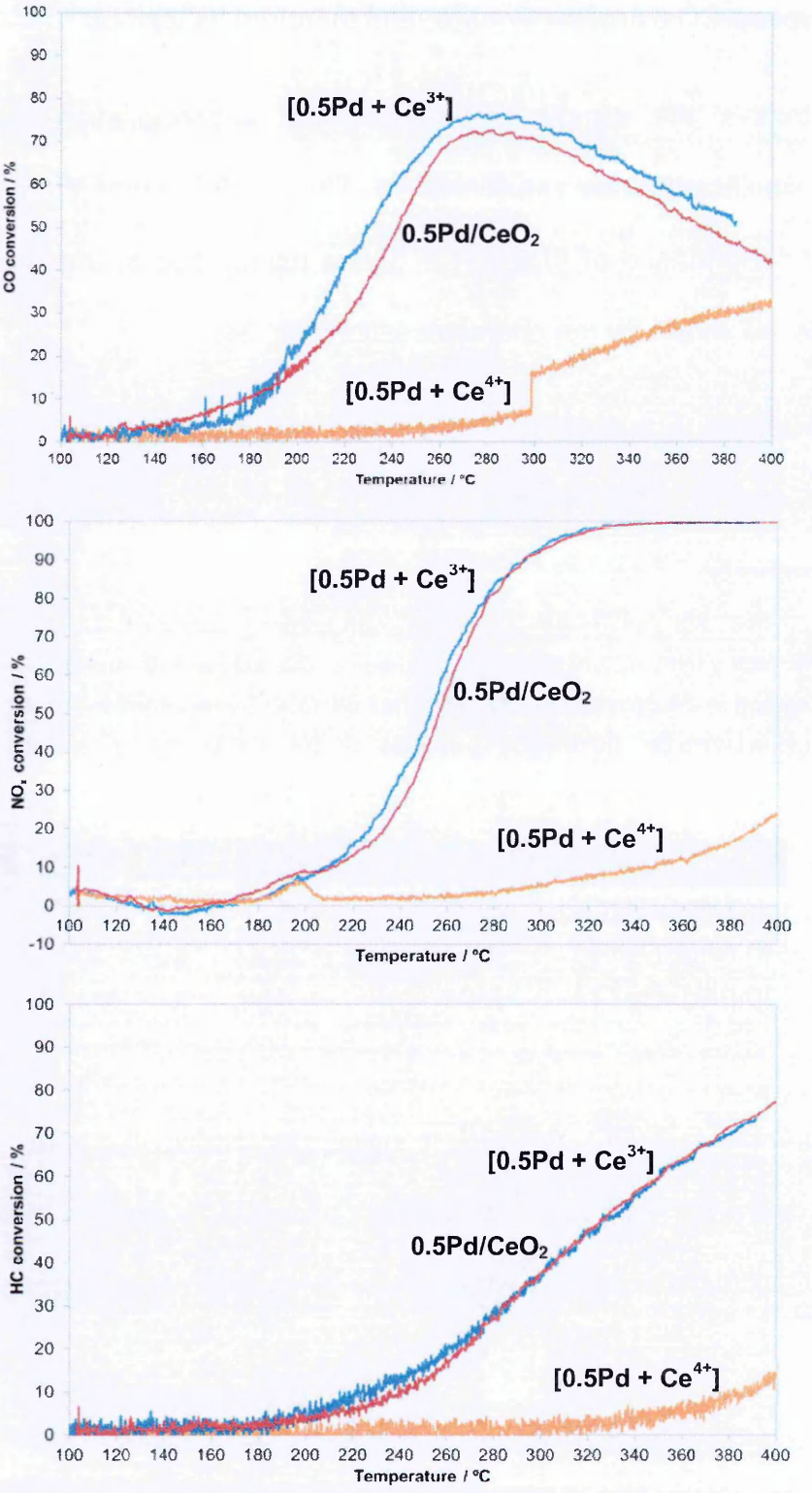

Figure 4-12: From top to bottom, CO, NO_x and HC light-off performance under constant lambda at 0.95 of 0.5Pd-CeO_2 catalysts prepared by impregnation (0.5Pd/CeO_2) and by co-precipitation using Ce^{3+} ([0.5Pd+Ce^{3+}]) and Ce^{4+} ([0.5Pd+Ce^{4+}]) precursors. The sample taken was 0.4 g (0.2 g sample + 0.2 g cordierite) and the gas flow rate 2 L min^{-1}. The catalyst was heated using a ramp rate of 10 °C min^{-1} from 100 to 400 °C.

4.1.6.2. Perturbed light-off

In a real system the catalyst will be also exposed to oscillations around lambda 1, and it is under these conditions that the OSC properties take more importance. For these reasons, the best catalysts ($0.5Pd/CeO_2$ and [$0.5Pd+Ce^{3+}$]) were also submitted to a perturbed test at lambdas 0.99 ± 0.05 (rich average lambda) and 1.01 ± 0.05 (lean average lambda), using 6 second cycles[11] (0.17 Hz). The conversion trends can be seen in Figure 4-13, and a summary of T50 values in Table 4-7.

It can be seen that [$0.5Pd+Ce^{3+}$] showed an improved light-off performance compared to $0.5Pd/CeO_2$ under all conditions. The difference was especially noticeable at the rich average lambda (0.99 ± 0.05). Under average rich conditions the T50 for [$0.5Pd+Ce^{3+}$] was 40 ºC lower for NO_x, 54 ºC lower for CO, and 19 ºC lower for HC compared to the values for $0.5Pd/CeO_2$; under average lean conditions T50 was 24 ºC lower for NO_x, 21 ºC lower for CO, and 19 ºC lower for HC. The better performance of [$0.5Pd+Ce^{3+}$] largely reflects the higher OSC of this catalyst compared to $0.5Pd/CeO_2$, as was discussed in section 2.1.2.

Table 4-7: Necessary temperature for 50% conversion of CO, NO_x and HC under perturbed conditions for 0.5Pd-CeO_2 catalysts prepared by impregnation ($0.5Pd/CeO_2$) and by co-precipitation using Ce^{3+} ([$0.5Pd+Ce^{3+}$]) and Ce^{4+} ([$0.5Pd+Ce^{4+}$]) precursors. Light-off instrument average standard error = ± 2 ºC.

	Lambda 0.99 ± 0.05			Lambda 1.01 ± 0.05		
	NO_x T50 / ºC	CO T50 / ºC	HC T50 / ºC	NO_x T50 / ºC	CO T50 / ºC	HC T50 / ºC
$0.5Pd/CeO_2$	238	248	253	230	206	222
[$0.5Pd+Ce^{3+}$]	194	198	234	185	206	203

[11] 1 cycle is considered [3 sec rich – 3 sec lean] switches.

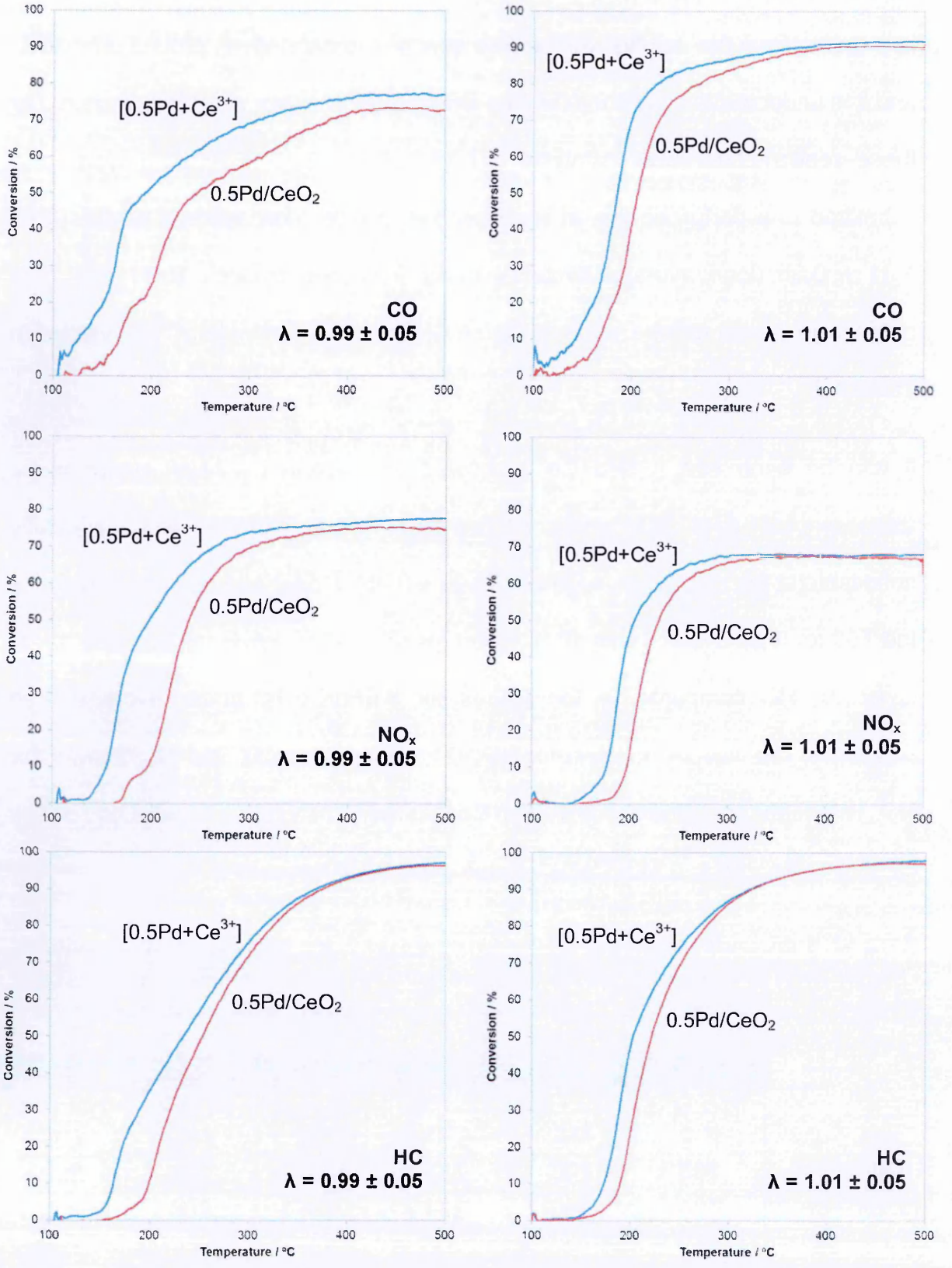

Figure 4-13: Light-off performance under perturbed conditions for 0.5Pd-CeO_2 catalysts prepared by impregnation (0.5Pd/CeO_2) and by co-precipitation using Ce^{3+} ([0.5Pd+Ce^{3+}]) precursor. From top to bottom, CO, NO_x and HC conversions; from left to right, light-offs at lambdas 0.99 ± 0 .05 and 1.01 ± 0.05. The sample size taken was 0.4 g (0.2 g sample + 0.2 g cordierite) and the gas flow rate 5 L min^{-1}. The catalyst was heated using a ramp rate of 10 °C min^{-1} from 110 to 500 °C.

4.1.7. Summary

Co-precipitation with a Ce^{4+} precursor resulted in a catalyst with poor surface area and little Pd surface content. The poor surface area obtained is suspected to be related to a higher agglomeration, which is believed to occur as a consequence of a higher supersaturation during the preparation of this sample [8]. ICP analyses also confirmed that this sample contained 0.38 wt% Pd instead of the theoretical Pd content calculated for this preparation (0.5 wt% Pd). The loss of Pd is suspected to be a consequence of small amounts of $Pd(OH)_2$ re-dissolving in water during the washes of the precipitate, however the supernatant of the filtrations was not analysed and this could not be concluded [9-11]. In addition, the Pd surface area of this material appeared to be even lower than that of a samples containing 1.5 times less Pd ($0.25Pd/CeO_2$) prepared by impregnation, suggesting that the loss of Pd surface area was not entirely related to the lower Pd content. Thus, it is likely that this preparation led to deeper encapsulation of the Pd particles by the ceria. It is also believed that the lower Pd surface area of this sample was not due to an increase of Pd particle size, as not shift towards lower temperature of the Pd-Ce reduction peak was detected during H_2-TPR experiments, compared to the $0.5Pd/CeO_2$ sample [3, 20]. The poor surface area and the low number of active sites on the surface resulted in poor catalytic performance in terms of light-off, pollutant conversion and OSC [33]. However, the sharp Pd-Ce reduction peak seen during H_2-TPR experiments and the lower E_a found for the CO oxidation reaction for this sample (compared to the $0.5Pd/CeO_2$ sample) suggests that there is an intimate contact between Pd and Ce atoms, which will facilitate the oxygen transfer [17].

In contrast, the catalyst prepared with the Ce^{3+} precursor showed a slightly better catalytic activity under cold-start conditions than an impregnated sample

($0.5Pd/CeO_2$) with the same Pd loading, and a significant improvement under perturbed conditions. XPS and TPR results showed that there was a significantly higher Pd-Ce interaction in this sample (XPS peaks shifted towards higher eV, sharp reduction peaks and higher H_2 consumption during H_2-TPR), which explains the important increase in the observed OSC and the consequent higher performance of the perturbed light-off [35, 36]. The lower E_a found for this sample was also a sign of the better oxygen transfer between the support and the palladium, due to a better Pd-Ce contact. Since the dispersion and metal surface area (based on CO chemisorption) of [$0.5Pd+Ce^{3+}$] only showed a small decrease compared to the impregnated $0.5Pd/CeO_2$ catalyst, the calculated XPS Ce:Pd atomic ratio was only slightly larger, and there was no shift in the Pd-Ce reduction peak towards lower temperature during H_2-TPR, it is concluded that the small decrease of Pd surface area is possibly due to some level of ceria encapsulation and not to an increase of Pd particle size. The supposed encapsulation obtained with the co-precipitation of Pd^{2+} with Ce^{3+} precursor seems to be partial or as a thin layer of CeO_2, where the pollutants and the oxygen atoms could still have access to the palladium particles. The higher Pd-Ce interaction seen in this sample is believed to be related to a larger number of Pd and Ce atoms in contact due to this partial encapsulation [17]. A higher number of Pd and Ce atoms in contact also means an increase in the number of Pd-Ce interface sites, which are the most active species for TWC reactions [2].

To conclude, the co-precipitation method for $0.5Pd-CeO_2$ sample preparation have shown to produce products with higher Pd-Ce contact, independently of the Ce-precursor. However, the choice of the Ce-precursor was seen to greatly impact the level of Pd in the sample, as well as its surface content, with Ce^{3+} leading to larger Pd surface areas than the Ce^{4+} precursor.

4.2. Pd-CeO_2 based catalysts: impact of the Pd loading

One of the limitations of the impregnation method is that when preparing catalysts with extremely low noble metal loadings (< 0.5 wt%), the dispersion obtained is so high that the particles finish locked in a less reactive state [1].

The co-precipitation method was extended to prepare a range of catalysts with different Pd loadings. Samples with loadings 0.25, 0.5, 0.75, 1 and 5 wt% Pd were prepared using the co-precipitation method with the Ce^{3+} precursor (which will be referred as [Pd+Ce^{3+}]). These samples were compared to same loaded samples prepared by wet impregnation (referred here as Pd/CeO_2).

4.2.1. Structural characterisation

Previously (section 4.1.2.1.), it was shown that compared to 0.5Pd/CeO_2 and [0.5Pd+Ce^{4+}], the [0.5Pd+Ce^{3+}] sample appeared to show a small lattice contraction; however, this contraction was too small to conclude that Pd was incorporated in the ceria structure. This may reflect the low loading of Pd in the initial catalyst (0.5 wt%), thus samples with higher Pd loadings were analysed by this method.

4.2.1.1. X-Ray Diffraction (XRD)

The samples with different Pd loadings prepared by the co-precipitation of [Pd+Ce^{3+}] were analysed by XRD. The lattice parameter *a* and the ceria crystallite size values are summarised in Table 4-8. As with the previous preparations, all the samples were formed of a cubic CeO_2 structure and no information regarding palladium could be obtained [7]. The diffraction patterns can be seen in Figure 4-14.

Table 4-8: Lattice parameter *a* and ceria crystallite size analysed by XRD, and specific surface area calculated by BET of Pd samples prepared by co-precipitation with Ce^{3+} precursor. Calculated errors for ceria crystallite size are reported in brackets; BET-SSA instrument standard error = ± 4 $m^2 g^{-1}$.

	a lattice parameter / Å	Crystallite size / nm	BET-SSA / $m^2 g^{-1}$	ICP / Pd wt%
CeO_2 XRD Reference [7]	5.411	-	-	-
[0.25Pd+Ce^{3+}]	5.408	4.59 (± 0.06)	131	0.21
[0.5Pd+Ce^{3+}]	5.409	5.51 (± 0.05)	114	0.51
[0.75Pd+Ce^{3+}]	5.407	4.62 (± 0.06)	145	0.81
[1Pd+Ce^{3+}]	5.415	5.75 (± 0.09)	106	1.06
[5Pd+Ce^{3+}]	5.421	4.87 (± 0.07)	131	4.91

A slight contraction in the lattice parameter was observed for those samples prepared by co-precipitation containing up to 0.75 wt% Pd. However, the contraction was not significant enough to determine definitely if there was any palladium incorporation into the ceria structure.

At higher palladium loadings (1 and 5 wt%) no shift to lower angles was apparent; in fact the lattice parameter values increased with increasing Pd loading (increase of 0.06% and 0.19% for 1 and 5 wt% Pd, respectively). This has been reported by other authors [37-40] who suggest that the lattice constant for small particle sizes (< 5 nm) can increase due to having a larger surface-to-volume ratio. Due to the small crystallite size the bonds Ce-O are too restricted, forcing the formation of oxygen vacancies to ease the space and consequently forming Ce^{3+} ions, which are bigger in size than Ce^{4+} [37-40]. However, the crystallite sizes obtained here were similar for all the samples (between 4.5-5.7 nm) thus it was not understood why this only occurred at higher Pd loadings.

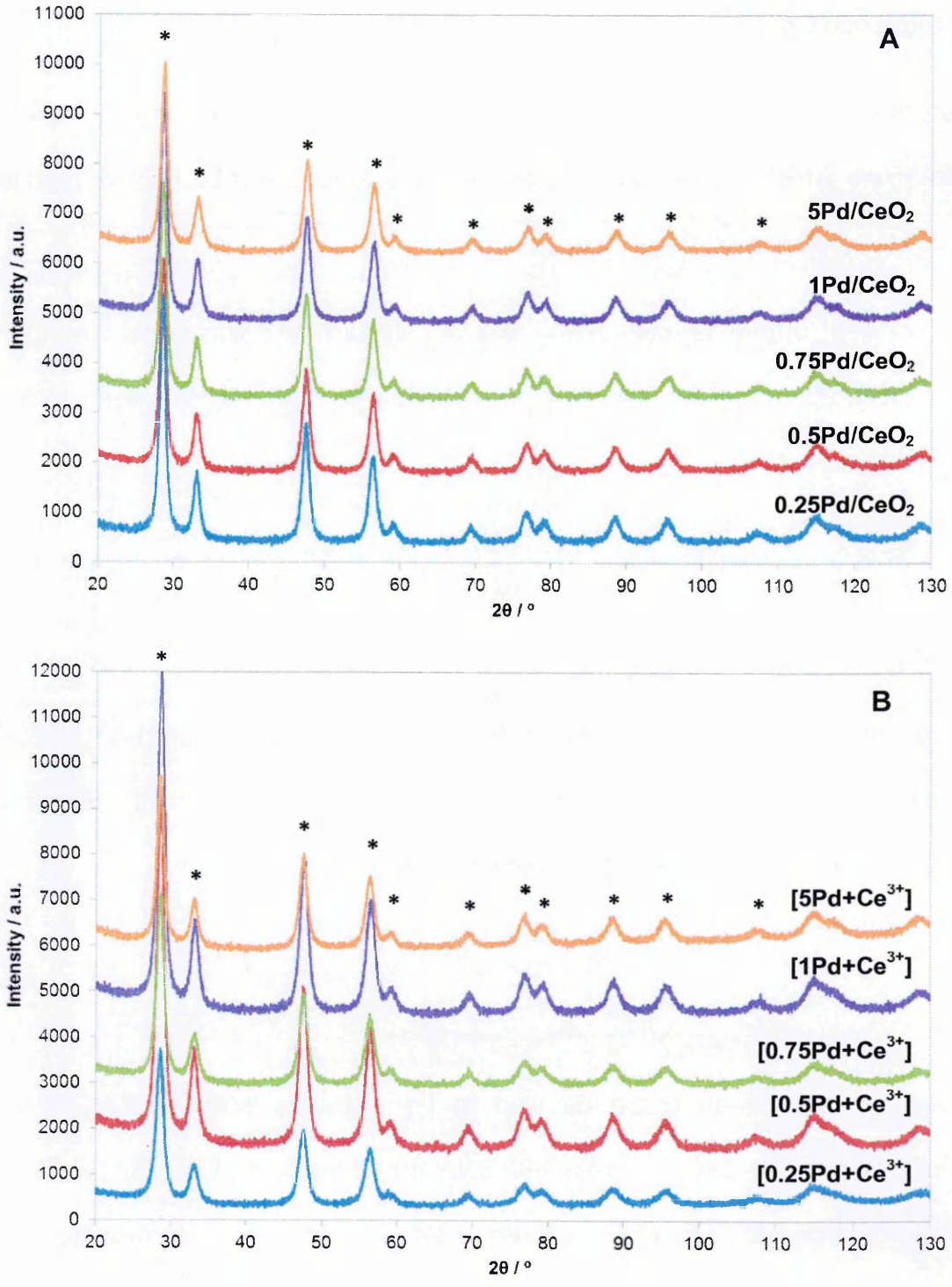

Figure 4-14: XRD patterns of Pd-CeO_2 samples with different loadings prepared by impregnation (A) and by co-precipitation with Ce^{3+} precursor (B). The peaks corresponding to the cubic CeO_2 phase are indicated as (*).

By contrast, in the case of the samples prepared by impregnation with equivalent Pd loading, the lattice parameter was essentially constant and agreed with that of the reference CeO_2.

There was no evidence of palladium particles even at higher loadings for either set of catalysts, which shows that the preparation methods described above both lead to extremely dispersed Pd particles.

As the extent of the cell contraction was not significant, it was concluded for the co-precipitated materials that there is no evidence that Pd has been included within the ceria lattice.

4.2.2. Surface characterisation

The change of the Pd particle size with Pd loading was monitored by XPS, CO chemisorption and EtOH-TPSR. The aim of this study was to quantify Pd surface area, as well as to define levels of interaction with ceria.

4.2.2.1. X-Ray Photoelectron Spectroscopy (XPS)

Similar conclusions to those detailed in the previous section (4.1.3.1) were obtained for the Pd-CeO_2 samples with different Pd loadings. CeO_2 and PdO were the main species present in both sets of samples (impregnated and co-precipitated), as shown in Figure 4-15 and Figure 4-16.

For the Ce3d spectra (Figure 4-15) CeO_2 can be identified as the main cerium species present in all these catalysts [14]. As seen previously, around 15-20 % of Ce^{3+} was also present in all the samples, possibly due to the reduction of Ce^{4+} induced by the X-ray beam [15]. The presence of Ce^{4+} as the main species

suggests that the majority of the cerium added during the co-precipitation preparation is oxidised during the calcination.

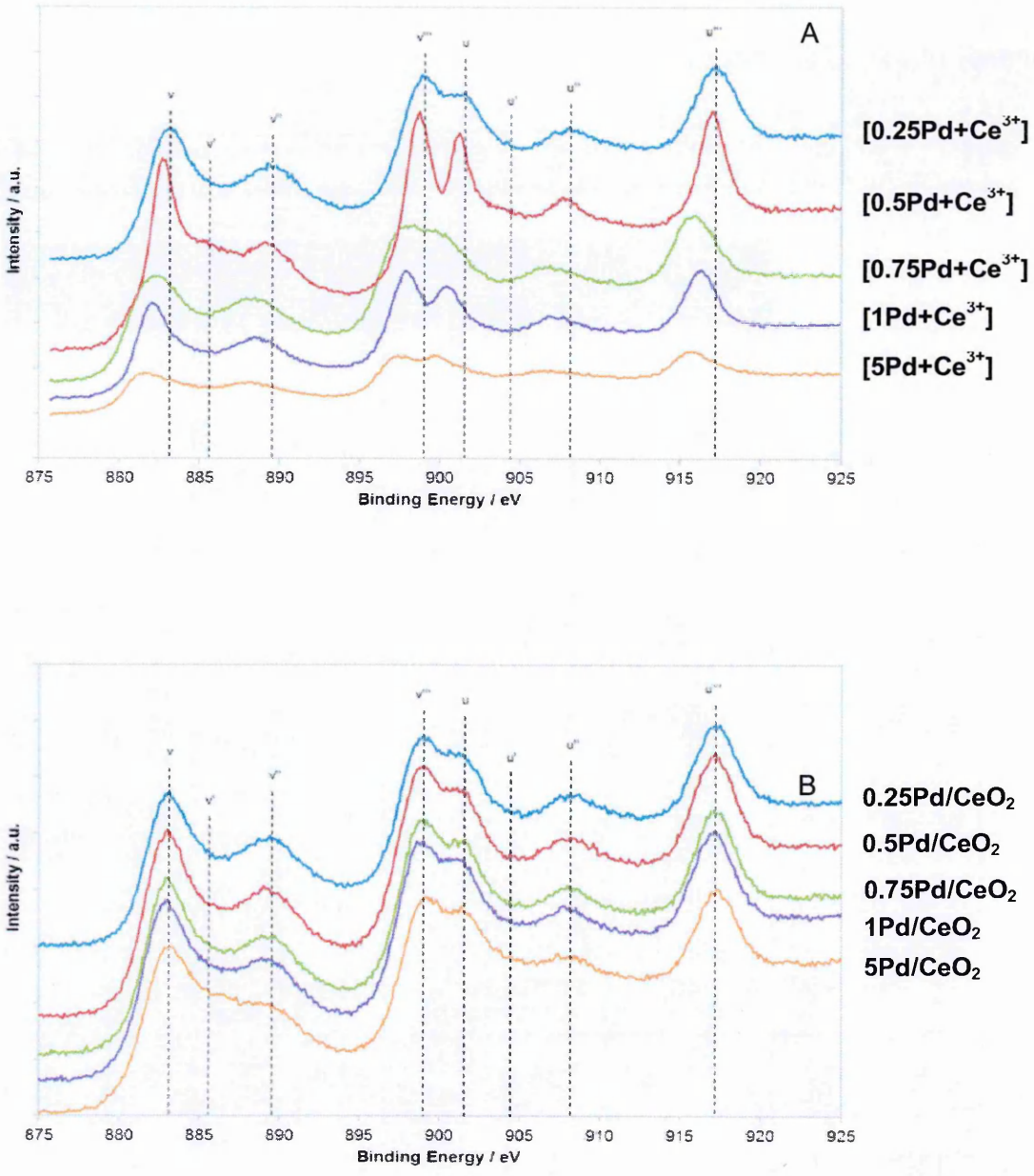

Figure 4-15: Ce3d XPS spectra. Comparison of Pd-CeO_2 samples with different Pd-loadings prepared by co-precipitation with Ce^{3+} precursor (A) and by wet impregnation (B). The bands u, v, u'', v'', u''' and v''' are related to Ce^{4+} species, whilst u' and v' are assigned to Ce^{3+}.

The palladium signal was poor for some samples due to the low amounts of palladium on the surface (i.e. 0.25 wt% Pd). The samples prepared by co-precipitation with Ce^{3+} showed bands corresponding to Pd-species with higher

oxidation states, associated with palladium species strongly interacting with ceria [13]. However, these bands were not present on those samples prepared by impregnation.Table 4-9 summarises the Pd species found in each of the catalysts, with their percentage based on total surface palladium calculated. The binding energy of the position of the bands is also detailed:

Table 4-9: Percentage of Pd-species found in the catalysts with different Pd-loadings prepared by wet impregnation (Pd/CeO_2) and by co-precipitation with Ce^{3+} precursor ([Pd+Ce^{3+}]) determined using XPS.

	Ce/Pd atomic ratio	Pd metal		Pd(II)		Pd(IV)	
Sample	a.u.	%	eV	%	eV	%	eV
[0.25Pd+Ce]	107.7	**0**	-	**100**	337.7 343.0	**0**	-
0.25Pd/CeO_2	67.0	**0**	-	**100**	337.7 343.0	**0**	-
[0.5Pd+Ce]	53.6	**0**	-	**51.8**	337.3 342.5	**48.2**	338.3 343.5
0.5Pd/CeO_2	34.1	**0**	-	**100**	337.6 342.9	**0**	-
[0.75Pd+Ce]	47.5	**0**	-	**44.2**	337.7 343.0	**55.8**	339.5 344.8
0.75Pd/CeO_2	29.9	**14.2**	336.5 341.8	**85.8**	337.8 343.0	**0**	-
[1Pd+Ce]	46.2	**0**	-	**100**	337.9 343.2	**0**	-
1Pd/CeO_2	25.5	**16.6**	336.3 341.9	**83.4**	337.6 343.0	**0**	-
[5Pd+Ce]	13.2	**23.4**	336.6 341.8	**76.6**	337.5 342.8	**0**	-
5Pd/CeO_2	10.6	**50.7**	336.2 341.5	**49.3**	337.9 343.1	**0**	-

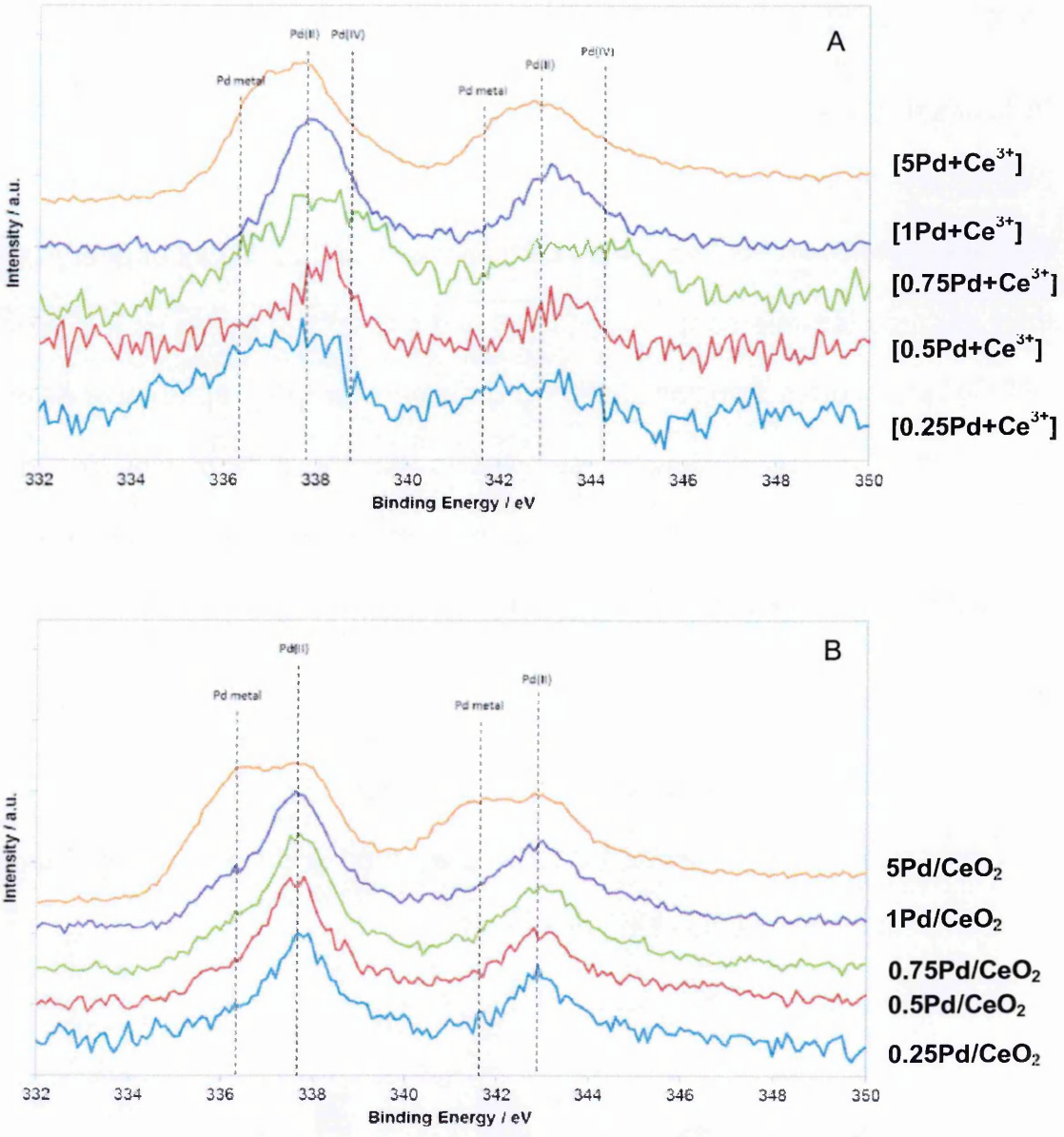

Figure 4-16: Pd3d XPS spectra. Comparison of Pd-CeO_2 samples with different Pd-loadings prepared by co-precipitation with Ce^{3+} precursor (A) and by wet impregnation (B). The vertical lines point the position of the different Pd species detected.

For the samples prepared by co-precipitation, the majority of Pd peaks were associated with Pd^{2+} and Pd^0 species [14]. It was also possible to notice an increase of the metallic Pd species when increasing Pd loading, likely due to an increase of Pd particle size. In addition, for the samples with low Pd loadings (0.5, and 0.75 wt%), there were also bands associated with higher Pd oxidation states,

contributing to the suggestion of a highly strong Pd-Ce interaction in these samples [13, 16].

In contrast, the samples prepared by impregnation did not show any shift in the binding energy with increasing Pd loading. The band with the maximum intensity was associated with Pd^{2+} species, which appeared shifted to higher energy values than the reported reference value (336.8 and 342.06 ± 0.2 eV), as it is typical in NM-CeO_2 supported samples due to Pd-Ce interaction [13, 16]. Another difference compared to the co-precipitated samples is the presence of metallic Pd from loadings as low as 0.5 wt% Pd; the amount of metallic species increased with Pd-loading due to the increase of particle size.

4.2.2.2. Metal dispersion analyses: CO chemisorption & EtOH-TPSR

The dispersion trends obtained for the impregnated and co-precipitated samples were different as can be seen in Figure 4-17.

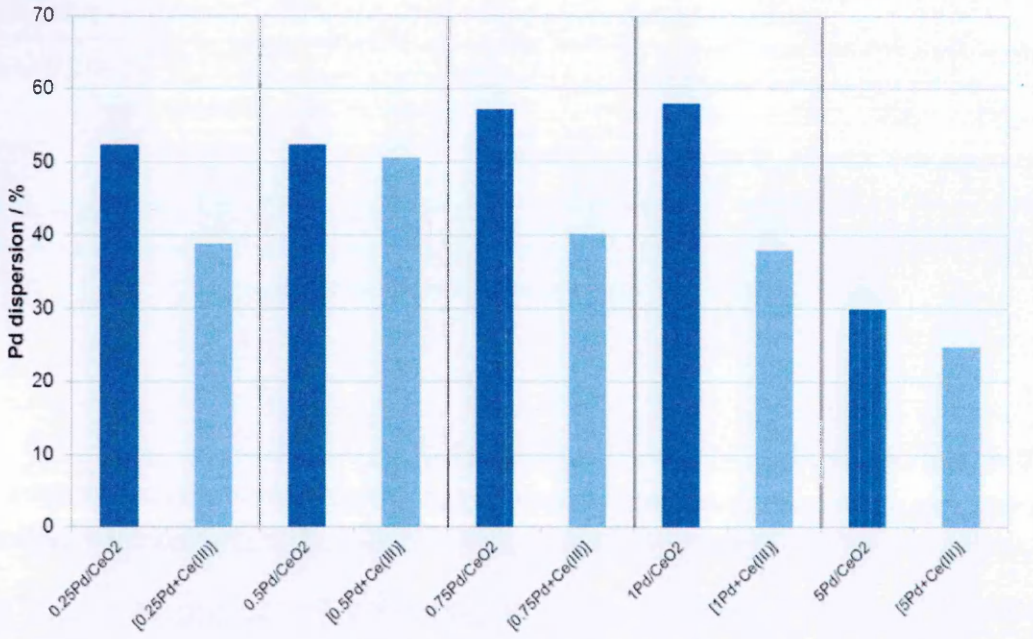

Figure 4-17: Comparison of Pd dispersion measured by CO chemisorption on Pd-CeO_2 samples with different Pd-loadings prepared by wet impregnation (dark blue) and by co-precipitation with Ce^{3+} precursor (light blue). Prior to the CO pulses, the samples were first pre-treated in H_2 at 300 °C for 30 min and cooled down to 30 °C in He.

The dispersion for those samples where Pd was impregnated on CeO_2 showed similar dispersion values (all around 55 %), except for 5Pd/CeO_2 which showed a significantly lower value (29 %), likely to be due to the formation of larger Pd particles. The dispersion values for the co-precipitated samples showed an initial increase when going from 0.25 wt% Pd to 0.5 wt% Pd (39 % and 51 %, respectively); following this, the increase of Pd loading led to a decrease in the dispersion (larger decrease than that seen for the impregnated catalysts). Overall, the impregnated samples showed a higher Pd dispersion compared to the co-precipitated samples.

In terms of Pd surface area, the values obtained from CO chemisorption and those obtained from EtOH-TPSR were plotted together for comparison (Figure 4-18).

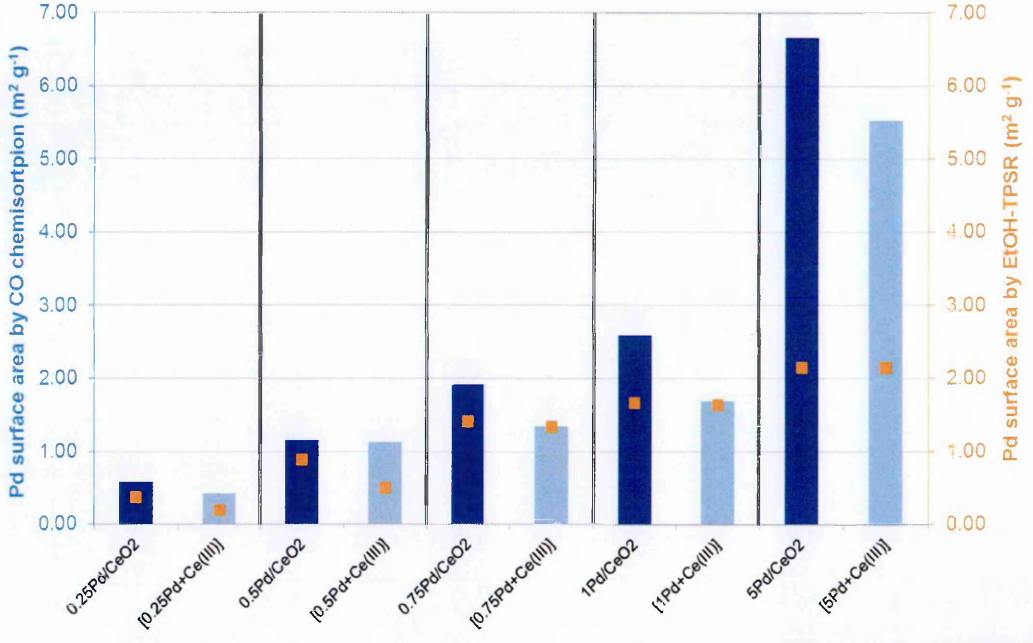

Figure 4-18: Comparison of Pd surface area on Pd-CeO_2 samples with different Pd-loadings prepared by wet impregnation (Pd/CeO_2) and by co-precipitation with Ce^{3+} precursor ([Pd+Ce^{3+}]). Comparison of the values obtained from the CO-chemisorption (blue bars) and the EtOH-TPSR (orange markers) methods.

Compared to the dispersion, the Pd surface area increased with Pd loading. This is because the metal surface area measures the total amount of surface Pd

without taking into account the total number of metal atoms in the sample; thus the higher the Pd loading is, the more surface Pd the sample will contain. However, dispersion calculations correlate the metal surface area with the total metal loading on the material, and therefore the metal particle size has a significant impact on the dispersion. At higher Pd loadings the particles were found to be larger and thus a higher number of Pd atoms will be lost inside them, leading to a decrease on the dispersion.

Table 4-10 summarises the dispersion and metal surface areas values found during these experiments:

Table 4-10: Palladium surface area calculated by CO chemisorption and by EtOH-TPSR. The excess of surface area measured by the CO chemisorption was also represented as % to study the contribution of Pd-Ce interface sites[12]. CO chemisorption instrument standard error = ± 2% (for metal dispersion) and ± 0.04 $m^2 g^{-1}$ (for metal surface area); EtOH-TPSR instrument standard error = ± 0.1 $m^2 g^{-1}$.

	CO chemisorption		EtOH-TPSR		Excess surface area measured on CO chemisorption
Sample	Pd dispersion / %	Pd surface area / $m^2 g^{-1}$	max ppm $CH_4 \cdot g^{-1}$ sample·ppm^{-1} EtOH	Pd surface area / $m^2 g^{-1}$	CO adsorption attributed to interface sites / %
$0.25Pd/CeO_2$	52	0.6	0.8	0.4	33
$[0.25Pd+Ce^{3+}]$	39	0.4	0.4	0.2	50
$0.5Pd/CeO_2$	52	1.2	1.9	0.9	25
$[0.5Pd+Ce^{3+}]$	51	1.1	1.1	0.5	54
$0.75Pd/CeO_2$	57	1.9	3.0	1.4	26
$[0.75Pd+Ce^{3+}]$	40	1.3	2.9	1.3	0
$1Pd/CeO_2$	58	2.6	3.6	1.7	35
$[1Pd+Ce^{3+}]$	38	1.7	3.5	1.6	6
$5Pd/CeO_2$	30	6.7	4.6	2.1	69
$[5Pd+Ce^{3+}]$	25	5.5	4.6	2.1	62

[12] This was done by calculating the difference between the Pd surface area values obtained from the CO chemisorption and from the EtOH-TPSR method, divided by the Pd surface area obtained from the CO chemisorption method and multiplied by 100 to express it as %.

It is possible to see that with both methods the Pd surface area increased with Pd loading, although a larger increase was observed when using the CO chemisorption method. As discussed previously, the values obtained from the EtOH-TPSR technique are exclusively associated to Pd, whilst those obtained from CO chemisorption are also associated with CO adsorption at the Pd-Ce interface [2, 17]. At Pd loadings higher than 0.75 wt%, when comparing samples with the same Pd loading similar Pd surface areas were obtained (based on EtOH-TPSR) independently of the preparation method. However, when performing the same comparison but based on the CO chemisorption results, these suggested that the impregnated samples contained a higher Pd surface content than the co-precipitated samples. By contrast, at low Pd loadings (0.25 and 0.5 wt% Pd), when comparing samples with the same Pd loading both methods (EtOH-TPSR and CO chemisorption) were in agreement showing a lower Pd surface area for the co-precipitated materials.

In addition, it was observed that the actual surface area values between these two methods were not the same, being in all cases lower for the EtOH-TPSR method. This was especially noticeable for the [0.5Pd+Ce^{3+}] sample. In Table 4-10 these differences are represented as a percentage; the bigger the percentage is, the larger the difference between CO chemisorption and EtOH-TPSR metal surface area values. These discrepancies suggested that for [0.5Pd+Ce^{3+}] there was more CO adsorbing at the interface of Pd-Ce on the co-precipitated materials, whilst at higher loadings this occurred in a larger extent for the impregnated catalysts. The significantly lower dispersion of the co-precipitated [1Pd+Ce^{3+}] and [5Pd+Ce^{3+}] materials suggests that this behaviour could be due to the formation of bigger Pd particles (and therefore lower number of Pd-Ce interface sites) on these samples compared to their impregnated equivalent.

4.2.3. Redox characterisation (TPR, OSC)

In section 4.1.4. it was shown that the samples prepared by co-precipitation had a sharper Pd-Ce reduction peak in H_2-TPR studies, suggesting a significant interaction between the Pd and Ce. In order to determine if this level of interaction is maintained with the different Pd loadings, the reducibility of the new set of samples was studied. OSC tests were also performed to correlate the results with the TPR data.

4.2.3.1. H_2-TPR

Figure 4-19 shows the H_2-TPR profiles of the samples with different Pd loadings; the figures are all represented on the same scale for direct comparison. The peaks associated to non-promoted surface and bulk ceria reduction, at 350 and 800 °C respectively, were practically identical in all cases for both sets of samples.

For the samples prepared by co-precipitation, the peak at low temperature associated to the Pd-Ce reduction shifted to lower temperature when the Pd loading was increased, most certainly due to an increase of Pd particle size [3, 20]. This peak was sharp, appearing approximately at 135 °C for 0.25 wt% Pd, at 110 °C for 0.5 wt% Pd, at 115 °C for 0.75 wt% Pd, at 105 °C for 1 wt% Pd, and at 80 °C for 5 wt% Pd. For the 5 wt% Pd the peak was wider with a clear shoulder at 95 °C, which indicates the existence of more than one type of Pd species [20].

For the impregnated samples the Pd-Ce reduction peak also shifted to lower temperature with increasing palladium loading, likely due to an increase of Pd particle size [3, 20]. In the case of the impregnated samples, the peak was wider and less intense. Moreover, multiple shoulders around the main peaks could be observed, indicating that these samples are more heterogeneous than the

samples prepared by co-precipitation. The reduction peak appeared approximately at 125 ºC and 235 ºC for 0.25 wt% Pd, at 90 ºC and 205 ºC for 0.5 wt% Pd, at 100 ºC for 0.75 wt% Pd, at 90 ºC for 1 wt% Pd, and at 50 ºC for 5 wt% Pd.

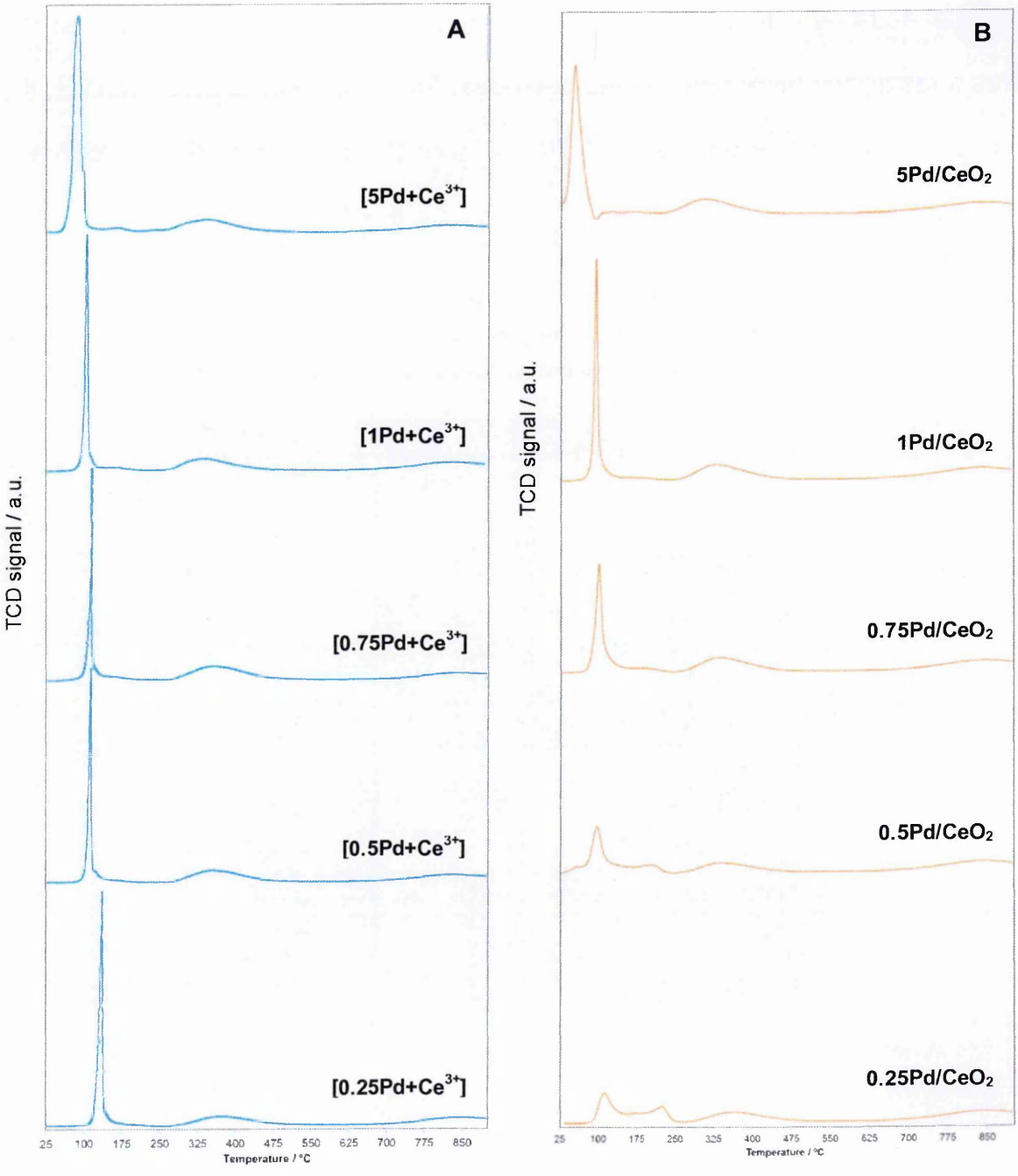

Figure 4-19: H_2-TPR of Pd-CeO_2 samples with different Pd-loadings prepared by co-precipitation with Ce^{3+} precursor (A) and by wet impregnation (B). The sample taken was ~0.2 g, and the flow used was 30 ml min^{-1} of 10% H_2/N_2 using 30 ml min^{-1} of N_2 as carrier gas. The same scale was used in all cases for a direct comparison of the peak intensities.

The H_2 consumption during this reduction, together with the peak temperature, can be seen in Table 4-11; it can be noticed that in all cases the samples prepared by co-precipitation consumed more H_2, especially at loadings ≤ 0.75 wt% Pd. This is likely to be due to a higher number of ceria atoms in contact with Pd undergoing simultaneous reduction [21]. Although the reduction of Pd-Ce indicated that this was a faster and more homogeneous process for the co-precipitated samples, the same reduction occurred overall at slightly lower temperature for the impregnated materials.

Table 4-11: Summary of peak positions and H_2 consumption during H_2-TPR experiments for Pd-CeO_2 samples with different Pd loadings prepared by impregnation (Pd/CeO_2) and by co-precipitation with Ce^{3+} precursor ([Pd+Ce^{3+}]). Average instrument standard error ± 0.02 mmol g^{-1}.

	PdO_x reduction	
Sample	Peak temperature / °C	H_2 consumed / mmol·g^{-1}
0.25Pd/CeO_2	125 °C 235 °C	0.54
[0.25Pd+Ce^{3+}]	135 °C	0.71
0.5Pd/CeO_2	90 °C 205 °C	0.58
[0.5Pd+Ce^{3+}]	110 °C	0.64
0.75Pd/CeO_2	100 °C	0.64
[0.75Pd+Ce^{3+}]	115 °C	0.78
1Pd/CeO_2	90 °C	0.66
[1Pd+Ce^{3+}]	105 °C	0.69
5Pd/CeO_2	50 °C	0.10
[5Pd+Ce^{3+}]	80 °C 95 °C	0.11

4.2.3.2. CO-TPR

The samples with different Pd-loadings were also evaluated by CO-TPR. The results can be seen in Figure 4-20 and Figure 4-21.

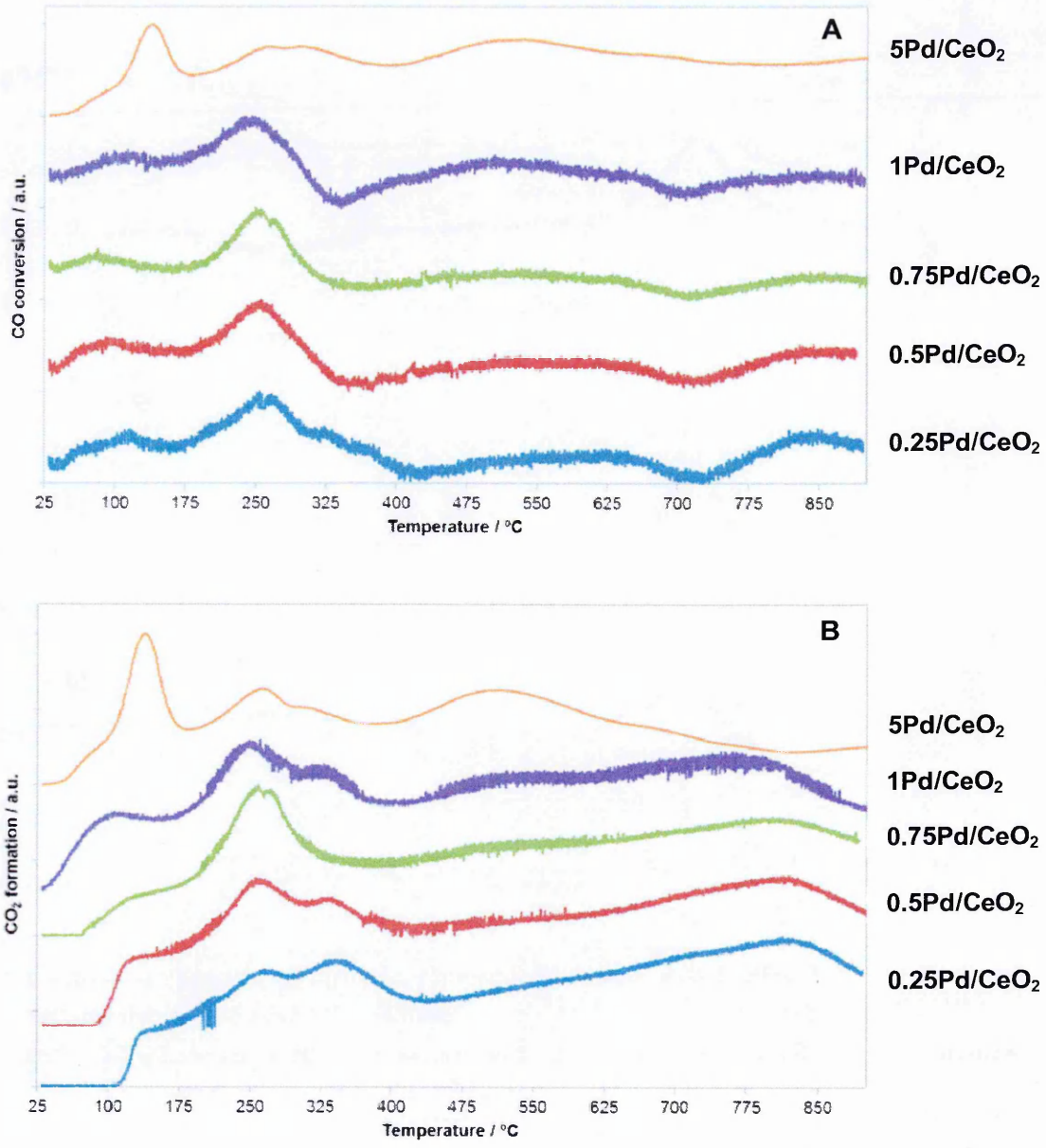

Figure 4-20: CO-TPR of Pd-CeO_2 samples with different Pd-loadings prepared by wet impregnation. CO consumption (A) and CO_2 formation (B) during CO-TPR. The samples were previously pre-treated under 50 ml min^{-1} of He at 500 °C. During the CO-TPR the flow consisted in 20 ml min^{-1} of 10%CO/He in 30 ml min^{-1} of He.

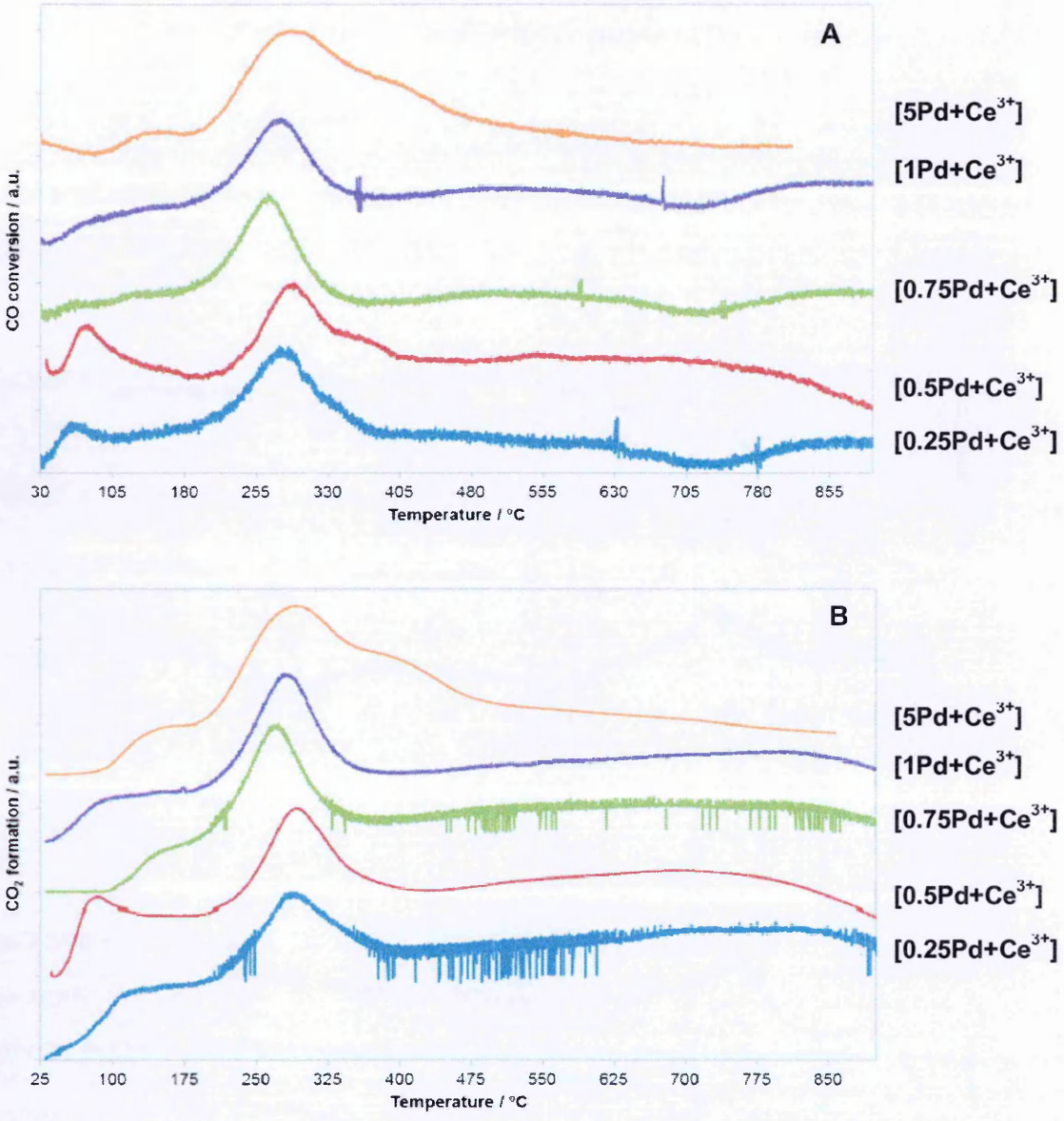

Figure 4-21: CO-TPR of Pd-CeO_2 samples with different Pd-loadings prepared by co-precipitation with Ce^{3+} precursor. (From top to bottom) CO consumption and CO_2 formation during CO-TPR. The samples were previously pre-treated under 50 ml min^{-1} of He at 500 °C. During the CO-TPR the flow consisted in 20 ml min^{-1} of 10%CO/He in 30 ml min^{-1} of He.

Similar to the results in section 1.4.2., for the impregnated samples with Pd loading lower than 1 wt%, CO consumption without consequent CO_2 formation is observed at low temperature (up to 125 °C), suggesting that the adsorption rate of CO is faster than the reaction with the oxygen to form CO_2. At higher Pd loadings, both profiles start following the same trend. For the co-precipitated materials, as

the reaction with the CO occurred in most cases simultaneously to the CO adsorption, it appears that they have better oxygen mobility (thus, better Pd-Ce interaction).

In these trends it is possible to recognise the main peaks associated with surface PdO_x reduction (peaks between 30-400 ºC), surface CeO_2 reduction (peaks between 400-600 ºC), and bulk CeO_2 reduction (peaks between 700-900 ºC) [13, 21].

The main differences between the two sets of samples were found for PdO_x reduction. Table 4-12 summarises the temperatures found for the reduction of surface PdO_x species, based on the CO consumption:

Table 4-12: Comparison of the temperatures corresponding to the surface PdO_x reduction, based on the CO consumption during CO-TPR, of Pd-CeO_2 samples with different Pd loadings prepared by impregnation and by co-precipitation with Ce^{3+} precursor.

	Surface PdO_x reduction (based on CO consumption)	
	Co-precipitation	Wet impregnation
0.25 wt% Pd	60 ºC 280 ºC Small shoulder at 340 ºC	Wide peak at 60 ºC Wide peak at 115 ºC 260 ºC
0.5 wt% Pd	75 ºC 290 ºC Small shoulder at 360 ºC	Wide peak at 60 ºC Wide peak at 100 ºC 260 ºC
0.75 wt% Pd	Shoulder at 65 ºC Shoulder 130 ºC 270 ºC	Wide peak at 80 ºC 250 ºC
1 wt% Pd	Shoulder 75 ºC Shoulder at 150 ºC 270 ºC	Wide peak at 110 ºC 240 ºC
5 wt% Pd	Shoulder at 60 ºC Shoulder 150 ºC 230 ºC Shoulder 405 ºC	Shoulder at 80 ºC Sharp peak at 140 ºC 260 ºC 300 ºC

For the co-precipitated materials, the samples with the lowest loadings (0.25 and 0.5 wt% Pd) showed two main peaks at 60-75 ºC and at 280-290 ºC for this reduction, whilst the same samples prepared by impregnation presented two

overlapping shoulders at ~60 ºC and 95-115 ºC, and a main peak at 260 ºC. The higher reduction temperature for the co-precipitated materials and the better definition of the reduction peaks suggests that the Pd particles are smaller and/or interacting more strongly with ceria than in the impregnated materials [20]. In addition, the lower number of peaks for the co-precipitated materials is an indication of a better homogeneity of the Pd particles in these samples.

For the samples with higher Pd loadings (0.75, 1 and 5 wt% Pd), the co-precipitated materials started losing the well-defined low-temperature reduction peak, and instead peaks appeared as small shoulders, suggesting the presence of multiple Pd species. By contrast, the low temperature reduction peak for the impregnated samples increased in intensity the higher the Pd loading was. The profile of 5Pd/CeO_2 differed from the profile of the other impregnated samples, where an extra peak at 140 ºC could be identified. Based in published work, the presence of this intense peak suggests the formation of large Pd species that were not present on the samples with lower Pd loadings [20].

In all cases, the increase in Pd loading shifted the reduction peak corresponding to the reduction of PdO_x species to lower temperature, most certainly due to an increase in Pd particle size [20]. Overall, those samples prepared by impregnation showed that the reduction occurred at slightly lower temperature than for those prepared by co-precipitation. The results seen here, agreed with the results obtained by H_2-TPR.

4.2.3.3. Oxygen Storage Capacity (OSC)

The impact of the Pd loading and the preparation method on the OSC was studied. Figure 4-22 shows the results obtained for the co-precipitated and

impregnated materials, respectively. For the co-precipitated set the OSC performance did not seem to depend highly on Pd loading; it was only at 5 wt% Pd that it was possible to see a significant increase in the OSC. The impregnated materials however showed a high dependence on palladium loading, with increasing OSC with increased loading.

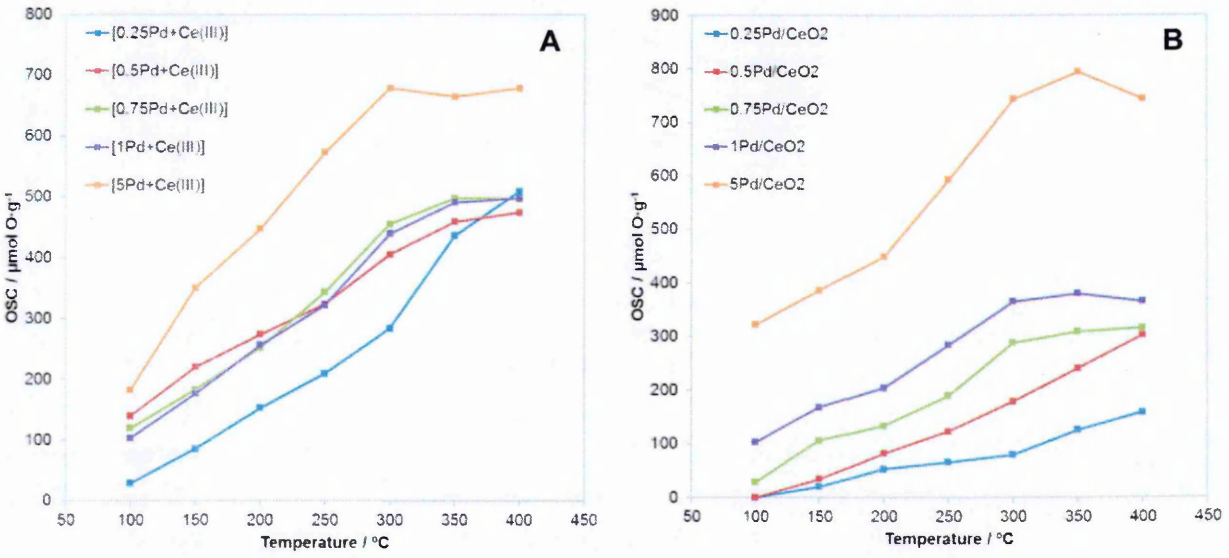

Figure 4-22: Oxygen storage capacity of Pd-CeO_2 samples with different Pd-loadings prepared by co-precipitation with Ce^{3+} precursor (A) and by wet impregnation (B). The OSC measurement was performed alternating switches between O_2 (10 ml min^{-1} of 5 %O_2/He) and CO (10 ml min^{-1} of 10 %CO/He) using He as a carrier gas (90 ml min^{-1}) at steady state temperatures. OSC instrument average standard error = ± 8 µmol O g^{-1}.

To compare the performance of both sets of samples the difference between the OSC values from the co-precipitated catalysts and the impregnated samples was calculated and represented against the temperature for each of the palladium loadings. The results can be seen in Figure 4-23. It is possible to appreciate that for low Pd loadings (< 1 wt%) the co-precipitation method led to higher OSC values than the impregnation method. For most loadings, the difference between the OSC values of the impregnated and co-precipitated materials was more evident with increasing temperature. At high temperature there is a higher contribution of unpromoted surface and bulk ceria (as indicated by the TPR

measurements), thus this could indicate that more oxygen is accessed on the co-precipitated materials.

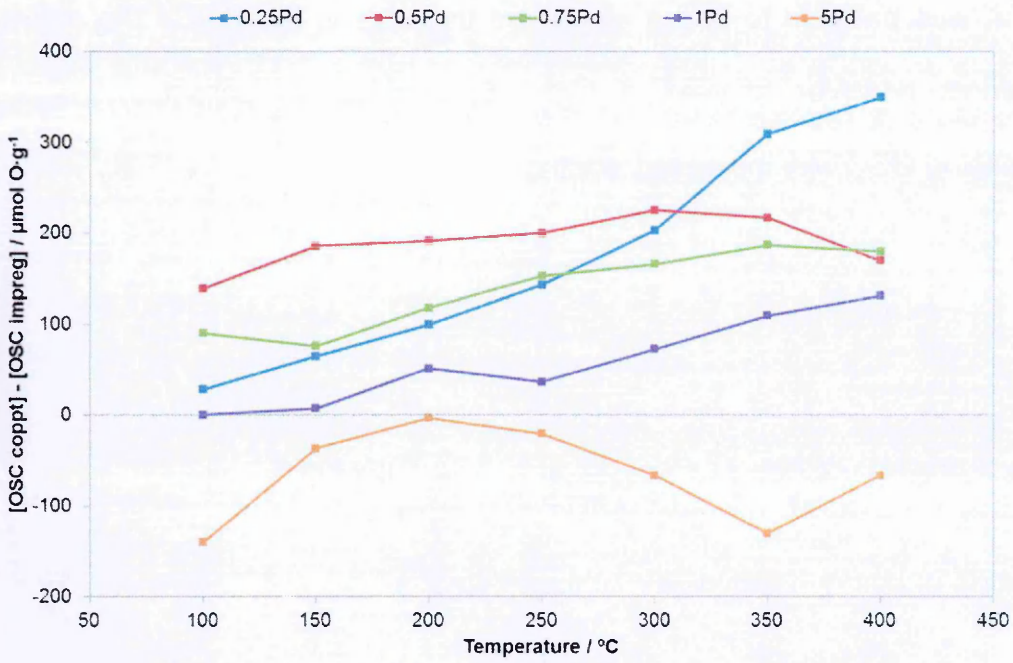

Figure 4-23: OSC difference between co-precipitated and impregnated Pd-CeO_2 materials with different Pd loadings. Positive numbers mean that the co-precipitated sample at that loading is superior, whilst negative values mean that the impregnated sample at that loading is better.

Ceria efficiency was also calculated. In order to focus only on ceria efficiency the contribution from palladium was extracted[13]. The values below 350 ºC should only be taken as qualitative information, as it was assumed that complete oxidation of PdO occurred. The efficiency has been represented against palladium loading at 100 ºC, 200 ºC, 300 ºC, and 400 ºC. The results for the co-precipitated and the impregnated samples are given in Figure 4-24.

It can be seen that the profiles for both sets of samples were different. For the co-precipitated set, the sample with the highest efficiency was 0.5 wt% Pd between 100-200 ºC, at higher temperatures also 0.25 wt% Pd (at 400 ºC) and 0.75 wt% Pd (at 300 ºC) showed similar or even higher values. For the impregnated set of samples, the increase of Pd loading led to an increase of ceria efficiency for OSC,

[13] Refer to *Appendix 2* for a detailed explanation of how to calculate ceria efficiency. Complete reduction of PdO is assumed for all the efficiency calculations.

resulting in 5 wt% Pd being the most efficient catalyst in terms of ceria utilisation. The negative values at 100 ºC were due to the extraction of palladium contribution, as it is assumed a 100% contribution from the noble metal, however at this temperature the complete reduction of Pd has not occurred (as CO-TPR showed). Therefore, these values appear lower than they should be.

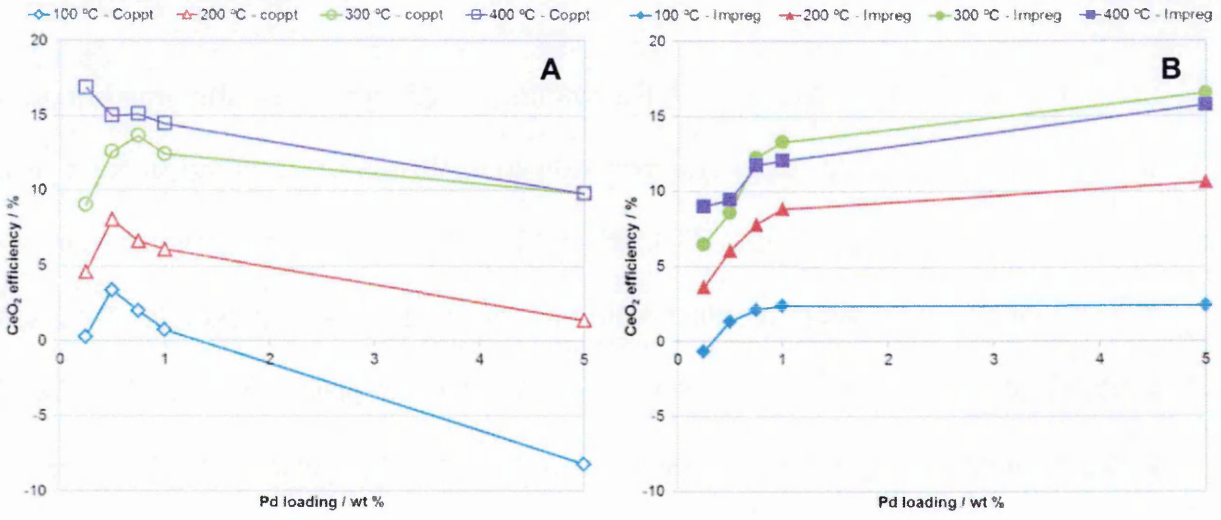

Figure 4-24: CeO_2 efficiency in terms of oxygen storage capacity for Pd-CeO_2 samples with different Pd-loadings prepared by co-precipitation with Ce^{3+} precursor (A) and by wet impregnation (B).

Overall, for up to 0.75 wt% Pd the catalysts prepared using the co-precipitation method showed a better usage of the oxygen from the ceria; this is particularly significant at temperatures of 300 ºC and higher. At higher Pd loadings it is the impregnation method which leads to a better oxygen usage. The overall improvement in OSC performance of the co-precipitated samples is likely to be a consequence of the higher number of Pd-Ce interfaces in these catalysts.

4.2.4. Kinetic characterisation: CO-SSITKA

The CO oxidation reaction rate was also studied for some of these catalysts. A sample with lower Pd loading (0.25 wt% Pd) and a sample with higher Pd loading (5 wt% Pd) were analysed in addition to the previously measured (0.5 wt% Pd), to see how the loading affects the reaction rate. These results can be seen in Figure 4-25.

For the samples with the lowest Pd loading (0.25 wt% Pd), the impregnated sample showed slightly faster reaction rate than the co-precipitated version. For the samples with the highest Pd loading (5 wt% Pd), the impregnated sample showed significantly faster reaction rate than the co-precipitated sample. This is in contrast to the results shown previously for the co-precipitated [0.5Pd+Ce^{3+}] catalyst, which showed a faster reaction rate than the impregnated 0.5Pd/CeO_2.

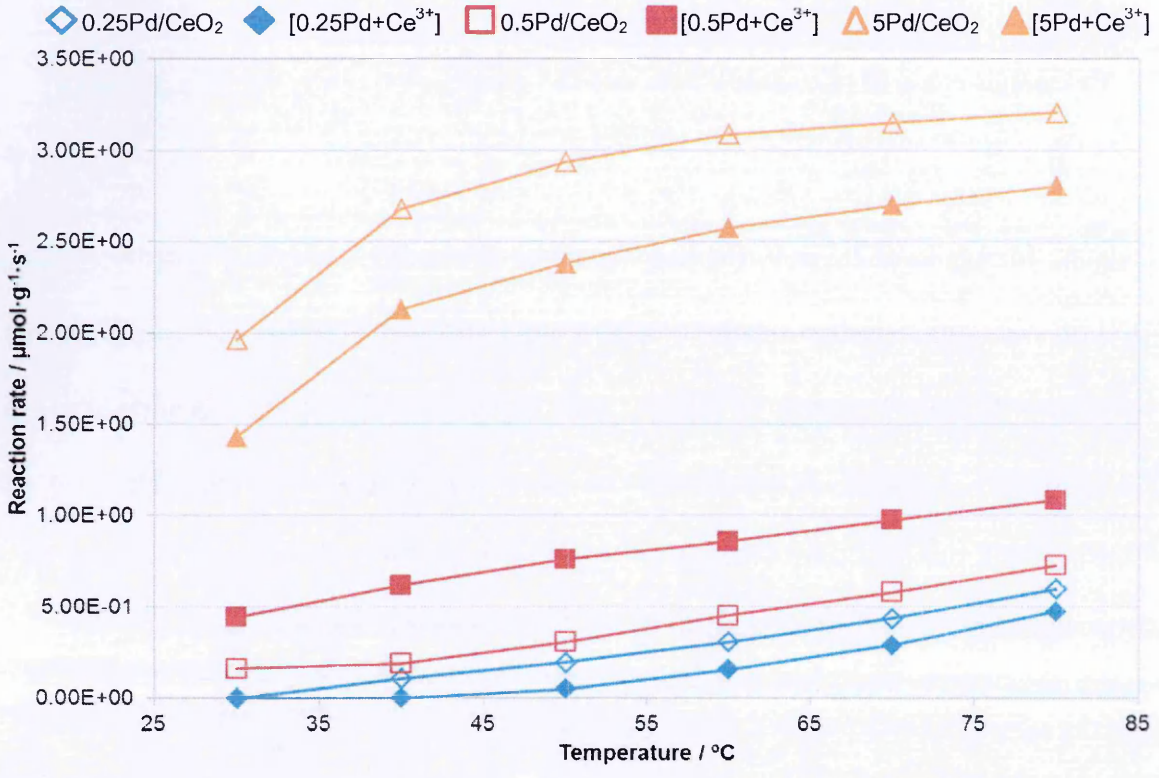

Figure 4-25: Comparison of the CO oxidation reaction rate at steady state temperatures for Pd-CeO_2 samples with different Pd-loadings, prepared by impregnation and by co-precipitation with Ce^{3+} precursor. The gas flows used were 52.5 ml min^{-1} of 5% O_2/He, 5.5 ml min^{-1} of 1%CO/5%Ar/He (^{12}C) and 5.5 ml min^{-1} of 1%CO/He (^{13}C). The average reaction rate standard error was ±0.01 µmol g^{-1} s^{-1}.

The reaction orders were also calculated for these samples. The equation rate and the activation energy (E_a) can be found in Table 4-13:

Table 4-13: Equation rate and E_a for CO oxidation over Pd-CeO_2 samples with different Pd-loadings prepared by wet impregnation (Pd/CeO_2) and by co-precipitation with Ce^{3+} precursor ([Pd+Ce^{3+}]). The standard errors for E_a are shown between brakets next to the values.

Sample	Equation rate	E_a / kJ·mol^{-1}
0.25Pd/CeO_2	$r = k$ [CO]	35 (± 1)
[0.25Pd+Ce^{3+}]	$r = k$ [CO]	54 (± 8)
0.5Pd/CeO_2	$r = k$ [CO]	27 (± 2)
[0.5Pd+Ce^{3+}]	$r = k$ [CO]	11 (± <1)
5Pd/CeO_2	$r = k$ [CO]	3 (± <1)
[5Pd+Ce^{3+}]	$r = k$ [CO]	5 (± <1)

All the reaction orders appeared to be zero with respect to O_2 concentration, and 1 with respect to CO concentration. No differences were found with respect to the Pd-loading, suggesting that all the catalysts followed the same mechanism based on the reaction between the CO adsorbed on Pd sites and the oxygen from the CeO_2 [27].

However, E_a decreased with increasing Pd-loading, most probably due to the creation of more active sites. In terms of the influence of the preparation method, only the sample with 0.5 wt% Pd prepared by co-precipitation showed a lower E_a value than the impregnated samples with the same loading; [0.25Pd+Ce^{3+}] and [5Pd+Ce^{3+}] showed a higher E_a value than 0.25Pd/CeO_2 and 5Pd/CeO_2, respectively. This is likely to be related to a lower Pd surface content, since [0.25Pd+Ce^{3+}] and [5Pd+Ce^{3+}] were seen to contain less surface Pd than 0.25Pd/CeO_2 and 5Pd/CeO_2 during metal surface area measurements (section 4.2.2.).

These results agree with the characterisation performed, which indicated that there is an optimum Pd loading to obtain the best Pd-Ce interaction with the

co-precipitation method over the impregnated version, which correspond to 0.5 wt% Pd (based on the loadings analysed in this study).

4.2.5. Light-off performance

The OSC has been seen to directly correlate with the final conversion of the pollutants during a perturbed light-off test. Thus, as the OSC of the Pd-CeO_2 samples with different Pd loadings was already evaluated, the perturbed light-off was not performed in this case.

However, the light-off temperature was seen to be largely influenced by the catalytic surface. Thus, the activity of the samples was only evaluated under cold-start conditions to study how the different surfaces impact the light-off, since significant differences were found on these catalysts depending on their preparation method (impregnation or co-precipitation).

4.2.5.1. Cold-start conditions

All the samples were tested under typical cold-start conditions. The profiles can be seen in Figure 4-26; in addition, to simplify their comparison, the results are summarised in Table 4-14 comparing the T50 for CO, NO_x, and HC. The values of the difference of T50 between co-precipitated and impregnated samples are also included in the table; positive numbers mean that the impregnated catalyst has a lower temperature light-off (meaning better performance), and negative values the opposite.

For this test, the co-precipitation method showed a small advantage over the impregnation method only for Pd loading of 0.5 wt% for CO oxidation light-off (as shown in section 4.1.6.1); all the other light-offs did not differ greatly between

samples prepared using the different techniques with similar Pd loadings. It was only the sample with 5 wt% Pd that showed the biggest difference in performance between both preparation methods, with the impregnated $5Pd/CeO_2$ showing better results than the [$5Pd+Ce^{3+}$] sample.

In previous experiments (section 4.1.6) it was shown that the light-off depended on palladium surface content (light-off temperature decreases with increasing Pd surface content) [33, 34, 41]. This is in accordance with the conclusions obtained during the characterisation of these samples, where it was seen, based on CO chemisorption, that the Pd surface areas (Pd together with Pd-Ce interface sites) were similar for equal Pd loadings independently of the preparation method. The differences between co-precipitated and impregnated materials were especially noticeable at 1 and 5 wt% Pd loadings, with the impregnated materials containing larger Pd surface areas. The higher surface Pd content of the impregnated $5Pd/CeO_2$ sample was then responsible of the better light-off performance.

Table 4-14: Necessary temperature for 50% conversion of CO, NO_x and HC during a light-off test under constant lambda at 0.95 for Pd-CeO_2 samples with different loadings prepared by impregnation (Pd/CeO_2) and by co-precipitation with Ce^{3+} precursor ([$Pd+Ce^{3+}$]). ΔT50 refer to the difference between the values obtained for the co-precipitated and the impregnated samples. Light-off instrument average standard error = ± 2 °C.

Sample	CO		NO_x		HC	
	T50 / °C	ΔT50 / °C	T50 / °C	ΔT50 / °C	T50 / °C	ΔT50 / °C
$0.25Pd/CeO_2$	275	-4	289	+5	359	+4
[$0.25Pd+Ce^{3+}$]	271		294		363	
$0.5Pd/CeO_2$	242	-14	257	-5	325	0
[$0.5Pd+Ce^{3+}$]	228		252		325	
$0.75Pd/CeO_2$	206	-6	223	-3	320	0
[$0.75Pd+Ce^{3+}$]	200		220		320	
$1Pd/CeO_2$	208	-2	222	+1	322	-9
[$1Pd+Ce^{3+}$]	206		223		313	
$5Pd/CeO_2$	133	+31	165	+19	306	+2
[$5Pd+Ce^{3+}$]	164		184		308	

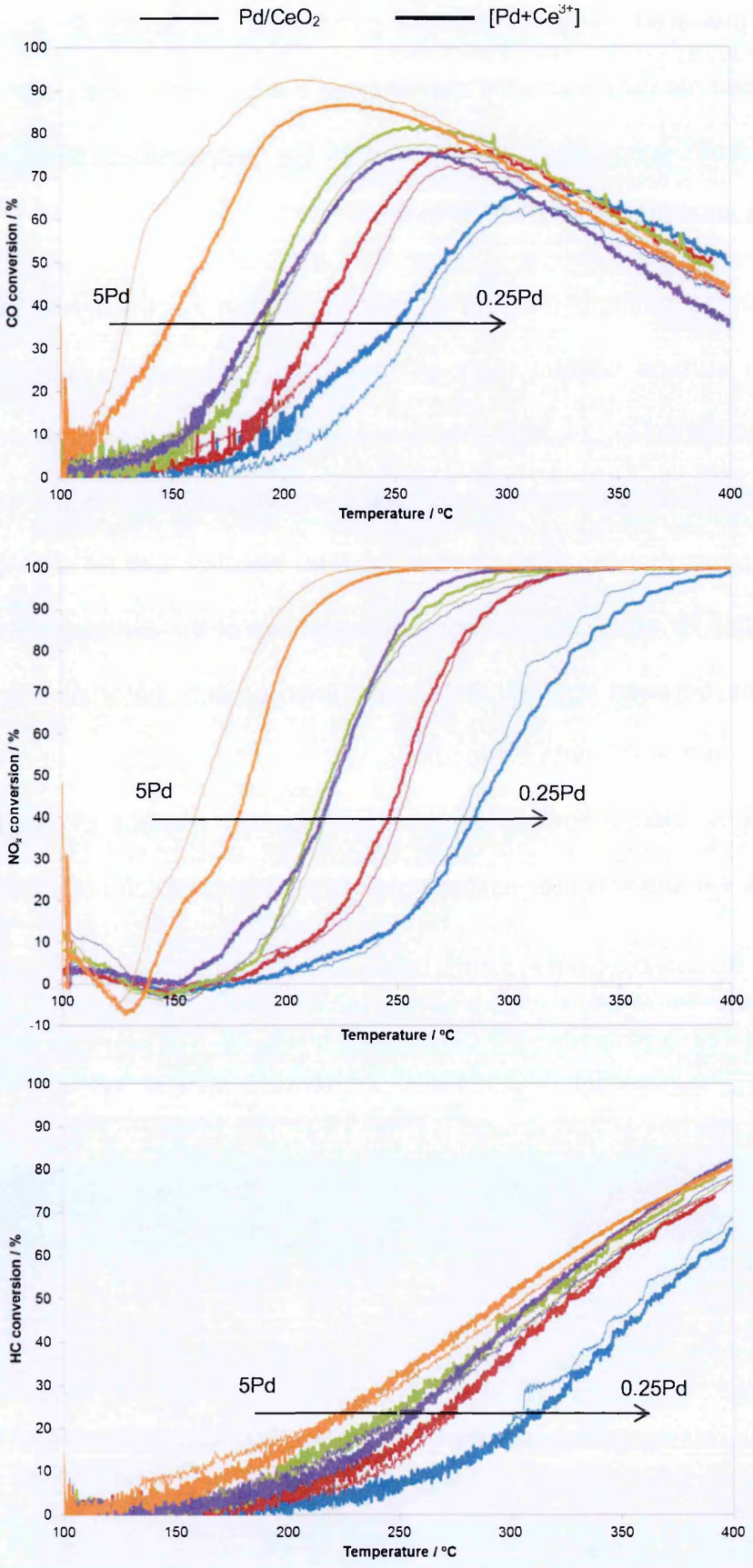

Figure 4-26: From top to bottom, CO, NO_x and HC light-off performance under constant lambda at 0.95 of Pd-CeO_2 catalysts prepared by impregnation (thin lines) and by co-precipitation using Ce^{3+} precursor (thicker lines). The sample taken was 0.4 g (0.2 g sample + 0.2 g cordierite) and the gas flow rate 2 L min^{-1}. The catalyst was heated using a ramp rate of 10 °C min^{-1} from 100 to 400 °C.

Overall, the co-precipitation method does not seem a good method to improve the light-off activity under these conditions, as similar performances were found independently of the preparation method. The biggest impact on the light-off was brought by the Pd loading, with higher Pd loadings leading to a shift in the light-off towards lower temperature. This is merely due to an increase of surface active sites.

4.2.6. Summary

As shown in section 4.1., the co-precipitation method has demonstrated an advantage over the impregnation method for catalysts with 0.5 wt% loading by increasing the number of Pd and Ce atoms in contact [4]. However, this method has been seen to be advantageous over the impregnation method only at low Pd-loadings (≤ 1 wt% Pd). These low Pd loaded catalysts prepared by co-precipitation presented an improved OSC, compared to their impregnated versions, due to an easier oxygen transfer [2, 17]. Unfortunately, the co-precipitation method led to higher light-off temperatures compared to the impregnation method. At Pd loadings lower than 1 wt%, the light-off profiles were almost identical when comparing the same Pd loadings, due to the similar Pd surface content of the samples, which was found to be independent of the preparation method used; at Pd loadings of 5 wt%, the impregnated sample showed a better performance due to a greater Pd surface content than the co-precipitated sample [33, 34, 41].

At higher Pd loadings (≥ 1 wt% Pd) the metal dispersion decreased suggesting the formation of bigger Pd particles, and therefore a lower presence of ionic dispersed species which are less active [1]. In addition, the impregnated catalysts contained

higher Pd-surface areas, as with this method the Pd is only placed at the surface of the support, whilst with the co-precipitation method some particles are embedded within the ceria or can agglomerate easily during the preparation leading to bigger Pd particle sizes [8]. Therefore, even if the co-precipitated materials still maintain a high interaction between Pd and Ce atoms (especially noticeable by the sharp peaks during the H_2-TPR), the lower availability of these sites makes them less active than the impregnated versions at these higher Pd loadings.

A summary of the key results can be seen in the following table (Table 4-15):

Table 4-15: Summary of the key results comparing Pd-CeO_2 samples prepared by impregnation and by co-precipitation at Pd loadings of and less than 0.75 wt% (left), and Pd loadings of and more than 1 wt% (right).

	< 1 wt% Pd		≥ 1 wt% Pd	
	Impregnated	Co-precipitated	Impregnated	Co-precipitated
XPS	Bands attributed to Pd^{2+} and Pd^0	Bands attributed to $Pd^{(2+\gamma)+}$	Bands attributed to Pd^{2+} and Pd^0	Bands attributed to Pd^{2+} and Pd^0
CO chemisorption & EtOH-TPSR	Less CO adsorbing at the Pd-Ce interface.	More CO adsorbing at the Pd-Ce interface.	More CO adsorbing at the Pd-Ce interface.	Less CO adsorbing at the Pd-Ce interface.
TPR	Multiple and wide Pd-Ce reduction peaks	Single sharp Pd-Ce reduction peak	Multiple and wide Pd-Ce reduction peaks	Sharp Pd-Ce reduction peak with shoulders
OSC	Worse	Better	Better	1Pd/CeO_2 still better, but 5Pd/CeO_2 worse
CO-ITK	0.25 wt% Pd had slightly higher rate 0.5 wt% Pd had slower rate	0.25 wt% Pd had slightly lower rate 0.5 wt% Pd had faster rate	5 wt% Pd had faster rate	5 wt% Pd had slower rate
Light-off temperature	Higher light-off T	Lower light-off T	Lower light-off T	Higher light-off T

References Chapter 4

[1] A. Satsuma, R. Sato, K. Osaki and K. Shimizu, Catalysis Today, 185 (2012) 61-65.

[2] M. Cargnello, V. V. T. Doan-Nguyen, T. R. Gordon, R. E. Diaz, E. A. Stach, R. J. Gorte, P. Fornasiero and C. B. Murray, Science, 341 (2013) 771-773.

[3] R. d. S. Monteiro, F. B. Noronha, L. C. Dieguez and M. Schmal, Applied Catalysis A: General, 131 (1995) 89-106.

[4] J. J. M. Jr, *Chemical Processing Handbook*, CRC Press, 1993.

[5] C. Knight (Editor), *Penny Cyclopaedia of the Society for the Diffusion of Useful Knowledge*, SDUK, 1840,

[6] F. Zereini and F. Alt (Editors), *Palladium Emissions in the Environment: Analytical Methods, Environmental Assessment and Health Effects*, Springer, 2006,

[7] ICDD, *PDF-4, COD (REV30738 2011.11.2)*, 2012.

[8] A. G. Jones, *Crystallization Process Systems*, Butterworth-Heinemann, 2002.

[9] J. M. Soriano-Rodríguez, V. E. Badillo-Almaraz, C. Alliot, F. Monroy-Guzmán and P. Vitorge, Journal of Radioanalytical and Nuclear Chemistry, 288 (2011) 645-652.

[10] ChemicalBook, *Chemical Book - Palladium hydroxide*, 2010, http://www.chemicalbook.com/ChemicalProductProperty_EN_CB3267682.htm [17-04-2014].

[11] T. Carlsson and U. Vuorinen, *The reliability of solubility data: Results from a limited literature survey focusing on Ni, Pd and Np*, Technical Research Centre of Finland, 1998.

[12] J. W. Niemantsverdriet, *Spectroscopy in Catalysis*, WILEY-VCH, 2007.

[13] A. I. Boronin, E. M. Slavinskaya, I. G. Danilova, R. V. Gulyaev, Y. I. Amosov, P. A. Kuznetsov, I. A. Polukhina, S. V. Koscheev, V. I. Zaikovskii and A. S. Noskov, Catalysis Today, 144 (2009) 201-211.

[14] A. V. Naumkin, A. Kraut-Vass, S. W. Gaarenstroom and C. J. Powell, *NIST X-ray Photoelectron Spectroscopy Database*, 2000.

[15] T. L. Barr, *Modern ESCA: The Principles and Practice of X-Ray Photoelectron Spectroscopy*, CRC Press, 1994.

[16] A. L. Guimarães, L. C. Dieguez and M. Schmal, Anais da Academia Brasileira de Ciências, 76 (2004) 825-832.

[17] R. Rao and B. G. Mishra, Bulletin of the Catalysis Society of India, 2 (2003) 122-134.

[18] L. S. F. Feio, C. E. Hori, S. Damyanova, F. B. Noronha, W. H. Cassinelli, C. M. P. Marques and J. M. C. Bueno, Applied Catalysis A: General, 316 (2007) 107-116.

[19] S. Damyanova, B. Pawelec, K. Arishtirova, M. V. M. Huerta and J. L. G. Fierro, Applied Catalysis A: General, 337 (2008) 86-96.

[20] M.-F. Luo and X.-M. Zheng, Applied Catalysis A: General, 189 (1999) 15-21.

[21] M. Kurnatowska, L. Kepinski and W. Mista, Applied Catalysis B: Environmental, 117–118 (2012) 135-147.

[22] H. Zhu, Z. Qin, W. Shan, W. Shen and J. Wang, Journal of Catalysis, 225 (2004) 267-277.

[23] A. Satsuma, K. Osaki, M. Yanagihara, J. Ohyama and K. Shimizu, Applied Catalysis B: Environmental, 132–133 (2013) 511-518.

[24] C. Higman and M. v. d. Burgt, *The kinetics of gasification and reactor theory*, in Elsevier (Editor), Gasification, Gulf Professional Publishing, 2011, p. 36.

[25] C. Descorme, S. Bedrane and D. Duprez, Catalysis Today, 75 (2002) 401-405.

[26] S. L. Shannon and J. G. Goodwin, Chemical Reviews, 95 (1995) 677-695.

[27] R. Rajasree, J. H. B. J. Hoebink and J. C. Schouten, Journal of Catalysis, 223 (2004) 36-43.

[28] R. H. Nibbelke, A. J. L. Nievergeld, J. H. B. J. Hoebink and G. B. Marin, Applied Catalysis B: Environmental, 19 (1998) 245-259.

[29] E. Bekyarova, P. Fornasiero, J. Kašpar and M. Graziani, Catalysis Today, 45 (1998) 179-183.

[30] S. Fuchs, T. Hahn and H. G. Lintz, Chemical Engineering and Processing: Process Intensification, 33 (1994) 363-369.

[31] R. H. Nibbelke, M. A. J. Campman, J. H. B. J. Hoebink and G. B. Marin, Journal of Catalysis, 171 (1997) 358-373.

[32] S. H. Oh and C. C. Eickel, Journal of Catalysis, 112 (1988) 543-555.

[33] G. Wang, M. Meng, Y. Zha and T. Ding, Fuel, 89 (2010) 2244-2251.

[34] A. Martínez-Arias, M. Fernández-García, A. Iglesias-Juez, A. B. Hungría, J. A. Anderson, J. C. Conesa and J. Soria, Applied Catalysis B: Environmental, 38 (2002) 151-158.

[35] H. S. Gandhi, G. W. Graham and R. W. McCabe, Journal of Catalysis, (2003) 433-442.

[36] A. Trovarelli, C. d. Leitenburg, M. Boaro and G. Dolcetti, Catalysis Today, 50 (1999) 353-367.

[37] M. Fukuhara, Physics Letters A, 313 (2003) 427-430.

[38] R. K. Hailstone, A. G. DiFrancesco, J. G. Leong, T. D. Allston and K. J. Reed, The Journal of Physical Chemistry C, 113 (2009) 15155-15159.

[39] J.-Y. Luo, M. Meng, J.-S. Yao, X.-G. Li, Y.-Q. Zha, X. Wang and T.-Y. Zhang, Applied Catalysis B: Environmental, 87 (2009) 92-103.

[40] S. Tsunekawa, J. T. Wang and Y. Kawazoe, Journal of Alloys and Compounds, 408–412 (2006) 1145-1148.

[41] H. Birgersson, L. Eriksson, M. Boutonnet and S. G. Järås, Applied Catalysis B: Environmental, 54 (2004) 193-200.

5. Co-precipitation of [Pd+Ce+Zr]

Contents

5. Co-precipitation of [Pd+Ce+Zr]

Ce-Zr mixed oxides are widely used in TWC as they show better durability than CeO_2, due to Zr higher thermal stability, and improved OSC [1-3]. The OSC can be 3-5 times higher when Zr is added to the ceria lattice; the incorporation of this smaller atom creates a distortion on the structure that improves the oxygen mobility (Ionic radius: Zr^{4+} = 0.84 Å; Ce^{4+} = 0.97 Å, Ce^{3+} = 1.14 Å) [4-7].

In an attempt to increase the thermal stability and the OSC of the improved co-precipitated [$Pd+Ce^{3+}$] samples, Zr was added to the ceria structure in a Ce:Zr 1:1 molar ratio. The reference palladium loading used was 0.5 wt% Pd (the same loading used to study the impact of the Ce-precursor); however, as it was seen that the Pd:Ce ratio was important for [$Pd+Ce^{3+}$] preparations, and that the highest performance was obtained for 0.5 wt% Pd-CeO_2, samples based on 0.25 wt% Pd-CeZr were also prepared to keep the same Pd:Ce ratio. The co-precipitated samples will be referred here as [Pd+Ce+Zr] and the impregnated as Pd/CeZr.

The reference materials were prepared by impregnation of $Pd(NO_3)_2$ solution on a CeZr (1:1 molar) support, previously prepared by co-precipitating $Ce(NO_3)_3 \cdot 6H_2O$ and $ZrO(NO_3)_2$. The samples were then dried at 105 ºC and calcined at 650 ºC for 2h for a completed decomposition of the precursors (based on TGA analyses). For more details about the preparation refer to *Chapter 2*.

5.1. Catalysis preparation: observations

During the precipitation of these catalysts it was observed that the redox reaction between Pd^{2+} and Ce^{3+} still occurred even in the presence of ZrO^{2+} ions. This was obvious due to the dark colour of the precipitate obtained, which is a sign of

metallic Pd [8]. The samples again turned yellow once calcined, suggesting the re-oxidation of metallic Pd to PdO.

5.2. Structural characterisation

The main aim of this characterisation was to determine whether Ce- and Zr-precursors formed the required CeZr mixed oxide, in a CeZr 1:1 molar ratio. In addition, the lattice parameter was carefully evaluated to look for any evidence of palladium in these samples.

5.2.1. X-Ray Diffraction (XRD)

XRD analyses showed that all samples presented tetragonal $Ce_xZr_{1-x}O_2$ like phases with low crystallinity (Figure 5-1). The main phase appeared to be a CeZr mixed oxide with lattice parameters close to, but smaller than $Ce_{0.5}Zr_{0.5}O_2$. Due to Zr^{4+} being a smaller ion than Ce^{4+}, the shift to lower angles suggests that this phase was slightly richer in Zr, [5, 6, 9].

The lattice parameters of the co-precipitated materials were directly compared to those of the impregnated reference samples. This can be seen in Table 5-1, where it is possible to appreciate that the lattice parameters practically remained unchanged, thus suggesting that no Pd was added to the CeZr structure. This is consistent with the results observed for the $Pd.CeO_2$ catalysts studied in *Chapter 4*, where in neither case were there any indications of Pd being added to the ceria structure.

The ceria crystallite size was similar for all catalysts but for the [0.5Pd+Ce+Zr] sample. The reason for this increase is unknown.

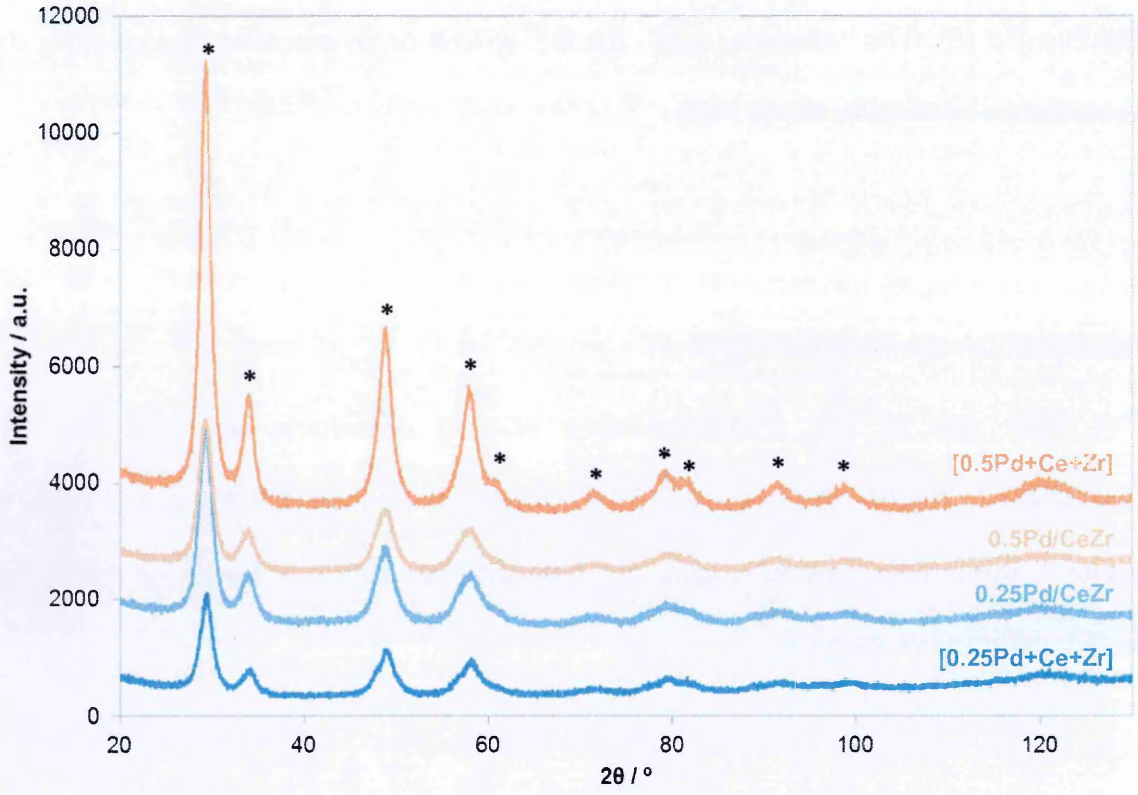

Figure 5-1: XRD patterns of Pd-CeZr samples with different Pd-loadings prepared by wet impregnation (Pd/CeZr) and by co-precipitation with Ce^{3+} precursor ([Pd+Ce+Zr]).The peaks corresponding to the tetragonal cubic $Ce_{0.5}Zr_{0.5}O_2$ phase are indicated as (*).

Table 5-1: Lattice parameters and CeZr crystallite size analysed by XRD, and specific surface area calculated by BET, of Pd-CeZr samples with different Pd loadings prepared by wet impregnation on CeZr (Pd/CeZr) and by co-precipitation with Ce^{3+} precursor ([Pd+Ce+Zr]). Calculated errors (reported in brackets) for crystallite size (nm) refer to the last significant figure; BET-SSA instrument standard error = ± 4 $m^2 g^{-1}$.

	lattice parameters / Å	Crystallite size / nm	BET – SSA / $m^2 g^{-1}$	ICP / Pd wt%
$Ce_{0.5}Zr_{0.5}O_2$ Reference [10]	*a* = 3.720 *c* = 5.304	-	-	-
0.25Pd/$Ce_{0.5}Zr_{0.5}O_2$	*a* = 3.702 *c* = 5.393	3.33 (± 0.05)	123	0.26
[0.25Pd+Ce+Zr]	*a* = 3.707 *c* = 5.357	3.39 (± 0.06)	125	0.24
0.5Pd/$Ce_{0.5}Zr_{0.5}O_2$	*a* = 3.703 *c* = 5.387	3.30 (± 0.05)	124	0.49
[0.5Pd+Ce+Zr]	*a* = 3.711 *c* = 5.348	4.58 (± 0.05)	121	0.51

The specific surface area was also compared in Table 5-1. All samples showed similar SSA values (between 121-125 $m^2 g^{-1}$). Therefore, the different palladium

loadings or the preparation methods used did not have any impact on the specific surface area. Since similar preparation conditions (i.e. precursors, temperature, precipitant base...) were used to precipitate the CeZr support for the impregnated catalysts, and for the co-precipitated materials, no changes in the specific surface area were expected.

5.3. Surface characterisation

The main interest in the surface characterisation was to study the surface composition of these new materials and explore how the different Pd-loadings affected the interaction with the support, depending on the preparation method used. The samples were analysed by XPS, CO chemisorption and EtOH-TPSR.

5.3.1. X-Ray Photoelectron Spectroscopy (XPS)

Ce3d XPS spectra were recorded for all the samples (Figure 5-2). No significant differences were found between the profiles, which showed that most of the ceria on the near surface was present as Ce^{4+}; only 25-27 % of the surface Ce was present as Ce^{3+} [11]. The realistic quantification of Ce^{3+} cations was not possible as Ce^{4+} can suffer spontaneous reduction under high vacuum condition and X-ray irradiation, thus the values shown here should be treated with caution [12]. These results agree with the previous results found for [Pd+Ce^{3+}], where it was shown that most of the Ce^{3+} was present as Ce^{4+} due to the re-oxidation of the Ce^{3+} from the precursor during the calcination process.

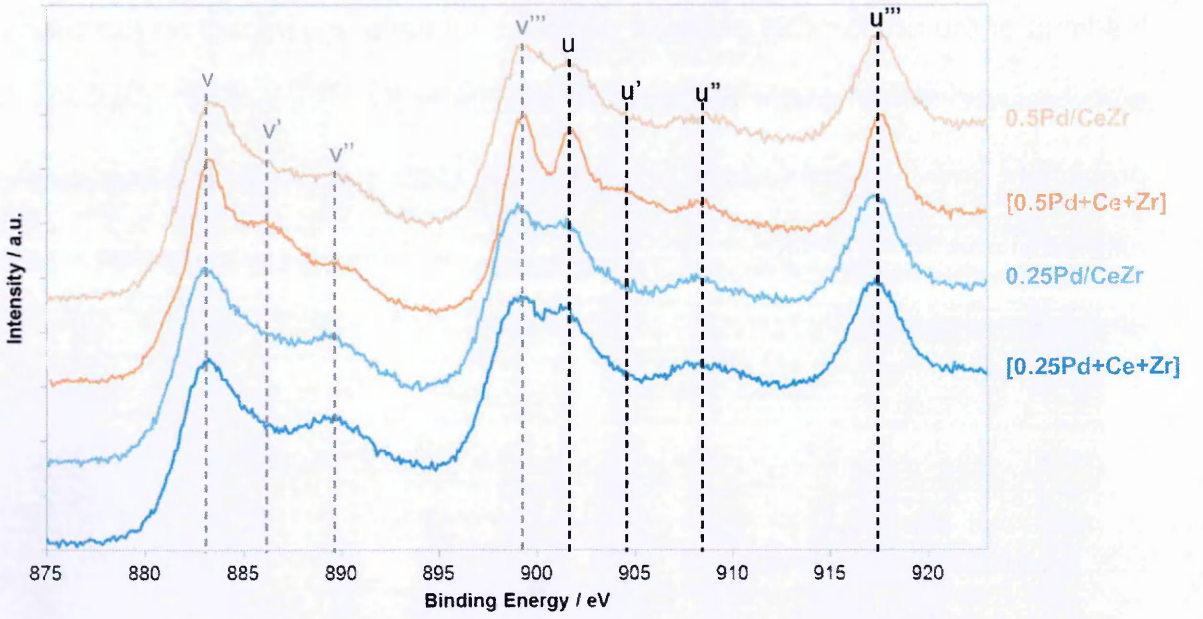

Figure 5-2: Ce3d spectra obtained by XPS comparing the cerium species found in Pd-CeZr samples with different Pd-loadings prepared by wet impregnation (Pd/CeZr) and by co-precipitation with Ce^{3+} precursor ([Pd+Ce+Zr]). The bands u, v, u'', v'', u''' and v''' are related to Ce^{4+} species, whilst u' and v' are assigned to Ce^{3+}.

In the case of CeZr-based materials it was not possible to interpret Pd3d signals due to the overlap with Zr3p peaks [11] (Figure 5-3). Therefore, no information regarding Pd-Ce interaction could be obtained from these analyses. Only a small shoulder at 337.7 eV ($Pd3d_{5/2}$) was detected for those samples containing 0.5 wt% Pd, which seemed to correspond to Pd^{2+}. As was mentioned in *Chapter 4*, Pd^{2+} bands should appear at 336.8 and 342.06 ± 0.2 eV; the presence of these bands would indicate a strong Pd-Ce interaction [13]. This shoulder had poor definition, thus it was not possible to conclude anything regarding the level of Pd-Ce interaction on the [0.5Pd+Ce+Zr] and 0.5Pd/CeZr samples.

Regarding near surface Zr, Zr3p bands from both sets of samples appeared at the same positions (332.7 and 346.4 eV) which both correspond to Zr^{4+} [11].

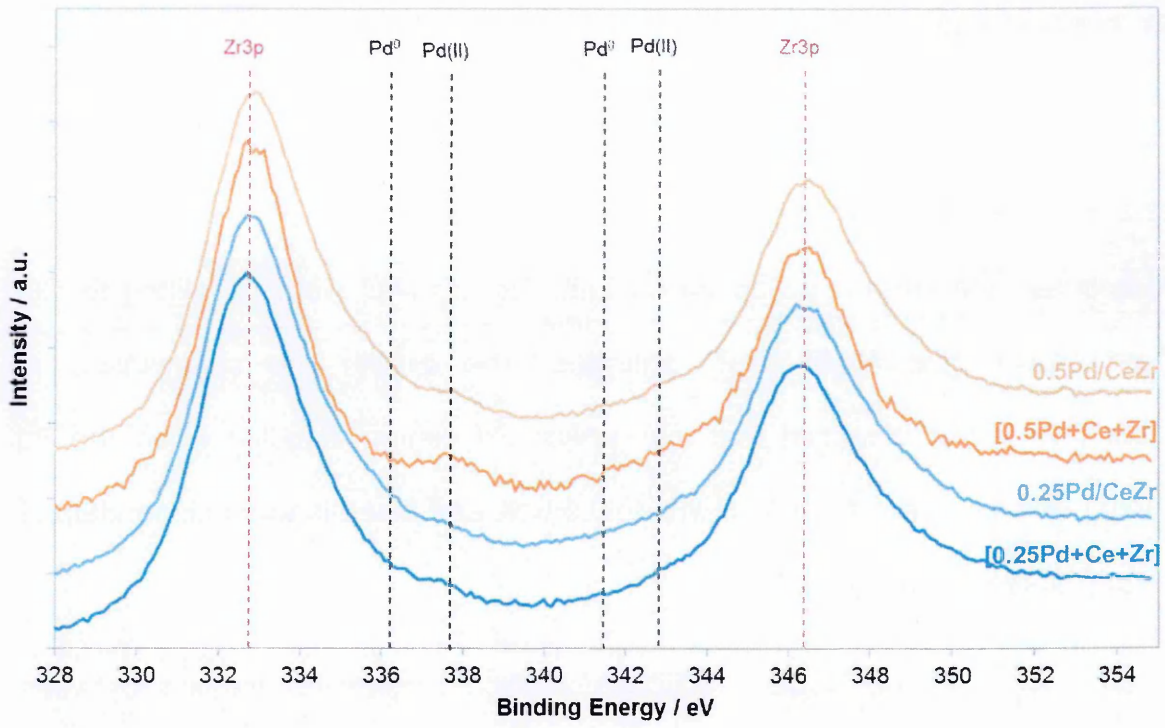

Figure 5-3: Pd3d and Zr3p spectra obtained by XPS comparing Pd-CeZr samples with different Pd-loadings prepared by wet impregnation (Pd/CeZr) and by co-precipitation with Ce^{3+} precursor ([Pd+Ce+Zr]).The red vertical lines point the positions of Zr3p bands, whilst the black vertical lines point the positions where the different Pd species should be detected (these last are not visible due to the overlap of Zr3p and Pd3d signals).

The Ce/Zr atomic ratio was also calculated to study the homogeneity of the CeZr mixed oxide at the surface. Table 5-2 shows these results.

Table 5-2: Ce/Zr atomic ratios calculated by XPS, comparing Pd-CeZr samples with different Pd-loadings prepared by wet impregnation (Pd/CeZr) and by co-precipitation with Ce^{3+} precursor ([Pd+Ce+Zr]).

Sample	Ce/Zr atomic ratio
[0.25Pd+Ce+Zr]	1.0
0.25Pd/CeZr	1.0
[0.5Pd+Ce+Zr]	0.9
0.5Pd/CeZr	0.9

XRD analyses showed that the mixed oxide formed was close to Ce:Zr 1:1 molar ratio (slightly richer in Zr), therefore a surface Ce/Zr atomic ratio close to 1.0 was

expected. The atomic ratios values were between 0.9 and 1.0, in agreement with the bulk composition obtained by XRD.

5.3.2. Metal dispersion analyses: CO chemisorption & EtOH-TPSR

To estimate the surface palladium content, the samples were submitted to CO chemisorption and EtOH-TPSR analyses. The results are summarised in Table 5-3. It was observed that the surface Pd content doubled when the Pd loading was increased from 0.25 wt% to 0.5 wt% and that this was independent of the preparation method used.

When comparing the values obtained for each preparation method between samples with similar Pd loadings different results were obtained from CO chemisorption and EtOH-TPSR methods. With the EtOH-TPSR, it was observed that the Pd surface areas obtained were identical irrespective of the preparation method; however, with CO chemisorption, a small decrease could be observed for the co-precipitated materials compared to the impregnated samples. This decrease was not significant for [0.25Pd+Ce+Zr] compared to 0.25Pd/CeZr, but it was slightly larger for [0.5Pd+Ce+Zr] compared to 0.5Pd/CeZr. Also, lower Pd dispersions were obtained for both co-precipitated samples in comparison with the impregnated catalysts, suggesting the formation of slightly bigger Pd particles, or some encapsulation or decoration by the CeZr.

In *Chapter 4* it was shown that Pd-CeO_2 samples prepared by co-precipitation always showed a smaller Pd surface area compared to the impregnated Pd/CeO_2 catalysts with similar loadings. Based on this and the other characterisation performed it was concluded that the lower Pd surface content obtained on the co-precipitated materials was due to a partial ceria decoration. Here, for Pd-CeZr

catalysts, no differences were found on Pd surface content (based on EtOH-TPSR results). Thus, based on these results only, no firm conclusions can be obtained, however this could initially suggest that low or no decoration occurred when Zr was present during the co-precipitation preparation. This could not be determined experimentally, as the quantification of Pd with XPS could not be possible due to the overlap with Zr3p peaks.

Table 5-3: Pd dispersion and Pd surface area measured by CO-chemisorption, and Pd surface area by EtOH-TPSR, of Pd-CeZr samples with different Pd-loadings prepared by wet impregnation (Pd/CeZr) and by co-precipitation with Ce^{3+} precursor ([Pd+Ce+Zr]). CO chemisorption instrument standard error = ± 2% (for metal dispersion) and ± 0.04 $m^2 g^{-1}$ (for metal surface area); EtOH-TPSR instrument standard error = ± 0.1 $m^2 g^{-1}$.

Method:	CO chemisorption		EtOH-TPSR	
Sample	Pd dispersion / %	Pd surface area / $m^2 g^{-1}$	max ppm CH_4 g sample^{-1} ppm $EtOH^{-1}$	Pd surface area / $m^2 g^{-1}$
0.25Pd/$Ce_{0.5}Zr_{0.5}O_2$	56	0.6	1.2	0.6
[0.25Pd+Ce+Zr]	43	0.5	1.2	0.6
0.5Pd/$Ce_{0.5}Zr_{0.5}O_2$	56	1.3	2.6	1.2
[0.5Pd+Ce+Zr]	40	0.9	2.5	1.2

In addition, compared to similar preparations on Pd-CeO_2, the metal surface area obtained on Pd-CeZr appeared higher than that on Pd-CeO_2 (Table 5-4). This could be due to their different thermal stabilities. CeO_2 suffers more sintering due to a poorer thermal stability than CeZr, promoting simultaneously the sintering of the supported metal [1, 2].

In contrast to Pd-CeO_2 catalysts, for the Pd-CeZr catalysts the metal surface areas obtained from both methods (CO chemisorption and EtOH-TPSR) did not differ significantly, suggesting little contribution from Pd-Ce interface sites or a change in CO:Pd stoichiometry during CO chemisorption (compared to the assumed stoichiometry for the Pd-CeO_2 samples).

Table 5-4: Pd surface area calculated by EtOH-TPSR, comparing samples based on Pd-CeO_2 and Pd-CeZr prepared by impregnation and by co-precipitation. Ce^{3+} precursor was used for all the different co-precipitations.

EtOH-TPSR:	Impregnated samples / $m^2\ g^{-1}$	Co-precipitated samples / $m^2\ g^{-1}$
0.25Pd-CeO_2	0.4	0.2
0.25Pd-CeZr	0.6	0.6
0.5Pd-CeO_2	0.9	0.5
0.5Pd-CeZr	1.2	1.2

5.4. Redox characterisation (TPR, OSC)

TPR experiments were found to be useful to study the reducibility in the Pd-Ce on Pd-CeO_2 catalysts, and understand more about the Pd-Ce interaction. The same approach was therefore used here.

OSC measurements were also performed. In this case, a significantly higher OSC, compared to the CeO_2 samples, was expected due to the distortion that Zr brings to the CeZr crystal structure [5-7, 12].

5.4.1. H_2-TPR

The H_2-TPR profiles of Pd-CeZr samples shown in Figure 5-4 contained two peaks. The peak at ~110 ºC corresponded to the reduction of PdO_x and promoted ceria, and the peak at ~350 ºC to the reduction of CeZr (bulk and non-promoted surface reduction occurs simultaneously in CeZr) [5, 14, 15].

The reduction temperature of Pd-Ce was not affected by the preparation method. It was only the increase of the Pd loading that shifted the reduction peak from ~105 ºC to ~95 ºC. Since the dispersion values shown in section 5.3.2. were

similar for 0.25 and 0.5 wt% Pd-CeZr samples prepared by the same method, the shift to lower temperature may not be related to an increase in Pd particle size; this could possibly have occurred due to a change in the strength of Pd-Ce interaction, with 0.25 wt% Pd samples leading to a stronger Pd-Ce interaction (the stronger the interaction with the support, the higher the reduction temperature) [9].

In terms of the peak's shape, the reduction seen for the co-precipitated samples occurred slightly faster (sharper peak) than for the impregnated sample, as was already seen previously for the Pd-CeO_2 co-precipitated samples in *Chapter 4*. A summary with the reduction temperatures and H_2 consumption for Pd-Ce and CeZr can be found in Table 5-5.

The amount of H_2 consumption associated to PdO_x was larger than the theoretical value, due to H_2 being spilled over from the Pd onto the support [9, 15, 16]. For this reason the reduction at this temperature is referred to as Pd-Ce reduction (PdO_x and promoted ceria). For the 0.25 wt% Pd samples, the co-precipitated material consumed more H_2 (0.54 mmol g^{-1} consumed by 0.25Pd/CeZr and 0.74 mmol g^{-1} by [0.25Pd+Ce+Zr]), whilst only a small increase was obtained for the 0.5 wt% Pd co-precipitated sample (0.70 mmol g^{-1} consumed by 0.5Pd/CeZr and 0.77 mmol g^{-1} by [0.5Pd+Ce+Zr]). This suggests that a larger number of Pd atoms could have been placed in contact with the ceria when using the co-precipitation method, especially at the lowest Pd loading [16, 17].

The total H_2 consumption during the reduction of CeZr (surface and bulk) appears to be affected by the preparation method used, but to be independent of Pd loading (0.23 – 0.28 mmol g^{-1} for the impregnated samples, and 0.16 – 0.17 mmol g^{-1} for the co-precipitated samples). Since the CeZr crystallite sizes and SSA-BET values of these samples were similar, the lower values for the co-precipitated samples could be due to a fewer number of un-promoted ceria

sites (not in contact with Pd), as these samples have shown to have a greater number of Pd sites in contact with Ce than those samples prepared by impregnation.

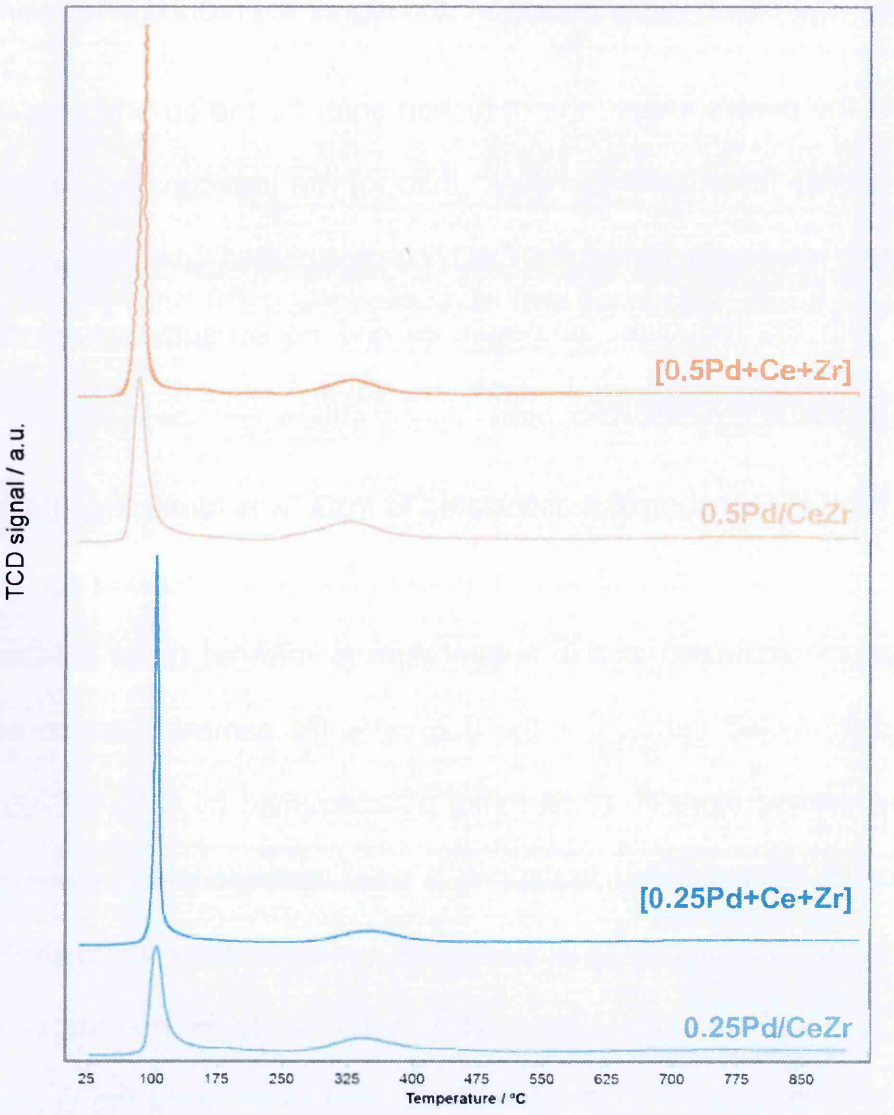

Figure 5-4: H_2-TPR of Pd-CeZr samples with different Pd-loadings prepared by wet impregnation (Pd/CeZr) and by co-precipitation with Ce^{3+} precursor ([Pd+Ce+Zr]). The sample taken was ~0.2 g, and the flow used was 30 ml min^{-1} of 10% H_2/N_2 using 30 ml min^{-1} of N_2 as carrier gas.

Overall, Pd-Ce reduction peak appeared particularly sharp for the co-precipitated materials, suggesting that a better Pd-Ce contact is created during the co-precipitation of [Pd+Ce+Zr].

Table 5-5: Summary of the temperatures corresponding to the PdO_x-Ce and CeZr reductions and their consequent H_2 consumption, for Pd-CeZr samples with different Pd-loadings prepared by wet impregnation (Pd/CeZr) and by co-precipitation with Ce^{3+} precursor ([Pd+Ce+Zr]). Average instrument standard error ± 0.02 mmol g^{-1}.

	Reduction of Pd-Ce		Reduction of CeZr	
Sample	Reduction temperature / °C	H_2 consumed / mmol g^{-1}	Reduction temperature / °C	H_2 consumed / mmol g^{-1}
0.25Pd/CeZr	104 °C	0.54	257 – 447 °C	0.23
[0.25Pd+Ce+Zr]	112 °C	0.74	271 – 436 °C	0.17
0.5Pd/CeZr	93 °C	0.70	225 – 441 °C	0.28
[0.5Pd+Ce+Zr]	99 °C	0.77	253 – 395 °C	0.16

5.4.2. CO-TPR

The CO-TPR profiles for these samples can be found in Figure 5-5. Similar to the H_2-TPR experiments, surface and bulk CeZr reduction occurred simultaneously around 350 – 400 °C; in addition, PdO_x reduction appeared at temperatures below 200 °C, and the reduction of Pd-Ce (PdO_x and promoted ceria) at ~ 300 °C [16].

CO consumption and CO_2 formation profiles showed a wide peak between 60 °C and 200 °C for all samples, which is associated with PdO_x reduction not in contact with Ce. It was noticed that this peak had a maximum at ~120 °C for 0.25Pd/CeZr and 0.5Pd/CeZr, and at ~140 °C for [0.25Pd+Ce+Zr] and [0.5Pd+Ce+Zr], with the reduction temperature just depending on the preparation method used and not on the Pd loading. Similarly, the reduction associated to PdO_x in contact with Ce (Pd-Ce) appeared approximately at 270 °C for 0.25Pd/CeZr and 0.5Pd/CeZr and at 300 °C for [0.25Pd+Ce+Zr] and [0.5Pd+Ce+Zr]. The slightly higher reduction temperatures obtained for the co-precipitated materials can be associated to smaller Pd particles and/or to a stronger interaction with Ce compared to the

impregnated catalysts [16]. Since surface analyses showed that Pd surface areas were similar for samples with the same loading prepared by the two different methods, this suggests that the shift to higher temperature was due to a higher Pd-Ce interaction.

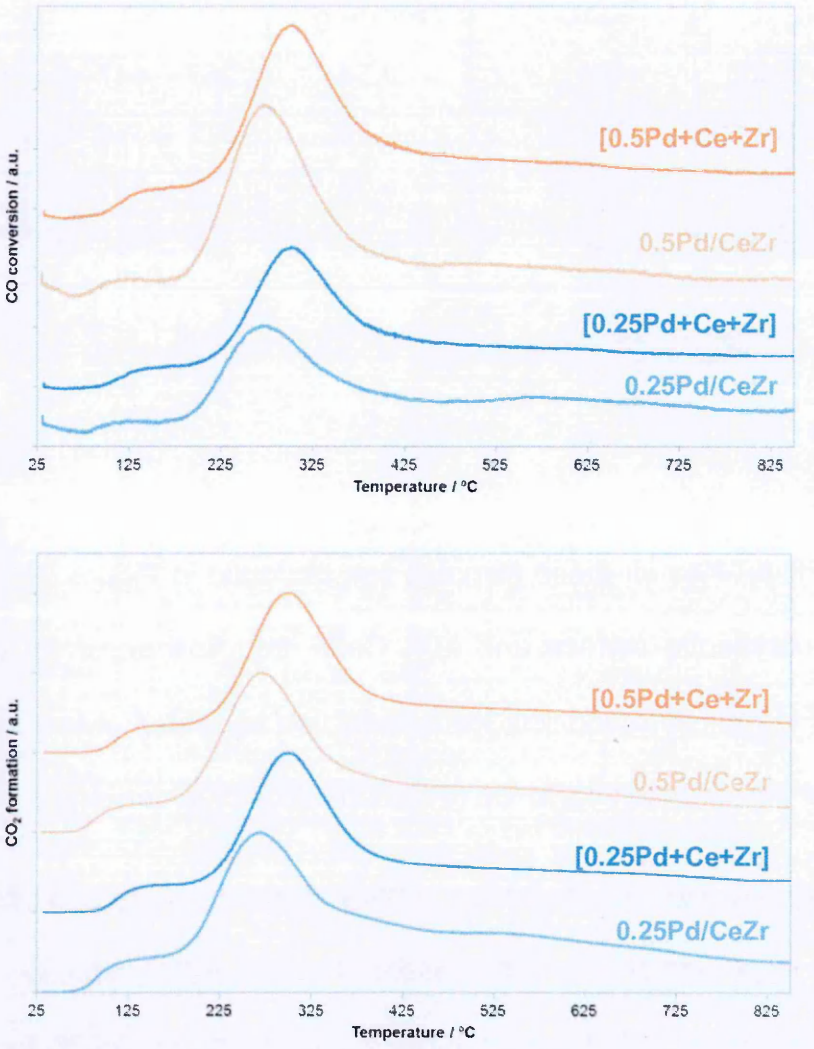

Figure 5-5: CO-TPR of Pd-CeZr samples with different Pd-loadings prepared by wet impregnation (Pd/CeZr) and by co-precipitation with Ce^{3+} precursor ([Pd+Ce+Zr]). (From top to bottom) CO consumption, and CO_2 formation during CO-TPR. The samples were previously pre-treated under 50 ml min^{-1} of He at 500 °C. During the CO-TPR the flow consisted in 20 ml min^{-1} of 10%CO/He in 30 ml min^{-1} of He.

The intensity of the Pd-Ce peak depends on Pd loading, as can be seen in Figure 5-5, where this peak was more intense for the samples with 0.5 wt% Pd due

to a higher number of Pd atoms. The wide shape of the Pd-Ce reduction peaks suggests that it overlaps with that for the reduction of CeZr (350-400 ºC) [16].

5.4.3. Oxygen Storage Capacity (OSC)

The OSC measured for these sets of samples can be seen in Figure 5-6, where the OSC values have been represented against temperature. Here the Pd-CeZr samples were also compared to an impregnated Pd-CeO_2 catalyst with similar noble metal content, to emphasise the increase of OSC achieved when using CeZr materials compared to CeO_2 [6, 7, 12].

As can be seen, the co-precipitated [0.5Pd+Ce+Zr] had a similar OSC in the low temperature region (100-250 ºC) as the equivalent sample prepared by impregnation, but measured a lower capacity at temperatures higher than 250 ºC (at 400 ºC, 0.5Pd/CeO_2 contained 574 µmol O g^{-1}, whilst [0.5Pd+Ce+Zr] only 382 µmol O g^{-1}). In contrast, the [0.25Pd+Ce+Zr] sample showed a better OSC than the equivalent impregnated sample at temperatures higher than 150 ºC (at 400 ºC, 0.25Pd/CeO_2 contained 432 µmol O g^{-1}, and [0.25Pd+Ce+Zr] 726 µmol O g^{-1}).

Compared to [0.5Pd+Ce^{3+}], the [0.5Pd+Ce+Zr] sample exhibited lower OSC values. Both samples followed the same trend, but [0.5Pd+Ce^{3+}] showed an improvement of 50 – 80 µmol O g^{-1} in the whole temperature region analysed here. On the other hand, [0.25Pd+Ce^{3+}] showed a lower OSC than [0.25Pd+Ce+Zr] at temperatures higher than 250 ºC. This improvement was of more than 200 µmol O g^{-1}.

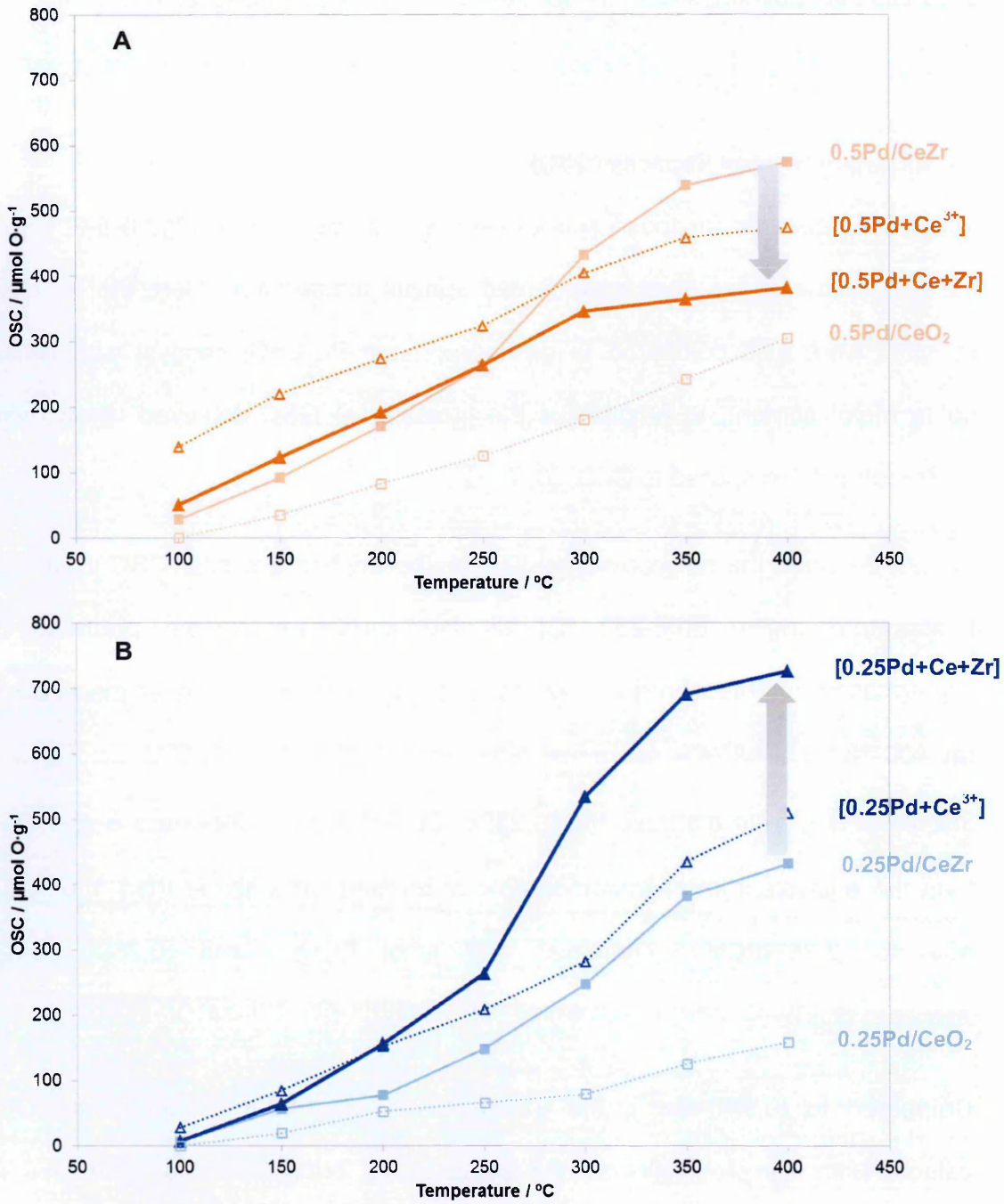

Figure 5-6: Comparison of the oxygen storage capacity of Pd-CeZr samples with different Pd-loadings prepared by wet impregnation (Pd/CeZr) and by co-precipitation with Ce^{3+} precursor ([Pd+Ce+Zr]). 0.5 wt% Pd loaded samples (A); 0.25 wt% Pd loaded samples (B). 0.25Pd-CeO_2 and 0.5Pd-CeO_2 prepared by impregnation and by co-precipitation have been also plotted to emphasise the increase of OSC when using CeZr materials. The OSC measurement was performed alternating switches between O_2 (10 ml min^{-1} of 5 %O_2/He) and CO (10 ml min^{-1} of 10 %CO/He) using He as a carrier gas (90 ml min^{-1}) at steady state temperatures. OSC instrument average standard error = ± 8 µmol O g^{-1}.

Overall, [0.25Pd+Ce+Zr] contained an even higher OSC than the impregnated 0.5Pd/CeZr, showing a better Pd-Ce efficiency. These results reinforce the idea postulated in *Chapter 4* for the Pd-CeO_2 co-precipitated catalysts, where the importance of the Pd:Ce ratio to promote Pd-Ce interaction using the co-precipitation method for a better performance was highlighted. It was observed that better OSC values were only obtained for the co-precipitated [Pd+Ce^{3+}] samples over the impregnated catalysts, at Pd loadings lower than 1%. If the same Pd:Ce ratios are also needed in the case of Pd-CeZr samples, this will mean that only those below 0.5 wt% Pd would show a benefit. The evaluation of further samples with different Pd loadings on Pd-CeZr samples was however beyond the scope of this thesis.

The efficiency of the CeZr support (considered as $Ce_{0.5}Zr_{0.5}O_2$) of Pd-CeZr samples was calculated (Figure 5-7). To focus only on the efficiency from the CeZr, the palladium contribution was removed. The trends obtained followed those of the OSC; 0.5Pd/CeZr had a higher efficiency than [0.5Pd+Ce+Zr] (at 400 ºC, 12 % more efficiency), whilst [0.25Pd+Ce+Zr] was more efficient than 0.25Pd/CeZr (at 400 ºC, 17 % more efficiency).

Comparing the efficiency values of Pd-CeZr and Pd-CeO_2 based samples it can be noticed that Pd-CeZr samples are significantly better (Table 5-6). When Ce^{4+} is reduced to Ce^{3+} the crystal structure suffers a stress due to the larger size of Ce^{3+} ion that restricts its redox properties; as Zr^{4+} is smaller, when it is added to the CeO_2 lattice, it compensates for the volume changes and facilitates the reduction/oxidation of $Ce^{4+/3+}$ (Ionic radius: Zr^{4+} = 0.84 Å; Ce^{4+} = 0.97 Å, Ce^{3+} = 1.14 Å) [7, 18].

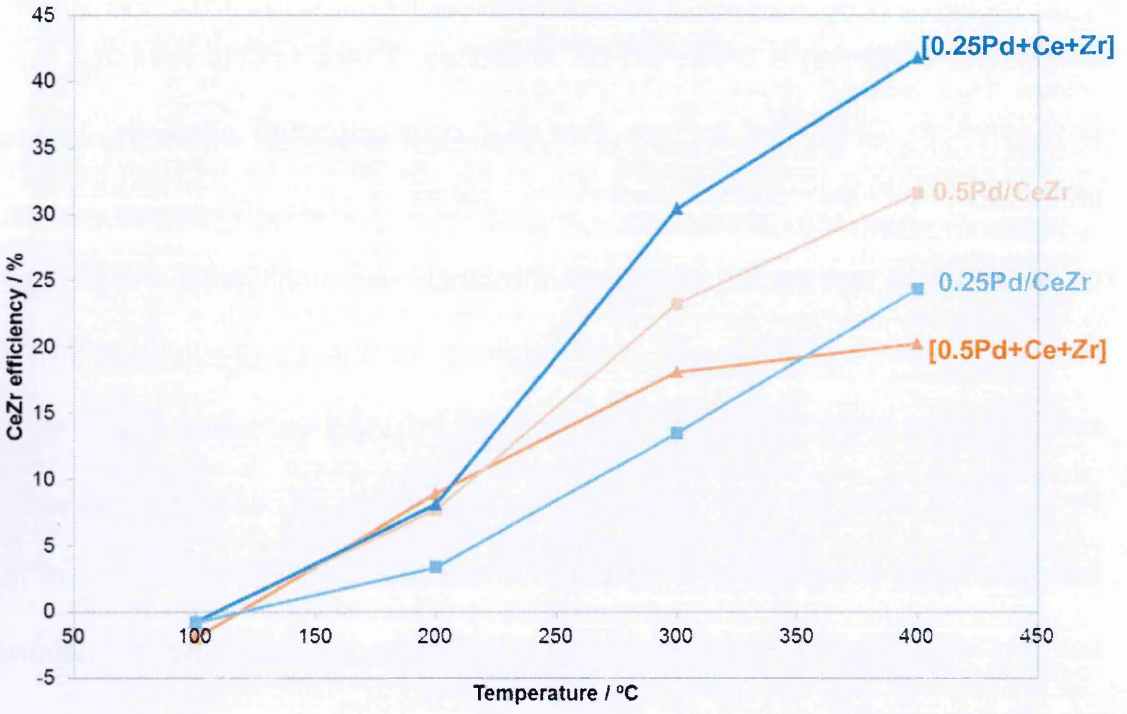

Figure 5-7: CeZr efficiency (%) during the OSC test of Pd-CeZr samples with different Pd-loadings prepared by wet impregnation (Pd/CeZr) and by co-precipitation with Ce^{3+} precursor ([Pd+Ce+Zr]) during an OSC test.

Table 5-6: CeZr efficiency (%) at 400 °C comparing Pd-CeZr samples with different Pd-loadings prepared by wet impregnation (Pd/CeZr) and by co-precipitation with Ce^{3+} precursor ([Pd+Ce+Zr]). The efficiency of a 0.5Pd/CeZr sample prepared by impregnation on a commercial support was also included for comparison.

Sample	Impregnated samples Ce-efficiency at 400 °C / %	Co-precipitated samples Ce-efficiency at 400 °C / %
0.25Pd-CeO_2	5	17
0.25Pd-CeZr	25	42
0.5Pd-CeO_2	9	15
0.5Pd-CeZr	32	20
0.5Pd-CeZr (commercial)	31	-

The efficiency of a 0.5Pd/CeZr sample prepared by wet impregnation on a commercial $Ce_{0.5}Zr_{0.5}O_2$ support was compared to the sample prepared by the

same method on the co-precipitated $Ce_{0.5}Zr_{0.5}O_2$ support synthesised for this work. Both samples showed similar efficiency values.

5.5. Kinetic characterisation: CO-SSITKA

The reaction rate and activation energy of CO oxidation over these samples was studied. The analysis was performed between 30 and 80 ºC in steps of 10 ºC. The comparison of the reaction rate of these samples can be seen in Figure 5-8.

Focusing on the preparation method, the reaction rate at the two lowest temperature points (30 ºC and 40 ºC) for the impregnated and co-precipitated samples appeared to be practically identical for the catalyst with 0.5 wt% Pd. However, when increasing the temperature, the reaction rate for both impregnated catalysts increased to a larger extent than for the co-precipitated samples (higher temperature coefficient). Based on metal surface area experiments (section 5.3.2.), the different preparation methods did not have a significant impact on the Pd surface content, which could explain the similar reaction rates obtained for these catalysts.

Pd loading had a significant impact on the value of the reaction rate, being higher those with the lowest Pd loading (0.25 wt% Pd). The characterisation performed on Pd-CeZr samples showed that the metal dispersion was similar between 0.25 and 0.5 wt% Pd samples prepared by the same method; thus, they are expected to have similar particle sizes. However, the reduction temperature associated to Pd-Ce during H_2-TPR experiments appeared at slightly higher temperature for 0.25 wt% Pd samples, independently of the preparation method. Based on these results, the higher CO reaction rate seen for the 0.25Pd-CeZr samples could be

justified as a stronger interaction between Pd and Ce atoms on these samples than on the 0.5Pd-CeZr catalysts.

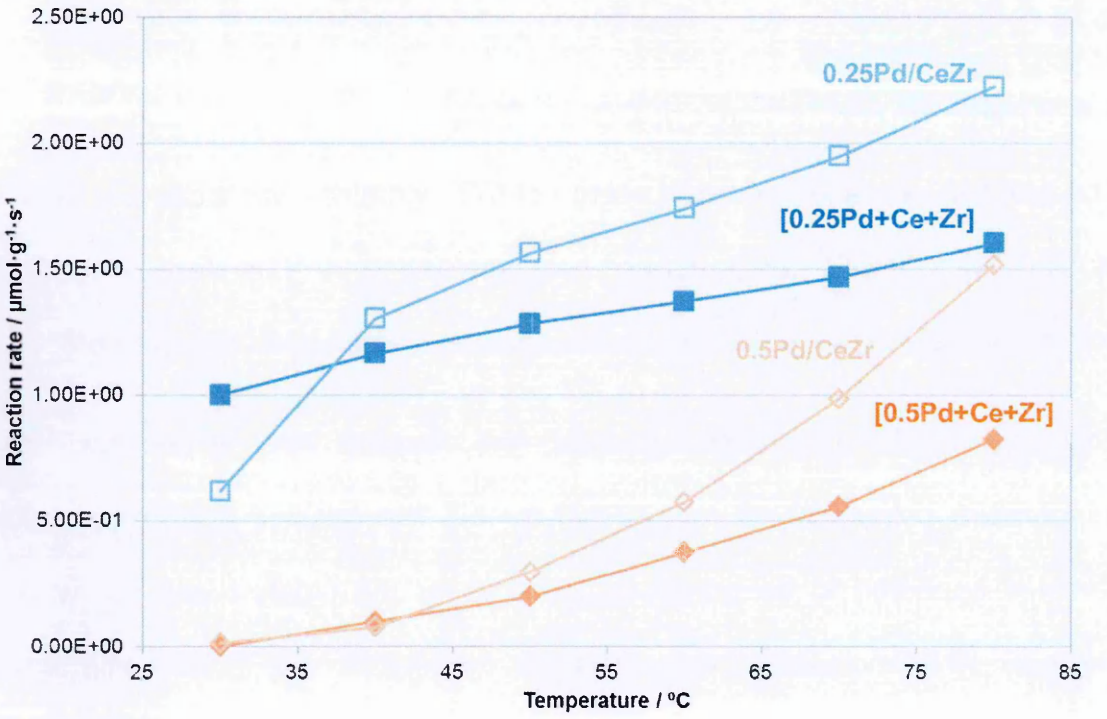

Figure 5-8: Comparison of CO oxidation reaction rate at steady temperatures of Pd-CeZr samples with different Pd-loadings prepared by wet impregnation (Pd/CeZr) and by co-precipitation with Ce^{3+} precursor ([Pd+Ce+Zr]). The gas flows used were 52.5 ml min^{-1} of 5% O_2/He, 5.5 ml min^{-1} of 1%CO/5%Ar/He (^{12}C) and 5.5 ml min^{-1} of 1%CO/He (^{13}C). The average reaction rate standard error was ±0.01 µmol g^{-1} s^{-1}.

This can be also seen when comparing the activation energy (E_a), which is shown in Table 5-7. The Pd-CeZr catalysts with 0.25 wt% Pd had lower E_a values than those with 0.5 wt% Pd, which is the opposite trend to that found for Pd-CeO_2 catalysts previously shown in *Chapter 4*. On Pd-CeO_2 samples, this trend suggested that bigger Pd particles were more active for this reaction; however, the similar Pd dispersion values found for Pd-CeZr samples (and thus similar Pd particles sizes) suggests that in this case the activity of Pd was dependent to a larger extent on the interaction with the CeZr support. As mentioned previously, this could be seen during H_2-TPR experiments, where the 0.25Pd-CeZr samples showed a stronger interaction with the Ce atoms than 0.5Pd-CeZr.

In contrast to the Pd loading, the preparation method did not have a significant impact on the E_a of Pd-CeZr samples. The E_a values and equations rate of Pd-CeO_2 catalysts have been also added to Table 5-6 for comparison. Similarly to Pd-CeO_2 catalysts, the reaction rate was not dependant on O_2 concentration (zero reaction order), and it had reaction order of 1 with respect to CO, suggesting that the CO oxidation occurred through the same mechanism as in Pd-CeO_2 catalysts. The suggested mechanism consists of the reaction between the adsorbed CO molecule on Pd and the oxygen from the CeZr support [19, 20].

Table 5-7: Equation rate and E_a for CO oxidation for Pd-CeZr samples with different Pd-loadings prepared by wet impregnation (Pd/CeZr) and by co-precipitation with Ce^{3+} precursor ([Pd+Ce+Zr]). For Pd-CeO_2 samples the E_a decreases when increasing Pd loading, and for Pd-CeZr the E_a decreases when decreasing it. The standard errors for E_a are shown between brakets next to the values.

Sample	Equation rate	E_a / kJ·mol^{-1}
0.25Pd/CeO_2	r = k [CO]	35 (± 1)
[0.25Pd+Ce^{3+}]	r = k [CO]	54 (± 8)
0.5Pd/CeO_2	r = k [CO]	27 (± 2)
[0.5Pd+Ce^{3+}]	r = k [CO]	11 (± <1)
0.25Pd/CeZr	r = k [CO]	12 (± <1)
[0.25Pd+Ce+Zr]	r = k [CO]	7 (± <1)
0.5Pd/CeZr	r = k [CO]	51 (± 3)
[0.5Pd+Ce+Zr]	r = k [CO]	48 (± 2)

5.6. Light-off performance

The light-off performance of the catalysts under cold-start and under perturbed conditions were also tested. The perturbed light-off was of special interest, as major differences during the characterisation performed were found for the OSC.

5.6.1. Cold-start conditions

Pd/CeZr catalysts prepared by wet impregnation and by co-precipitation were tested under cold light-off conditions (see *Chapter 2* for a description of the test). The comparison can be seen in Figure 5-9. A summary of the necessary temperatures to obtain 50% conversion of the pollutants (T50) for each of these catalysts can be also found in Table 5-8.

Only small differences were obtained comparing the catalysts prepared using the different two methods. The biggest impact in the light-off was brought by Pd loading, with 0.5 wt% Pd leading to lower light-off temperatures due to a higher number of surface active sites [21, 22].

In section 5.3.2. it was shown that 0.25 wt% Pd samples prepared by co-precipitation and by impregnation contained similar amounts of surface palladium; however, [0.25Pd+Ce+Zr] showed a faster Pd-Ce reduction and a higher H_2 consumption during H_2-TPR experiments, indicating that a larger number of Ce atoms were promoted by Pd creating better oxygen mobility. This interaction was reflected in the NO_x and CO profiles, where it could be noticed that the light-off for [0.25Pd+Ce+Zr] was sharper than that for 0.25Pd/CeZr, giving higher conversion values after 250 ºC.

Table 5-8: Necessary temperature for 50% conversion of CO, NO_x and HC for Pd-CeZr samples with different Pd-loadings prepared by wet impregnation (Pd/CeZr) and by co-precipitation with Ce^{3+} precursor ([Pd+Ce+Zr]), during a cold-start light-off test at λ = 0.95. Light-off instrument average standard error = ± 2 ºC.

Sample	CO		NO_x		HC	
	T50 / ºC	ΔT50 / ºC	T50 / ºC	ΔT50 / ºC	T50 / ºC	ΔT50 / ºC
0.25Pd/$Ce_{0.5}Zr_{0.5}O_2$	239	-4	257	0	373	-24
[0.25Pd^{2+}+Ce^{3+}+ZrO^{2+}]	243		257		349	
0.5Pd/ $Ce_{0.5}Zr_{0.5}O_2$	212	10	233	9	361	1
[0.5Pd^{2+}+Ce^{3+}+ZrO^{2+}]	222		242		362	

[0.5Pd+Ce+Zr] presented a slightly worse light-off performance (higher temperature) than 0.5Pd/CeZr. This could be associated to a smaller Pd surface content on the co-precipitated material, as shown by CO chemisorption analyses (1.3 m^2 g^{-1} and 0.9 m^2 g^{-1} for the impregnated and co-precipitated samples, respectively) [21].

Similar conclusions were found previously in *Chapter 4* for Pd-CeO_2 samples with different Pd loadings prepared by impregnation on CeO_2 and by co-precipitation with Ce^{3+} precursor, where it was seen that the light-off temperature strongly depended on their metal surface areas.

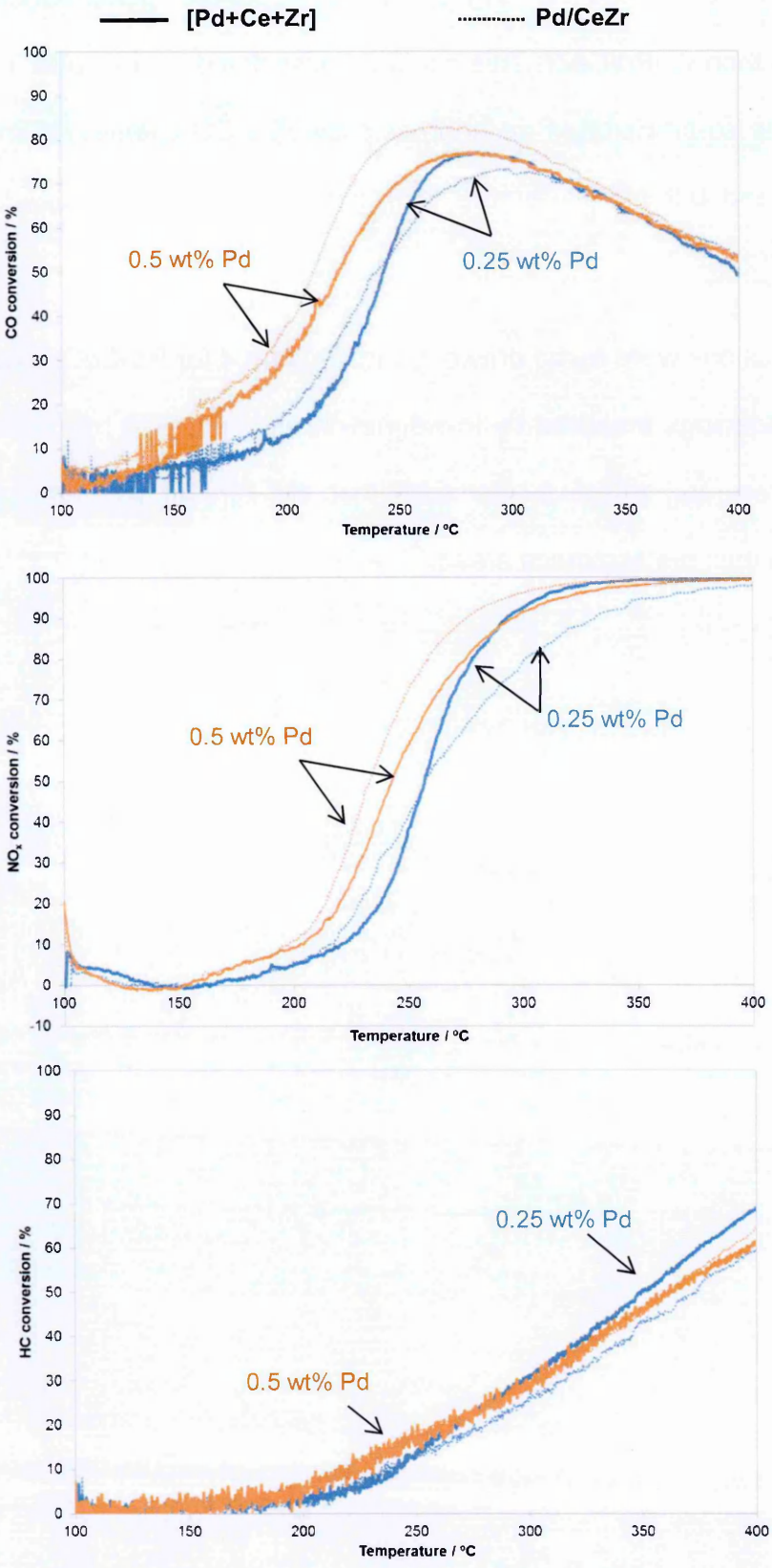

Figure 5-9: CO, NO_x and HC light-off performance under constant lambda at 0.95 of Pd-CeZr samples with different Pd-loadings prepared by wet impregnation (Pd/CeZr) and by co-precipitation with Ce^{3+} precursor ([Pd+Ce+Zr]). The sample taken was 0.4 g (0.2 g sample + 0.2 g cordierite) and the gas flow rate 2 L min^{-1}. The catalyst was heated using a ramp rate of 10 °C min^{-1} from 100 to 400 °C.

5.6.2. Perturbed light-off

Since the main difference between these catalysts appeared to be their OSC performance, it was expected that their activities under perturbed conditions could also emphasise their differences in terms of catalytic activities. The results for lambdas 0.99 ± 0.05 and 1.01 ± 0.05 can be seen in Figure 5-10.

The light-off temperatures for [0.5Pd+Ce+Zr] appeared at higher values than for its reference sample 0.5Pd/CeZr under all the conditions tested here (~20 °C higher in most cases). The lower light-off temperature shown by the 0.5Pd/CeZr sample is likely to be due to a higher Pd surface content than on [0.5Pd+Ce+Zr], as shown by CO chemisorption analyses [21, 22]. On the other hand, the final conversion at temperatures higher than 300 °C appeared to be practically identical. These results were not expected, since the OSC at temperatures higher than 250 °C was better for the impregnated sample, and thus, higher conversions were expected for the 0.5Pd/CeZr sample. No explanation was found to justify this behaviour.

Different results were obtained for the 0.25Pd-CeZr samples. Practically no differences were found between the light-offs of these samples, agreeing with the metal surface quantification performed previously where it was shown that 0.25Pd/CeZr and [0.25Pd+Ce+Zr] contained similar Pd surface areas. Regarding their final conversion at high temperature (T > 250 °C), the [0.25Pd+Ce+Zr] performed slightly better than 0.25Pd/CeZr (~3-5% higher conversion than 0.25Pd/CeZr). This small improvement is likely to be related with the higher OSC performance shown by [0.25Pd+Ce+Zr], however is not as significant as would have been predicted from the OSC measurements.

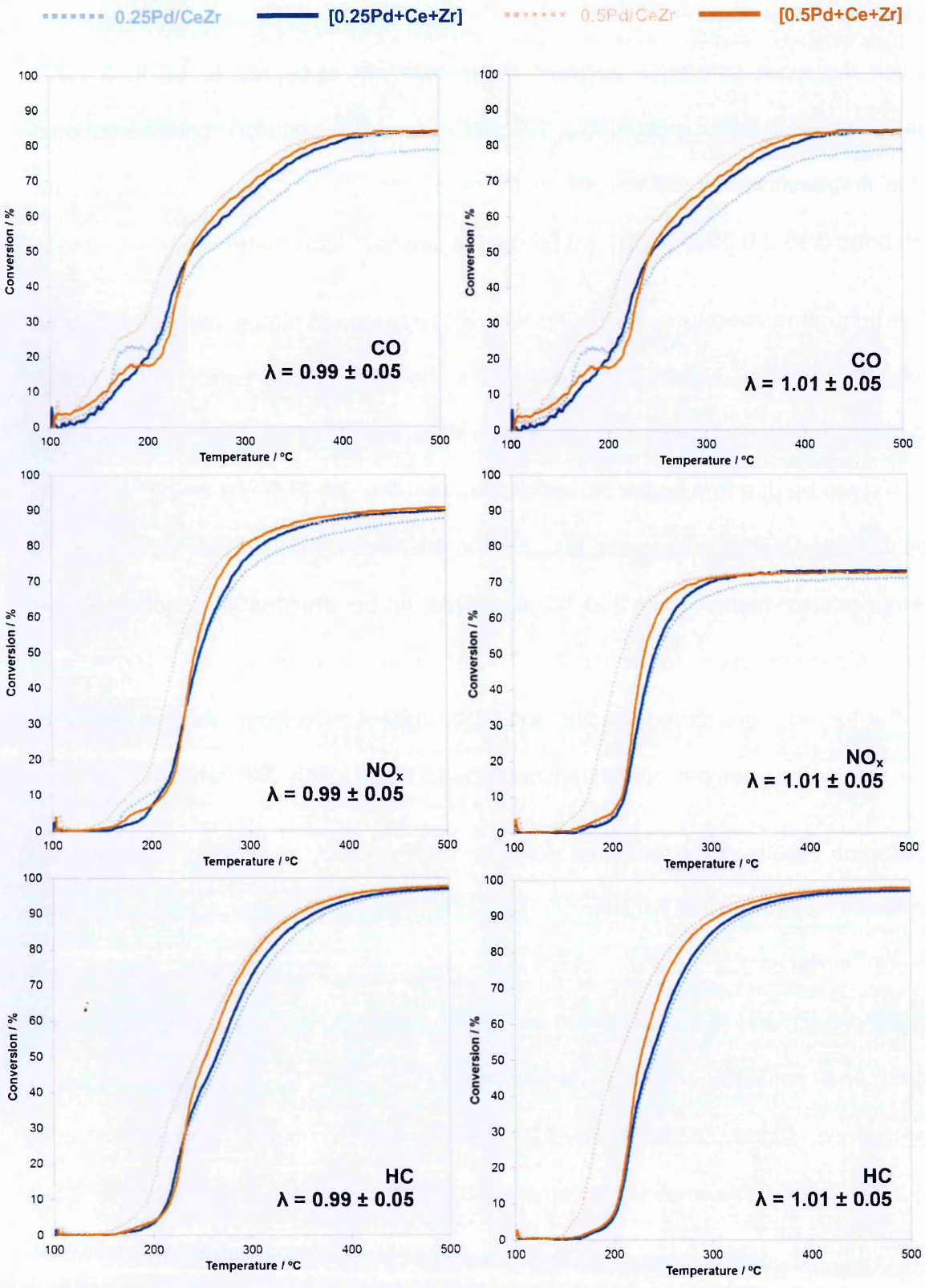

Figure 5-10: Light-off performance under perturbed conditions of Pd-CeZr samples with different Pd-loadings prepared by wet impregnation (Pd/CeZr) and by co-precipitation with Ce^{3+} precursor ([Pd+Ce+Zr]). From top to bottom, CO, NO_x and HC conversions; from left to right, light-offs at lambdas 0.99 ± 0 .05 and 1.01 ± 0.05. The sample size taken was 0.4 g (0.2 g sample + 0.2 g cordierite) and the gas flow rate 5 L min^{-1}. The catalyst was heated using a ramp rate of 10 °C min^{-1} from 110 to 500 °C.

A summary of the necessary temperature to achieve 50% conversion and the conversion obtained at 350 °C can be found in Table 5-9:

Table 5-9: Necessary temperature for 50% conversion of CO, NO_x and HC, and conversion values at 350 °C during a perturbed light-off test, for Pd-CeZr samples with different Pd-loadings prepared by wet impregnation (Pd/CeZr) and by co-precipitation with Ce^{3+} precursor ([Pd+Ce+Zr]). Light-off instrument average standard error = ± 2 °C.

	T50 / °C						Conversion at 350 °C / %					
	0.99			1.01			0.99			1.01		
	NO_x	HC	CO	NO_x	HC	CO	NO_x	HC	CO	NO_x	HC	CO
0.25Pd/CeZr	249	269	263	246	240	220	80	85	69	70	92	91
[0.25Pd+Ce+Zr]	248	264	244	243	236	216	85	88	75	73	93	94
0.5Pd/CeZr	225	242	224	210	204	177	86	91	80	72	96	96
[0.5Pd+Ce+Zr]	244	253	243	233	226	217	87	90	78	72	95	95

As an observation, in Figure 5-10, a small inflection is present during the CO light-off profiles (between 150 – 220 °C). This is related to the competition between CO and HC oxidation reactions. CO oxidation occurs at lower temperature than HC, but once HC starts reacting (at the temperature where the bump in the CO light-off is formed) both molecules compete for oxygen, and it is this that creates the distortion during the CO light-off.

5.7. Summary

The use of the co-precipitation method to prepare Pd-CeZr catalysts did not show a significant improvement over the impregnation method. Instead, the Pd loading was seen to have a more significant impact on Pd surface area, Pd-Ce interaction, and light-off performance with either preparation method.

EtOH-TPSR analyses revealed that both preparations led to products with similar Pd surface areas (at similar loadings). However, CO-chemisorption showed that

this was still the case for the samples with low Pd loading (0.25 wt%), but not at high loadings (0.5 wt%), where Pd metal area was slightly higher for the impregnated sample. Moreover, the value obtained from the CO-chemisorption for [0.5Pd+Ce+Zr] was lower than that obtained with the EtOH-TPSR method, suggesting that [0.5Pd+Ce+Zr] adsorbed less CO per Pd-site than 0.5Pd/CeZr, possibly due to a change in the Pd:CO stoichiometry[1]. The change in Pd:CO stoichiometry seemed to be a key parameter to explain the differences between the activities of these catalysts. The stoichiometry is usually determined by evaluation of the CO adsorption using infrared spectroscopy [23], however this could not be done for the Pd-CeO_2 and Pd-CeZr samples due to issues regarding the sample preparation for this analysis[2]. Thus, this theory could not be demonstrated. If a change in CO:Pd stoichiometry has occurred, based on published literature, the CO:Pd stoichiometry typically depends on the nature of the metal and the support, as well as on the interaction between them [23]. Since a more intimate contact is created between Pd and Ce when co-precipitated together, the interaction is expected to be different to the interaction found in the impregnated catalysts, which could explain a change in stoichiometry of adsorption.

The light-off performance is strongly related to Pd surface content, and this could also be seen during the experiments performed here [21, 22]. The samples based on 0.25Pd-CeZr presented similar light-off temperatures as both catalysts contained similar Pd surface areas; however, the [0.5Pd+Ce+Zr] sample showed a slightly higher light-off temperature than 0.5Pd/CeZr, suspected to be due to the

[1] There are typically three different chemisorption conformations: linear, bridge, and twin type.

[2] For the analysis of the type of CO adsorption through DRIFTS it was necessary to prepare the samples as pellets. Due to the large quantities of H_2O that the Ce-based materials adsorb from the atmosphere, these pellets could not be formed. Even after the samples were dried in air at 105 °C, the samples seemed to still contain water, which made them to stick to the dice used to prepare them, and constantly broke during their preparation.

lower adsorption capacity of the [0.5Pd+Ce+Zr] sample (based on CO chemisorption results) as mentioned previously. Thus, based on the results obtained here, the light-off temperature seems to have a stronger dependence on the adsorption capacities than on the overall Pd surface content.

In terms of Pd-Ce interaction, H_2-TPR experiments revealed that, even though the reduction of Pd-Ce appeared as a sharp peak for both co-precipitated samples, a higher H_2 consumption (compared to the equivalent impregnated catalyst) was only achieved for [0.25Pd+Ce+Zr], suggesting that a higher number of Pd and Ce atoms were in contact than on the 0.25Pd/CeZr sample [16, 17]. However, a similar H_2 consumption was obtained for [0.5Pd+Ce+Zr] compared to 0.5Pd/CeZr. In addition, the Pd-Ce reduction peak appeared at higher temperatures for the samples containing 0.25 wt% Pd, suggesting a stronger Pd-Ce interaction in the low loaded samples.

In *Chapter 4* it was shown that the XPS profiles were also important to clarify the level of Pd-Ce interaction; however in this case, Pd3d and Zr3p signals overlapped and no information regarding Pd oxidation state or level of Pd-Ce interaction could be obtained [11].

The bigger promotion of Ce-atoms by Pd seen in [0.25Pd+Ce+Zr], compared to 0.25Pd/CeZr, led to an increase in the OSC capacity and a small improvement in the final pollutant conversions during perturbed light-off conditions; in contrast, the co-precipitation of [0.5Pd+Ce+Zr] led to lower OSC capacity and similar conversions during the perturbed light-off, compared to the results obtained for 0.5Pd/CeZr.

To summarise, the Pd:Ce ratio is a key parameter for improving the Pd-Ce contact when using the co-precipitation method, where an improvement was only achieved

with the low Pd loaded sample ([0.25Pd+Ce+Zr]). This agrees with the results seen previously based on Pd-CeO_2 materials presented in *Chapter 4*, where only an improvement was achieved at Pd loadings lower than 1 wt%. In addition, similar or worst performances were seen during the light-offs as a consequence of similar or slightly lower adsorption capacities [21, 22]. Moreover, the almost identical Pd surface areas obtained with the EtOH-TPSR method between impregnated and co-precipitated samples when comparing equal Pd loadings, suggests that no encapsulation occurred for the co-precipitated [Pd+Ce+Zr] samples.

References Chapter 5

[1] C. Descorme, S. Bedrane and D. Duprez, Catalysis Today, 75 (2002) 401-405.

[2] H. S. Gandhi, G. W. Graham and R. W. McCabe, Journal of Catalysis, (2003) 433-442.

[3] M. Ozawa, Journal of Alloys and Compounds, 275-277 (1998) 886-890.

[4] D. Belton, C. E. Hori, H. Permana, K. Y. S. Ng, A. Brenner, K. More and K. M. Rahmoeller, Applied Catalysis B: Environmental, 16 (1998) 105-117.

[5] J. Wang, M. Zhao and M. Shen, Journal of Catalysis, 248 (2007) 258-267.

[6] F. Dong, A. Suda, T. Tanabe, Y. Nagai, H. Sobukawa, H. Shinjoh, M. Sugiura, C. Descorme and D. Duprez, Catalysis Today, 93-95 (2004) 827-832.

[7] Y. Nagai, T. Yamamoto, T. Tanaka, S. Yoshida, T. Nonaka, T. Okamoto, A. Suda and M. Sugiura, Catalysis Today, 74 (2002) 225-234.

[8] F. Zereini and F. Alt (Editors), *Palladium Emissions in the Environment: Analytical Methods, Environmental Assessment and Health Effects*, Springer, 2006,

[9] B. Zhao, G. Li, C. Ge, Q. Wang and R. Zhou, Applied Catalysis B: Environmental, 96 (2010) 338-349.

[10] International Centre for Diffraction Data (ICDD), *PDF-4, COD (REV30738 2011.11.2)*, 2012.

[11] A. V. Naumkin, A. Kraut-Vass, S. W. Gaarenstroom and C. J. Powell, *NIST X-ray Photoelectron Spectroscopy Database*, 2000.

[12] A. Trovarelli, *Catalysis by Ceria and Related Materials*, Imperial College Press, 2002.

[13] A. I. Boronin, E. M. Slavinskaya, I. G. Danilova, R. V. Gulyaev, Y. I. Amosov, P. A. Kuznetsov, I. A. Polukhina, S. V. Koscheev, V. I. Zaikovskii and A. S. Noskov, Catalysis Today, 144 (2009) 201-211.

[14] A. Trovarelli, E. Aneggi, M. Boaro, C. d. Leitenburg and G. Dolcetti, Journal of Alloys and Compounds, 408-412 (2006) 1096-1102.

[15] R. Zhou, B. Zhao, G. Li, C. Ge and Q. Wanga, Applied Catalysis B: Environmental, 96 (2010) 338-349.

[16] M.-F. Luo and X.-M. Zheng, Applied Catalysis A: General, 189 (1999) 15-21.

[17] Y. Cao, R. Ran, X. Wu, B. Zhao, J. Wan and D. Weng, Applied Catalysis A: General, 457 (2013) 52-61.

[18] A. Martorana, G. Deganello, A. Longo, A. Prestianni, L. Liotta, A. Macaluso, G. Pantaleo, A. Balerna and S. Mobilioc, Journal of Solid State Chemistry, 117 (2004) 1268-1275.

[19] R. H. Nibbelke, A. J. L. Nievergeld, J. H. B. J. Hoebink and G. B. Marin, Applied Catalysis B: Environmental, 19 (1998) 245-259.

[20] R. Rajasree, J. H. B. J. Hoebink and J. C. Schouten, Journal of Catalysis, 223 (2004) 36-43.

[21] G. Wang, M. Meng, Y. Zha and T. Ding, Fuel, 89 (2010) 2244-2251.

[22] H. Birgersson, L. Eriksson, M. Boutonnet and S. G. Järås, Applied Catalysis B: Environmental, 54 (2004) 193-200.

[23] K. Nakai and K. Nakamura, *Pulse Chemisorption Method: Metal Dispersion Measurement*, 2003, http://www.tdno.ru/files/file/CAT-APP-002%28E%29.pdf [13-12-2013].

6. Impact of the noble metal on NM-CeO_2 co-precipitation (NM = Pd, Pt, Rh)

Contents

6. Impact of the noble metal on NM-CeO_2 co-precipitation (NM = Pd, Pt, Rh)

Pd, Pt and Rh are often used in TWC formulations, typically as a combination of Pt and Rh, or Pd and Rh, or even combining the three noble metals together [1]. Pd and Pt are mainly used for oxidation reactions, whilst Rh is mostly used for reduction reactions [1-3]. The choice of noble metal and loading usually depends on their predicted future prices. As an example of the changes they can suffer, Figure 6-1 shows the prices of Pd, Pt, and Rh between the years 2010 and 2014.

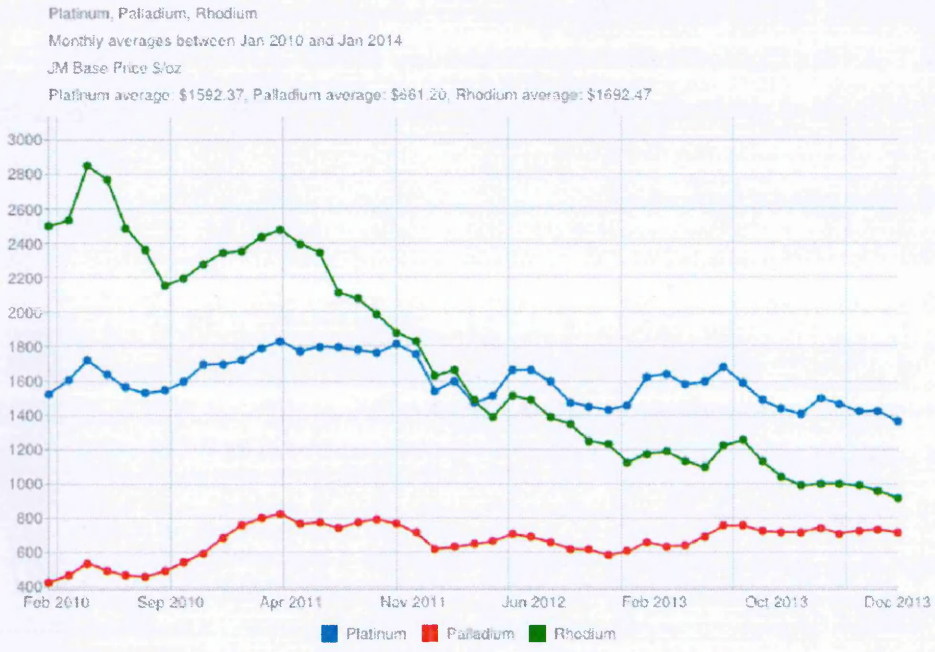

Figure 6-1: Monthly average price of Pd, Pt, and Rh between the years 2010 and 2014. (Source - Johnson Matthey).

As previously seen in *Chapter 4 and 5*, the co-precipitation of Pd with a Ce^{3+} precursor can lead to catalysts with a larger content of Ce atoms promoted by Pd, which as a consequence increases the oxygen storage capacity. This was also seen to be dependent on Pd:Ce ratio.

With the aim of studying if similar improvements can be obtained for Pt-CeO_2 and Rh-CeO_2 catalysts, Pt-CeO_2 and Rh-CeO_2 samples were also prepared by the

redox method described in *Chapter 2* and compared to catalysts with similar noble metal (NM) loadings prepared by wet impregnation. The co-precipitated catalysts will be referred as [NM+Ce^{3+}], and the impregnated as NM/CeO_2 (NM = Pd, Pt, Rh).

For a direct comparison with the results obtained in *Chapter 4* (based on 0.5Pd-CeO_2 catalysts), 0.5 wt% of each noble metal was used for these preparations. In addition, a catalyst with 0.1 wt% Rh was also synthesised to mimic closer loadings to those used in real catalysts.

6.1. Catalysis preparation observations

Similar to the results obtained for [0.5Pd+Ce^{3+}], the co-precipitation of [0.5Pt+Ce^{3+}] also led to a dark grey coloured sample (suggesting the reduction of Pt^{4+} to metallic Pt), which turned light brown once it was calcined (suggesting oxidation of Pt to PtO_2) [4]. In contrast, the co-precipitation of [0.5Rh+Ce^{3+}] and [0.1Rh+Ce^{3+}] led to a white precipitate that turned brown at ambient temperature (typical colour of Rh_2O_3, suggesting no reduction of Rh^{3+} to metallic Rh), and no colour change was observed during the calcination, suggesting that Rh and Ce did not suffer further changes regarding their oxidation states [4-6]. Figure 6-2 shows the different colours obtained for these materials:

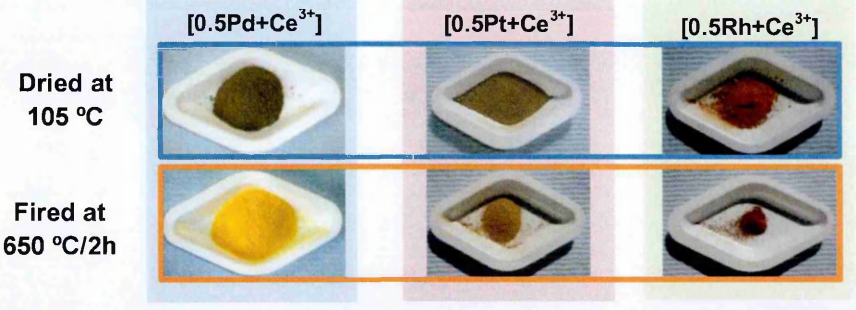

Figure 6-2: Pd-, Pt-, and Rh-CeO_2 catalysts prepared by co-precipitation with Ce^{3+} precursor, dried at 105 °C overnight, and calcined at 650 °C for 2 hours in air.

6.2. Structural characterisation

In order to understand if changing the noble metal (NM) during the co-precipitation affects the structure of the catalysts, the samples were evaluated by XRD. As mentioned in the previous chapters, one of the main objectives was to determine if the NM was placed within the ceria structure.

6.2.1. X-Ray Diffraction (XRD)

All catalysts, independent of the noble metal used, presented a cubic-CeO_2 structure [7]. No information regarding the noble metal could be obtained, implying that the NM particles are small and well dispersed [8]. The lattice parameters *a* and the ceria crystallite sizes are shown in Table 6-1. The XRD profiles are shown in Figure 6-3.

Table 6-1: Lattice parameter *a* and ceria crystallite size analysed by XRD, and specific surface area calculated by BET, of 0.5Pd-, 0.5Pt-, 0.5Rh- and 0.1Rh-CeO_2 samples prepared by wet impregnation on CeO_2 (NM/CeO_2) and by co-precipitation with Ce^{3+} precursor ([NM+Ce^{3+}]). Calculated errors (reported in brackets) for crystallite size (nm) refer to the last significant figure; BET-SSA instrument standard error = ± 4 m^2 g^{-1}.

	lattice parameters / Å	Crystallite size / nm	BET – SSA / m^2 g^{-1}	ICP / NM wt%
CeO_2 XRD Reference [7]	*a* = 5.411	-	-	-
0.5Pd/CeO_2	5.410	5.83 (± 0.07)	138	0.51
[0.5Pd+Ce^{3+}]	5.409	5.51 (± 0.05)	114	0.50
0.5Pt/CeO_2	5.410	6.55 (± 0.08)	107	0.54
[0.5Pt+Ce^{3+}]	5.409	5.68 (± 0.05)	102	0.48
0.5Rh/CeO_2	5.410	6.42 (± 0.06)	110	0.53
[0.5Rh+Ce^{3+}]	5.406	3.76 (± 0.04)	142	0.47
0.1Rh/CeO_2	5.410	6.61 (± 0.08)	106	0.13
[0.1Rh+Ce^{3+}]	5.407	5.66 (± 0.08)	124	0.12

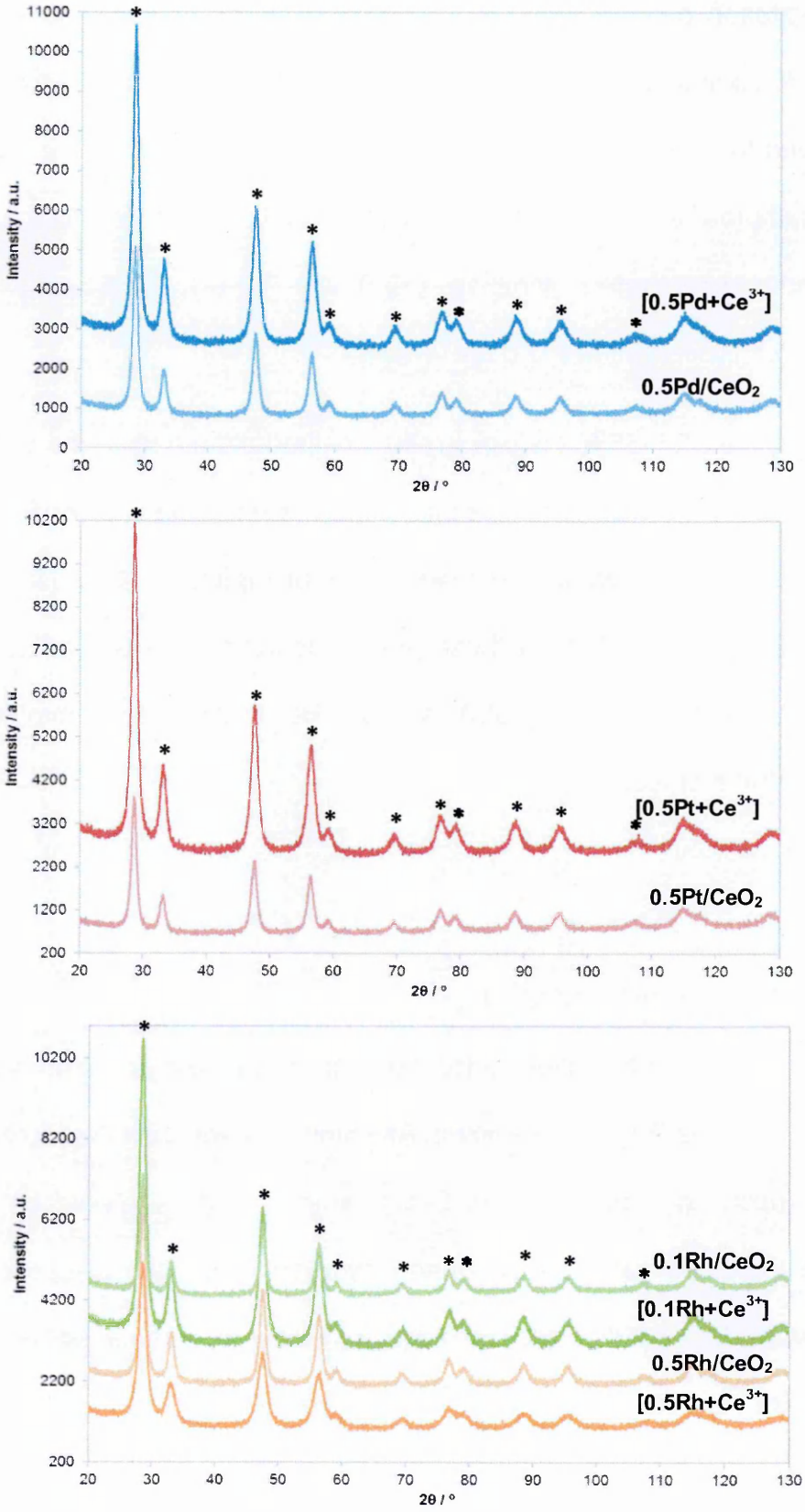

Figure 6-3: XRD profiles for NM-CeO_2 samples prepared by impregnation (NM/CeO_2) and by co-precipitation with Ce^{3+} precursors ([NM+Ce^{3+}]). The peaks corresponding to the cubic CeO_2 phase are indicated as (*).

As was previously seen for the Pd-CeO_2 catalysts, those catalysts prepared by the co-precipitation method showed a small contraction in the ceria structure (less than 0.1% contraction), but not significant enough to conclude if any metallic atom was added to the lattice of the CeO_2. In addition, the crystallite size was smaller for those samples prepared with the co-precipitation method compared to their equivalent impregnated samples (~0.9 nm lower), particularly evident for [0.5Rh+Ce^{3+}] preparation (~2.6 nm lower).

Regarding the BET-SSA, the preparation method did not have a significant impact when using Pt, however, the specific surface areas obtained for Rh were higher when the materials were prepared by co-precipitation. In addition, the SSA increased with Rh loading for these preparations. In contrast, the co-precipitation with Pd and Ce^{3+} led to SSA slightly lower than that obtained with the impregnation method.

6.2. Surface characterisation

The surface characterisation performed for these catalysts was similar to that performed for the Pd-CeO_2 samples. All samples were submitted to XPS and CO-chemisorption; in addition the Pt-CeO_2 samples were analysed by EtOH-TPSR and the Rh-CeO_2 samples by ethane hydrogenolysis. As discussed previously (*Chapter 3*) EtOH-TPSR can be used to measure surface Pd and Pt but not surface Rh, therefore a different method selective to surface Rh was needed (i.e. ethane hydrogenolysis). EtOH-TPSR and ethane hydrogenolysis techniques are detailed in *Chapter 3*.

6.2.1. X-Ray Photoelectron Spectroscopy (XPS)

XPS results were used to determine the level of interaction between the noble metal and the ceria for Pd-CeO_2 samples. For similar reasons, Pt- and Rh-ceria samples were submitted for these analyses. Pt4f and Rh3d signals can be seen in Figure 6-5 and Figure 6-6, respectively; Pd3d profiles are also shown here for comparison in Figure 6-4.

As was shown in *Chapter 4*, 0.5Pd-CeO_2 samples presented peaks associated with PdO species (at 337.6 and 342.9 eV for Pd/CeO_2, and at 337.3 and 342.5 eV for [0.5Pd+Ce^{3+}]), appearing shifted towards higher binding energies than those reported in the literature for PdO (which should appear at 336.8 and 342.06 ± 0.2 eV) indicating that a strong Pd-Ce interaction existed [9]. In addition to these bands, [0.5Pd+Ce^{3+}] also produced bands at positions associated with Pd species with higher oxidation states (338.3 and 343.5 eV), suggesting that the Pd-Ce interaction was stronger in this sample [9].

Similarly all the Pt-CeO_2 samples contained Pt4f bands in the PtO_2 region [10, 11]. These bands did not appear shifted towards higher binding energy for the [0.5Pt+Ce^{3+}] sample compared to 0.5Pt/CeO_2 which gave values similar to those predicted from the literature. Thus, based on this, both Pt-Ce samples appeared to have the same level of interaction [11]. Looking at the Ce/Pt calculated atomic ratio, [0.5Pt+Ce^{3+}] contained a significantly higher amount of Ce on the surface compared to 0.5Pt/CeO_2 (Ce/Pt atomic ratios of 118 and 65, respectively, a 45% increase), suggesting some Pt encapsulation by ceria and/or an increase of Pt particle size.

The binding energies of $Rh3d_{5/2}$ and $Rh3d_{3/2}$ in all Rh containing catalysts were attributed to Rh_2O_3 [10, 12]. Similar to the results for the Pt-CeO_2 samples, no change in the position of the peaks was seen for the co-precipitated [0.5Rh+Ce^{3+}]

compared to 0.5Rh/CeO_2. Also in this case the Ce/Rh atomic ratio was higher for [0.5Rh+Ce^{3+}] (216 for 0.5Rh/CeO_2 and 255 for [0.5Rh+Ce^{3+}], meaning an 18% increase). The larger SSA found for [0.5Rh+Ce^{3+}] compared to 0.5Rh/CeO_2 could have contributed to this increase.

From the Ce/NM atomic ratios it was observed that 0.5Pd-CeO_2, 0.5Pt-CeO_2 and 0.5Rh-CeO_2 catalysts contained very different amounts of surface noble metal[1]. In 0.5Rh-CeO_2 samples this ratio was significantly lower than for 0.5Pd-CeO_2 and 0.5Pt-CeO_2 samples, suggesting the formation of larger noble metal particles and/or greater ceria encapsulation. Using the impregnated catalysts as references (as most of the noble metal should be located on the surface of the material) it was possible to observe that 0.5Pd/CeO_2 had lower calculated Ce/NM atomic ratio value than 0.5Pt/CeO_2, suggesting that the impregnation of Pt on CeO_2 led to larger metal particles; moreover, 0.5Rh/CeO_2 showed a significantly higher calculated Ce/NM atomic ratio compared to Pd and Rh impregnated catalysts, suggesting that Rh particles were even larger than Pt particles. Therefore, based on the impact of the noble metal on the particle size, it could be possible that the higher Ce/NM value found for [0.5Rh+Ce^{3+}] compared to [0.5Pd+Ce^{3+}] and [0.5Pt+Ce^{3+}] could be associated with the formation of larger Rh particles, than for Pd and Pt catalysts. However, based only on XPS characterisation, it was not possible to determine the exact metal particle sizes of the co-precipitated materials, as the higher Ce/NM atomic ratios could also be due to a higher ceria-encapsulation.

[1] Based on XPS analyses, which are typically 5 nm in depth.

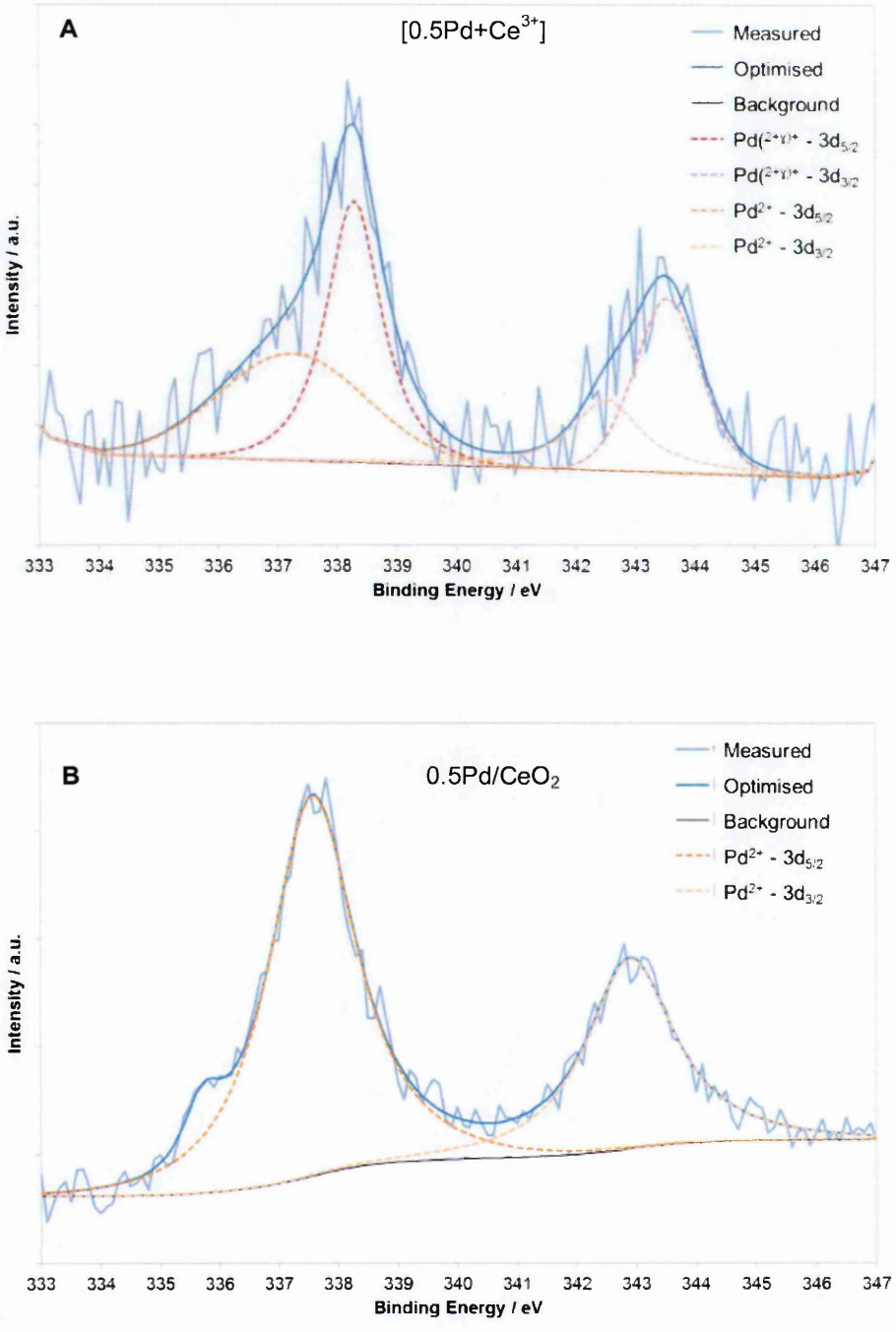

Figure 6-4: Deconvolution of Pd3d XPS peaks for 0.5Pd-CeO_2 samples prepared by co-precipitation with Ce^{3+} precursor ([0.5Pd+Ce^{3+}] (A)) and by impregnation on CeO_2 (0.5Pd/CeO_2 (B)).

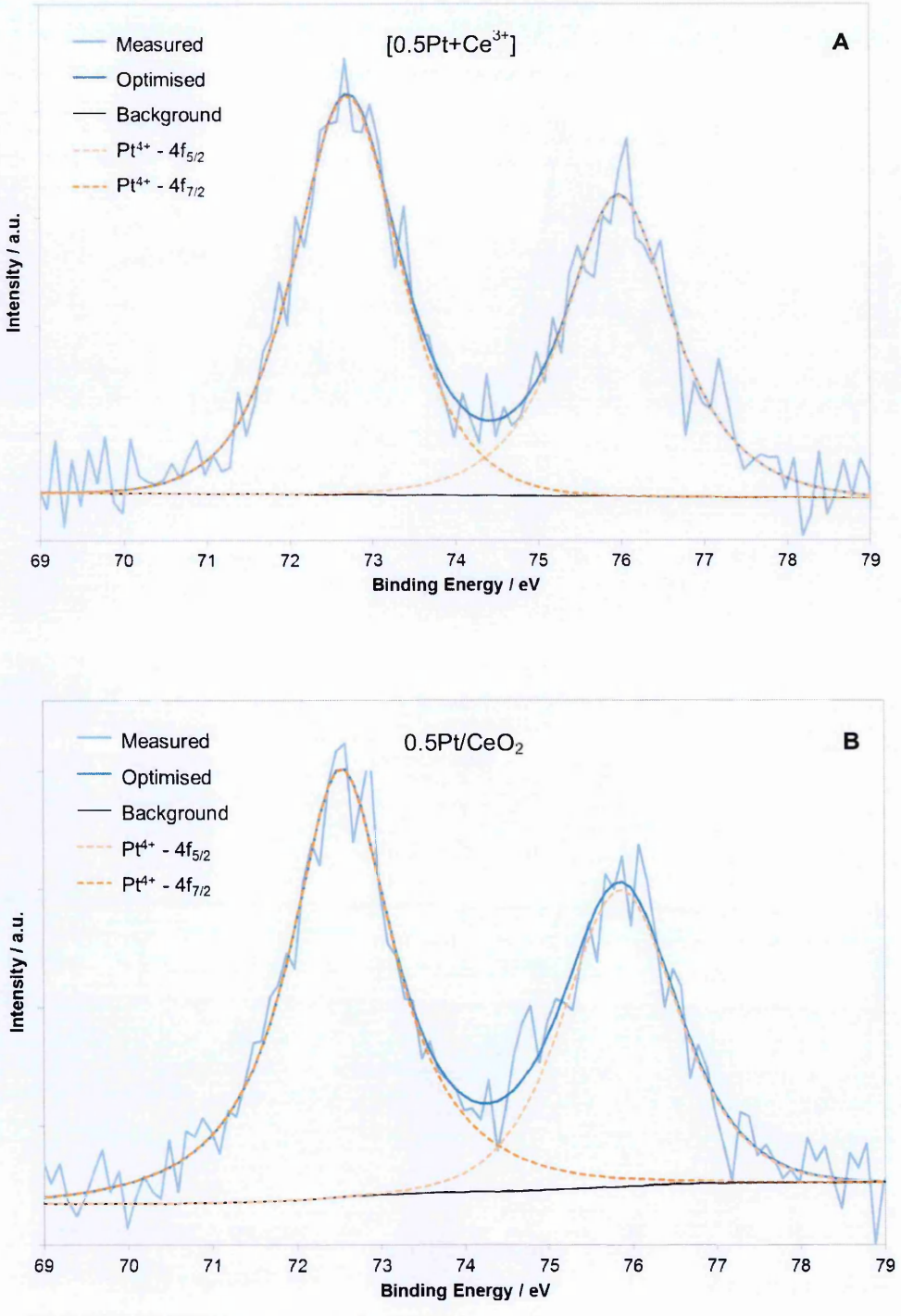

Figure 6-5: Deconvolution of Pt4f XPS peaks for 0.5Pt-CeO_2 samples prepared by co-precipitation with Ce^{3+} precursor ([0.5Pt+Ce^{3+}] (A)) and by impregnation on CeO_2 (0.5Pt/CeO_2 (B)).

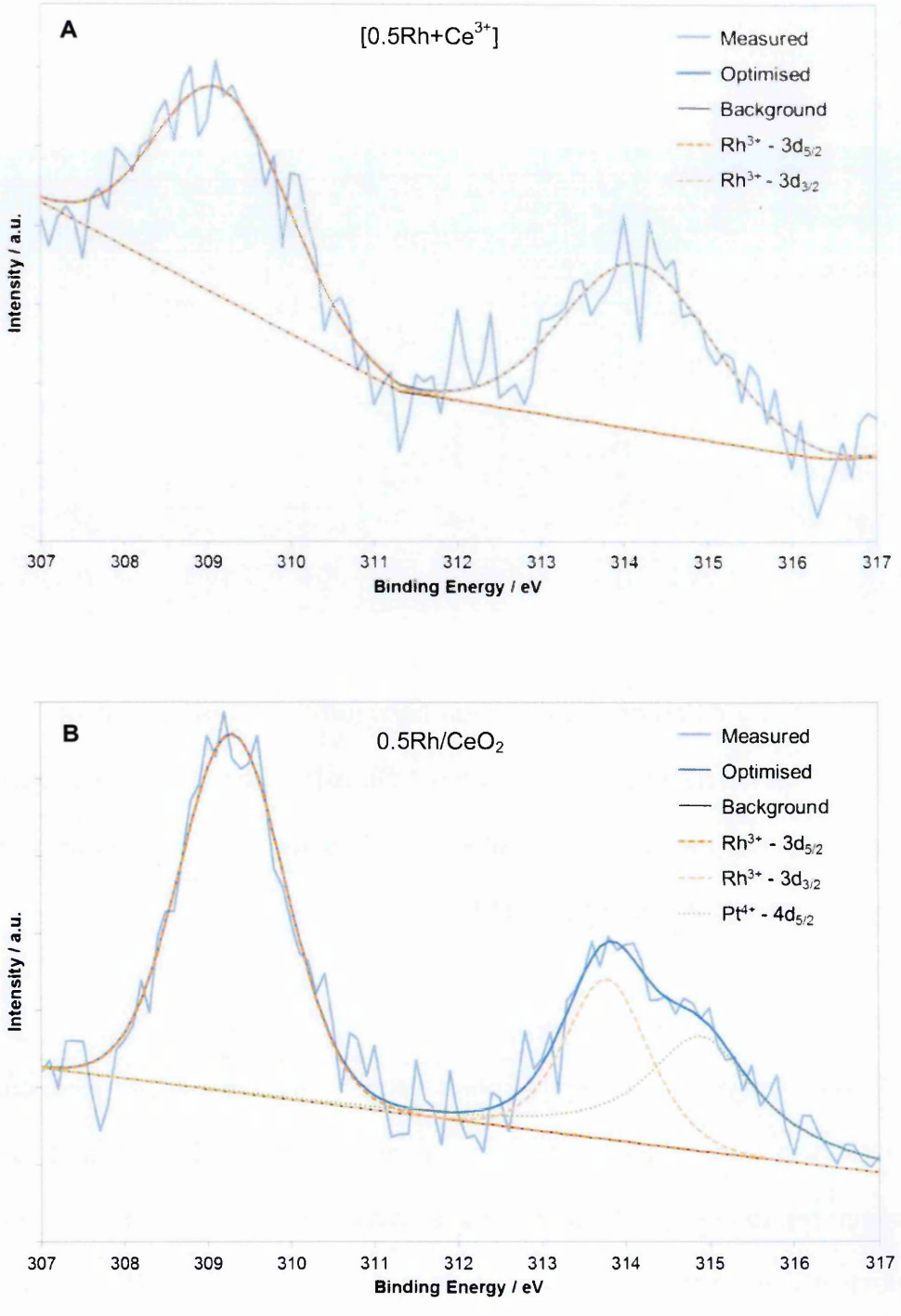

Figure 6-6: Deconvolution of Rh3d XPS peaks for 0.5Rh-CeO_2 samples prepared by co-precipitation with Ce^{3+} precursor ([0.5Rh+Ce^{3+}] (A)) and by impregnation on CeO_2 (0.5Rh/CeO_2 (B)). Pt4d XPS signal has been added to Figure B to show the contribution of Pt.

Table 6-2 summarises Pd3d, Pt4f and Rh3d band positions for Pd-CeO_2, Pt-CeO_2 and Rh-CeO_2, respectively, as well as the Ce/NM atomic ratios calculated by XPS:

Table 6-2: Summary of the XPS bands positions for Pd3d, Pt4f, and Rh3d, and calculated Ce/NM atomic ratio for samples prepared by co-precipitation with Ce^{3+} precursor ([(NM+Ce^{3+}]) and by impregnation on CeO_2 (NM/CeO_2).

Sample	Pd3d / eV		Pt4f / eV		Rh3d / eV		Ce/NM atomic ratio
	$3d_{5/2}$	$3d_{3/2}$	$4f_{7/2}$	$4f_{5/2}$	$3d_{5/2}$	$3d_{3/2}$	
0.5Pd/CeO_2	337.6	342.9	-	-	-	-	34
[0.5Pd+Ce^{3+}]	337.3 338.3	342.5 343.5	-	-	-	-	53
0.5Pt/CeO_2	-	-	72.5	75.9	-	-	65
[0.5Pt+Ce^{3+}]	-	-	72.7	76.0	-	-	118
0.5Rh/CeO_2	-	-	-	-	309.3	313.8	216
[0.5Rh+Ce^{3+}]	-	-	-	-	309.1	314.1	255

Regarding Ce, no differences were seen between the three sets of samples. All profiles (not shown here) showed that most Ce existed as CeO_2. As explained in previous chapters, traces of Ce^{3+} were also detected as a consequence of the reduction caused by the XPS beam [13].

6.2.2. Surface analyses: CO chemisorption, EtOH-TPSR, and ethane hydrogenolysis

The metal dispersion of these samples was measured by CO-chemisorption. This was compared to the Ce/NM atomic ratios calculated by XPS. In addition, in order to selectively estimate the Pd- and Pt-surface area, Pd-CeO_2 and Pt-CeO_2 samples were also analysed by EtOH-TPSR[2]; and to selectively estimate Rh-surface area, Rh-CeO_2 samples were analysed by the ethane hydrogenolysis

[2] See *Chapter 3* for a detailed description of EtOH-TPSR and ethane hydrogenolysis techniques. Separate calibration curves were used to correlate the CH_4 formation during the EtOH-TPSR with metal surface area, for the Pd and Pt samples.

technique [14]. As no calibration was performed for the Rh-samples on the ethane hydrogenolysis technique, the values can only be used only for comparative purposes. All these results are summarised in Table 6-3:

Table 6-3: Quantitative and qualitative analyses of metal surface area calculated by XPS, by CO chemisorption, by EtOH-TPSR (in the case of Pd- and Pt-CeO_2 samples) and by ethane hydrogenolysis (in the case of Rh-CeO_2 samples). Comparison of samples prepared by wet impregnation on CeO_2 (NM/CeO_2) and by co-precipitation with Ce^{3+} precursor ([NM+Ce^{3+}]). CO chemisorption instrument standard error = ± 2% (for metal dispersion) and ± 0.04 m^2 g^{-1} (for metal surface area); EtOH-TPSR instrument standard error = ± 0.1 m^2 g^{-1}; Ethane hydrogenolysis instrument standard error = ± 4 °C.

Sample	XPS	CO chemisorption		EtOH-TPSR	Ethane hydrogenolysis
Sample	Ce/Metal atomic ratio / a.u.	Metal dispersion / %	Metal surface area / m^2 g^{-1}	Metal surface area / m^2 g^{-1}	T50 / °C
0.5Pd/CeO_2	34	52	1.2	0.9	-
[0.5Pd+Ce^{3+}]	54	51	1.1	0.5	-
0.5Pt/CeO_2	65	55	0.7	1.3	-
[0.5Pt+Ce^{3+}]	118	25	0.3	0.5	-
0.5Rh/CeO_2	216	43	0.9	-	304
[0.5Rh+Ce^{3+}]	255	22	0.5	-	320
0.1Rh/CeO_2	-	56	0.2	-	321
[0.1Rh+Ce^{3+}]	-	11	0.1	-	414

The CO adsorption stoichiometry assumed here for CO chemisorption calculations was CO:NM 1:1. However, it is known that the stoichiometry is different between these noble metals. Based on published work on Pd, Pt and Rh supported on alumina, this stoichiometry is believed to be 0.5 for CO/Pd [15], 0.5-1 for CO/Pt [16], and 2 for CO/Rh [17]. The different stoichiometries are related with how the CO bonds to the metal, as explained in *Chapter 2*; linear adsorption occurs when one CO molecule adsorbs on one metal site (CO/M stoichiometry 1), bridge type when one CO molecule adsorbs in two metal sites (CO/M stoichiometry 0.5), and twin type when two CO molecules adsorb in one metal site (CO/M stoichiometry

2). The type of adsorption not only depends on the type of metal, but also on the particle size and its surface [18]. Thus, if this is taken into account, the dispersion values obtained for Pd and Pt should be lower than the real values and higher for Rh. Considering this, Rh particles would be larger than those of Pd and Pt.

In terms of metal surface area, all the techniques were in good agreement. They all showed that the samples prepared by impregnation contained higher metal surface content than those co-precipitated.

For Pd-CeO_2 samples, the increase of the calculated Ce/Pd atomic ratio of the co-precipitated catalyst compared to the impregnated material was associated to ceria decoration, as the Pd surface area values calculated by CO chemisorption and EtOH-TPSR were similar. But for Pt- and Rh-CeO_2 co-precipitated samples, the increase of the calculated Ce/NM atomic ratio was also accompanied by a decrease of the metal surface area (by about 50%), compared to their reference impregnated catalysts. This can either suggest an increase of particle size or a higher ceria encapsulation; based on this characterisation this could not be concluded.

Focusing on the selective reactive characterisation, the trends obtained between the EtOH-TPSR and the CO chemisorption for 0.5Pt/CeO_2 and [0.5Pt+Ce^{3+}] were in good agreement, showing a lower Pt surface area for [0.5Pt+Ce^{3+}] than the impregnated sample. However, the metal surface area values obtained with the EtOH-TPSR were higher than those obtained with the CO chemisorption method. This could indicate that the CO/Pt adsorption stoichiometry during the CO chemisorpition was lower than 1, as already suggested by published literature [16].

In the case of the Rh-CeO_2 samples, the results from the ethane hydrogenolysis also showed a significant decrease in Rh surface area for the co-precipitated

samples compared to the impregnated catalysts with comparable loading, agreeing with the results obtained from the CO chemisorption experiments (Figure 6-7).

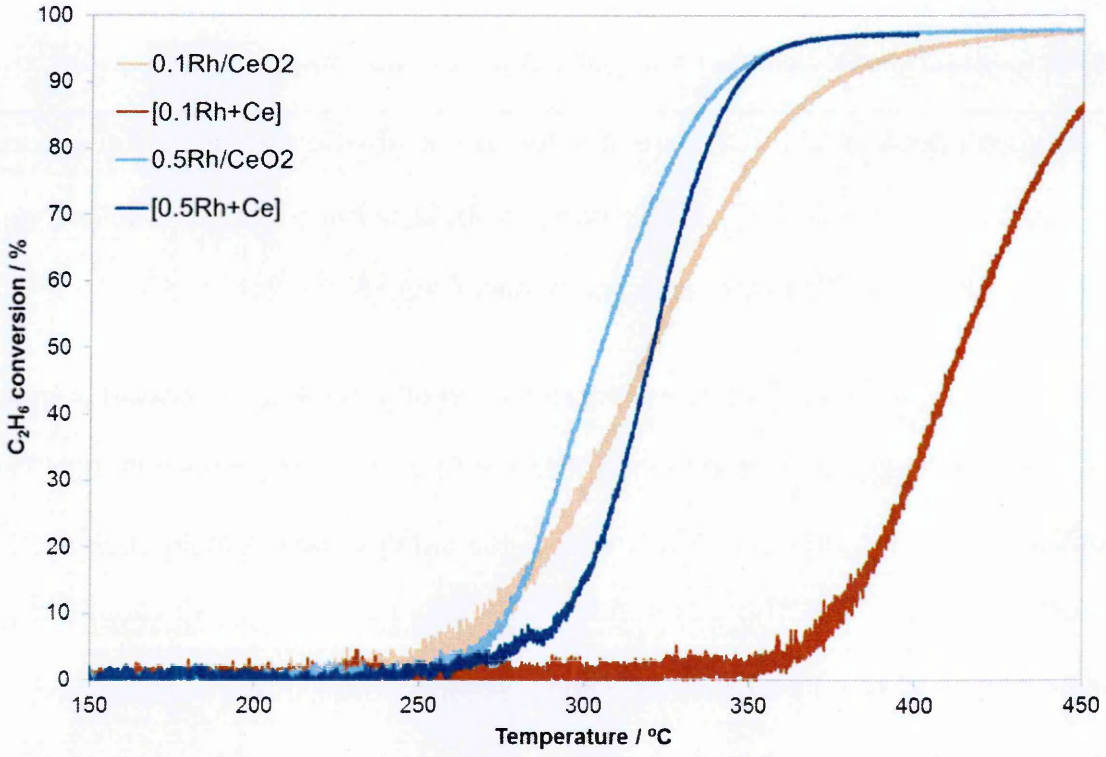

Figure 6-7: Ethane hydrogenolysis profiles performed on Rh-CeO_2 samples with 0.5 wt% Rh and 0.1 wt% Rh prepared by co-precipitation with Ce^{3+} precursor ([Rh+Ce^{3+}]) and by impregnation on CeO_2 (Rh/CeO_2). Each sample was firstly pre-treated under He at 300 °C for 30 minutes. Following this, the sample was cooled down to 150 °C and the gas flows set to 50 ml min^{-1} 10%H_2/N_2 and 10 ml min^{-1} 10%C_2H_6/N_2. Once a stable signal was obtained, a temperature ramp of 10 °C min^{-1} was applied up to 450 °C.

The results shown here suggest that the sample with the lowest Rh loading prepared by co-precipitation ([0.1Rh+Ce^{3+}]) has suffered a higher level of encapsulation than the [0.5Rh+Ce^{3+}] sample.

6.3. Redox characterisation

H_2-TPR was performed in order to study the reducibility of the samples, as well as the NM-Ce interaction. CO-TPR was mainly used to focus on the reducibility of the

NM, as spillover occurs to a lesser extent when using CO [19]. In addition, the total oxygen storage capacity (OSC) was also measured.

6.3.1. H_2-TPR

H_2-TPR profiles of Pd-, Pt- and Rh-CeO_2 samples are shown in Figure 6-8. The first reduction peak (< 250 °C) corresponded to the NM-Ce reduction, the second peak (between 250 – 500 °C) to the non-promoted surface CeO_2 reduction, and the third peak (> 600 °C) to the reduction of bulk CeO_2 [8, 20, 21].

Similar to the [0.5Pd+Ce^{3+}] samples, the reduction of [0.5Pt+Ce^{3+}] showed a sharp peak at 180 °C, suggesting that the reduction of PtO_x is a fast process [8, 22]. The reduction of PtO_x for the equivalent impregnated catalyst gave a main peak at 200 °C and two shoulders at 100 and 140 °C, indicating the presence of several PtO_x species [22]. The slightly higher reduction temperature for 0.5Pt/CeO_2 (based on the largest peak) compared to the co-precipitated catalyst also suggests smaller Pt particles or Pt particles that interact stronger with the support [23]. The reduction of surface and bulk ceria gave the two typical peaks at 370 and 805 °C for the impregnated samples, and at 390 and 840 °C for the co-precipitated material, respectively [24]. These peaks were very similar for both samples.

The Rh_2O_3 reduction for [0.5Rh+Ce^{3+}] also appeared as a sharp peak at 150 °C; the same reduction peak for 0.5Rh/CeO_2 appeared as a less intense peak at 120 °C with a prominent shoulder at 225 °C [24, 25]. As explained previously, the appearance of multiple peaks is related to the presence of several RhO_x species [12].

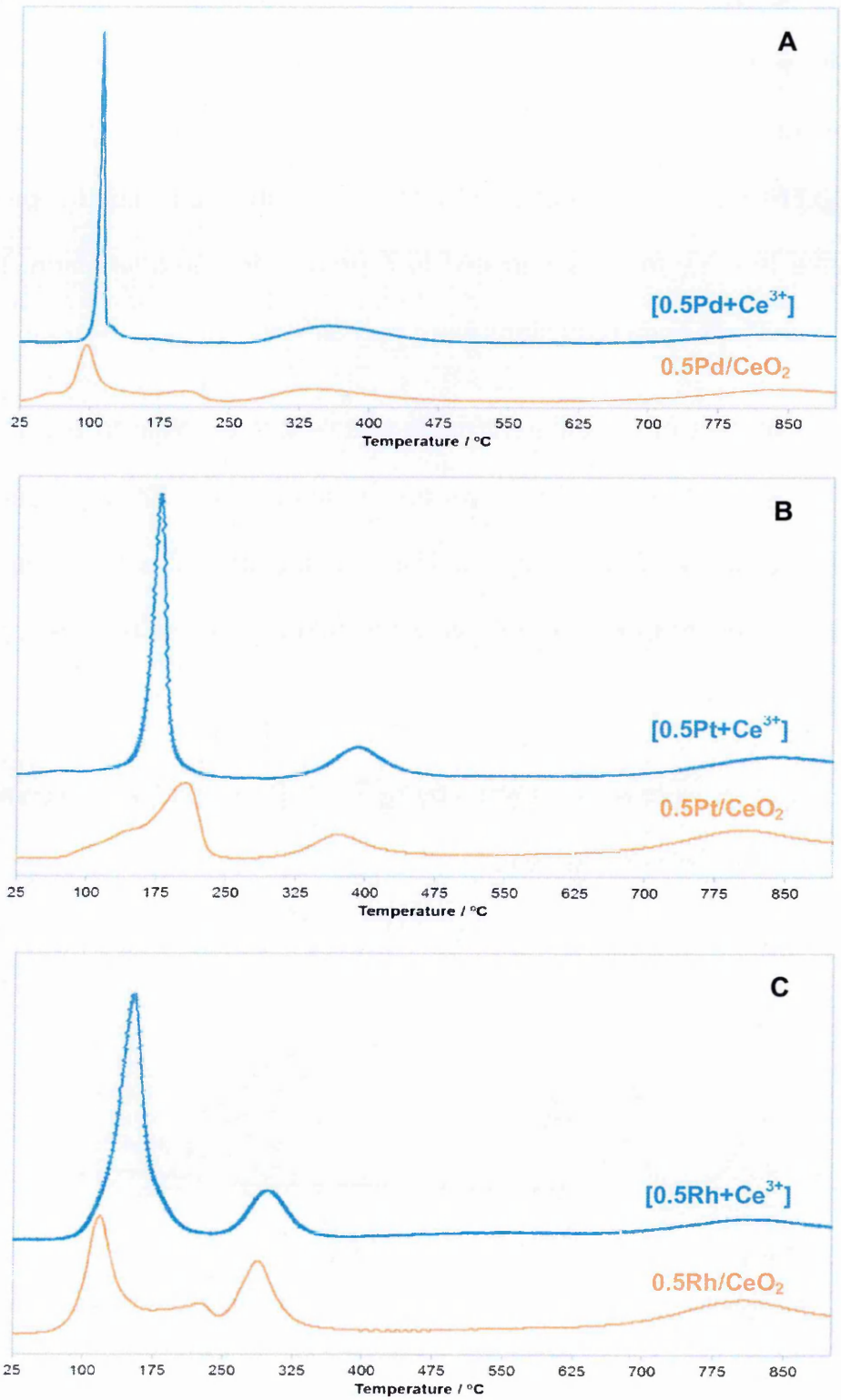

Figure 6-8: H_2-TPR of Pd-CeO_2 (A), Pt-CeO_2 (B) and Rh-CeO_2 (C) samples prepared by co-precipitation with Ce^{3+} precursor (blue) and by impregnation on CeO_2 (orange). The sample taken was ~0.2 g, and the flow used was 30 ml min^{-1} of 10% H_2/N_2 using 30 ml min^{-1} of N_2 as carrier gas.

Overall, the position of the Rh-Ce reduction peak at slightly higher temperature for [0.5Rh+Ce^{3+}] suggests the presence of either smaller Rh particles or Rh interacting in a stronger level with ceria [23]. The surface characterisation performed on this sample did not give any evidence of the existence of smaller Rh particles in [0.5Rh+Ce^{3+}] (see section 6.2), thus the higher reduction temperature for this sample is likely to be associated to a greater Rh-Ce interaction. In this case, surface and bulk ceria reductions were very similar.

Comparing the profiles of the different noble metals it is possible to see that the surface CeO_2 reduction occurred at lower temperature for the Rh-CeO_2 samples, compared to Pd- and Pt-CeO_2 samples. This is evidence of the higher spillover capacity of Rh, compared to Pd and Pt, which is able to promote a higher number of Ce atoms [26].

0.1Rh-CeO_2 samples were also analysed by H_2-TPR. These profiles are compared with those for 0.5Rh-CeO_2 in Figure 6-9.

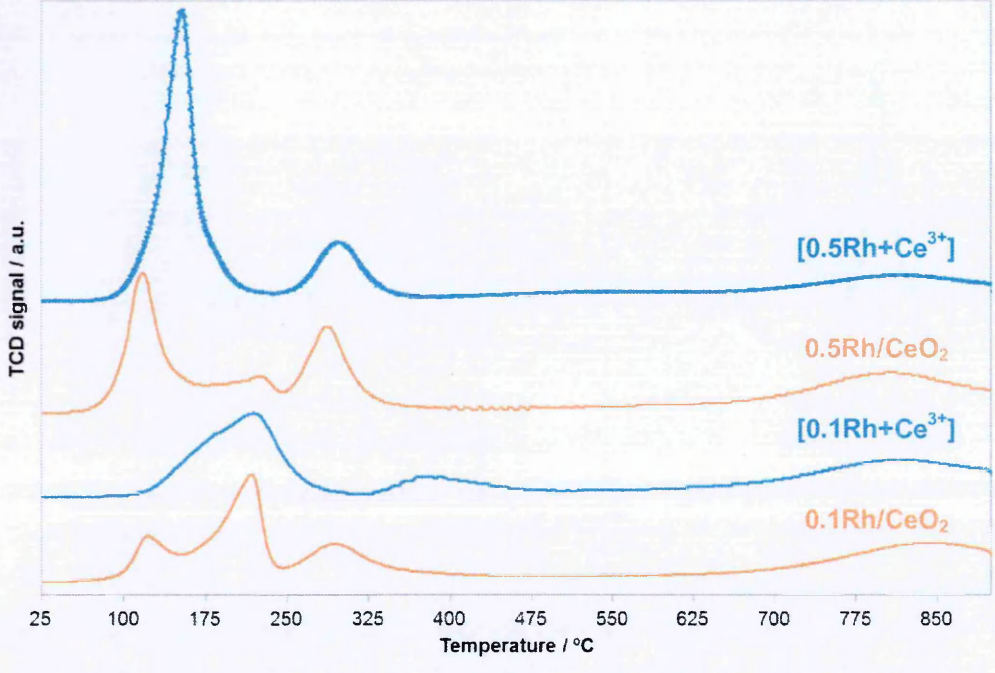

Figure 6-9: H_2-TPR profiles of Rh-CeO_2 samples with 0.5 wt% Rh and 0.1 wt% Rh prepared by co-precipitation with Ce^{3+} precursor (blue) and by impregnation on CeO_2 (orange). The sample taken was ~0.2 g, and the flow used was 30 ml min^{-1} of 10% H_2/N_2 using 30 ml min^{-1} of N_2 as carrier gas.

The reduction of Rh-Ce on 0.1Rh/CeO_2 also appeared as two peaks, however in this case the most prominent peak was the one at higher temperature (215 ºC), suggesting the existence of smaller Rh particles than in 0.5Rh/CeO_2. The same sample prepared by co-precipitation did not show a sharp reduction peak, as was observed for all the other co-precipitated samples tested; in this case, Rh-Ce reduction appeared as a wide peak where it was possible to notice the overlap of multiple peaks, with a maximum at 220 ºC, which was similar to the reduction temperature found for 0.1Rh/CeO_2. The surface and bulk ceria reductions were also similar.

Table 6-4 summarises the reduction temperatures for the metals and ceria species as well as the H_2 consumption. In all cases, the H_2 consumption obtained for the NM-O_x reduction was higher than the theoretical due to the extra contribution from the near-by CeO_2 (surface ceria promoted by the NM)[3].

As was shown previously in *Chapter 4*, the co-precipitated [0.5Pd+Ce^{3+}] sample consumed more H_2 during the reduction of Pd-Ce species than 0.5Pd/CeO_2, meaning that there was a better Pd-Ce contact. In contrast to this, the amount of H_2 consumed during the Pt-Ce reduction was similar for all Pt-CeO_2 samples. However, the sharpness of the peak shown by [0.5Pt+Ce^{3+}] indicated that this was a faster process, possibly as a consequence of a better Pt-Ce contact. Previous surface characterisation (CO chemisorption, EtOH-TPSR, XPS Ce/Pt atomic ratio) showed a significantly lower number of active sites in [0.5Pt+Ce^{3+}] than in 0.5Pt/CeO_2. Based on the surface characterisation and the H_2-TPR experiments, it was suggested that for the [0.5Pt+Ce^{3+}] sample the improved Ce-reduction by Pt

[3] For the 0.5Pd-CeO_2 and 0.5Pt-CeO_2 samples the theoretical H_2 consumption for a complete reduction of PdO and PtO_2 is 0.05 mmol H_2 g^{-1}; and for the 0.5Rh-CeO_2 and 0.1Rh-CeO_2 samples the theoretical H_2 consumption for a complete reduction of Rh_2O_3 is 0.14 mmol H_2 g^{-1} and 0.03 mmol H_2 g^{-1}, respectively.

(due to a higher number of Pt and Ce atoms in contact) could have been counteracted by the lower Pt surface area, leading to a similar H_2 consumption as for the 0.5Pt/CeO_2 sample.

Table 6-4: Summary of peak positions and H_2 consumption during the H_2-TPR experiments on Pd-, Pt-, and Rh-CeO_2 samples prepared by co-precipitation with Ce^{3+} precursor ([NM+Ce^{3+}]) and by impregnation on CeO_2 (NM/CeO_2). Average instrument standard error ± 0.02 mmol g^{-1}.

	NM-Ce reduction		Surface CeO_2 reduction		Bulk CeO_2 reduction	
Sample	Peak temperature / °C	H_2 consumed / mmol·g^{-1}	Peak temperature / °C	H_2 consumed / mmol·g^{-1}	Peak temperature / °C	H_2 consumed / mmol·g^{-1}
0.5Pd/CeO_2	90 °C 50, 205 °C (shoulders)	0.58	250 – 505 °C	0.30	580 - >900 °C	0.47
[0.5Pd+Ce^{3+}]	110 °C 120, 160 °C (shoulders)	0.64	260 – 535 °C	0.40	580 - >900 °C	0.38
0.5Pt/CeO_2	200 °C Shoulders at 100 and 140 °C	0.59	285 – 465 °C	0.18	580 - >900 °C	0.33
[0.5Pt+Ce^{3+}]	180 °C Shoulder at 70 °C	0.58	295 – 505 °C	0.21	580 - >900 °C	0.34
0.5Rh/CeO_2	120 °C Shoulder at 225 °C	0.48	245 – 375 °C	0.22	580 - >900 °C	0.32
[0.5Rh+Ce^{3+}]	150 °C	0.74	240 – 375 °C	0.18	580 - >900 °C	0.27
0.1Rh/CeO_2	120 °C 215 °C	0.46	245 – 360 °C	0.12	580 - >900 °C	0.45
[0.1Rh+Ce^{3+}]	75 – 305 °C (wide peak, max at 220 °C)	0.60	330 – 530 °C	0.11	580 - >900 °C	0.47

In the case of Rh-CeO_2 samples, those prepared by co-precipitation showed a slightly sharper Rh-Ce reduction peak and significantly higher H_2 consumption than the impregnated versions. This can be attributed to a higher H_2 spillover in the co-precipitated samples due to a higher number of Rh and Ce atoms in contact. Therefore, even if Rh particles were larger for [0.5Rh+Ce^{3+}], the partial decoration of these particles with ceria allowed a significantly greater Rh-Ce interaction than in 0.5Rh/CeO_2.

6.3.2. CO-TPR

With the aim of focusing on the understanding of the noble metal reduction, CO-TPR was performed on Pt-CeO_2 and Rh-CeO_2 samples and compared to those previously obtained for Pd-CeO_2 samples. The CO consumption and CO_2 formation are represented in Figure 6-10 for Pd-CeO_2, in Figure 6-11 for Pt-CeO_2, and in Figure 6-12 for Rh-CeO_2 samples. H_2 is not shown here as practically no H_2 formation was detected during these experiments.

The three characteristic regions of peaks identified corresponded to the reduction of surface NM and promoted surface CeO_2 (between 50 – 350 ºC), to non-promoted CeO_2 reduction and water gas shift (between 400 – 700 ºC), and to bulk CeO_2 reduction (> 700 ºC) [9, 19, 27]. For Pd-CeO_2 samples these peaks could be determined; however, for the Pt-CeO_2 and Rh-CeO_2 samples, CO consumption and CO_2 formation profiles were less well defined (due to the overlap of the reduction peaks), making their separation difficult.

Table 6-5 summarises the temperatures found for the noble metal reduction during the CO-TPR experiments:

Table 6-5: Comparison of the peak temperatures corresponding to the surface NM-O_x reduction of NM-CeO_2 samples prepared by wet impregnation and by co-precipitation with Ce^{3+} precursor, based on the CO consumption during CO-TPR experiments.

	Temperature NM-O_x reduction (based on CO consumption)	
	Co-precipitation	Wet impregnation
0.5Pd-CeO_2	75 ºC 290 ºC Small shoulder at 360 ºC	Wide peak at 60 ºC Wide peak at 100 ºC 260 ºC
0.5Pt-CeO_2	200 ºC 270 ºC	185 ºC 270 ºC 355 ºC
0.5Rh-CeO_2	Shoulder at 160 ºC 300 ºC 335 ºC	Wide peak from 155 to 480 ºC

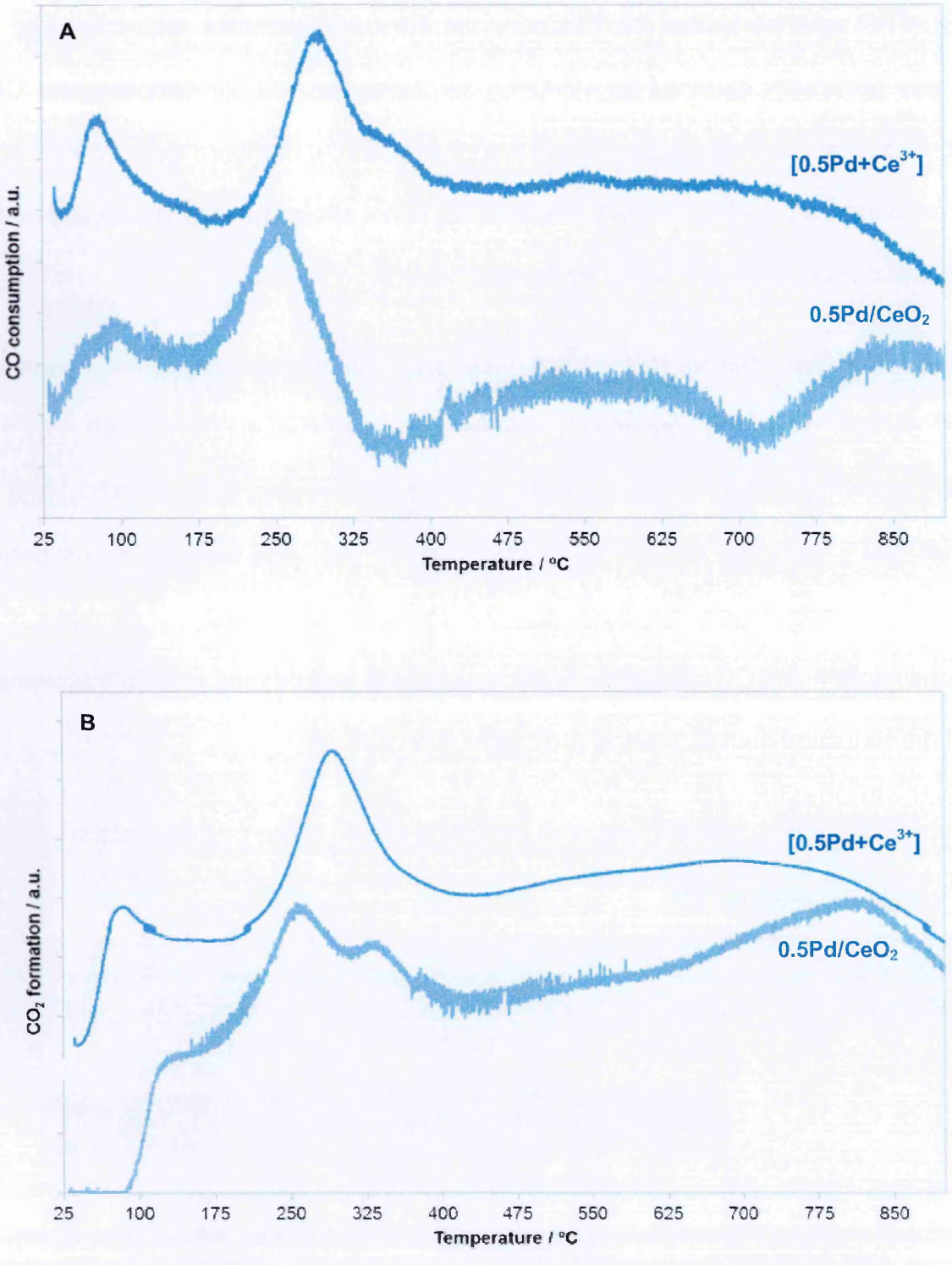

Figure 6-10: CO consumption (A) and CO_2 formation (B) during CO-TPR experiments for Pd-CeO_2 samples prepared by co-precipitation with Ce^{3+} precursor ([Pd+Ce^{3+}]) and by impregnation on CeO_2 (Pd/CeO_2). The samples were previously pre-treated under 50 ml min^{-1} of He at 500 °C. During the CO-TPR the flow consisted in 20 ml min^{-1} of 10%CO/He in 30 ml min^{-1} of He.

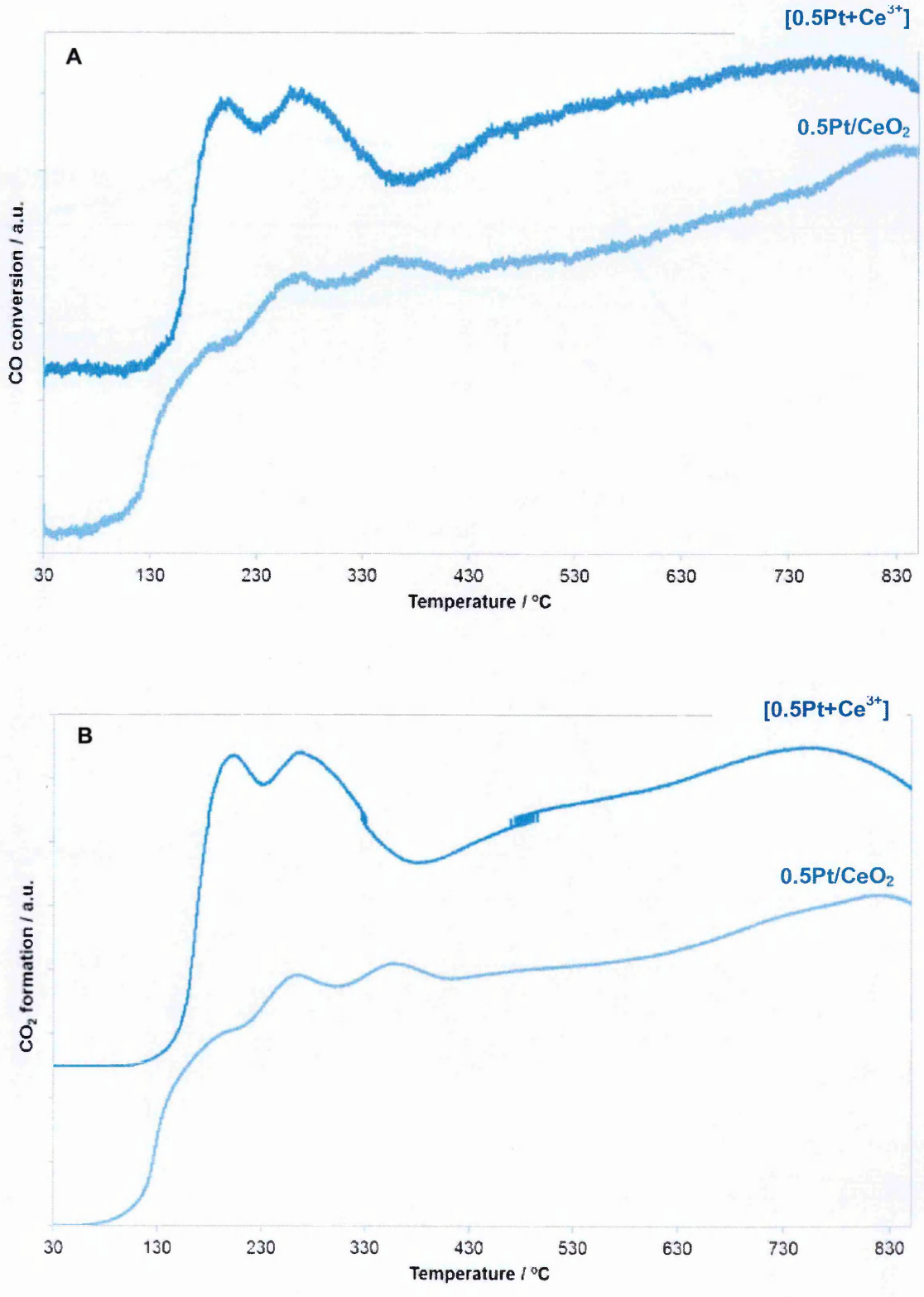

Figure 6-11: CO consumption (A) and CO_2 formation (B) during CO-TPR experiments for Pt-CeO_2 samples prepared by co-precipitation with Ce^{3+} precursor ([Pt+Ce^{3+}]) and by impregnation on CeO_2 (Pt/CeO_2). The samples were previously pre-treated under 50 ml min^{-1} of He at 500 °C. During the CO-TPR the flow consisted in 20 ml min^{-1} of 10%CO/He in 30 ml min^{-1} of He.

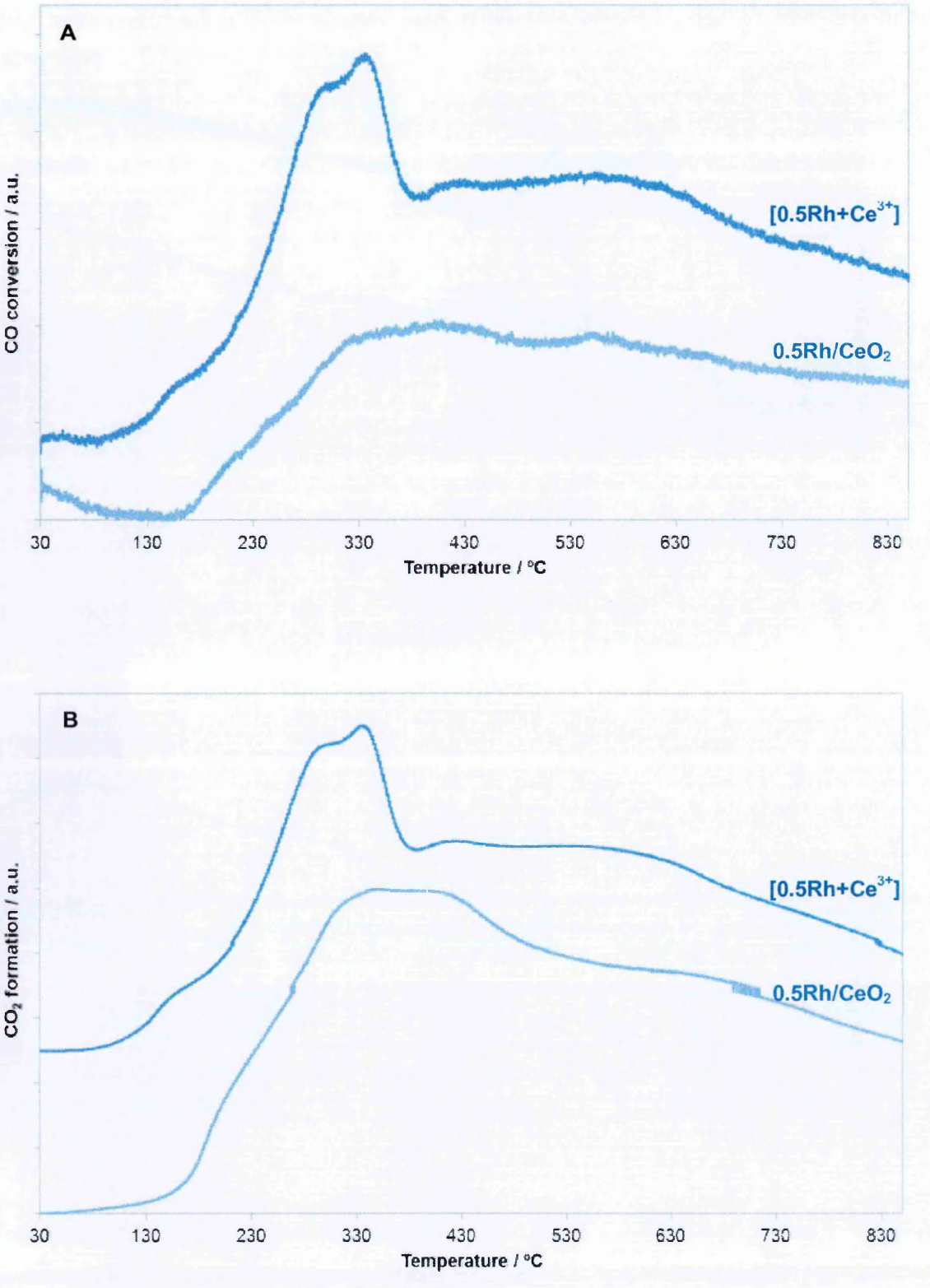

Figure 6-12: CO consumption (A) and CO_2 formation (B) during CO-TPR experiments for Rh-CeO_2 samples prepared by co-precipitation with Ce^{3+} precursor ([Rh+Ce^{3+}]) and by impregnation on CeO_2 (Rh/CeO_2). The samples were previously pre-treated under 50 ml min^{-1} of He at 500 °C. During the CO-TPR the flow consisted in 20 ml min^{-1} of 10%CO/He in 30 ml min^{-1} of He.

PtO reduction appeared at slightly lower temperature for 0.5Pt/CeO_2 than for [0.5Pt+Ce^{3+}], possibly due to a greater interaction between Pt and the support on [0.5Pt+Ce^{3+}] [27]. Similar results were also obtained during H_2-TPR experiments.

The comparison of Rh-CeO_2 samples was complicated, as no well-defined peaks were identified for the 0.5Rh/CeO_2 sample, which suggested the formation of multiple Rh particle types. However, these peaks were sharper and better defined for [0.5Rh+Ce^{3+}], which could be associated to a strong interaction between Rh and Ce and a more homogeneous distribution of Rh particles compared to the impregnated catalyst. These results also agree with the H_2-TPR profiles, where the reduction of Rh-Ce led to wide peaks, suggesting the presence of multiple Rh species; also during these experiments the reduction of Rh-Ce for the co-precipitated [0.5Rh+Ce^{3+}] led to a slightly sharper peak and at higher temperature than for the 0.5Rh/CeO_2 sample.

No CO-TPR data was found in the literature for Rh-catalysts; all the available TPR data was performed under H_2 instead of CO for this type of experiments, possibly due to the complexity of the CO-TPR profiles, as shown here. Thus, the profiles and the peak positions could not be compared with any published data.

6.3.3. Oxygen Storage Capacity (OSC)

The impact of the noble metal on the OSC was evaluated. The results can be found in Figure 6-13. As can be seen, all the samples prepared by co-precipitation showed improved OSC compared to the impregnated samples. However, other than [0.5Pd+Ce^{3+}], this improvement was only noticeable at temperatures higher than 200 ºC in most cases.

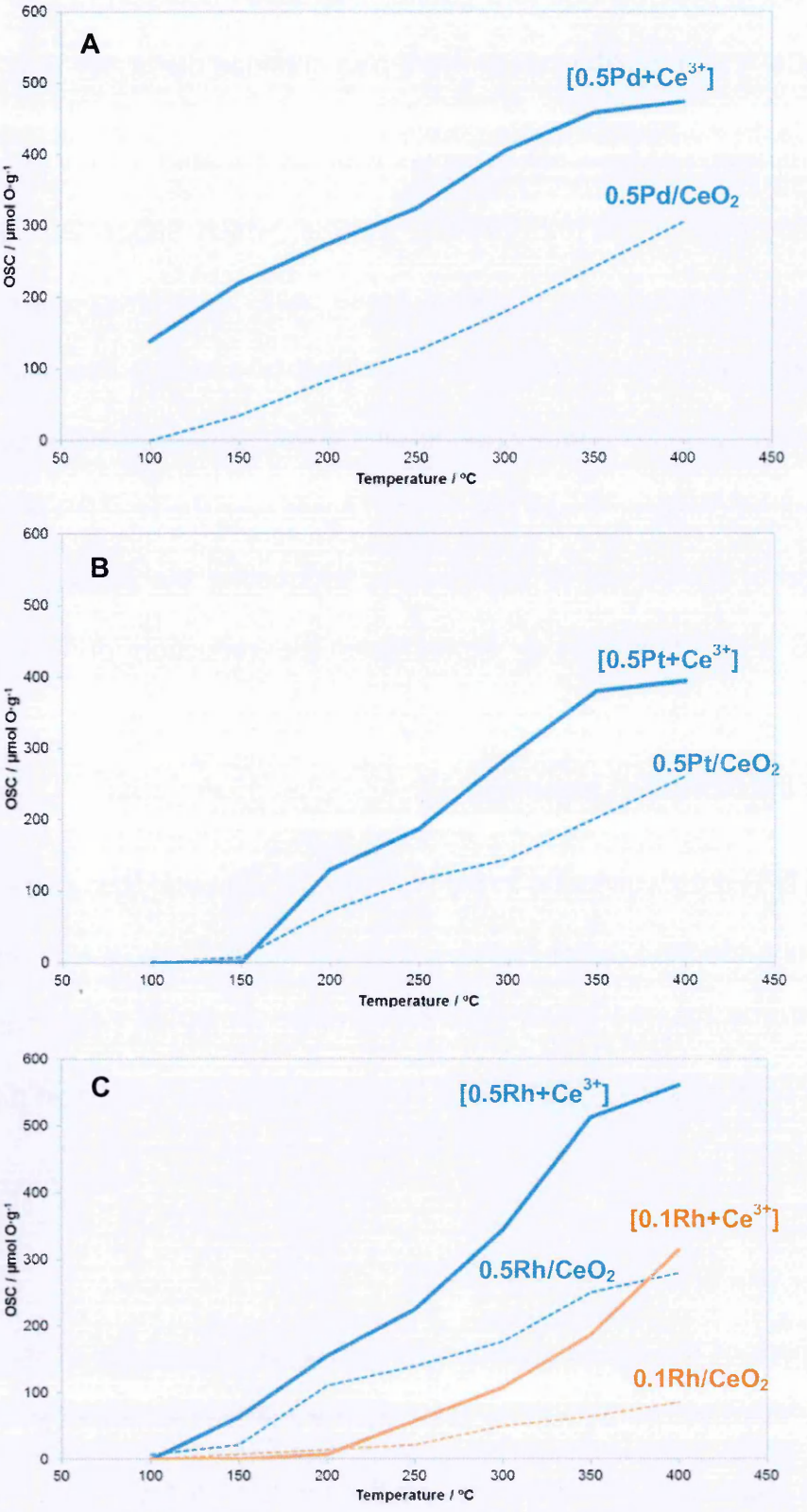

Figure 6-13: OSC profiles of Pd-, Pt-, and Rh-CeO_2 samples prepared by co-precipitation and by impregnation. The OSC measurement was performed alternating switches between O_2 (10 ml min^{-1} of 5 %O_2/He) and CO (10 ml min^{-1} of 10 %CO/He) using He as a carrier gas (90 ml min^{-1}) at steady state temperatures. OSC instrument average standard error = ± 8 µmol O g^{-1}.

The lack of improvement in the low temperature region for Pt-CeO_2 and Rh-CeO_2 samples could be associated with a lower number of surface active sites on the co-precipitated materials compared to the reference catalysts. In CeO_2-based samples the low temperature OSC (< 300 ºC) is dominated by the surface and the high temperature OSC (> 300 ºC) by the bulk [20, 26, 28]. At 400 ºC, the OSC for the co-precipitated sample compared to the impregnated sample increased by 170 µmol O g^{-1} for Pd, and 34 µmol O g^{-1} for Pt. The improvement of these samples was significantly lower than that of the [0.5Rh+Ce^{3+}] sample which improved by 282 µmol O g^{-1} compared to 0.5Rh/CeO_2. Comparing the Rh-CeO_2 samples with different loadings, [0.1Rh+Ce^{3+}] showed a similar improvement as [0.5Rh+Ce^{3+}] compared to its equivalent impregnated catalysts, improving by 229 µmol O g^{-1}. Overall, comparing the samples prepared by co-precipitation, Rh was a better noble metal to obtain high OSC at temperatures higher than 300 ºC, and Pd to obtain high OSC at temperatures lower than 300 ºC.

The efficiency from ceria (without the noble metal contribution) was calculated. The trends can be found in Figure 6-14 and Table 6-6.

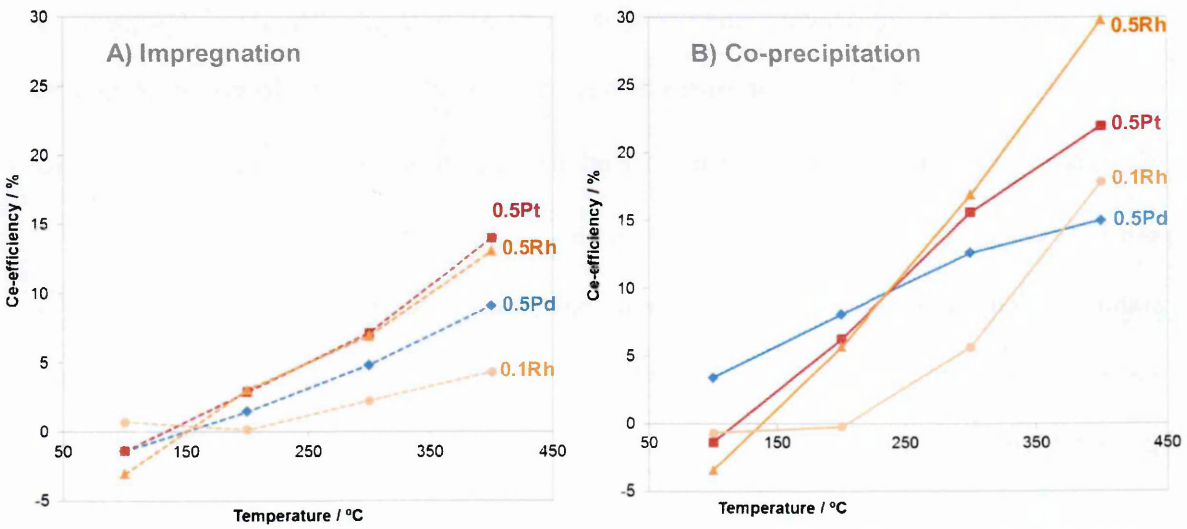

Figure 6-14: Ceria efficiency during the OSC test of Pd-, Pt-, and Rh-CeO_2 samples prepared by wet impregnation on CeO_2 (A) and by co-precipitation with Ce^{3+} precursor (B).

Table 6-6: Ce-efficiency at 400 °C during the OSC test of Pd-, Pt-, and Rh-CeO_2 samples prepared by impregnation and by co-precipitation.

Sample	Impregnated samples Ce-efficiency at 400 °C / %	Co-precipitated samples Ce-efficiency at 400 °C / %
0.5Pd-CeO_2	9	15
0.5Pt-CeO_2	14	22
0.5Rh-CeO_2	13	30
0.1Rh-CeO_2	4	18

Three different effects can be seen. The largest factor on which the ceria-efficiency depended appears to be the NM loading used (the increase of NM increased the efficiency) followed by the preparation method, as shown for the Rh-CeO_2 catalysts [24]. All the samples prepared by co-precipitation were more efficient than those prepared by impregnation. This is believed to occur as a consequence of a higher number of NM and Ce atoms in contact, which allowed easier oxygen transfer.

The type of NM also had an influence, with the efficiency following the trend: Rh ≥ Pt > Pd, agreeing with studies already published [26, 28, 29]. This trend is shown in Table 6-6, which compares the efficiency values of these samples at 400 °C. The higher efficiency of Rh is related to its higher oxygen activation, due to contain a high population of oxygen species loosely bounded to the surface when oxidised [26]. The greater reducibility of Rh could also be noticed during H_2-TPR experiments, where Rh-CeO_2 samples presented the lowest reduction temperature peaks of un-promoted surface ceria.

6.4. Kinetic characterisation: CO-SSITKA

The kinetics of the CO oxidation reaction were studied by CO-SSITKA. The range of temperature evaluated was changed for each sample, in order to maintain 5 – 10% CO conversion. For the Pd-CeO_2 samples the temperature range studied was between 30 to 80 ºC, for Pt-CeO_2 samples between 180 to 230 ºC, and for Rh-CeO_2 samples between 100 to 150 ºC. The reaction rates obtained can be seen in Figure 6-15.

[0.5Pd+Ce^{3+}] was the only co-precipitated sample to show a higher reaction rate than the equivalent impregnated catalyst. [0.5Pt+Ce^{3+}] appeared to have a similar reaction rate to 0.5Pt/CeO_2, and [0.5Rh+Ce^{3+}] showed a significantly lower reaction rate compared to 0.5Rh/CeO_2. The lower reaction rates obtained for [0.5Pt+Ce^{3+}] and [0.5Rh+Ce^{3+}] could be associated with a lower number of surface active sites compared to their reference impregnated materials, as observed by the surface characterisation performed on these samples (CO chemisorption, EtOH-TPSR, and ethane hydrogenolysis) shown in section 6.2.2.

The different noble metals used in these catalysts did not have an impact on the reaction order, with a reaction order of zero with respect to O_2 and 1 with respect to CO. Since the reaction seems to be independent of the O_2 concentration in the feed, this suggests that the reaction occurs through the mechanism where CO is first adsorbed on the NM particle and subsequently reacts on the NM-Ce interface with oxygen from the support, which has either diffused from the CeO_2 surface or from the bulk [30, 31].

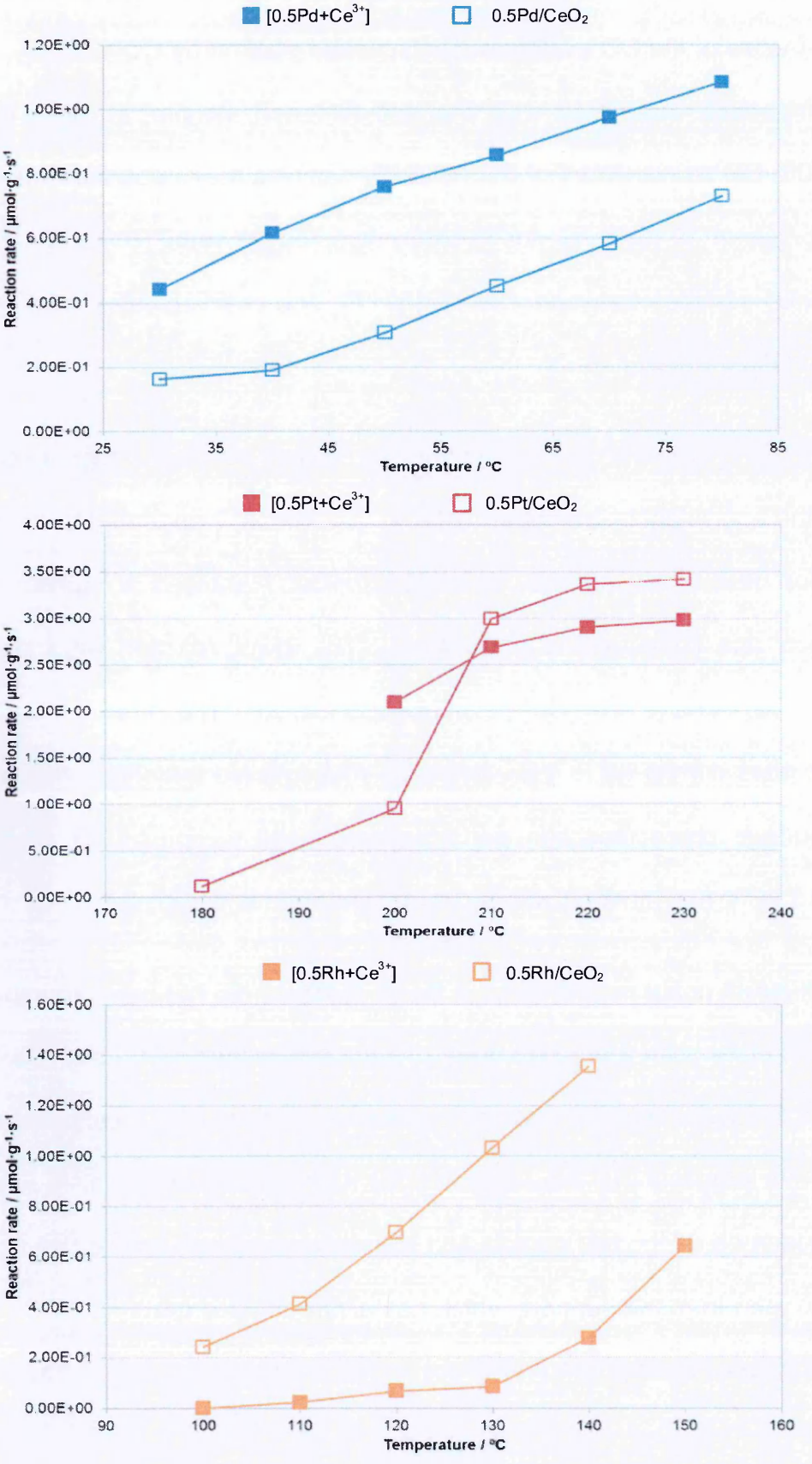

Figure 6-15: CO oxidation reaction rate of Pd-, Pt-, and Rh-CeO_2 samples prepared by impregnation on CeO_2 (NM/CeO_2) and by co-precipitation with Ce^{3+} precursor ([NM+Ce^{3+}]). The gas flows used were 52.5 ml min^{-1} of 5% O_2/He, 5.5 ml min^{-1} of 1%CO/5%Ar/He (^{12}C) and 5.5 ml min^{-1} of 1%CO/He (^{13}C). The average reaction rate standard error was ±0.01 µmol g^{-1} s^{-1}.

Table 6-7: Estimated equation rates of CO oxidation reaction and activation energies (E_a) for Pd-, Pt-, and Rh-CeO_2 samples prepared by wet impregnation on CeO_2 (NM/CeO_2) and by co-precipitation with Ce^{3+} precursor ([NM+Ce^{3+}]). The standard errors for E_a are shown between brakets next to the values.

Sample	Equation rate	E_a / kJ·mol^{-1}
0.5Pd/CeO_2	r = k [CO]	27 (± 2)
[0.5Pd+Ce^{3+}]	r = k [CO]	11 (± <1)
0.5Pt/CeO_2	r = k [CO]	13 (± 2)
[0.5Pt+Ce^{3+}]	r = k [CO]	10 (± 3)
0.5Rh/CeO_2	r = k [CO]	56 (± 3)
[0.5Rh+Ce^{3+}]	r = k [CO]	108 (± 3)

In contrast, the activation energy (E_a) was affected by the preparation method depending on the type of NM used; [0.5Pd+Ce^{3+}] showed a lower E_a value than 0.5Pd/CeO_2 (11 and 27 kJ mol^{-1}, respectively), whilst 0.5Pt/CeO_2 and [0.5Pt+Ce^{3+}] samples showed similar E_a values (between 13 and 10 kJ mol^{-1}, respectively) independent of the preparation method used. Rh-CeO_2 samples showed significantly higher E_a values than Pd- and Pt-CeO_2 samples; however, the E_a of the Rh sample prepared by impregnation was about half of the value of that prepared by co-precipitation (56 and 108 kJ mol^{-1}, respectively). The different E_a values between Pd-, Pt- and Rh- could be associated to the different metal particle sizes, the particle morphology and/or the metal-support interaction, which can affect the oxygen activation process [29]. A summary of the E_a values can be found in Table 6-7.

Since no exact quantification of particle size or morphology could be performed on these catalysts, the justification of the E_a values obtained can only be speculated.

The lower E_a value for [0.5Pd+Ce^{3+}] compared to 0.5Pd/CeO_2 suggests a better interaction between Pd-Ce in the co-precipitated sample, which would allow a faster oxygen transfer for the CO oxidation reaction.

The similar E_a values between [0.5Pt+Ce^{3+}] and 0.5Pt/CeO_2 suggests that the better Pd-Ce interaction created during the co-precipitation of [0.5Pt+Ce^{3+}] (shown by TPR and OSC experiments) could have been counteracted by a decrease of Pt surface area (as shown during CO chemisorption and EtOH-TPSR analyses).

The lower E_a values obtained for [0.5Rh+Ce^{3+}] compared to 0.5Rh/CeO_2 suggests that the counteracted effects due to the loss of Rh surface area in the co-precipitated material (shown during CO chemisorption and ethane hydrogenolysis) could have had a significant impact in the oxygen activation.

6.5. Light-off performance

As in the previous chapters, the activities of the samples were tested under continuous cold-start conditions and perturbed conditions. The results can be found in the following sections.

6.5.1. Cold start conditions

Figure 6-16 compares CO, NO_x and HC light-off profiles under cold-start conditions for Pd-CeO_2 samples and Figure 6-17 for Pt-CeO_2 and Rh-CeO_2 samples.

To aid comparison, Table 6-8 summarises T50 for CO and NO_x, and T30 for HC found during this test. The T50 and T30 difference between impregnated and co-precipitated values (ΔT50 and ΔT30) was calculated and is also shown in this table. Positive values mean a shift towards higher temperature and a negative value a shift towards lower temperature, based on the comparison of the co-precipitated material with the impregnated catalyst.

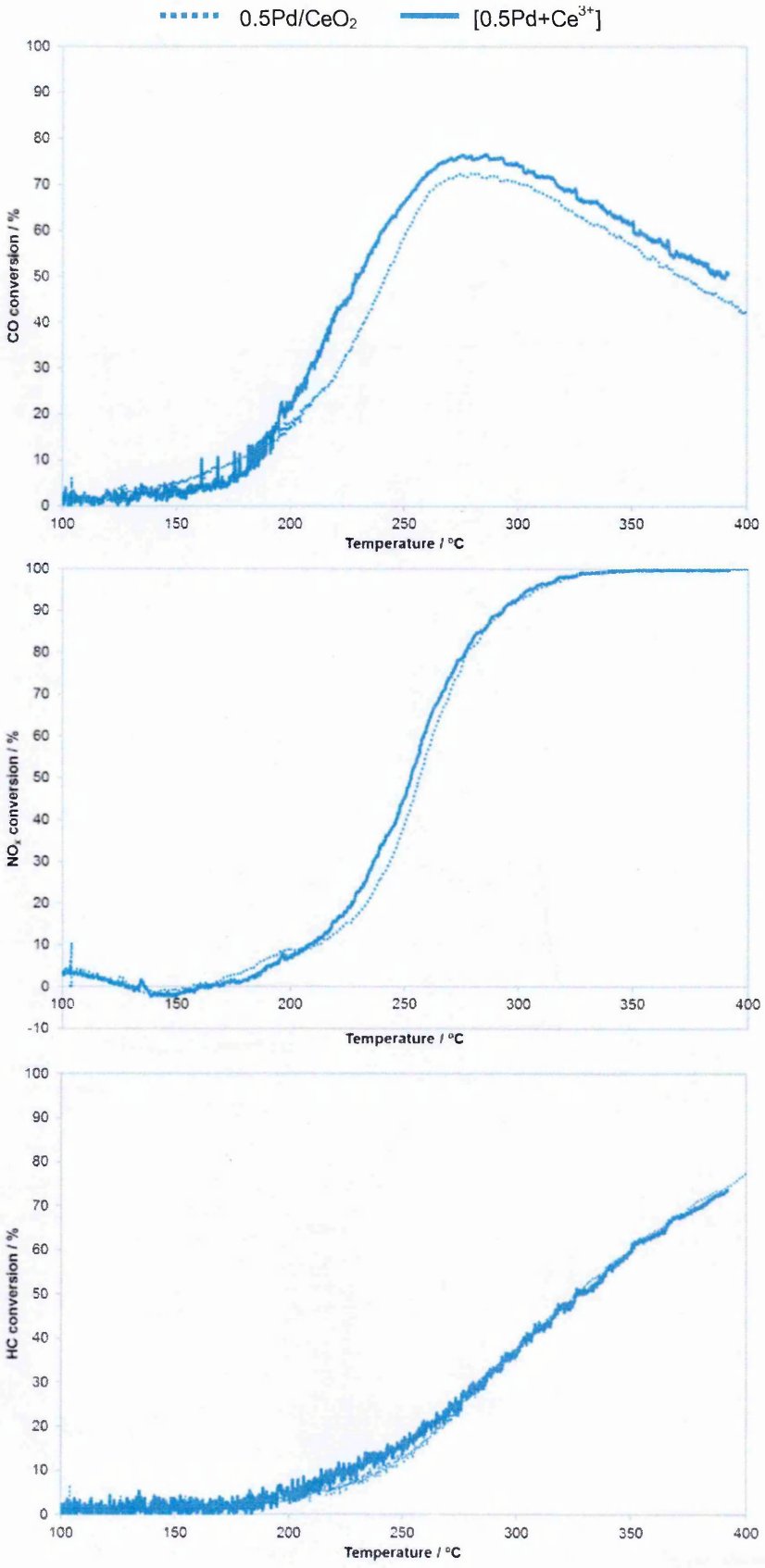

Figure 6-16: From top to bottom, CO, NO_x and HC light-off performance under constant lambda at 0.95 of 0.5Pd-CeO_2 catalysts prepared by impregnation (0.5Pd/CeO_2) and by co-precipitation using Ce^{3+} ([0.5Pd+Ce^{3+}]) and Ce^{4+} ([0.5Pd+Ce^{4+}]) precursors. The sample taken was 0.4 g (0.2 g sample + 0.2 g cordierite) and the gas flow rate 2 L min^{-1}. The catalyst was heated using a ramp rate of 10 °C min^{-1} from 100 to 400 °C.

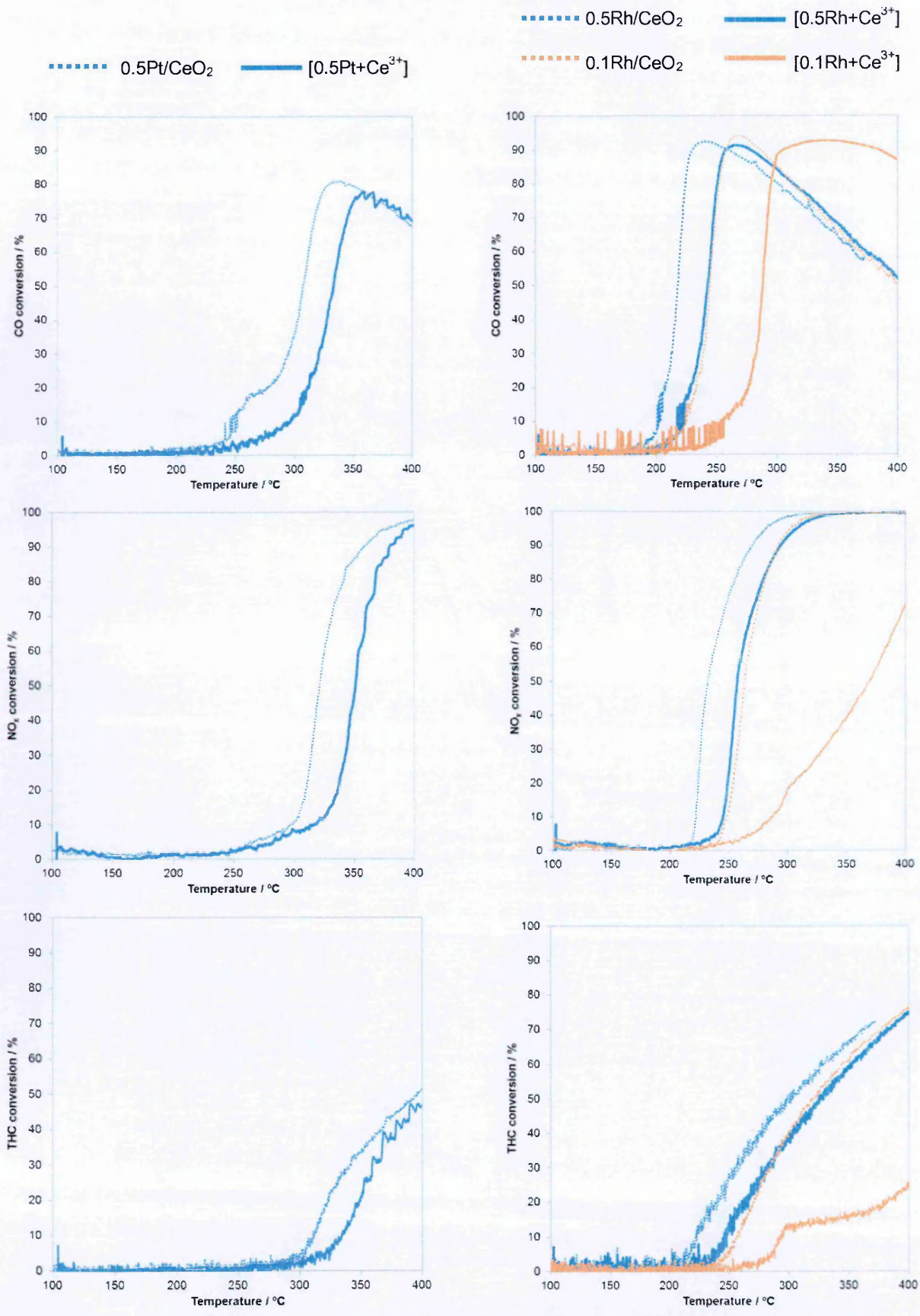

Figure 6-17: From top to bottom, CO, NO_x and HC light-off performance under constant lambda at 0.95 of Pt-, and Rh-CeO_2 samples prepared by impregnation on CeO_2 (NM/CeO_2) and by co-precipitation with Ce^{3+} precursor ([NM+Ce^{3+}]). The sample taken was 0.4 g (0.2 g sample + 0.2 g cordierite) and the gas flow rate 2 L min^{-1}. The catalyst was heated using a ramp rate of 10 °C min^{-1} from 100 to 400 °C.

Table 6-8: Necessary temperature to achieve 50% conversion of CO and NO_x and to achieve 30% conversion of HC during a light-off test under constant lambda at 0.95 for Pd-, Pt-, and Rh-CeO_2 samples prepared by impregnation and by co-precipitation. Light-off instrument average standard error = ± 2 °C.

Sample	CO		NO_x		HC	
	T50 / °C	ΔT50 / °C	T50 / °C	ΔT50 / °C	T30 / °C	ΔT30 / °C
0.5Pd/CeO_2	242	-14	257	-5	284	+1
[0.5Pd+Ce^{3+}]	228		252		285	
0.5Pt/CeO_2	307	+25	321	+29	340	+17
[0.5Pt+Ce^{3+}]	332		350		357	
0.5Rh/CeO_2	217	+26	232	+25	259	+25
[0.5Rh+Ce^{3+}]	243		257		284	
0.1Rh/CeO_2	243	+44	236	+133	284	> +116
[0.1Rh+Ce^{3+}]	287		369		> 400	

* ΔT = difference between impregnated and co-precipitated temperature values.

It can be seen that, in contrast to the 0.5Pd-CeO_2 samples, under these conditions the 0.5Pt-CeO_2 and 0.5Rh-CeO_2 samples prepared by impregnation showed a better performance (lower light-off temperature) than those prepared by co-precipitation. This lower performance of the co-precipitated materials was most certainly due to a lower number of surface active sites, as shown previously in section 6.2.2. [25, 32-34].

Overall, comparing samples with equal NM loading, Rh was the noble metal that led to lower light-off temperatures, followed closely by Pd. Pt showed the highest light-off temperatures.

6.5.2. Perturbed light-off

The samples were analysed under perturbed conditions at lambda values of 0.99 ± 0.05 (rich) and 1.01 ± 0.05 (lean). The aim of this perturbed-test was to force the catalysts to use their OSC during the lambda changes. The results can be seen in Figure 6-19 and Figure 6-20.

The 0.5Pt/CeO_2 and [0.5Pt+Ce^{3+}] samples showed similar performances, with [0.5Pt+Ce^{3+}] leading to slightly higher conversions. These agreed with the characterisation performed previously, where it was shown that the deeper ceria encapsulation of Pt particles during the co-precipitation preparation could have counteracted the better Pt-Ce contact obtained with this preparation.

In the case of Rh, the co-precipitated materials showed an advantage over the impregnated catalysts. 0.5Rh-CeO_2 samples prepared by both methods showed practically identical light-off temperatures, however the final pollutant conversions were significantly higher for [0.5Rh+Ce^{3+}]. The superior performance of [0.5Rh+Ce^{3+}] could be associated with the improved OSC that this sample showed, which is believed to be a consequence of a better Rh-Ce interaction.

For the low Rh-loading samples, the light-off of the co-precipitated material was clearly at higher temperature than for the impregnated catalyst, but NO_x and CO final conversions were better. On the other hand, HC conversions were higher for the 0.1Rh/CeO_2 sample. The significantly lower activity of [0.1Rh+Ce^{3+}] was associated with a lower number of active sites on the surface [25]. However, the supposed improved Rh-Ce interaction (and therefore higher OSC) helped it to achieve better CO and NO_x final conversions. It is known that the mechanism for HC conversion follows a different route which is not based on the activation of the oxygen, therefore the improved OSC would not have any impact here. Based on

the characterisation performed here it was not possible to explain the lower HC conversion given by the co-precipitated material.

A summary of the conversion values can be found in Table 6-9 for the rich lambda and in Table 6-10 for the lean lambda. Pd-CeO_2 samples have been added for comparison. Also here, the difference between the conversion obtained with the co-precipitated sample and the conversion obtained with the impregnated catalysts was calculated (Δ%). Overall, the conversion improvements were not highly significant (mostly <10 %). Comparing the different NM, the co-precipitated material with Rh was the sample that showed the most improved conversion, especially for NO_x.

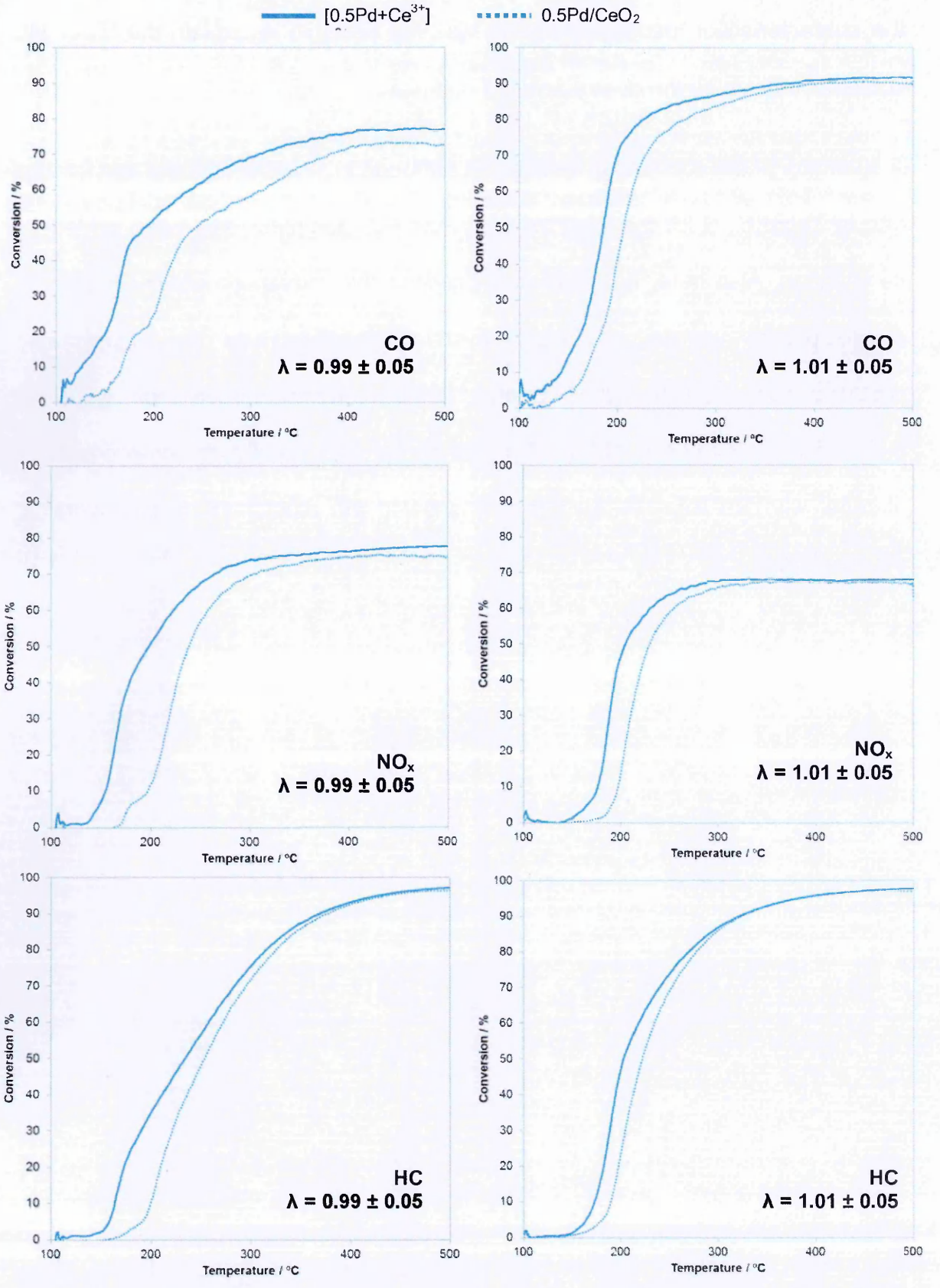

Figure 6-18: Light-off performance under perturbed conditions for 0.5Pd-CeO_2 catalysts prepared by impregnation (0.5Pd/CeO_2) and by co-precipitation using Ce^{3+} ([0.5Pd+Ce^{3+}]) precursor. From top to bottom, CO, NO_x and HC conversions; from left to right, light-offs at lambdas 0.99 ± 0 .05 and 1.01 ± 0.05. The sample size taken was 0.4 g (0.2 g sample + 0.2 g cordierite) and the gas flow rate 5 L min^{-1}. The catalyst was heated using a ramp rate of 10 °C min^{-1} from 110 to 500 °C.

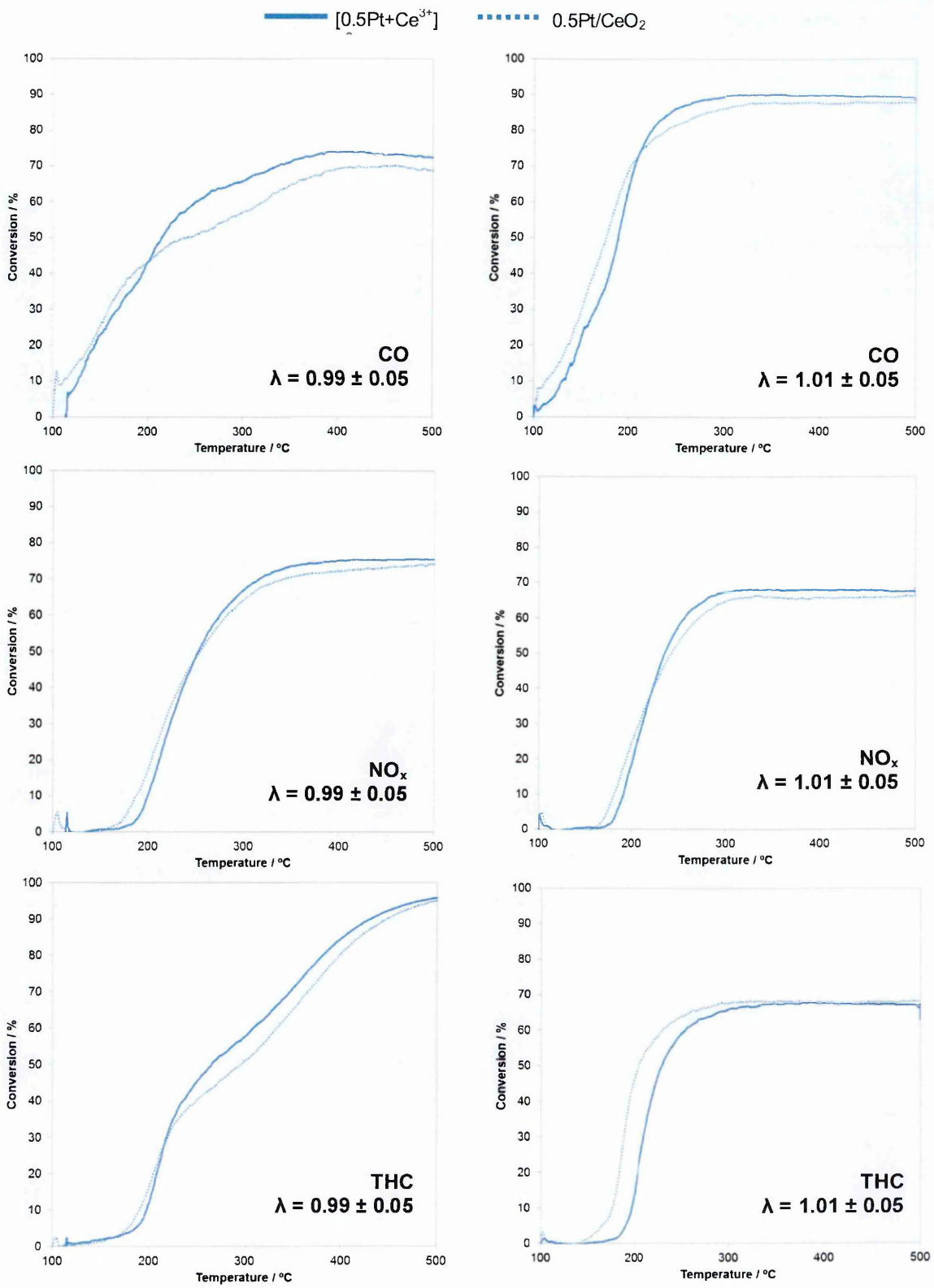

Figure 6-19: Light-off performance under perturbed conditions of Pt-CeO_2 catalysts prepared by co-precipitation with Ce^{3+} and by impregnation on CeO_2. From top to bottom, CO, NO_x and HC conversions; from left to right, light-offs at lambdas 0.99 ± 0.05 and 1.01 ± 0.05. The sample size taken was 0.4 g (0.2 g sample + 0.2 g cordierite) and the gas flow rate 5 L min^{-1}. The catalyst was heated using a ramp rate of 10 °C min^{-1} from 110 to 500 °C.

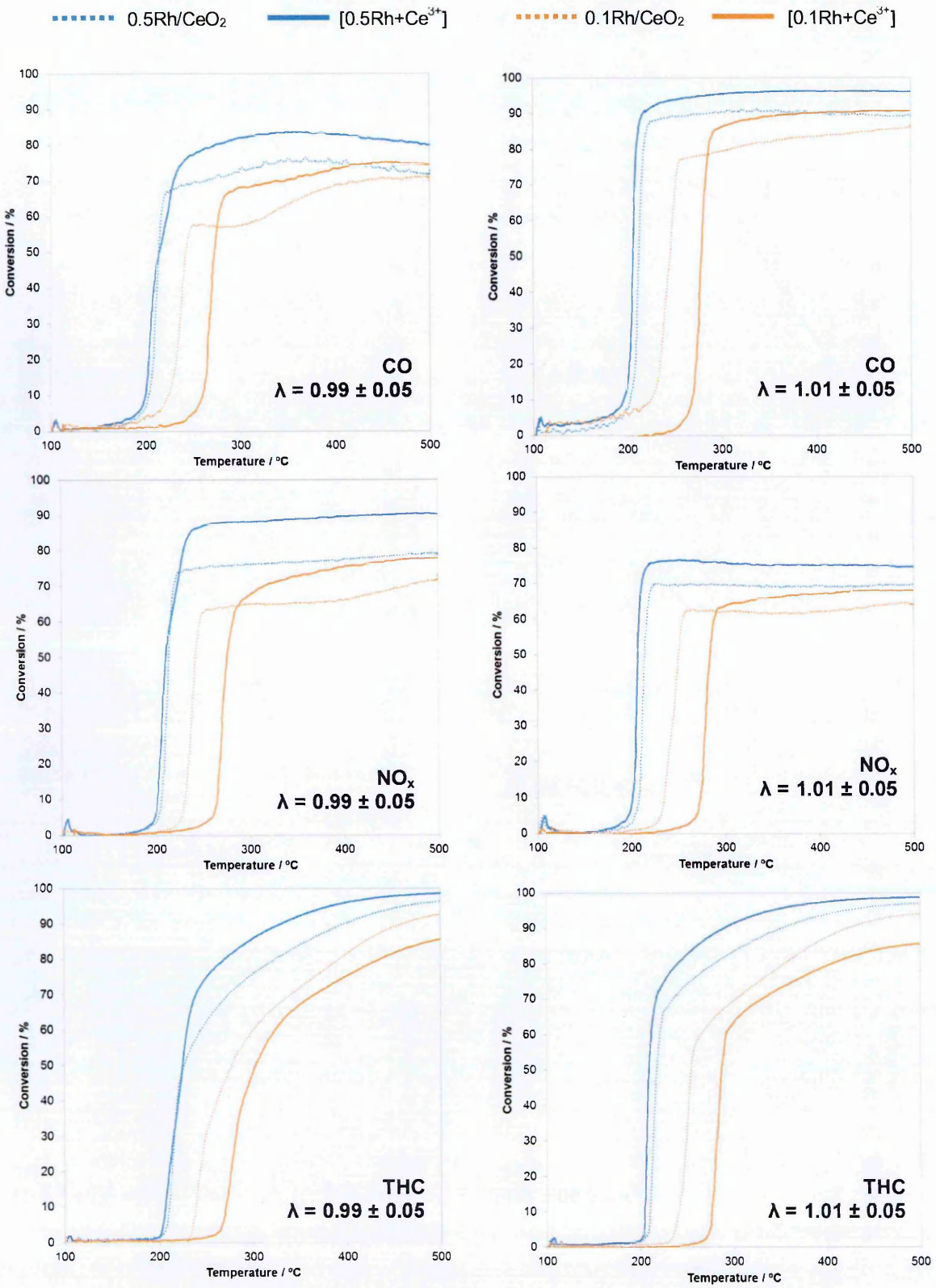

Figure 6-20: Light-off performance under perturbed conditions of Rh-CeO_2 catalysts prepared by co-precipitation with Ce^{3+} and by impregnation on CeO_2. From top to bottom, CO, NO_x and HC conversions; from left to right, light-offs at lambdas 0.99 ± 0.05 and 1.01 ± 0.05. The sample size taken was 0.4 g (0.2 g sample + 0.2 g cordierite) and the gas flow rate 5 L min^{-1}. The catalyst was heated using a ramp rate of 10 °C min^{-1} from 110 to 500 °C.

Table 6-9: Summary of the CO, NO_x and HC conversions achieved at 350 °C at lambda 0.99 ± 0.05. Δ% values refer to the difference between the conversions from the co-precipitated material minus the conversions from the impregnated material.

0.99 ± 0.05

Sample	CO conversion		NO_x conversion		HC conversion	
	At 350 °C / %	Δ%	At 350 °C / %	Δ%	At 350 °C / %	Δ%
$0.5Pd/CeO_2$	66	+7	73	+2	86	+1
$[0.5Pd+Ce^{3+}]$	73		75		87	
$0.5Pt/CeO_2$	65	+6	70	+4	65	+6
$[0.5Pt+Ce^{3+}]$	71		74		71	
$0.5Rh/CeO_2$	76	+7	77	+12	84	+8
$[0.5Rh+Ce^{3+}]$	83		89		92	
$0.1Rh/CeO_2$	63	+7	65	+8	72	-5
$[0.1Rh+Ce^{3+}]$	70		73		67	

Table 6-10: Summary of the CO, NO_x and HC conversions achieved at 350 °C at lambda 1.01 ± 0.05. Δ% values refer to the difference between the conversions from the co-precipitated material minus the conversions from the impregnated material.

1.01 ± 0.05

Sample	CO conversion		NO_x conversion		HC conversion	
	At 350 °C / %	Δ%	At 350 °C / %	Δ%	At 350 °C / %	Δ%
$0.5Pd/CeO_2$	88	+1	67	0	93	0
$[0.5Pd+Ce^{3+}]$	89		67		93	
$0.5Pt/CeO_2$	88	+2	66	+2	80	+4
$[0.5Pt+Ce^{3+}]$	90		68		84	
$0.5Rh/CeO_2$	91	+5	69	+6	90	+6
$[0.5Rh+Ce^{3+}]$	96		75		96	
$0.1Rh/CeO_2$	82	+7	61	+5	79	-6
$[0.1Rh+Ce^{3+}]$	89		66		73	

6.6. Summary

The co-precipitation method led to different catalytic morphologies depending on the noble metal used. In all the cases evaluated here, the co-precipitation method improved NM-Ce interaction; however, the amount of surface metal exposed varied depending on the noble metal.

As previously shown in *Chapter 4*, the co-precipitation of palladium and cerium (III) led to a catalyst with a similar Pd surface area to the impregnated version but with a significantly improved Pd-Ce interaction, due to the larger number of Ce atoms promoted by Pd. It was concluded that this improvement was possibly a consequence of a partial ceria decoration on the Pd particles [24, 35].

For [0.5Pt+Ce^{3+}] the co-precipitation also led to a product with an improved Pt-Ce interaction due to a larger number of Pt atoms in close contact with Ce atoms [8]. This could be especially noticed when comparing the amounts of H_2 consumed during H_2-TPR experiments (which was the largest for the [0.5Pt+Ce^{3+}] sample), and by comparing the OSC values (which again were higher for the co-precipitated material). However, based on CO chemisorption, EtOH-TPSR and calculated XPS Ce/Pt atomic ratio, in the co-precipitated sample the Pt particles appeared to be either larger in size or to contain a larger amount of CeO_2 covering them (compared to the amount seen on [0.5Pd+Ce^{3+}]), which would have decreased the pollutants adsorption capacity [36]. Therefore, even if the Pt-Ce interaction was improved allowing better oxygen mobility, the poorer Pt surface area counteracted the improvement, leading to similar catalytic activities between the co-precipitated catalyst and the impregnated reference (in terms of light-off and pollutant conversions) [33, 37].

Regarding the preparations with Rh, catalysts with significantly larger Rh particles were obtained in comparison to Pd and Pt preparations, either by the impregnation

or the co-precipitation routes (as CO chemisorption dispersion values stated). Similar to the Pt-CeO_2 samples, the surface characterisation (CO chemisorption, ethane hydrogenolysis, and XPS calculated Ce/Rh atomic ratios) also showed that the metal surface area was significantly lower for the [0.5Rh+Ce^{3+}] sample than for 0.5Rh/CeO_2. Compared to the impregnated catalyst, the lower Rh surface area affected the cold-start light-off, shifting it to higher temperatures [25, 34]. However, the partial ceria-decoration, which is believed to occur during the co-precipitation, greatly improved the Rh-Ce interaction (especially obvious when comparing the H_2 consumption during H_2-TPR experiments). As a consequence, a significant improvement in the OSC properties of the Rh co-precipitated catalyst was seen, which could also be linked to higher conversions obtained during perturbed light-off tests [24].

From all the catalysts evaluated here, [0.5Rh+Ce^{3+}] was the catalyst that presented the largest improvement in terms of NM-Ce interaction compared to its impregnated version. Based on reported studies, this could be associated to a higher spillover capacity of Rh, which can promote a higher number of ceria atoms than Pt or Pd [26, 28, 29].

Table 6-11 summarises the main properties of these materials:

Table 6-11: Results obtained on the co-precipitated materials with Ce^{3+} precursor. The results shown here are based on the comparison with the reference impregnated materials.

	[0.5Pd+Ce^{3+}]	[0.5Pt+Ce^{3+}]	[0.5Rh+Ce^{3+}]
XRD	Pd outside structure	Pt outside structure	Rh outside structure
XPS	Shift of Pd3d to higher binding energy. Ce/NM atomic ratio: 36% increase.	No shift of Pt4f to higher binding energy. Ce/NM atomic ratio: 48% increase.	No shift of Rh3d to higher binding energy. Ce/NM atomic ratio: 18% increase.
Metal surface area	3.5% lower	54% lower	48% lower
TPR	Sharp reduction Higher H_2 consumption	Sharp reduction Similar H_2 consumption	Sharp reduction Significantly higher H_2 consumption
Cold light-off T	Similar	Worse	Worse
Perturbed final conversion	Better	Slightly better	Significantly better

References Chapter 6

[1] M. V. Twigg, Applied Catalysis B: Environmental, (2007) 2-15.

[2] M. V. Twigg, Catalysis Today, 117 (2006) 407-418.

[3] R. M. Heck and R. J. Farrauto, *Catalytic air pollution control - Commercial Technology*, Willey-Interscience, 2002.

[4] C. Knight (Editor), *Penny Cyclopaedia of the Society for the Diffusion of Useful Knowledge*, SDUK, 1840,

[5] H. Watts, *A Dictionary of Chemistry*, Longman, Green, Roberts & Green, 1868.

[6] M. Eagleson, *Concise Encyclopedia Chemistry*, Walter de Gruyter, 1994.

[7] International Centre for Diffraction Data (ICDD), *PDF-4, COD (REV30738 2011.11.2)*, 2012.

[8] Y. Zhang, J. Zhou, Z. Wang, J. Liu and K. Cen, International Journal of Hydrogen Energy, 33 (2008) 2211-2217.

[9] A. I. Boronin, E. M. Slavinskaya, I. G. Danilova, R. V. Gulyaev, Y. I. Amosov, P. A. Kuznetsov, I. A. Polukhina, S. V. Koscheev, V. I. Zaikovskii and A. S. Noskov, Catalysis Today, 144 (2009) 201-211.

[10] A. V. Naumkin, A. Kraut-Vass, S. W. Gaarenstroom and C. J. Powell, *NIST X-ray Photoelectron Spectroscopy Database*, 2000.

[11] P. Bera, K. R. Priolkar, A. Gayen, P. R. Sarode, M. S. Hegde, S. Emura, R. Kumashiro, V. Jayaram and G. N. Subbanna, Chemistry of Materials, 15 (2003) 2049-2060.

[12] A. Gayen, K. R. Priolkar, P. R. Sarode, V. Jayaram, M. S. Hegde, G. N. Subbanna and S. Emura, Chemistry of Materials, 16 (2004) 2317-2328.

[13] T. L. Barr, *Modern ESCA: The Principles and Practice of X-Ray Photoelectron Spectroscopy*, CRC Press, 1994.

[14] A. Cimino, M. Boudart and H. S. Taylor, Journal of Physical Chemistry, 58 (1954) 796.

[15] P. Canton, G. Fagherazzi, M. Battagliarin, F. Menegazzo, F. Pinna and N. Pernicone, Langmuir, 18 (2002) 6530-6535.

[16] J. Freel, Journal of Catalysis, 25 (1972) 149-160.

[17] H. F. J. V. t. Blik, J. B. A. D. V. Zon, D. C. Koningsberger and R. Prins, Journal of Molecular Catalysis, 25 (1984) 379-396.

[18] T. Schalow, B. Brandt, D. E. Starr, M. Laurin, S. K. Shaikhutdinov, S. Schauermann, J. Libuda and H. J. Freund, Physical Chemistry Chemical Physics, 9 (2007) 1347-1361.

[19] M. Kurnatowska, L. Kepinski and W. Mista, Applied Catalysis B: Environmental, 117–118 (2012) 135-147.

[20] A. Trovarelli, E. Aneggi, M. Boaro, C. d. Leitenburg and G. Dolcetti, Journal of Alloys and Compounds, 408-412 (2006) 1096-1102.

[21] C. Larese, M. L. Granados, F. C. Galisteo, R. Mariscal and J. L. G. Fierro, Applied Catalysis B: Environmental, 62 (2006) 132-143.

[22] D. M. Fernandes, C. F. Scofield, A. A. Neto, M. J. B. Cardoso and F. M. Z. Zotin, Chemical Engineering Journal, 160 (2010) 85-92.

[23] P. Fornasiero, J. Kaspar, T. Montini, M. Graziani, V. Dal Santo, R. Psaro and S. Recchia, Journal of Molecular Catalysis A: Chemical, 204–205 (2003) 683-691.

[24] R. Rao and B. G. Mishra, Bulletin of the Catalysis Society of India, 2 (2003) 122-134.

[25] I. Heo, D. Y. Yoon, B. K. Cho, I.-S. Nam, J. W. Choung and S. Yoo, Applied Catalysis B: Environmental, 121–122 (2012) 75-87.

[26] C. Descorme and D. Duprez, Applied Catalysis A: General, 202 (2000) 231-241.

[27] C. Hardacre, T. Rayment and R. M. Lambert, Journal of Catalysis, 158 (1996) 102-108.

[28] C. Descorme, S. Bedrane and D. Duprez, Catalysis Today, 75 (2002) 401-405.

[29] S. Bedrane, C. Descorme and D. Duprez, Applied Catalysis A: General, 289 (2005) 90-96.

[30] R. H. Nibbelke, A. J. L. Nievergeld, J. H. B. J. Hoebink and G. B. Marin, Applied Catalysis B: Environmental, 19 (1998) 245-259.

[31] R. Rajasree, J. H. B. J. Hoebink and J. C. Schouten, Journal of Catalysis, 223 (2004) 36-43.

[32] G. Wang, M. Meng, Y. Zha and T. Ding, Fuel, 89 (2010) 2244-2251.

[33] A. S. Ivanova, E. M. Slavinskaya, R. V. Gulyaev, V. I. Zaikovskii, O. A. Stonkus, I. G. Danilova, L. M. Plyasova, I. A. Polukhina and A. I. Boronin, Applied Catalysis B: Environmental, 97 (2010) 57-71.

[34] H. Birgersson, L. Eriksson, M. Boutonnet and S. G. Järås, Applied Catalysis B: Environmental, 54 (2004) 193-200.

[35] M. Cargnello, V. V. T. Doan-Nguyen, T. R. Gordon, R. E. Diaz, E. A. Stach, R. J. Gorte, P. Fornasiero and C. B. Murray, Science, 341 (2013) 771-773.

[36] E. L. Wilson, W. A. Brown and G. Thornton, Surface Science, 600 (2006) 2555-2561.

[37] M. Hatanaka, N. Takahashi, T. Tanabe, Y. Nagai, K. Dohmae, Y. Aoki, T. Yoshida and H. Shinjoha, Applied Catalysis B: Environmental, 99 (2010) 336-342.

7. Bimetallic catalysts based on 0.5Pd-0.1Rh-CeO_2

Contents

7. Bimetallic catalysts based on 0.5Pd-0.1Rh-CeO_2

Commercial TWC usually contain Pd and Rh, typically in a weight ratio of approximately 5:1. These metals can be found separated in 2-layer formulations or together in 1-layer forming an alloy. However, the interaction of Pd and Rh has been seen to have a negative impact on the activity of the catalyst, as depending on the type of ageing experienced the composition of the alloy changes. Rich ageing segregates Rh out of the alloy to cover the Pd; under oxidising conditions at high temperature (< 600 ºC) Pd segregates as PdO, covering the Pd-Rh alloy, which results in the suppression of Rh activity to reduce NO_x [1]. Therefore, separation of the noble metals to avoid these Pd-Rh interactions is desired, which can significantly increase the complexity of the catalyst system [2].

With the aim of studying how the different preparations affect Pd-Rh interaction, 0.1Rh-0.5Pd-CeO_2 catalysts were synthesised by different routes:

1) Co-impregnation of Rh and Pd (0.1Rh-0.5Pd/CeO_2).
2) Impregnation of Rh on co-precipitated Pd and Ce (0.1Rh/[0.5Pd+Ce]).
3) Co-precipitation of Rh, Pd and Ce simultaneously [0.1Rh+0.5Pd+Ce].

In all catalysts the Pd:Rh ratio used was 5:1 with a weight loading of 0.5 wt% Pd and 0.1 wt% Rh. The ceria precursor used for the co-precipitated materials in all cases was $Ce(NO_3)_3 \cdot 6H_2O$ (Ce^{3+} precursor), supplied by Alfa Aesar. The precursor used for Pd was $Pd(NO_3)_2$ solution supplied by Johnson Matthey. The choice of Rh precursor depended on the preparation method as will be explained in the following sections, where $Rh(NO_3)_3$ or Rh (II) citrate were used; both solutions were also supplied by Johnson Matthey.

7.1. Catalysts preparation: observations

As detailed above, three different catalysts were prepared by different routes. The co-impregnation and the co-precipitation of Pd and Rh were performed with the aim of maximising Pd-Rh contact; the impregnation of Rh on the co-precipitated material [0.5Pd+Ce^{3+}] was an attempt to minimise their interaction within the same component.

For the impregnation of Rh on [0.5Pd+Ce^{3+}] an organic precursor was used to decrease the acidity during the preparation, as a too acidic medium could re-dissolve any NM already present while the new metals are being impregnated [3]. For this reason the precursor used was Rh(II) citrate: $(Rh_2(H_2cit)_4)$[1].

The colour of these samples remained unchanged in all cases, suggesting no modifications in the oxidation state of the metals, which were already present as oxides.

7.1.1. 0.1Rh-0.5Pd co-impregnation on CeO_2

Rh nitrate and Pd nitrate solutions were mixed together in a beaker and diluted with a 20% excess of demineralised H_2O to fully fill all pores of the CeO_2 support. The solution was added with a pipette and mixed to achieve maximum homogeneity. The sample was dried at 105 °C overnight and calcined at 650 °C for 2h.

7.1.2. 0.1Rh impregnation on [0.5Pd+Ce^{3+}]

Rh(II) citrate was diluted with 20% excess of demineralised H_2O to fully fill all pores of the [0.5Pd+Ce^{3+}] catalyst. The solution was added with a pipette and

[1] Cit = citrate $(C_3H_4O_6\text{-}OH)^{3-}$

mixed to achieve maximum homogeneity. The sample was dried at 105 ºC overnight and calcined at 650 ºC for 2h.

Note that [0.5Pd+Ce^{3+}] had been previously calcined at 650 ºC/2h before Rh impregnation; therefore, overall this support was exposed for a total of 4 hours to 650 ºC.

7.1.3. Co-precipitation of [0.1Rh+0.5Pd+Ce^{3+}]

The same procedure described in *Chapter 2* was used for this preparation. Rh nitrate, Pd nitrate and Ce(III) nitrate precursors were mixed in 150 ml of demineralised H_2O. This solution was then added with a peristaltic pump to the basified solution.

The precipitate obtained was dark grey. Since previously a similar preparation based on [Rh+Ce^{3+}] did not reduce Rh, the dark colour is assumed to be only related to the presence of metallic Pd. After the calcination this material changed colour to yellow, suggesting the oxidation of metallic Pd to PdO [4].

7.2. Structural characterisation

The structural characterisation was done by XRD. The aim of this study was to identify differences in the ceria structure between the samples prepared by the different methods, especially for the co-precipitated materials where any impact caused by the addition of multiple noble metals (NM) during the preparation was monitored. In most of the characterisation results, the mono-metallic catalysts based on 0.1Rh-CeO_2 and 0.5Pd-CeO_2 have been also included for comparison.

7.2.1 X-Ray Diffraction (XRD)

All three bimetallic catalysts presented cubic ceria structure and no information regarding the NM was obtained, suggesting that the NM were highly dispersed [5]. The XRD profiles can be seen in Figure 7-1:

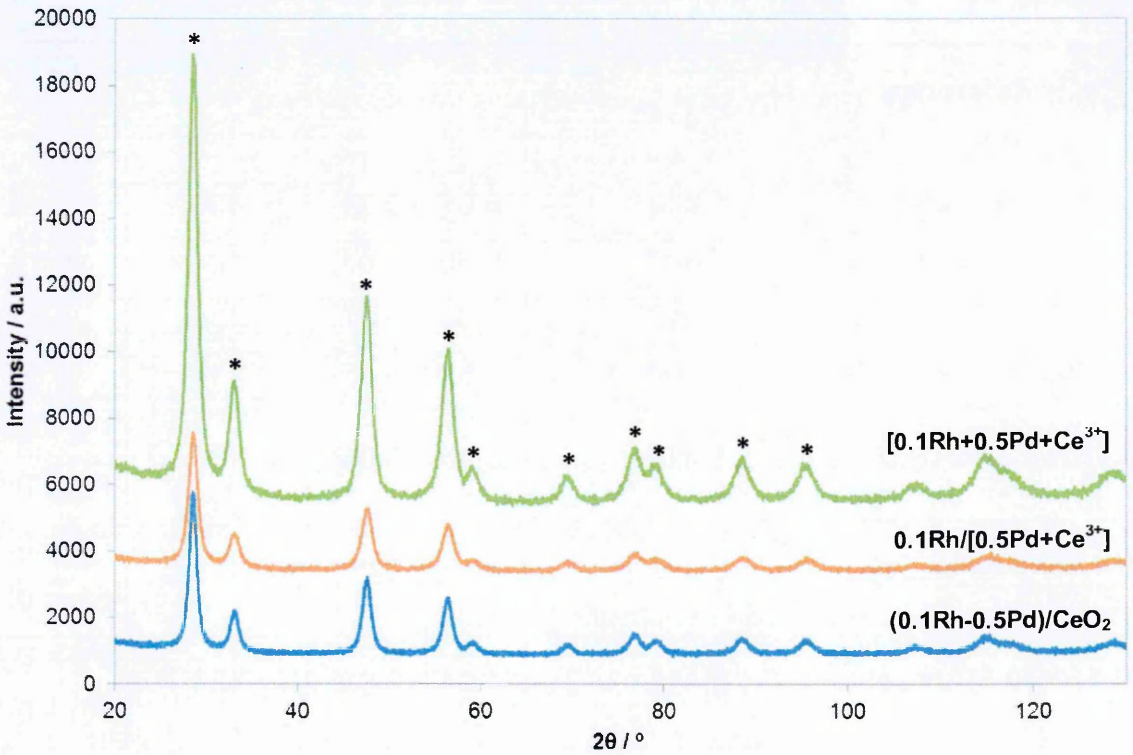

Figure 7-1: XRD profiles for Pd-Rh-CeO_2 samples prepared by co-precipitation with Ce^{3+} precursor ([Rh+Pd+Ce^{3+}]), by wet impregnation on CeO_2 (Rh-Pd/CeO_2), and by a combination of both methods (Rh/[Pd+Ce^{3+}]). The peaks corresponding to the cubic CeO_2 phase are indicated as (*).

Table 7-1 summarises the lattice parameter *a* and the ceria crystallite size values, as well as their BET-SSA. Compared to the mono-metallic catalysts, the bimetallic samples did not differ significantly. Similar lattice parameters and ceria crystallite size were obtained.

Table 7-1: Lattice parameter *a* and ceria crystallite size analysed by XRD, and specific surface area calculated by BET, of Pd-CeO_2, Rh-CeO_2, and Pd-Rh-CeO_2 samples prepared by co-precipitation with Ce^{3+} precursor ([(NM+Ce^{3+}]), by wet impregnation on CeO_2 (NM/CeO_2), and by a combination of both methods (Rh/[Pd+Ce^{3+}]). Calculated errors (reported in brackets) for crystallite size (nm) and lattice parameter data (Å) refer to the last significant figure; BET-SSA instrument standard error = ± 4 m^2 g^{-1}.

	lattice parameter *a* / Å	Crystallite size / nm	BET – SSA / m^2 g^{-1}	ICP / NM wt%
CeO_2 Reference [5]	5.411	-	-	-
0.1Rh/CeO_2	5.410	6.61 (±0.08)	106	0.13
[0.1Rh+Ce]	5.407	5.66 (±0.08)	124	0.12
0.5Pd/CeO_2	5.410	5.83 (±0.07)	138	0.51
[0.5Pd+Ce]	5.409	5.51 (±0.05)	114	0.50
0.1Rh-0.5Pd/CeO_2	5.410	5.65 (±0.06)	131	Pd = 0.51 Rh = 0.13
0.1Rh/[0.5Pd+Ce]	5.407	4.62 (±0.05)	114	Pd = 0.49 Rh = 0.12
[0.1Rh+0.5Pd+Ce]	5.411	4.64 (±0.05)	135	Pd = 0.46 Rh = 0.12

7.3. Surface characterisation

7.3.1. X-Ray Photoelectron Spectroscopy (XPS)

The bimetallic 0.1Rh-0.5Pd-CeO_2 catalysts prepared by the different routes were submitted for XPS analyses and compared to 0.1Rh- and 0.5Pd-CeO_2 catalysts prepared by impregnation and by co-precipitation. A summary of Pd3d and Rh3d bands positions, as well as the calculated Ce/NM atomic ratios obtained from these analyses can be found in Table 7-2.

Table 7-2: Summary of the XPS bands positions for Pd3d and Rh3d, and calculated Ce/NM and Pd/Rh atomic ratio for Pd-, Rh- and Rh-Pd-CeO_2 samples prepared by co-precipitation with Ce^{3+} precursor ([(NM+Ce^{3+}]), by wet impregnation on CeO_2 (NM/CeO_2), and by a combination of both methods (Rh/[Pd+Ce^{3+}]).

Sample	Ce/NM atomic ratio / a.u.	Pd/Rh atomic ratio / a.u.	Pd3d bands / eV			Rh3d bands / eV
			Pd^0	PdO	PdO_2	Rh_2O_3
0.1Rh/CeO_2	Rh = 111	-	-			308.1 313.1
[0.1Rh+Ce]	*Rh not detectable	-	-			*Rh not detectable
0.5Pd/CeO_2	Pd = 34	-	-	337.6 342.9	-	-
[0.5Pd+Ce]	Pd = 54	-	-	337.3 342.5	338.3 343.5	-
(0.1Rh-0.5Pd)/CeO_2	*Rh not detectable Pd = 48	*Rh not detectable	335.8 341.1	337.6 342.8	339.5 344.8	* Rh not detectable
0.1Rh/[0.5Pd+Ce]	Rh = 216 Pd = 87	2.5	335.8 341.1	337.8 343.0	-	309.1 314.0
[0.1Rh+0.5Pd+Ce]	*Rh not detectable Pd = 82	*Rh not detectable	335.7 341.2	337.7 343.0	-	*Rh not detectable

In most cases Rh could not be detected. Rh3d bands were only visible for 0.1Rh/[0.5Pd+Ce], suggesting a larger surface Rh concentration than for (0.1Rh-0.5Pd)/CeO_2 and [0.1Rh+0.5Pd+Ce] (Figure 7-2). These bands appeared at 309.1 ($Rh3d_{5/2}$) and at 314.0 eV ($Rh3d_{3/2}$), and were attributed to Rh_2O_3 [6, 7]. For (0.1Rh-0.5Pd)/CeO_2 and [0.1Rh+0.5Pd+Ce] samples, it could be possible that the intimate contact between Pd and Rh would have promoted the formation of a Pd-Rh alloy. It is also well reported that the exposure of Pd-Rh alloys to oxidation conditions at high temperature segregates Pd as PdO, covering the Pd-Rh alloy, and thus decreasing the number of Rh surface sites [1, 8]. This could have occurred during the calcination of these catalysts at 650 ºC, which would explain the lower Rh surface concentration of (0.1Rh-0.5Pd)/CeO_2 and [0.1Rh+0.5Pd+Ce] samples compared to 0.1Rh/[0.5Pd+Ce].

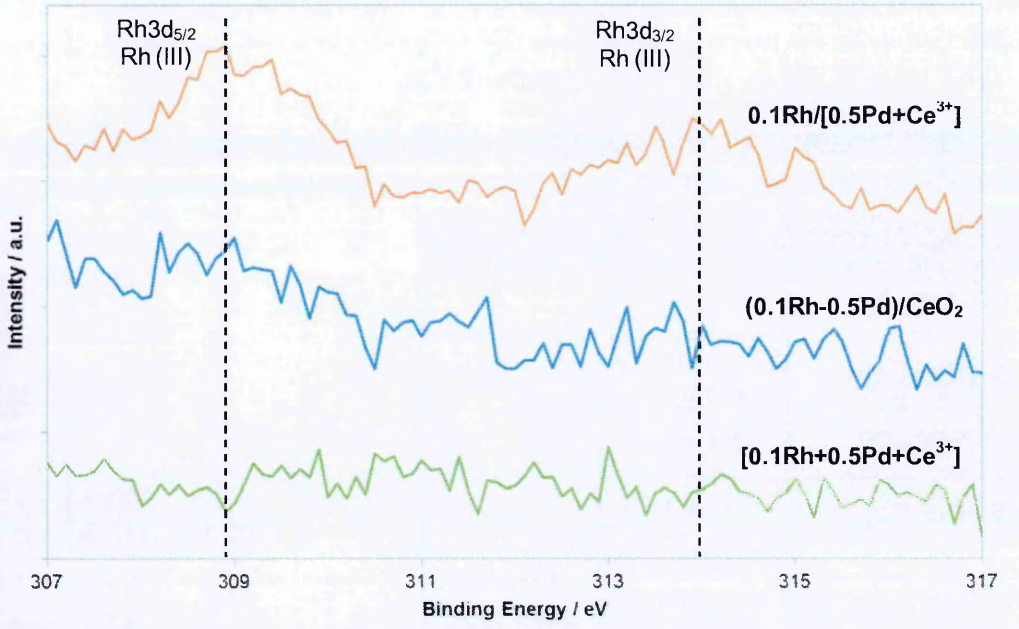

Figure 7-2: Rh3d XPS spectra of Rh-Pd-CeO_2 samples prepared by co-precipitation with Ce^{3+} precursor ([(Rh+Pd+Ce^{3+}]), by wet impregnation on CeO_2 (Rh-Pd/CeO_2), and by a combination of both methods (Rh/[Pd+Ce^{3+}]). The vertical lines point the position of the Rh species detected.

Rh3d bands for 0.1Rh/[0.5Pd+Ce], appeared at the same position as those for 0.1Rh/CeO_2 (see Table 7-2). Regarding Rh surface content, the 0.1Rh/[0.5Pd+Ce] sample had a calculated Ce/Rh atomic ratio of 216 which was considerably higher than that for 0.1Rh/CeO_2 (111). Since in both cases Rh was added by impregnation, it was expected to find all the Rh metal on the surface with minimum encapsulation. The higher Ce/Rh atomic ratio of the bimetallic sample could be related to the presence of larger Rh particles or due to encapsulation by PdO particles, this however could not be concluded from this characterisation.

In contrast to Rh, Pd3d bands could be detected in all these samples due to the higher Pd loading. Different Pd species were found in each of the materials evaluated (see below) [6]:

(0.1Rh-0.5Pd)/CeO_2: 63% PdO, 15% Pd metal, 22% PdO_2.

0.1Rh/[0.5Pd+Ce]: 84% PdO, 16% Pd metal.

[0.1Rh+0.5Pd+Ce]: 92% PdO, 8% Pd metal.

In all cases, the main Pd species existed as PdO and metallic Pd. A higher Pd oxidation state (bands positions related to PdO_2) was only detected for (0.1Rh-0.5Pd)/CeO_2, which contained a higher content of these species than metallic Pd (22% and 15%, respectively). The detection of these bands indicated that there was an electronic interaction, either with the support or with the Rh, which was stronger than for 0.1Rh/[0.5Pd+Ce] and [0.1Rh+0.5Pd+Ce] [9, 10]. This differs with the results seen previously for [0.5Pd+Ce] and 0.5Pd/CeO_2 samples, where XPS bands close to those associated to PdO_2 were only detected for the co-precipitated material but not for the impregnated sample.

The formation of metallic Pd could suggest the presence of Pd-Rh alloy [8]. Based on this, (0.1Rh-0.5Pd)/CeO_2 and 0.1Rh/[0.5Pd+Ce] would appear to contain a higher content of Pd-Rh alloy than [0.1Rh+0.5Pd+Ce]. This would suggest that the impregnation of Rh on [0.5Pd+Ce] has not stopped Pd and Rh from interacting.

Figure 7-3 compares the Pd3d bands obtained for the bimetallic catalysts:

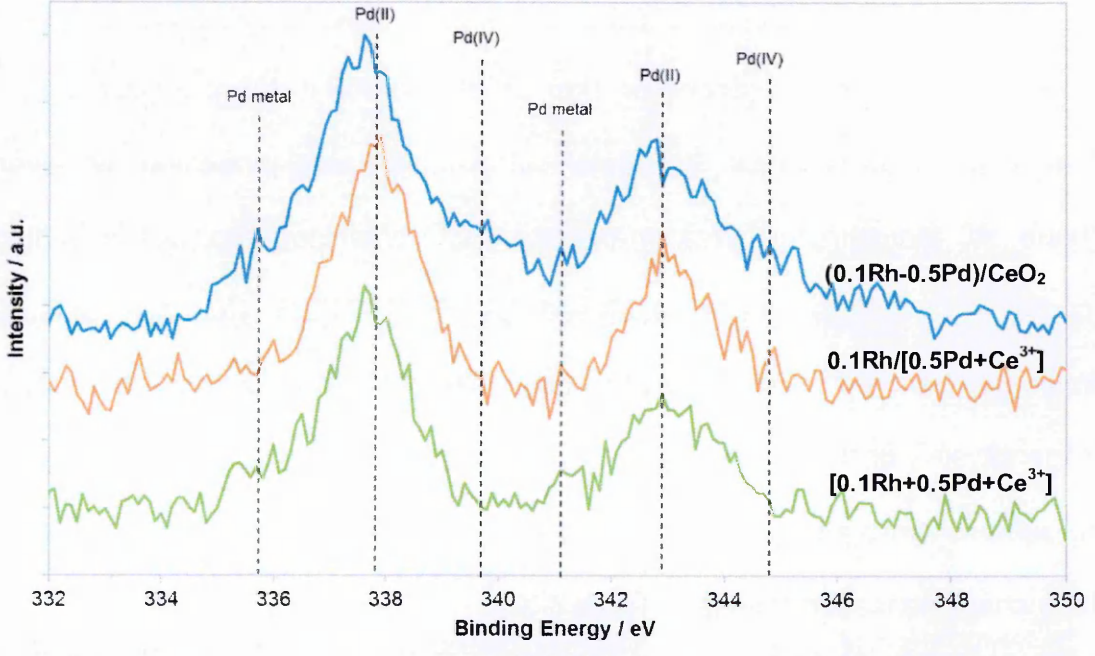

Figure 7-3: Pd3d XPS spectra of Rh-Pd-CeO_2 samples prepared by co-precipitation with Ce^{3+} precursor ([(Rh+Pd+Ce^{3+}]), by wet impregnation on CeO_2 (Rh-Pd/CeO_2), and by a combination of both methods (Rh/[Pd+Ce^{3+}]). The vertical lines point the position of the different Pd species detected.

0.1Rh-0.5Pd/CeO_2 was the bimetallic sample with the most surface Pd based on the comparison of the calculated Ce/Pd atomic ratios. However, this Ce/Pd atomic ratio was higher than that for 0.5Pd/CeO_2. As previously mentioned, since these catalysts were prepared by impregnation, minimum ceria decoration is expected and therefore the increase of Ce/Pd atomic ratio for 0.1Rh-0.5Pd/CeO_2 could be related with the presence of larger Pd particles.

0.1Rh/[0.5Pd+Ce] and [0.1Rh+0.5Pd+Ce] contained similar Ce/Pd atomic ratios, which were higher than that found for 0.1Rh-0.5Pd/CeO_2. Just based on these analyses it was not possible to conclude if the higher Ce/Pd atomic ratio was due to a higher ceria decoration and/or to larger Pd particles. Compared to [0.5Pd+Ce], the Ce/Pd atomic ratios of the bimetallic samples were also higher.

Similar to results found in previous chapters, Ce3d signals (not shown here) showed that most of the ceria was present as Ce^{4+}, suggesting the oxidation of Ce^{3+} to Ce^{4+} during the calcination process.

7.3.2. Surface analyses: CO chemisorption, EtOH-TPSR, and ethane hydrogenolysis

Similar to previous samples, the metal surface area was evaluated by several methods. All the samples were analysed by CO chemisorption, but in addition Pd-containing samples were analysed by EtOH-TPSR (for the selective quantification of Pd surface area), and Rh-containing samples by ethane hydrogenolysis (for the selective characterisation of Rh surface area). The profiles of the ethane hydrogenolysis can be found in Figure 7-4 and a summary of all the surface characterisation results in Table 7-3.

Table 7-3: Quantitative and qualitative analyses of metal surface area calculated by XPS, by CO chemisorption, by EtOH-TPSR (in the case of Pd) and by ethane hydrogenolysis (in the case of Rh) for Rh-, Pd- and Rh-Pd-CeO_2 catalysts prepared by co-precipitation with Ce^{3+} precursor ([(NM+Ce^{3+}]), by wet impregnation on CeO_2 (NM/CeO_2), and by a combination of both methods (Rh/[Pd+Ce^{3+}]). CO chemisorption instrument standard error = ± 2% (for metal dispersion) and ± 0.04 $m^2 g^{-1}$ (for metal surface area); EtOH-TPSR instrument standard error = ± 0.1 $m^2 g^{-1}$; Ethane hydrogenolysis instruments standard error = ± 4 °C.

	XPS	CO chemisorption		Ethane hydrogenolysis for Rh surface area	EtOH-TPSR for Pd surface area	
	Ce/NM atomic ratio / a.u.	Metal dispersion / %	Metal surface area / $m^2 g^{-1}$	T50 / °C	max ppm CH_4 g sample^{-1} ppm $EtOH^{-1}$	Pd surface area / $m^2 g^{-1}$
0.1Rh/CeO_2	Rh = 111	56	0.2	321	-	-
[0.1Rh+Ce]	-	11	0.1	414	-	-
0.5Pd/CeO_2	Pd = 34	52	1.2	-	1.9	0.9
[0.5Pd+Ce]	Pd = 53	51	1.1	-	1.1	0.5
0.5Pd-0.1Rh/CeO_2	Pd = 48	62	1.7	397	1.8	0.8
0.1Rh/[0.5Pd+Ce]	Rh = 216 Pd = 86	53	1.4	351	1.4	0.6
[0.1Rh+0.5Pd+Ce]	Pd = 82	48	1.3	388	1.1	0.5

The same general trends were observed for CO chemisorption and EtOH-TPSR for metal surface area. The CO chemisorption results appeared to be always higher with the Pd-Rh-CeO_2 samples as besides measuring the total surface area of both metals (it is not a selective technique), it also measures the extra contribution of the adsorption at the NM-Ce interface [11]. In addition, the CO adsorption stoichiometry is known to be different between Pd and Rh, which can also result in misleading dispersion values [12-15].

If the bimetallic catalysts are compared, based on the ethane hydrogenolysis and EtOH-TPSR results, 0.1Rh/[0.5Pd+Ce] contained more surface Rh but less Pd than 0.1Rh-0.5Pd/CeO_2. On the other hand, the co-precipitated

[0.1Rh+0.5Pd+Ce], contained significantly less Pd at the surface, but slightly more surface Rh than 0.1Rh-0.5Pd/CeO_2. This agrees with the conclusions obtained by XPS. As already mentioned, it is possible that on the co-impregnated sample (0.1Rh-0.5Pd/CeO_2) Pd could have been placed on top of Rh during the calcination process, blocking the Rh sites [8].

Summarising, from less to more metal surface area:

- Pd on surface (based on EtOH-TPSR): [0.1Rh+0.5Pd+Ce] < 0.1Rh/[0.5Pd+Ce] < 0.1Rh-0.5Pd/CeO_2
- Rh on surface (based on ethane hydrogenolysis): 0.1Rh-0.5Pd/CeO_2 < [0.1Rh+0.5Pd+Ce] < 0.1Rh/[0.5Pd+Ce].

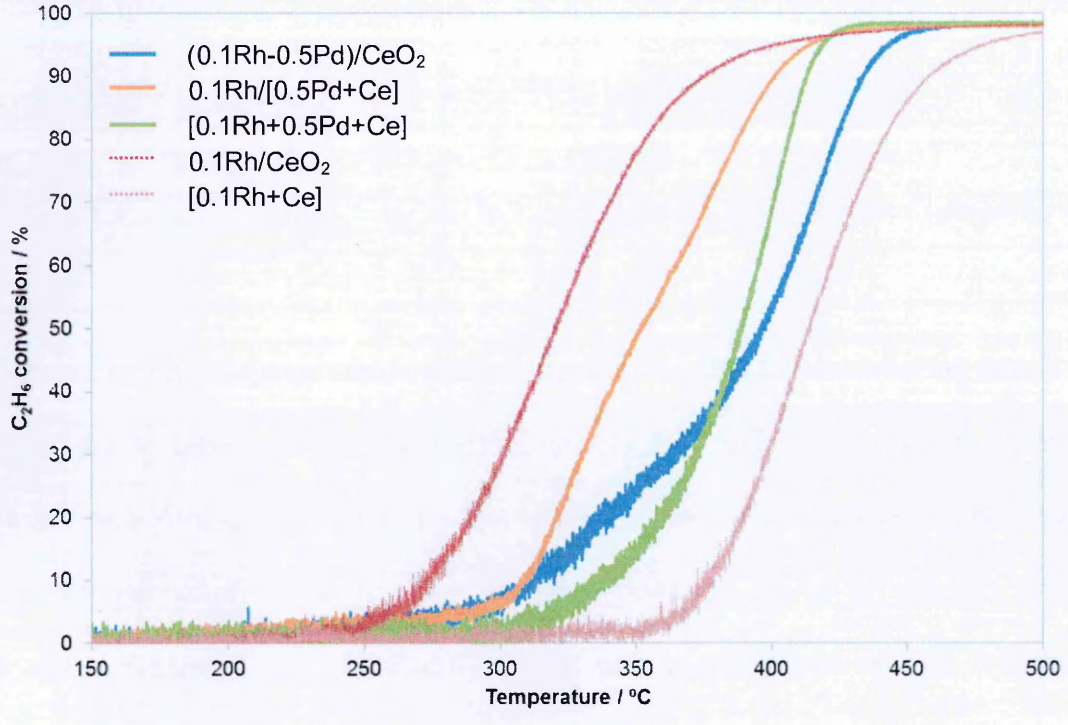

Figure 7-4: Ethane hydrogenolysis profiles performed on Rh-CeO_2 and Rh-Pd-CeO_2 samples prepared by co-precipitation with Ce^{3+} precursor ([(NM+Ce^{3+}]), by wet impregnation on CeO_2 (NM/CeO_2), and by a combination of both methods (Rh/[Pd+Ce^{3+}]). Each sample was firstly pre-treated under He at 300 °C for 30 minutes. Following this, the sample was cooled down to 150 °C and the gas flows set to 50 ml min^{-1} 10%H_2/N_2 and 10 ml min^{-1} 10%C_2H_6/N_2. Once a stable signal was obtained, a temperature ramp of 10 °C min^{-1} was applied up to 450 °C.

The results obtained here for the bimetallic catalysts were also compared to those obtained for 0.5Pd-CeO_2 and 0.1Rh-CeO_2 catalysts:

- 0.1Rh-0.5Pd/CeO_2 was compared to 0.1Rh/CeO_2 and 0.5Pd/CeO_2. It was seen that Pd surface area was similar to that of 0.5Pd/CeO_2. However, the calculated XPS Ce/Pd atomic ratio was slightly higher for 0.1Rh-0.5Pd/CeO_2 than for 0.5Pd/CeO_2. Since both samples contained similar amounts of surface Pd, the small increase of Ce/Pd atomic ratio is possibly associated with some Pd particles forming part of a Pd-Rh alloy on the bimetallic catalyst. This would agree with the presence of metallic Pd already seen during the XPS peak analysis.

  The Rh surface area was lower than 0.1Rh/CeO_2. The lower Rh surface area is believed to be due to the Pd coverage of the Rh particles.

- 0.1Rh/[0.5Pd+Ce] was compared to 0.1Rh/CeO_2 and [0.5Pd+Ce]. Similar Pd surface areas were found for 0.1Rh/[0.5Pd+Ce] and [0.5Pd+Ce]; however, in this case the Ce/Pd atomic ratio was significantly higher for 0.1Rh/[0.5Pd+Ce], which suggest a considerable increase in ceria decoration in the bimetallic sample. This is likely to be associated to a higher sintering suffered by the bimetallic catalyst due to the second calcination performed on the [0.5Pd+Ce] component after Rh impregnation.

  The Rh surface area appeared to be slightly lower than on 0.1Rh/CeO_2; in addition, XPS Ce/Rh atomic ratio was also significantly higher for the bimetallic catalyst. This could occur as a consequence of an increase of Ce-decoration, and/or Pd segregation placed on Rh particles.

- [0.1Rh+0.5Pd+Ce] was compared to [0.1Rh+Ce] and [0.5Pd+Ce]. Pd surface areas between [0.1Rh+0.5Pd+Ce] and [0.5Pd+Ce] were similar; however, the XPS Ce/Pd atomic ratio was significantly higher for the bimetallic catalyst. This suggests an increase of ceria decoration on Pd particles.

  The Rh surface area was higher for the bi-metallic catalyst compared to [0.1Rh+Ce]. It is unknown if this occurred due to Rh being less encapsulated by ceria or to the formation of smaller Rh particles. From this characterisation reported here this could not be concluded.

7.4. Redox characterisation

7.4.1. H_2-TPR

The three samples were analysed by H_2-TPR; an overlay of the spectra can be found in Figure 7-5. All three samples presented three reduction regions between 110 – 200 ºC (NM-Ce reduction), 240 – 430 ºC (unpromoted surface CeO_2), and 600 – 900 ºC (bulk CeO_2) [16-18].

0.1Rh/[0.5Pd+Ce] followed a similar profile to that of [0.1Rh+0.5Pd+Ce], which showed very sharp NM-Ce reduction peaks at 110 and 115 ºC, respectively. These profiles were also highly similar to that of [0.5Pd+Ce^{3+}] sample, suggesting that the bimetallic catalysts contain a good Pd-Ce contact. The intensity of their bulk ceria reduction was practically identical (between 600 – 900 ºC), but the un-promoted surface ceria reduction (between 240 – 430 ºC) was lower for the co-precipitated material. Since the specific surface areas were similar between these catalysts, the lower intensity of this peak cannot be associated to a lower number of surface Ce atoms. This matter will be further evaluated below.

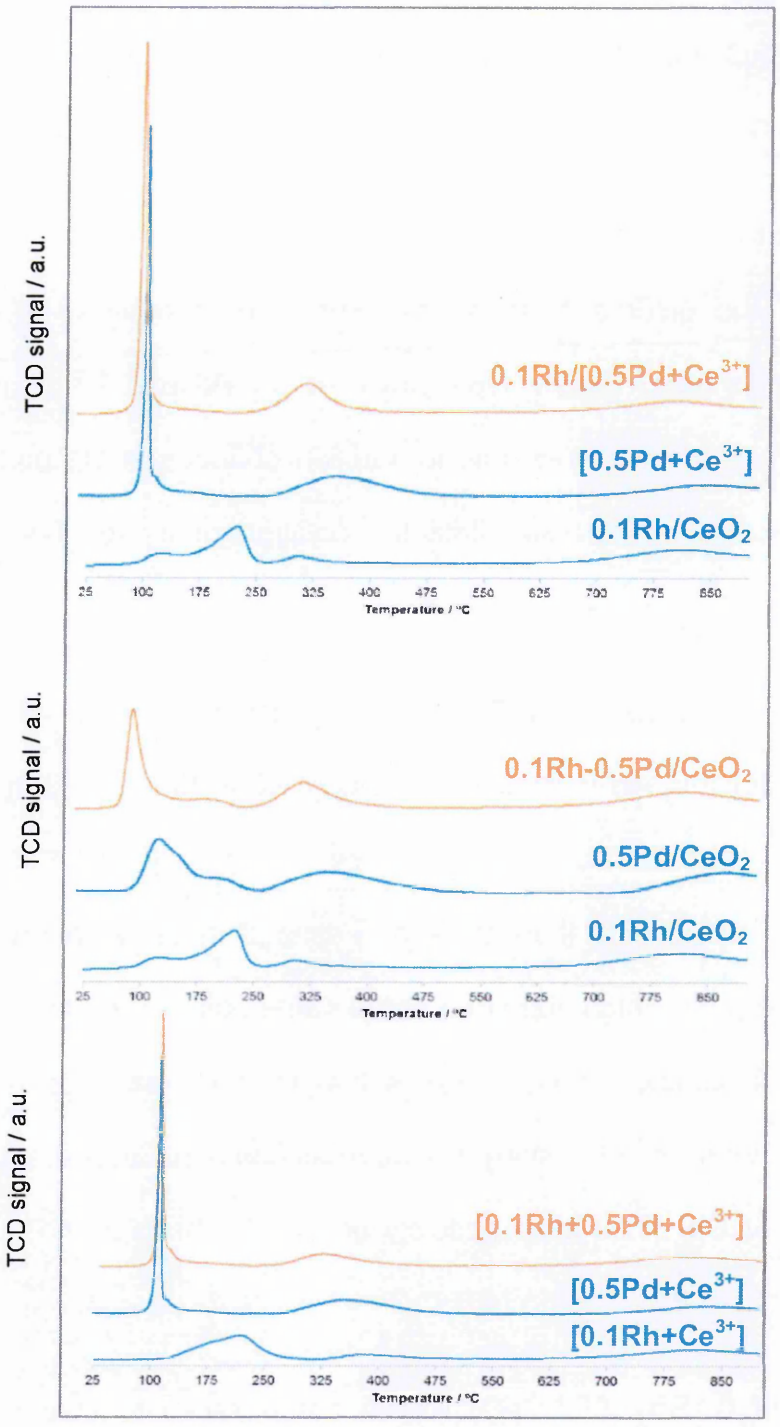

Figure 7-5: H_2-TPR of Rh-, Pd- and Rh-Pd-CeO_2 catalysts prepared by co-precipitation with Ce^{3+} precursor ([(NM+Ce^{3+}]), by wet impregnation on CeO_2 (NM/CeO_2), and by a combination of both methods (Rh/[Pd+Ce^{3+}]). The sample taken was ~0.2 g, and the flow used was 30 ml min^{-1} of 10% H_2/N_2 using 30 ml min^{-1} of N_2 as carrier gas.

0.1Rh-0.5Pd/CeO_2 followed closely the profile of 0.1Rh/[0.5Pd+Ce] in terms of the reduction of un-promoted surface and bulk ceria. However, the NM-Ce reduction

was significantly less intense and appeared as two distinct peaks for the 0.5Pd-0.1Rh/CeO_2 sample, with the largest peak at 105 ºC and the smallest at 190 ºC.

As an attempt to identify which peaks correspond to the reduction of each of the noble metals, the profiles of these samples were compared to those of the individual components (Figure 7-5). However as Pd and Rh reduction peaks appear at similar temperatures, and in addition changes in the particle size and level of interaction would also affect the position of those, this could not be performed exactly.

The reduction associated with Rh-Ce seen previously for the [0.1Rh+Ce] and 0.1Rh/CeO_2 samples, led to reduction peaks at 80 – 305 ºC and at 120 and 215 ºC positions, respectively. In the case of the [0.1Rh+0.5Pd+Ce] and 0.1Rh/[0.5Pd+Ce] samples there were no peaks at these temperatures, only the sharp reduction peak which appeared at the same position as Pd-Ce reduction on the [0.5Pd+Ce] sample. Thus, it seems that in those samples where Pd was co-precipitated with Ce^{3+}, the sharp Pd-Ce reduction dominates the profile, even in the presence of Rh. This could possibly be due to the higher Pd loading used compared to that of Rh.

In the case of 0.1Rh-0.5Pd/CeO_2 it was not possible to clearly assign each reduction peak to each metal, as Pd-Ce and Rh-Ce reduction on 0.5Pd/CeO_2 and 0.1Rh/CeO_2 occurred at similar positions. 0.5Pd/CeO_2 contained two peaks, the largest at ~95 ºC and a shoulder at 205 ºC; 0.1Rh/CeO_2 also contained two peaks, the main one at 215 ºC and a shoulder at 120 ºC. In addition, the co-existence of Pd and Rh would affect the NM stabilities and this could have had an impact on the position of their reduction peaks. If, as suggested by XPS characterisation,

some Pd and Rh particles formed an alloy, this would have increased the stability of the NM particles, but also decreased the level of interaction with the ceria. In the case of 0.1Rh-0.5Pd/CeO_2 two peaks were observed in the 50 to 250 ºC region; based on the assumptions, the peak at ~105 ºC could be associated with the reduction of the noble metals with less contact with ceria, whilst the peak at ~190 ºC could be related with the reduction of NM particles with greater contact with ceria. Table 7-4 summarises the reduction temperatures for the metals and ceria species as well as the H_2 consumption:

Table 7-4: Summary of peak positions and H_2 consumption during the H_2-TPR experiments on Rh-Pd-CeO_2 catalysts prepared by co-precipitation with Ce^{3+} precursor ([(Rh+Pd+Ce^{3+}]), by wet impregnation on CeO_2 (Rh-Pd/CeO_2), and by a combination of both methods (Rh/[Pd+Ce^{3+}]). Average instrument standard error ± 0.02 mmol g^{-1}.

	NM-Ce reduction		Surface CeO_2 reduction		Bulk CeO_2 reduction	
Sample	Peak temperature / ºC	H_2 consumed / mmol g^{-1}	Peak temperature / ºC	H_2 consumed / mmol g^{-1}	Peak temperature / ºC	H_2 consumed / mmol g^{-1}
0.1Rh-0.5Pd/CeO_2	105 Shoulder at 190	1.08	240 – 430	0.60	600 – 900	0.58
0.1Rh/[0.5Pd+Ce]	110	1.14	240 – 430	0.62	600 – 900	0.44
[0.1Rh+0.5Pd+Ce]	115	0.89	240 – 430	0.38	600 – 900	0.58

Besides the different peak shapes obtained, all three catalysts consumed similar amounts of H_2 during the NM-Ce reduction, with the sample [0.1Rh+0.5Pd+Ce] consuming just slightly less H_2 compared to the other two catalysts. Thus, besides the different surface NM contents and compositions, the combination of NM and promoted Ce reduction has led to similar H_2 consumption. This suggests that in those catalysts which appear to have lower NM surface areas, a larger number of Ce atoms were promoted (i.e. [0.1Rh+0.5Pd+Ce]) compared to the catalysts found to have higher surface NM content (i.e. 0.1Rh-0.5Pd/CeO_2). This indicates that

despite the lower NM surface areas achieved with the co-precipitation method compared to the impregnation synthesis, a larger number of NM and Ce atoms are placed in intimate contact.

Regarding the unpromoted surface ceria reduction, the [0.1Rh+0.5Pd+Ce] sample consumed less H_2, compared to 0.1Rh-0.5Pd/CeO_2 and 0.1Rh/[0.5Pd+Ce] samples. Since the ceria crystallite sizes and the catalysts specific surface areas were similar for these catalysts, this could suggest that a higher number of surface ceria atoms were promoted by the NM, which had been already reduced at the lowest temperature reduction region (as already suggested above). On the other hand, the bulk ceria reduction was similar for all the bimetallic catalysts.

7.4.2. CO-TPR

Similar reduction profiles were obtained for the three bimetallic catalysts, all of them showing peaks corresponding to the reduction of surface NM and promoted surface CeO_2 (between 50 – 350 ºC), to non-promoted CeO_2 reduction and water gas shift (between 400 – 700 ºC), and to bulk CeO_2 reduction (> 700 ºC) [9, 19, 20]. The CO consumption and CO_2 formation are represented in Figure 7-6.

In terms of NM reduction, all three samples showed a shoulder at about 130 ºC and a more intense peak close to 300 ºC, most certainly due to the different reductions of each of the noble metals. The initial shoulder appeared at similar temperatures for all these bi-metallic samples, whilst the more intense peak appeared at 270 ºC for 0.5Pd-0.1Rh/CeO_2, at 285 ºC for [0.1Rh+0.5Pd+Ce], and at 290 ºC for 0.1Rh/[0.5Pd+Ce]. A summary can be found in Table 7-5. The small differences in the position of this peak are an indication of different NM particle sizes and/or different level of interactions with the support and between the noble

metals; the lower the temperature of the reduction peak, the less stable these particles are [9, 19]. Based on previous surface area measurements (*section 7.3*), the shift of the NM reduction to slightly higher temperature for 0.1Rh/[0.5Pd+Ce] and [0.1Rh+0.5Pd+Ce] compared to 0.1Rh-0.5Pd/CeO_2, could be related to a higher NM-Ce interaction, as 0.1Rh/[0.5Pd+Ce] and [0.1Rh+0.5Pd+Ce] contained more NM and Ce atoms in contact. These results also agree with those obtained during H_2-TPR experiments.

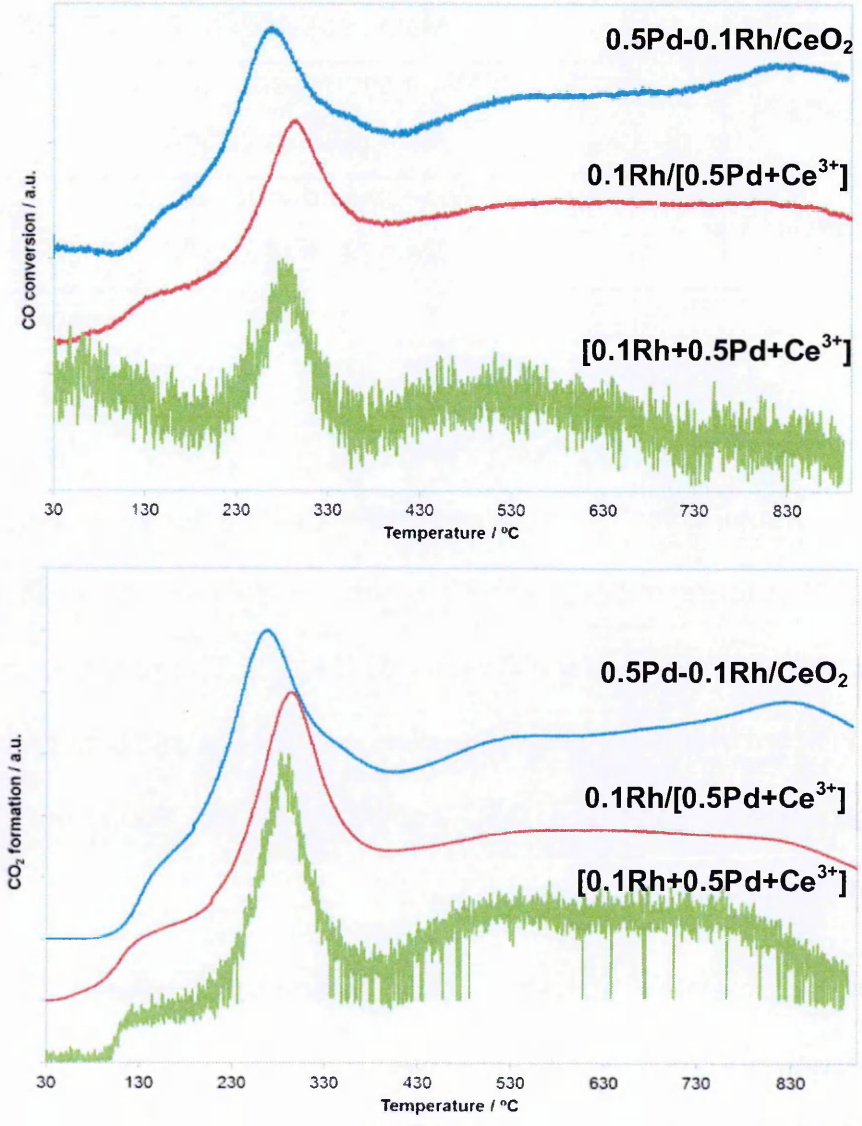

Figure 7-6: CO-TPR of Rh-Pd-CeO_2 catalysts prepared by co-precipitation with Ce^{3+} precursor ([(Rh+Pd+Ce^{3+}]), by wet impregnation on CeO_2 (Rh-Pd/CeO_2), and by a combination of both methods (Rh/[Pd+Ce^{3+}]). (From top to bottom) CO consumption and CO_2 formation during CO-TPR. The samples were previously pre-treated under 50 ml min^{-1} of He at 500 ºC. During the CO-TPR the flow consisted in 20 ml min^{-1} of 10%CO/He in 30 ml min^{-1} of He.

The reduction of surface CeO_2 was highly similar between the samples, however bulk CeO_2 reduction appeared at lower temperature for 0.1Rh/[0.5Pd+Ce] and [0.1Rh+0.5Pd+Ce] than for 0.1Rh-0.5Pd/CeO_2. This lower reduction temperature suggests better oxygen mobility in these samples.

Table 7-5: Comparison of the peak temperatures corresponding to the surface NM-O_x reduction of Rh-Pd-CeO_2 catalysts prepared by co-precipitation with Ce^{3+} precursor ([(Rh+Pd+Ce^{3+}]), by wet impregnation on CeO_2 (Rh-Pd/CeO_2), and by a combination of both methods (Rh/[Pd+Ce^{3+}]).

Sample	Surface NM-O_x reduction (based on CO consumption)
0.1Rh-0.5Pd/CeO_2	Shoulder at 155 ºC Main peak at 270 ºC
0.1Rh/[0.5Pd+Ce^{3+}]	Wide shoulder at 135 ºC Main peak at 295 ºC
[0.1Rh+0.5Pd+Ce^{3+}]	Wide shoulder at 120 ºC Main peak at 285 ºC

7.4.3. Oxygen Storage Capacity (OSC)

In the previous chapters, 0.1Rh-CeO_2 and 0.5Pd-CeO_2 catalysts were shown to behave differently in terms of OSC, with Rh a better noble metal to obtain a higher OSC and CeO_2-OSC efficiency (see *Chapter 6*) [21, 22]. The preparation method also had a significant impact on their capacities, with all the samples prepared by co-precipitation showing improved OSC compared to the equivalent catalysts prepared by impregnation.

In the case of the bimetallic catalysts, not only interactions between the NM and the Ce are present, but also interactions between the two NM, which based on the characterisation performed, seem to be different depending on the preparation method. Thus, the impact of these interactions in the OSC is of great interest.

The OSC for the bimetallic 0.1Rh-0.5Pd-CeO_2 samples can be seen in Figure 7-7. The three bimetallic catalysts were also compared to [0.5Pd+Ce], 0.5Pd/CeO_2 and 0.1Rh/CeO_2.

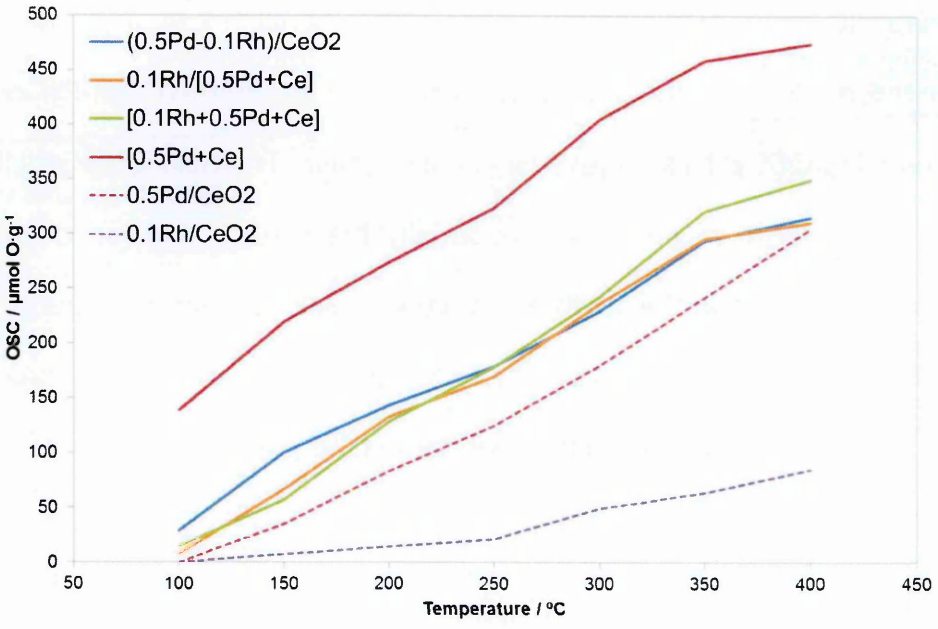

Figure 7-7: OSC profiles of Pd-CeO_2, Rh-CeO_2, and Pd-Rh-CeO_2 samples prepared by co-precipitation with Ce^{3+} precursor ([(NM+Ce^{3+}]), by wet impregnation on CeO_2 (NM/CeO_2), and by a combination of both methods (Rh/[Pd+Ce^{3+}]).The OSC measurement was performed alternating switches between O_2 (10 ml min^{-1} of 5 %O_2/He) and CO (10 ml min^{-1} of 10 %CO/He) using He as a carrier gas (90 ml min^{-1}) at steady state temperatures. OSC instrument average standard error = ± 7.9 µmol O g^{-1}.

No significant differences were found between the profiles of the bimetallic catalysts, with all of them overlapping at slightly higher values than those found for 0.5Pd/CeO_2.

The results obtained for the impregnated 0.1Rh-0.5Pd/CeO_2 catalyst were expected to be higher than 0.5Pd/CeO_2, as the addition of Rh will increase the amount of promoted surface ceria atoms. However, the 0.1Rh/[0.5Pd+Ce] sample was expected to appear at similar or higher values to those of [0.5Pd+Ce] (as the same material was used to prepared the bimetallic catalyst), but it showed a significantly lower performance. As mentioned previously, this could be due to Pd being segregated to the surface during the impregnation of Rh, decreasing in this

way the Pd-Ce contact, and/or to a deeper Ce-decoration of the Pd particles due to the sintering suffered during the extra calcination step. Lastly, [0.1Rh+0.5Pd+Ce] catalyst was expected to have a higher or at least similar oxygen capacity as [0.5Pd+Ce] as in addition of containing more noble metal, the co-precipitation method has previously been seen to improve NM-Ce contact (thus, promoting OSC). This however was not the case. The results agree with the previous characterisation performed, especially the results obtained during H_2-TPR, where it was shown that all three catalysts consumed similar amounts of H_2 during NM-Ce reduction, concluding that the combination of NM and promoted ceria reduction was similar overall between these catalysts.

7.5. Light-off performance

Due to the similar behaviour of these samples shown during OSC experiments, and the different surface area compositions that they contain, only cold-start light-off conditions were used to evaluate their catalytic activity.

7.5.1. Cold-start conditions

During this work it has been shown that the light-off under continuous lambda at cold-start conditions are highly dependent on the number of active sites on the surface [23, 24]. Thus, this test was ideal to analyse the bimetallic catalysts, as they all contained very different surface compositions. The results for CO, NO_x and HC conversion can be found in Figure 7-8.

The three profiles followed the same trends, where 0.1Rh-0.5Pd/CeO_2 was the sample with the lowest light-off temperature, followed by 0.1Rh/[0.5Pd+Ce] and by

[0.1Rh+0.5Pd+Ce]. These results agreed with the metal surface area characterisation performed by CO chemisorption where it was seen that the co-impregnated material (0.1Rh-0.5Pd/CeO_2) contained the most surface NM, followed by 0.1Rh/[0.5Pd+Ce] and by [0.1Rh+0.5Pd+Ce], even if these differences were small. Based on this, it seems that the total noble metal content affects the light-off temperature to a larger extent than the surface composition in terms of surface Pd:Rh ratio.

Table 7-6 summarises and compares the T50 for CO and the T30 for NO_x of the bimetallic and the monometallic catalysts. It can be seen that in most cases all bimetallic catalysts showed a lower light-off temperature than the monometallic catalysts, most likely due to the overall higher NM content [23, 24].

Table 7-6: Necessary temperature to achieve 50% conversion of CO and NO_x and to achieve 30% conversion of HC during a light-off test under constant lambda at 0.95 for Rh-Pd-CeO_2 catalysts prepared by co-precipitation with Ce^{3+} precursor ([(Rh+Pd+Ce^{3+}]), by wet impregnation on CeO_2 (Rh-Pd/CeO_2), and by a combination of both methods (Rh/[Pd+Ce^{3+}]). Light-off instrument average standard error = ± 2 °C.

Samples	CO T50 / °C	NO_x T50 / °C	HC T30 / °C
0.1Rh/CeO_2	243	236	284
[0.1Rh+Ce]	287	369	> 400
0.5Pd/CeO_2	242	257	284
[0.5Pd+Ce]	228	252	285
0.5Pd-0.1Rh/CeO_2	210	225	270
0.1Rh/[0.5Pd+Ce]	221	232	281
[0.1Rh+0.5Pd+Ce]	227	240	281

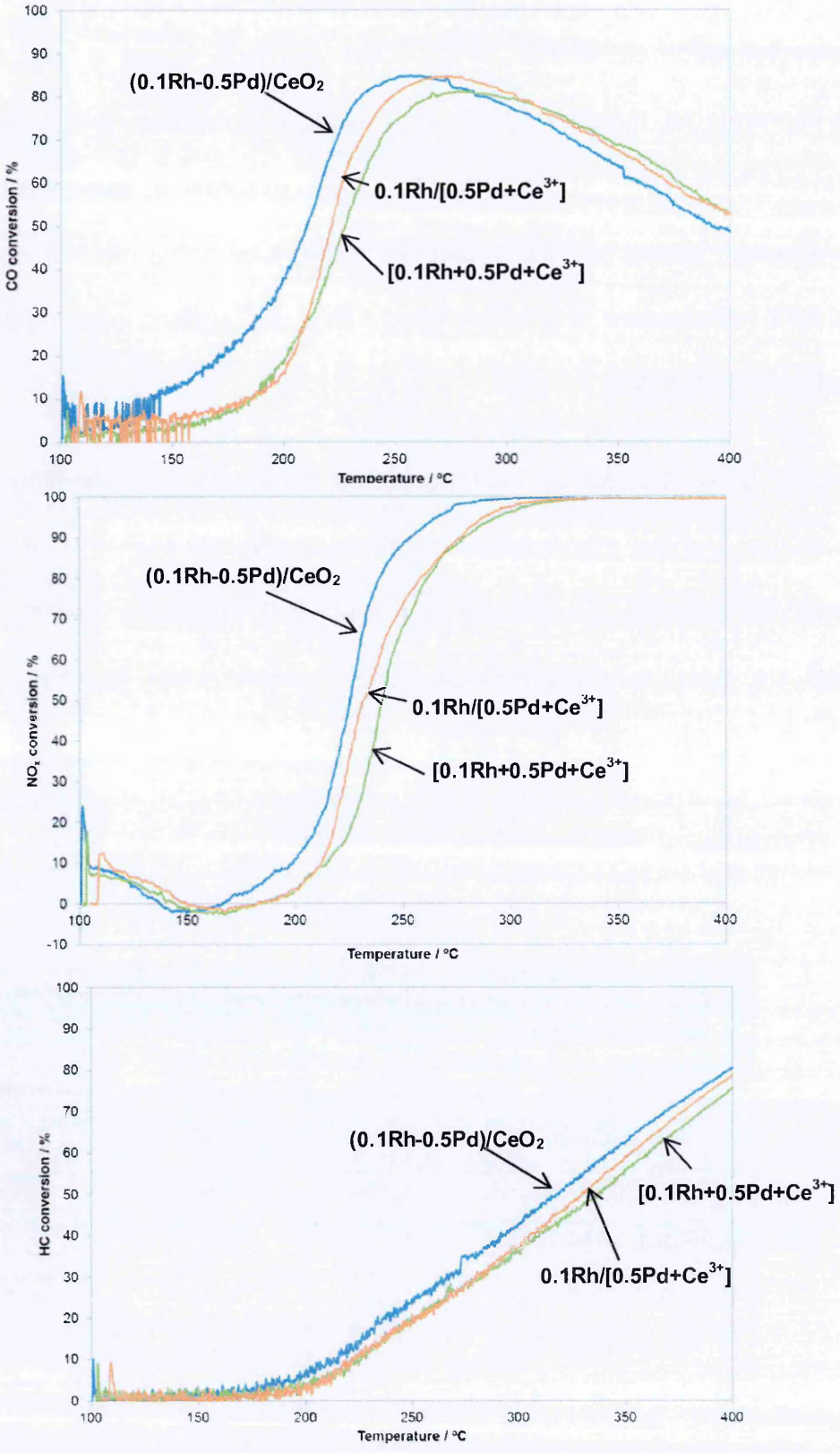

Figure 7-8: CO, NO_x and HC light-off performance under constant lambda at 0.95 of Rh-Pd-CeO_2 catalysts prepared by co-precipitation with Ce^{3+} precursor ([(Rh+Pd+Ce^{3+}]), by wet impregnation on CeO_2 (Rh-Pd/CeO_2), and by a combination of both methods (Rh/[Pd+Ce^{3+}]).The sample taken was 0.4 g (0.2 g sample + 0.2 g cordierite) and the gas flow rate 2 L min^{-1}. The catalyst was heated using a ramp rate of 10 °C min^{-1} from 100 to 400 °C.

7.6. Summary

Different preparation methods were evaluated as possible tools to modify the way that Pd and Rh interact on CeO_2 catalysts.

It was seen that when Pd and Rh are co-impregnated on a CeO_2 support, a catalyst with higher metallic surface area is obtained. However, Pd is believed to be reside on top of Rh particles when exposed to high temperature under oxidising conditions (i.e. the calcination process used here), decreasing the Rh surface area [1, 8].

Another preparation evaluated consisted of the impregnation of Rh on [0.5Pd+Ce] which was previously prepared by co-precipitation. The idea behind this was to stop Pd and Rh from interacting and to increase the Rh surface area. However, there are indications of some Pd segregating during the impregnation process, which could have interacted with some of the Rh particles [3]. In addition, this possible Pd segregation would have decreased the improved Pd-Ce contact achieved with the co-precipitation method to prepare the [0.5Pd+Ce] sample. The characterisation of this sample showed that a higher Rh surface content was in fact achieved, but at the expense of Pd surface area, as deeper ceria decoration was found on the Pd particles. The reason for the change in ceria-decoration is unknown, but since this material is exposed to a second calcination at 650 ºC (the first one during the synthesis of [0.5Pd+Ce] and a second one after the impregnation of Rh) physical changes were expected.

The last preparation was based on the co-precipitation of all the metals simultaneously ([0.1Rh+0.5Pd+Ce]). The aim of this preparation was to create an intimate contact between all the metals, especially between each of the noble metals with the ceria to further promote a larger number of ceria atoms and improve the OSC. However, although a larger number of Ce atoms appear to have

been promoted (based on H_2-TPR experiments), the OSC was not better than either of the other two bimetallic samples. This behaviour is suspected to be related to a lower number of surface sites [22] and/or a possible strong Pd-Rh interaction during the preparation, which could have prevented them from interacting with ceria to the same extent as on the monometallic catalysts prepared by co-precipitation. In terms of available surface sites, this catalyst contained the least metal surface content, due to greater ceria encapsulation.

Regarding OSC, all the catalysts appeared to have similar capacities, which agreed with the overall H_2 consumption associated to NM-Ce reduction during H_2-TPR, since the consumed H_2 was similar between all the three samples.

To conclude, different surface areas and compositions were obtained depending on the preparation method used. The catalysts with the highest metal content was 0.1Rh-0.5Pd/CeO_2 followed by 0.1Rh/[0.5Pd+Ce] and by [0.1Rh+0.5Pd+Ce]. The catalyst that contained the most surface Rh was 0.1Rh/[0.5Pd+Ce] and the least 0.1Rh-0.5Pd/CeO_2 (due to Pd covering Rh particles). The catalyst with the highest Pd content was 0.1Rh-0.5Pd/CeO_2 and the one containing the least was [0.1Rh+0.5Pd+Ce].

Overall, besides the different surface compositions, all the catalysts presented similar OSC, which in agreement with H_2-TPR results suggests that the improved NM-Ce contact during the co-precipitation is counteracted by the poorer availability of surface active sites [22]. In terms of light-off temperature, the profile was seen to be directly linked with the total amount of NM surface content [23, 24], independent of its composition. Thus, the different preparations of bimetallic 0.1Rh-0.5Pd-CeO_2 catalysts did not lead to an improvement in terms of OSC or light-off temperature compared to the reference catalyst prepared by co-impregnation, showing similar behaviours between them. This finding is in

contrast to what was seen for monometallic catalysts prepared by co-precipitation with Ce^{3+} precursor, which showed an improved OSC compared to the equivalent catalysts prepared by impregnation.

References Chapter 7

[1] H. S. Gandhi, G. W. Graham and R. W. McCabe, Journal of Catalysis, (2003) 433-442.

[2] C.-H. Wu and R. H. Hammerle, Industrial And Engineering Chemistry, Product Research And Development, 22 (1983) 559-565.

[3] S. Harjanto, Y. Cao, A. Shibayama, I. Naitoh, T. Nanami, K. Kasahara, Y. Okumura, K. Liu and T. Fujita, Materials Transactions, 47 (2006) 129-135.

[4] F. Zereini and F. Alt (Editors), *Palladium Emissions in the Environment: Analytical Methods, Environmental Assessment and Health Effects*, Springer, 2006,

[5] International Centre for Diffraction Data (ICDD), *PDF-4, COD (REV30738 2011.11.2)*, 2012.

[6] A. V. Naumkin, A. Kraut-Vass, S. W. Gaarenstroom and C. J. Powell, *NIST X-ray Photoelectron Spectroscopy Database*, 2000.

[7] A. Gayen, K. R. Priolkar, P. R. Sarode, V. Jayaram, M. S. Hegde, G. N. Subbanna and S. Emura, Chemistry of Materials, 16 (2004) 2317-2328.

[8] M. Taillades-Jacquin, D. J. Jones, J. Rozière and E. Rodríguez-Castellón, Applied Catalysis A: General, 340 (2008) 250-256.

[9] A. I. Boronin, E. M. Slavinskaya, I. G. Danilova, R. V. Gulyaev, Y. I. Amosov, P. A. Kuznetsov, I. A. Polukhina, S. V. Koscheev, V. I. Zaikovskii and A. S. Noskov, Catalysis Today, 144 (2009) 201-211.

[10] A. L. Guimarães, L. C. Dieguez and M. Schmal, Anais da Academia Brasileira de Ciências, 76 (2004) 825-832.

[11] M. Cargnello, V. V. T. Doan-Nguyen, T. R. Gordon, R. E. Diaz, E. A. Stach, R. J. Gorte, P. Fornasiero and C. B. Murray, Science, 341 (2013) 771-773.

[12] P. Canton, G. Fagherazzi, M. Battagliarin, F. Menegazzo, F. Pinna and N. Pernicone, Langmuir, 18 (2002) 6530-6535.

[13] R. M. Lambert and G. Pacchioni, *Chemisorption and Reactivity on Supported Clusters and Thin Films: Towards an Understanding of Microscopic Processes in Catalysis*, Kluwer Academic Publishers, 1997.

[14] H. F. J. V. t. Blik, J. B. A. D. V. Zon, D. C. Koningsberger and R. Prins, Journal of Molecular Catalysis, 25 (1984) 379-396.

[15] J. Freel, Journal of Catalysis, 25 (1972) 149-160.

[16] Y. Zhang, J. Zhou, Z. Wang, J. Liu and K. Cen, International Journal of Hydrogen Energy, 33 (2008) 2211-2217.

[17] A. Trovarelli, E. Aneggi, M. Boaro, C. d. Leitenburg and G. Dolcetti, Journal of Alloys and Compounds, 408-412 (2006) 1096-1102.

[18] C. Larese, M. L. Granados, F. C. Galisteo, R. Mariscal and J. L. G. Fierro, Applied Catalysis B: Environmental, 62 (2006) 132-143.

[19] M. Kurnatowska, L. Kepinski and W. Mista, Applied Catalysis B: Environmental, 117–118 (2012) 135-147.

[20] C. Hardacre, T. Rayment and R. M. Lambert, Journal of Catalysis, 158 (1996) 102-108.

[21] C. Descorme, S. Bedrane and D. Duprez, Catalysis Today, 75 (2002) 401-405.

[22] C. Descorme, R. Taha, N. Mouaddib-Moral and D. Duprez, Applied Catalysis A: General, 223 (2002) 287-299.

[23] I. Heo, D. Y. Yoon, B. K. Cho, I.-S. Nam, J. W. Choung and S. Yoo, Applied Catalysis B: Environmental, 121–122 (2012) 75-87.

[24] G. Wang, M. Meng, Y. Zha and T. Ding, Fuel, 89 (2010) 2244-2251.

8. Conclusions

Contents

8.1. Effect of Ce-precursor

The effect of the Ce-precursor used in the co-precipitation was evaluated; the Ce-precursor was found to have a great impact on the structure of the final product. The co-precipitation of Pd^{2+} and Ce^{3+} led to a catalyst with similar Pd surface area to the material prepared by impregnation but with a significantly better Pd-Ce interaction, which is believed to be due to the partial ceria decoration of the Pd particles [1, 2]. The higher number of Pd and Ce atoms in contact led to an improved OSC and CO oxidation rate.

The co-precipitation of Pd^{2+} and Ce^{4+} produced a catalyst with lower specific surface area and lower Pd content. The loss of Pd is believed to occur as a consequence of $Pd(OH)_2$ leaching during the washes of the precipitant during the preparation [3-5]. However, it was noticed that the Pd surface area was significantly lower than for the reference material and that this decrease could not be entirely related to the overall lower Pd content. Characterisation of this sample indicated that the loss of Pd surface area could also be related to an increase of ceria encapsulation of the Pd particles (based on CO chemisorption, EtOH-TPSR, XPS and TPR). This is suspected to occur as a result of the formation of large particles due to particle agglomeration during the preparation, which could have trapped the Pd particles leading to deeper encapsulation by the ceria. High agglomeration could have occurred as a consequence of a higher supersaturation during the preparation of this sample [6].

8.2. Effect of noble metal

0.5Pt-CeO_2 and 0.5Rh-CeO_2 catalysts were also studied. The co-precipitation of these NM with Ce^{3+} also led to products with an improved NM-Ce interaction.

However, the choice of NM had an impact on the final structure of the catalyst. The co-precipitated Pd catalyst ([0.5Pd+Ce^{3+}]) was found to have a very similar amount of surface Pd to the impregnated 0.5Pd/CeO_2 catalyst; in contrast, the co-precipitated Pt and Rh catalysts ([0.5Pt+Ce^{3+}] and [0.5Rh+Ce^{3+}]) contained a lower content of surface noble metal compared to their reference catalysts prepared by impregnation (0.5Pt/CeO_2 and 0.5Rh/CeO_2). The co-precipitation of [0.5Pt+Ce^{3+}] led to a product with Pt particles deeply encapsulated by ceria, and the co-precipitation of [0.5Rh+Ce^{3+}] to a product with larger Rh particles than the reference sample, partially decorated with ceria.

It could be seen that in all co-precipitated samples, better NM-Ce contact (higher number Ce atoms promoted by the NM) improved the NM-Ce reduction during H_2-TPR experiments as a consequence of a higher H_2 spillover. In addition, due to a larger number of ions being in contact, the OSC improved as a consequence of a better oxygen mobility [1]. This led to a small improvement in the pollutants conversion under perturbed light-off conditions; however, the improvement achieved was unexpectedly low, compared to the level of OSC improvement. This suggests that the conversion was not only controlled by the total oxygen storage capacity of the material, but also by its kinetics (i.e. how fast the oxygen can be accessed) [7-9].

In terms of OSC for the co-precipitated samples, Pd was the noble metal that led to a greater improvement at low temperature (< 300 ºC), whilst Rh was significantly better in the high temperature region (> 300 ºC) compared to their impregnated versions. The improvement obtained for the co-precipitated [0.5Pt+Ce^{3+}] sample compared to the impregnated 0.5Pt/CeO_2 catalyst was lower when compared to the improvement achieved for Pd and Rh sets (At 400 ºC, the OSC for the co-precipitated sample compared to the impregnated sample

increased by 170 μmol O g^{-1} for Pd, 34 μmol O g^{-1} for Pt, and 282 μmol O g^{-1} for Rh).

On the other hand, the performances of the light-off temperature and low temperature OSC (< 300 ºC) were seen to be closely linked to the amount of active surface metal [10-12]. Because of this, there was no light-off improvement for [0.5Pt+Ce^{3+}] and [0.5Rh+Ce^{3+}] samples (i.e. CO-T50 at 307 ºC for 0.5Pt/CeO_2 and 332 ºC for [0.5Pt+Ce^{3+}], and at 217 ºC for 0.5Rh/CeO_2 and at 243 ºC for [0.5Rh+Ce^{3+}]), as they contained a significantly lower surface area of NM compared to their reference catalysts prepared by impregnation. The [0.5Pd+Ce^{3+}] sample was the only catalyst that showed similar or slightly lower light-off temperature than the impregnated equivalent sample 0.5Pd/CeO_2 (i.e. CO-T50 at 242 ºC for 0.5Pd/CeO_2 and 228 ºC for [0.5Pd+Ce^{3+}]). This occurred due to both catalysts containing similar amounts of Pd surface areas.

8.3. Effect of Pd loading

The effects of the NM loading were also evaluated focusing on the co-precipitation of Pd^{2+} and Ce^{3+} ([Pd+Ce^{3+}]) preparations. It was seen that the co-precipitation technique was advantageous over the impregnation method only at loadings lower than 0.75 wt% Pd. As explained in *Chapter 4*, the reason for this is that when impregnating low amounts of Pd on CeO_2, the Pd particles finish extremely dispersed, which makes them interact too strongly with the support, leaving them less reactive [2, 13, 14]. At Pd loadings < 0.75 wt% there seemed to be a higher contribution from the Pd-Ce interface sites[1] when the samples were prepared with the co-precipitation method; this changed to be the opposite at Pd loadings

[1] Based on the comparison of Pd surface area obtained from EtOH-TPSR and CO chemisorption experiments.

> 0.75 wt%, where there was a higher contribution of the interface sites for the impregnated samples.

In addition, based on CO chemisorption results, the Pd surface area appeared to be similar for the catalysts produced by both methods at low Pd loadings, whilst it was noticeably lower for the co-precipitated materials at loadings > 0.75 wt% Pd compared to the equivalent samples prepared by impregnation. All these results suggest that at low Pd loadings both methods lead to similar Pd particle sizes, but the co-precipitation leads to a higher number of Pd and Ce atoms in contact (as suggested by XPS Ce/Pd atomic ratios and H_2-TPR), adding more highly active Pd-Ce interface sites where the pollutants can be adsorbed [2]. Instead, at higher Pd loadings, the characterisation performed suggested that bigger Pd particles were obtained with the co-precipitation method (decrease in Pd dispersion), which as a consequence would have a detrimental impact on the number of highly active interface sites.

The differences found depending on the Pd loading cannot be easily justified. However, the different OSC trends observed for the catalysts prepared by impregnation and by co-precipitation, where there was a gradual increase of the OSC with the Pd loading for the impregnated materials, but no significant changes for the co-precipitated samples, suggests that the Pd loading has a bigger impact in the impregnation method.

Based on this study, the co-precipitation method seems a better preparation technique to prepare Pd-CeO_2 catalysts with Pd loadings lower than 0.75 wt%, whilst the impregnation method should be chosen for the preparation of higher Pd loadings.

8.4. Co-precipitation of Pd, Ce and Zr

The impact of Pd:Ce ratio was also noticeable when evaluating the Pd-CeZr samples. Here only two different palladium loadings were evaluated, 0.25 and 0.5 wt% Pd. In this case, only the sample prepared by co-precipitation containing 0.25 wt% Pd ([0.25Pd+Ce+Zr]) had a higher OSC than the sample with similar Pd loading prepared by impregnation. The [0.5Pd+Ce+Zr] sample had a lower oxygen storage capacity than the 0.5Pd/CeZr catalyst. One of the differences found between the two sets of samples was the different surface metal adsorption. Similar Pd surface areas were found between the methods CO chemisorption and EtOH-TPSR methods for the [0.25Pd+Ce+Zr] sample; however, the Pd surface content obtained for [0.5Pd+Ce+Zr] was higher during the EtOH-TPSR analysis compared to the value obtained from the CO chemisorption. This suggests that less CO was adsorbing per Pd site on the [0.5Pd+Ce+Zr] sample, which could be due to a change in the CO:Pd adsorption stoichiometry. This could not be confirmed.

The lower CO adsorption seems to be responsible for the higher light-off temperature found for the [0.5Pd+Ce+Zr] catalyst compared to 0.5Pd/CeZr during the activity tests under cold-start and perturbed conditions (i.e. CO-T50 under cold start test of 222 ºC for [0.5Pd+Ce+Zr] and of 212 ºC for 0.5Pd/CeZr; CO-T50 under perturbed conditions of 244 ºC for [0.5Pd+Ce+Zr] and of 225 ºC for 0.5Pd/CeZr). On the other hand, similar light-off temperatures were found for the 0.25Pd-CeZr samples prepared by co-precipitation and impregnation (i.e. CO-T50 under cold start test of 243 ºC for [0.25Pd+Ce+Zr] and of 239 ºC for 0.25Pd/CeZr; CO-T50 under perturbed conditions of 248 ºC for [0.25Pd+Ce+Zr] and of 249 ºC for 0.25Pd/CeZr), most certainly due to the similar Pd surface areas found for these materials (as evidenced by CO chemisorption and EtOH-TPSR).

8.5. Impact of the preparation method on bimetallic Rh-Pd-CeO_2 catalysts

The final part of this work was based on the preparation of bimetallic catalysts, based on 0.1Rh-0.5Pd-CeO_2, by different preparation routes to promote or avoid Pd-Rh interaction, as well as the interaction with the CeO_2. In this case, three catalysts were prepared based on the co-impregnation of Rh and Pd on CeO_2 (0.1Rh-0.5Pd/CeO_2), on the impregnation of Rh on a previously co-precipitated [0.5Pd+Ce^{3+}] (0.1Rh/[0.5Pd+Ce]), and on the co-precipitation of Rh, Pd and Ce ([0.1Rh+0.5Pd+Ce]). For the 0.1Rh-0.5Pd/CeO_2 and [0.1Rh+0.5Pd+Ce] samples the aim was to promote Pd-Rh interaction, and for 0.1Rh/[0.5Pd+Ce] to avoid it. The different preparations led to products with different metal surface area compositions, with the sample prepared by impregnation containing the most NM on the surface (1.7 m^2 g^{-1} in 0.1Rh-0.5Pd/CeO_2, 1.4 m^2 g^{-1} in 0.1Rh/[0.5Pd+Ce], and 1.3 m^2 g^{-1} in [0.1Rh+0.5Pd+Ce], based on CO chemisorption analyses). In terms of metal surface composition they also appeared to be different, with 0.1Rh/[0.5Pd+Ce] sample containing the most Rh on the surface and 0.1Rh-0.5Pd/CeO_2 the least and 0.1Rh-0.5Pd/CeO_2 containing the most surface Pd and [0.1Rh+0.5Pd+Ce] the least. However, the characterisation performed in these catalysts showed that the combination of NM and promoted Ce reduction led to similar H_2 consumption during H_2-TPR. This indicated that besides the lower NM surface areas achieved with the co-precipitation method compared to the impregnation synthesis, a larger number of NM and Ce atoms were being promoted by the NM in the co-precipitated samples. The results obtained from the OSC tests agreed with the H_2-TPR experiments, as they all showed similar OSC capacities. Thus, it is suggested that the improved NM-Ce contact created during the co-precipitation was counteracted by the poorer availability of surface active sites compared to the sample prepared by impregnation [15].

Thus, for these preparations the co-precipitation method did not further improve the NM-Ce promotion. In the case of [0.1Rh+0.5Pd+Ce] this is suspected to be related to a lower number of surface sites [15] and/or a possible stronger interaction occurring between Rh and Pd, than with the Ce; and for 0.1Rh/[0.5Pd+Ce], the loss of the improved Pd-Ce contact of [0.5Pd+Ce] is suspected to be due to Pd segregation during the impregnation of Rh [16]. In terms of light-off performance, the 0.1Rh-0.5Pd/CeO_2 showed the lowest light-off temperature due to containing a higher metal surface area [12, 17].

8.6. Summary

In most cases, the co-precipitation improved the promotion of surface ceria, most likely due to the creation of a partial ceria decoration on the NM particles. As a consequence, the improved NM-Ce promotion has increased the oxygen storage capacity and the pollutants conversions compared to the equivalent impregnated versions due to the increase of NM-Ce interface sites which are highly active. However, in most cases this method has also led to materials with a lower metal surface content which could have a detrimental effect in their light-off temperature.

The Pd:Ce ratio had a significant impact on the activity of these catalysts, and it was only at low Pd loadings that the co-precipitation method presented advantages over the impregnation preparation. A similar behaviour for other noble metals would also be expected. This study suggests that an optimal loading exist to obtain the highest efficiency and performance with samples prepared by co-precipitation with a Ce^{3+} precursor.

In this work, only the fresh catalysts were evaluated. However, TWC are usually exposed to high temperatures (~1000 ºC), thus the evaluation of these catalysts

after high temperature ageing is suggested. In addition, this work has also shown that the type of cerium precursor has a significant impact in the final structure of the catalyst, thus other parameters (such as the noble metal precursor, temperature of precipitation or precipitant addition) should be evaluated.

Moreover, the EtOH-TPSR technique created during this work will be further developed. In-situ infrared spectroscopy will be used to monitor the EtOH adsorption on noble metals supported on different substrates and to evaluate its changes with the temperature to understand more about the reactivity of different metallic sites.

References Conclusions

[1] R. Rao and B. G. Mishra, Bulletin of the Catalysis Society of India, 2 (2003) 122-134.

[2] M. Cargnello, V. V. T. Doan-Nguyen, T. R. Gordon, R. E. Diaz, E. A. Stach, R. J. Gorte, P. Fornasiero and C. B. Murray, Science, 341 (2013) 771-773.

[3] J. M. Soriano-Rodríguez, V. E. Badillo-Almaraz, C. Alliot, F. Monroy-Guzmán and P. Vitorge, Journal of Radioanalytical and Nuclear Chemistry, 288 (2011) 645-652.

[4] ChemicalBook, *Chemical Book - Palladium hydroxide*, 2010, http://www.chemicalbook.com/ChemicalProductProperty_EN_CB3267682.htm [17-04-2014].

[5] T. Carlsson and U. Vuorinen, *The reliability of solubility data: Results from a limited literature survey focusing on Ni, Pd and Np*, Technical Research Centre of Finland, 1998.

[6] A. G. Jones, *Crystallization Process Systems*, Butterworth-Heinemann, 2002.

[7] M. Zhao, M. Shen and J. Wang, Journal of Catalysis, 248 (2007) 258-267.

[8] P. Kumar, T. Gu, K. Grigoriadis, M. Franchek and V. Balakotaiah, Chemical Engineering Science, 111 (2014) 180-190.

[9] S. Bedrane, C. Descorme and D. Duprez, Catalysis Today, 73 (2002) 233-238.

[10] A. Trovarelli, E. Aneggi, M. Boaro, C. d. Leitenburg and G. Dolcetti, Journal of Alloys and Compounds, 408-412 (2006) 1096-1102.

[11] C. Descorme, S. Bedrane and D. Duprez, Catalysis Today, 75 (2002) 401-405.

[12] G. Wang, M. Meng, Y. Zha and T. Ding, Fuel, 89 (2010) 2244-2251.

[13] A. Satsuma, R. Sato, K. Osaki and K. Shimizu, Catalysis Today, 185 (2012) 61-65.

[14] R. d. S. Monteiro, F. B. Noronha, L. C. Dieguez and M. Schmal, Applied Catalysis A: General, 131 (1995) 89-106.

[15] C. Descorme, R. Taha, N. Mouaddib-Moral and D. Duprez, Applied Catalysis A: General, 223 (2002) 287-299.

[16] S. Harjanto, Y. Cao, A. Shibayama, I. Naitoh, T. Nanami, K. Kasahara, Y. Okumura, K. Liu and T. Fujita, Materials Transactions, 47 (2006) 129-135.

[17] I. Heo, D. Y. Yoon, B. K. Cho, I.-S. Nam, J. W. Choung and S. Yoo, Applied Catalysis B: Environmental, 121–122 (2012) 75-87.

Appendix

Contents

A1. BET-Specific Surface Area

The specific surface area was calculated by the BET method, based on N_2-physisorption at sub-ambient temperature (at the boiling temperature of liquid nitrogen, 77 K).

Stephen Brunauer, Paul Hugh Emmett, and Edward Teller (BET) developed this theory using Langmuir's theory as a base. Langmuir's theory is based on monolayer molecular adsorption, while the BET theory is based on a multilayer gas adsorption. For the BET theory the following hypotheses need to be assumed [1, 2]:

- The adsorbent surface is homogeneous.
- There are no lateral interactions between the adsorbant molecules.
- Gas molecules physically adsorb infinitely as layers on a solid.
- At equilibrium the rate of adsorption is equal to the rate of desorption.

The resulting equation from this theory can be found below (A1-1) [1, 2]. This equation can be represented as a linear regression (y = c + mx):

$$\frac{1}{V\left[\frac{P}{P_0}-1\right]} = \frac{1}{V_m C} + \frac{C-1}{V_m C}\left(\frac{P}{P_0}\right) \qquad \text{(A1-1)}$$

$$y = c + m \cdot x$$

where
- V amount of gas adsorbed (volume units)
- V_m amount of gas adsorbed on the monolayer (volume units)
- P equilibrium pressure of adsorbates at the temperature of adsorption (pressure units)
- P_0 saturation pressure of adsorbates at the temperature of adsorption (pressure units)
- C BET constant

The BET constant is expressed as

$$C = \left(\frac{E_1 - E_L}{RT}\right) \qquad \text{(A1-2)}$$

where E_1 heat of adsorption for the first layer (J)

E_L heat of adsorption for the second and higher layers (J)

R gas constant (8.31 J mol^{-1} K^{-1})

T temperature (K)

By plotting $(1/V[P/P_0 - 1])$ versus (P/P_0) a straight line is obtained (Figure A1-1). This plot is known as a BET plot. The linear relationship is only maintained in the range of 0.5 < (P/P_0) < 0.35. Using the slope (m) and y-interception (c) values it is possible to calculate the monolayer adsorbed gas quantity (V_m) and the BET constant (C) using the equations below:

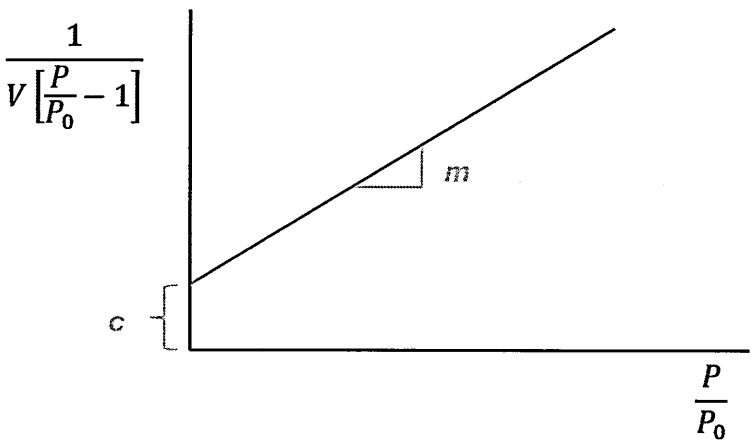

Figure A1-1: Example of BET plot.

$$m = \frac{C\text{-}1}{V_m C} \qquad \text{(A1-3)} \qquad\qquad c = \frac{1}{V_m C} \qquad \text{(A1-4)}$$

With this, is then possible to calculate the total surface area (S_{total}) and the specific surface area (SSA or S_{BET}) using the following equations:

$$S_{total} = \frac{V_m N_A s}{MV} \quad \text{(A1-5)} \qquad S_{BET} = \frac{S_{total}}{a} \quad \text{(A1-6)}$$

where

S_{total}	total surface area (m^2)
S_{BET}	specific surface area ($m^2\ g^{-1}$)
V_m	amount of gas adsorbed on the monolayer (m^3)
N_A	Avogadro's number (6.022×10^{23} molecule mol^{-1})
s	adsorption cross section of the adsorbing species (m^2 molecule)
MV	molar volume of adsorbate gas ($m^3\ mol^{-1}$)
a	mass of adsorbent (g)

The N_2 adsorption was performed at 77 K using an Autosorb-1 analyser from Quantachrome. Prior to the analysis the samples were outgassed at 350 °C to remove any moisture or unwanted adsorbed species that may have been present on the surface.

A2. Calculation of CeO_2-OSC efficiency

CeO_2 is not a material that uses its full oxygen capacity (not 100% efficient). The addition of dopants and/or noble metals usually promotes its efficiency [3-5].

To calculate the efficiency of the materials presented in this work, the next steps were followed:

1. Quantification of CeO_2 moles (exclusion of moles from noble metal):

Supposing that 0.0982 g of (0.5 wt% Pd)-CeO_2 were used, it is possible to calculate how much correspond to grams of Pd [6]:

$$0.0982\ \text{g sample} \cdot \frac{0.5\ \text{g Pd}}{100\ \text{g sample}} = 4.91\text{x}10^{-4}\ \text{g Pd}$$

It is supposed that all the Pd exists as PdO, thus the grams of Pd need to be expressed as grams of PdO (molar weight of Pd = 106.42 g mol^{-1}, and PdO = 122.42 g mol^{-1}) [6, 7]:

$$4.91\text{x}10^{-4}\ \text{g Pd} \cdot \frac{1\ \text{mol Pd}}{106.42\ \text{g Pd}} \cdot \frac{1\ \text{mol PdO}}{1\ \text{mol Pd}} \cdot \frac{122.42\ \text{g PdO}}{1\ \text{mol PdO}} = 5.65\text{x}10^{-4}\ \text{g PdO}$$

By extracting the grams corresponding to PdO from the total weight of the sample, it is possible to calculate the weight related to CeO_2:

$$0.0982\ g\ sample - 5.65x10^{-4}\ g\ PdO = 0.0976\ g\ CeO_2$$

The grams of CeO_2 are then transformed to moles (molar weight of CeO_2 = 172.12 g mol^{-1}) [6, 7]:

$$0.0976\ \text{g CeO}_2 \cdot \frac{1\ \text{mol CeO}_2}{172.12\ \text{g CeO}_2} = 5.67\text{x}10^{-4}\ \text{mol CeO}_2$$

2. Calculation of theoretical maximum OSC based on the reduction of CeO_2:

$$2CeO_2 \rightleftharpoons Ce_2O_3 + 1/2O_2$$

Based on the equation above, for each 2 moles of CeO_2, 0.5 moles of O_2 will be released (theoretically) [6, 8].

$$5.67x10^{-4}\ \text{mol}\ CeO_2 \cdot \frac{0.5\ \text{mol}\ O_2}{2\ \text{mol}\ CeO_2} = 1.42x10^{-4}\text{mol}\ O_2$$

And then in 1 mol of O_2 there are 2 moles of O. The units are also transformed to µmol at the end. This value corresponds to the total amount of oxygen that CeO_2 can use, theoretically.

$$1.42x10^{-4}\ \text{mol}\ O_2 \cdot \frac{2\ \text{mol}\ O}{1\ \text{mol}\ O_2} \cdot \frac{10^6 \mu\text{mol}}{1\ \text{mol}} = 283.85\ \mu\text{mol}\ O$$

3. Calculation of OSC from the noble metal, supposing 100% reduction:

$$PdO \rightleftharpoons Pd + 1/2O_2$$

In point 1, the amount of PdO was calculated, which corresponded to $5.65 \cdot 10^{-4}$ g PdO. The grams of PdO are transformed to moles (molar weight of PdO = 122.42 g mol^{-1}) [6, 7].

$$5.65x10^{-4}\ \text{g PdO} \cdot \frac{1\ \text{mol PdO}}{122.42\ \text{g PdO}} = 4.61x10^{-6}\ \text{mol PdO}$$

To reduce 1 mol of PdO, 0.5 moles of O_2 are needed.

$$4.61x10^{-6}\ \text{mol PdO} \cdot \frac{0.5\ \text{mol}\ O_2}{1\ \text{mol PdO}} = 2.31x10^{-6}\ \text{mol}\ O_2$$

The moles of O_2 are transformed to moles of O, and to µmol units.

$$2.31x10^{-6}\ \text{mol}\ O_2 \cdot \frac{2\ \text{mol}\ O}{1\ \text{mol}\ O_2} \cdot \frac{10^6 \mu\text{mol}}{1\ \text{mol}} = 4.61\ \mu\text{mols}\ O$$

4. Assuming complete reduction of PdO, the theoretical OSC contribution from the noble metal is extracted from each of the experimental OSC values (Experimental OSC – Theoretical OSC from NM). The value obtained should be the OSC contribution from the CeO_2:

Temperature / °C	Experimental OSC / µmol O	Theoretical OSC from PdO / µmol O	Experimental OSC from CeO_2 / µmol O
100	13.63	4.61	9.02
200	26.88		22.27
300	39.75		35.14
400	46.57		41.96

5. The experimental OSC values from CeO_2 are divided by the theoretical OSC value and multiplied by 100 to obtain the efficiency in percentage:

Temperature / °C	Experimental OSC from CeO_2 / µmol O	Theoretical OSC from CeO_2 / µmol O	CeO_2-OSC efficiency / %
100	9.02	283.85	3.2
200	22.27		7.8
300	35.14		12.4
400	41.96		14.8

A3. Steady-State Isotopic Transient Kinetics Analysis (SSITKA) - Example

SSITKA was used to study the kinetics of the CO oxidation reaction over the different catalysts. This technique enables the simultaneous quantification of the number of active catalytic sites on the catalyst and the activity of these catalytic sites under *in-situ* conditions.

This method is based on the monitoring of the reactant species in the reactor feed during a switch in which one of the reactants is switched to its isotopic labelled equivalent (i.e. ^{12}CO is switched to ^{13}CO). To maintain isothermal and isobaric reaction conditions, all the gas concentrations and flows need to remain undisturbed during the step change. As the gas reactants will be the same, the intermediates formed will not change, and this allows the steady-state kinetic behaviour of the surface of the catalyst to be studied [9].

A3.1. Obtaining reaction rate

0.0099 g of sample were placed in the middle of a quartz reactor held by quartz wool in each side. The reactor was then placed inside the furnace and connected to the gas lines and a mass spectrometer.

CO oxidation reactor was monitored at different temperatures: 30, 40, 50, 60, 70 and 80 ºC. The gas flows used were:

a) Part I: CO (^{12}C)

52.5 ml min^{-1} of 5% O_2/He

5.5 ml min^{-1} of 1%CO/5%Ar/He

b) Part II: CO (^{13}C)

52.5 ml min^{-1} of 5% O_2/He

5.5 ml min^{-1} of 1%CO/He

In order to calculate the reaction rate at each temperature, the catalyst was under conditions specified in Part I (unlabelled CO) for 30 s before switching to the conditions of Part II (labelled CO).

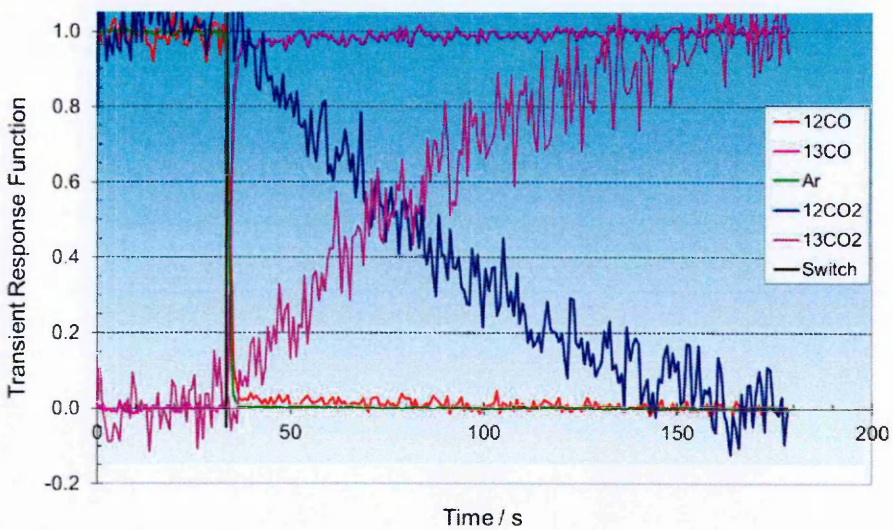

Figure A3-1: Evolution of gas concentrations during CO-SSITKA analysis.

The conversion of CO (^{13}C) to CO_2 (^{13}C) after 3 minutes was calculated. Previously, a blank reactor was used to measure the signal of unreacted CO (^{13}C) in order to be able to calculate this conversion:

$$\%\, CO\ conversion = 100 - \left(\left(\frac{CO\ measured - CO\ minimum}{CO\ blank - CO\ minimum}\right)100\right)$$

Where CO *measured*: CO mass spectrometer signal during the test

CO *minimum*: CO mass spectrometer signal when there is no CO in the gas feed.

CO *blank*: CO mass spectrometer signal during the test with a blank reactor.

Knowing the reactant flow (5.5 ml min^{-1} 1%CO/5%Ar/He = 0.055 ml min^{-1} CO) and the fraction of it that is reacting is possible to calculate the rate:

1. The flow is transformed to l s^{-1}.

$$\frac{0.055\ \text{ml CO}}{\text{min}} \cdot \frac{1\ \text{min}}{60\ s} \cdot \frac{1\ \text{l}}{1000\ \text{ml}} = 9.17\text{x}10^{-7}\ \text{l}\ s^{-1}$$

Then, knowing the CO conversion (here it is supposed 29% CO conversion), it is possible to calculate the litres of CO that are reacting [6].

$$\frac{9.17\text{x}10^{-7}\ \text{l CO fed}}{s} \cdot \frac{29\ \text{l CO reacting}}{100\ \text{l CO fed}} = 2.658\text{x}10^{-7}\ \text{l}\ s^{-1}$$

2. The volumetric flow is then converted to molar flow by using the ideal gas law [6, 10]:

$$PV = nRT \quad \rightarrow \quad \frac{n}{V} = \frac{P}{RT}$$

It is assumed ideal gas conditions, therefore

P = 100 kPa

T = 298 K

R = 8.314 l kPa $\underline{K}^{-1}$ mol^{-1}

$$\frac{n}{V} = \frac{100\ \text{kPa}}{(8.314\ \text{l kPa mol}^{-1}\ \text{K}^{-1})(298\ \text{K})} = 40.362\text{x}10^{-3}\ \text{mol l}^{-1}$$

The molar flow is then obtained using this conversion factor:

$$\frac{2.658\text{x}10^{-7}\ \text{l}}{s} \cdot \frac{40.362\text{x}10^{-3}\ \text{mol}}{1\ \text{l}} \cdot \frac{10^{6}\ \mu\text{mol}}{1\ \text{mol}} = 0.0107\ \mu\text{mol}\ s^{-1}$$

Volumetric flow Molar flow

3. Finally, the reaction rate is calculated by dividing the molar flow by the sample weight:

$$r = \frac{0.0107\ \mu mol\ s^{-1}}{0.0099\ g} = 1.0808\ \mu mol\ s^{-1}\ g^{-1}$$

Reaction rate

A3.2. Obtaining reaction orders

To define the reaction orders, the reaction rate is calculated at a fixed temperature under different gas conditions, where the concentration of one of the reactants is modified and the other one maintained constant [11]:

Table A3-1: Gas concentrations used to calculate reaction orders with respect to CO and O_2.

To calculate reaction order of [CO]		To calculate reaction order of [O_2]	
Concentration of A and B / mol l^{-1}	**Concentration of C / mol l^{-1}**	**Concentration of A and B / mol l^{-1}**	**Concentration of C / mol l^{-1}**
$2.25x10^{-6}$	$2.20x10^{-3}$	$2.14x10^{-5}$	$2.28x10^{-3}$
$1.12x10^{-5}$			$1.83x10^{-3}$
$2.25x10^{-5}$			$1.37x10^{-3}$
$4.51x10^{-5}$			$4.57x10^{-4}$

*A = 1%CO(^{12}C)/5%Ar/He; B= 1%CO(^{13}C)/He; C = 5%O_2/He

As explained in *Chapter 2*, if one of the reactants' concentrations is maintained constant, the reaction rate can be expressed as:

$$\ln(r) = \ln(k) + b\ln([B]) + a\ln([A])$$

$$y = c + m\ x$$

Therefore, from the graphical representation of ln(r) vs ln[A] is possible to calculate the reaction order, which corresponds to the slope of the regression line.

The example corresponds to the calculation of the reaction order with respect of [CO]:

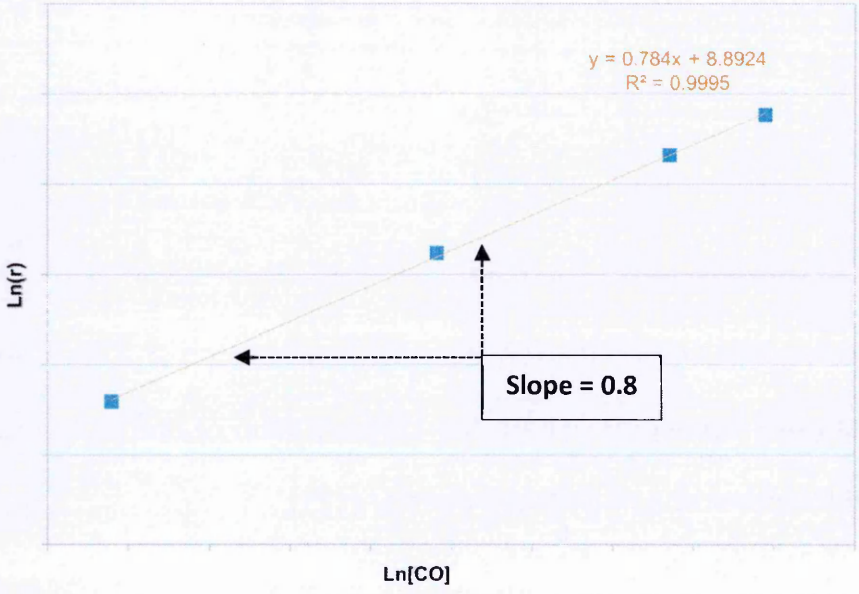

Figure A3-2: Regression line obtained from the ln[CO] and ln(*r*). Rate values (*r*) obtained from SSITKA experiments.

A3.3. Obtaining *k* and E_a from Arrhenius equation

Once the reaction orders are known, it is possible to calculate *k* from the graphical representation of the naperial version of the Arrhenius equation [11]:

$$\ln(k) = \ln(A) - \frac{E_a}{R}\frac{1}{T}$$

$$y = c + m\,x$$

Since the reaction rate had already been calculated at different temperatures, it is just a matter of calculating *k* at each of these temperatures.

Table A3-2: Parameters used for the representation of the regression line to calculate E_a.

[0.5Pd+Ce^{3+}]: $r = k$ [CO]				
T / K	Rate / μmol s^{-1} g^{-1}	k = r/[CO]	1/T	ln(k)
323	0.76	50559	3.10×10^{-3}	10.83
333	0.86	57120	3.00×10^{-3}	10.95
343	0.98	64905	2.92×10^{-3}	11.08
353	1.08	72118	2.83×10^{-3}	11.19

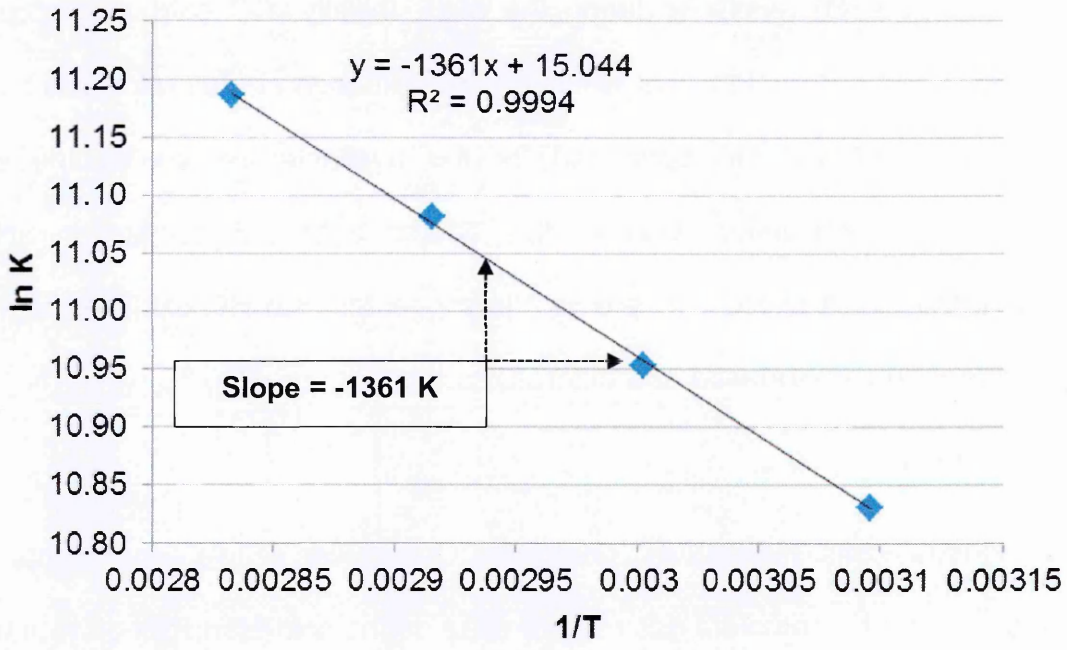

Figure A3-3: Regression line from the representation of 1/T vs Ln(k) to calculate the slope of the line to obtain E_a.

If the slope corresponds to $-E_a/R$ (and R is the ideal gas constant, 8.314 J K^{-1} mol^{-1}), is then possible to calculate E_a:

$$E_a = (1361\ \text{K})(8.314\ \text{J K}^{-1}\ \text{mol}^{-1}) = 11315\ \text{J mol}^{-1} = 11.3\ \text{KJ mol}^{-1}$$

A4. Explanation for the CO profile during light-off at λ = 0.95

As the light-off was performed under rich lambda (λ = 0.95) this means there was an excess of reducing species, therefore 100% conversion of CO and HC could not be achieved because there was not enough available oxygen for their oxidation (1.6% O_2 is needed to completely oxidise C_3H_6, C_3H_8, and CO, and there was only 0.95% O_2 available during the test). Initially, CO oxidation occurred (increase of CO conversion), but when the HC oxidation started later at a higher temperature, CO and HC competed for the available oxygen leading to a decreased CO conversion. Due to this decrease in CO conversion and a continuous increase of HC conversion it is suggested that HC oxidation is more favourable than CO oxidation at temperatures higher than ~280 °C when they are in competition.

To demonstrate this, Figure A4-1 shows the CO profiles of two experiments. For one experiment the complete gas mixture used during cold-start light-off was used (λ = 0.95), and for the other experiment the HC (C_3H_8 and C_3H_6) was removed (λ = 1.02). By removing HC, a lean lambda is obtained, which means there is an excess of oxidant species in the flow. As Figure A4-1 shows, under this lean lambda (λ = 1.02) the complete oxidation of CO is possible.

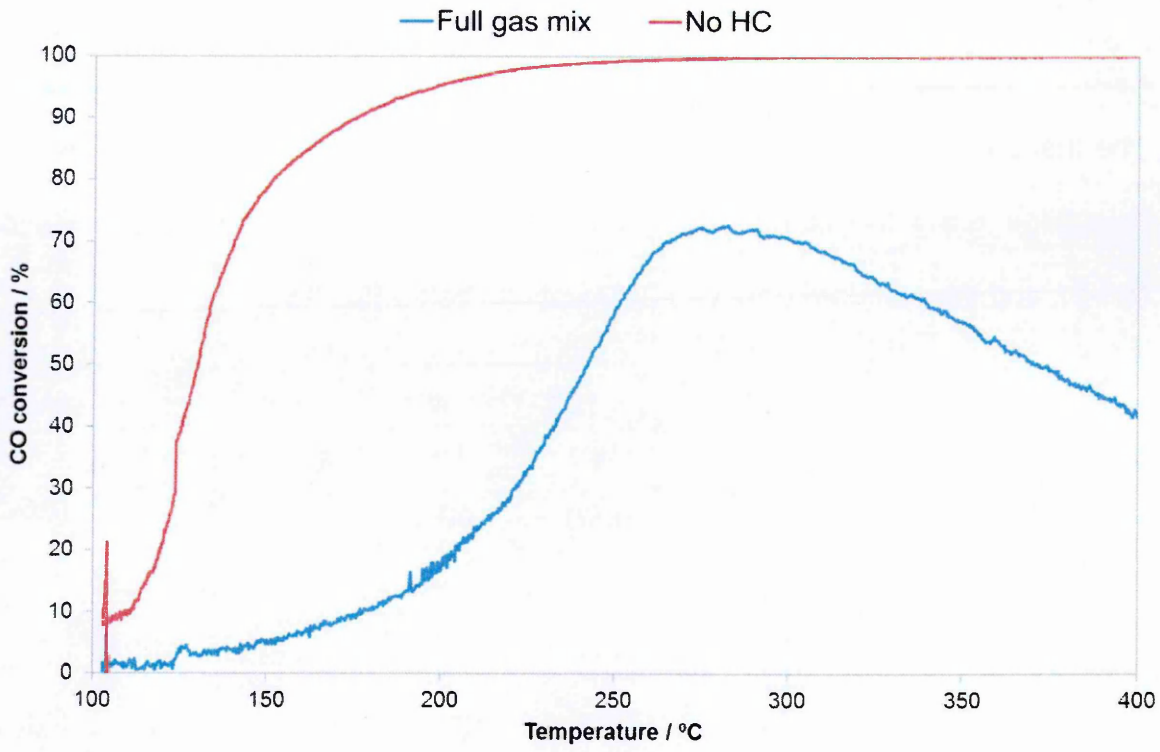

Figure A4-1: CO light-off performance under constant lambda at 0.95 (full gas mix) and constant lambda at 1.02 (no HC) of 0.5Pd/CeO_2 sample prepared by impregnation on CeO_2. The sample taken was 0.4 g (0.2 g sample + 0.2 g cordierite) and the gas flow rate 2 L min^{-1}. The catalyst was heated using a ramp rate of 10 °C min^{-1} from 100 to 400 °C.

A5. Standard instrument error calculation

The instrument standard error for most of the techniques used in this thesis was calculated using the standard deviation (A5-1), the relative standard deviation (A5-2), and the standard error (A5-3) equations below [12, 13]:

$$s = \sqrt{\frac{\sum_{i=1}^{N}(x_i - \bar{x})^2}{N-1}} \quad \text{(A5-1)}$$

$$RSD = \frac{s}{\bar{x}}\,100 \quad \text{(A5-2)}$$

$$SE_{\bar{x}} = \frac{s}{\sqrt{N}} \quad \text{(A5-3)}$$

Where

s	standard deviation
x_i	measured value
$\bar{x}$	average value
N	population
$SE_{\bar{x}}$	standard error
RSD	relative standard deviation

A5.1. XRD

The errors associated to XRD results were calculated automatically by computer software based on Rietveld[1] and Pawley[2] analysis. These measurements were performed by Dr Hoi Jobson (jobsoh@matthey.com) and Dr Edward Bilbe (BilbeE01@matthey.com).

[1] Powder diffraction pattern fitting using full structural models including atomic positions.
[2] Powder diffraction pattern fitting using unit cell only models.

A5.2. BET-SSA

The specific surface area of a CeZr 1:1 molar ratio was measured by the BET method. The measurement was performed 3 times under the same conditions, previously outgassing at 350 ºC. The SSA-BET values and the standard error obtained from this can be found in Table A5-1:

Table A5-1: Calculation of BET-SSA instrument standard error.

Measurement	BET-SSA / $m^2 g^{-1}$	Standard error / $m^2 g^{-1}$	RSD / %
A	76	± 4	8
B	86		
C	89		

A5.3. CO chemisorption

The metal surface area of a Pd-CeO_2 sample was measured by the CO-chemisorption method. The measurement was performed 3 times under the same conditions. The values and the standard error obtained from this can be found in Table A5-2:

Table A5-2: Calculation of CO chemisorption instrument standard error.

Measurement	Metal dispersion / %	Standard error / %	RSD / %	Metal surface area / $m^2 g^{-1}$ sample	Standard error / $m^2 g^{-1}$ sample	RSD / %
A	50.6	± 1.9	6	1.13	± 0.04	6
B	54.6			1.21		
C	57.1			1.27		

A5.4. EtOH-TPSR

The metal surface area of several Pd-CeO_2 samples was measured by the EtOH-TPSR method. The measurement was performed twice for each of these samples under the same conditions (A and B). The values and the standard error obtained from this can be found in Table A5-3:

Table A5-3: Calculation of EtOH-TPSR instrument standard error.

Measurement	Metal surface area / m^2 g^{-1} sample	Standard error / m^2 g^{-1} sample	RSD / %	Average standard error / m^2 g^{-1} sample	Average RSD / %
A	0.33	0.01	2	± 0.07	16
B	0.32				
A	1.88	0.09	6		
B	2.07				
A	1.07	0.17	20		
B	1.43				
A	0.09	0.03	35		
B	0.15				
A	0.55	0.06	17		
B	0.43				

A5.5. Ethane Hydrogenolysis

The ethane hydrogenolysis of a Rh-CeO_2 sample was performed twice under the same conditions. The values and the standard error obtained from this can be found in Table A5-4:

Table A5-4: Calculation of ethane hydrogenoysis instrument standard error.

Measurement	T50 / °C	Standard error / °C	Average RSD / %
A	296	± 4	2
B	305		

A5.6. H_2-TPR & CO-TPR

The H_2-TPR of a Pd-CeO_2 sample and the CO-TPR of a Rh-Pd-CeO_2 sample were performed twice each under the same conditions. The values and the standard errors obtained can be found in Table A5-5, A5-6 and A5-7:

Table A5-5: Calculation of H_2-TPR instrument standard error regarding peak position.

	Main NM-Ce reduction			Surface Ce reduction			Bulk Ce reduction		
Measurement	Peak T / °C	Standard error / °C	RSD / %	Peak T / °C	Standard error / °C	RSD / %	Peak T / °C	Standard error / °C	RSD / %
A	96	± 16	10	333	± 18	3	840	± 10	1
B	112			351			850		
Average standard error: ± 14 °C									
Average RSD: 4 %									

Table A5-6: Calculation of H_2 consumption instrument standard error based on the integration of the NM-Ce reduction during a H_2-TPR experiment.

	Main NM-Ce reduction			Surface Ce reduction			Bulk Ce reduction		
Measurement	Integration / mmol g^{-1}	Standard error / mmol g^{-1}	RSD / %	Integration / mmol g^{-1}	Standard error / mmol g^{-1}	RSD / %	Integration / mmol g^{-1}	Standard error / mmol g^{-1}	RSD / %
A	0.58	± 0.01	2	0.30	± 0.02	10	0.47	± 0.03	9
B	0.60			0.35			0.41		
Average standard error: ± 0.02 mmol g^{-1}									
Average RSD: 7 %									

Table A5-7: Calculation of CO-TPR instrument standard error regarding peak position, based on CO_2 formation.

	Main NM-Ce reduction			Surface Ce reduction			Bulk Ce reduction		
Measurement	Peak T / °C	Standard error / °C	RSD / %	Peak T / °C	Standard error / °C	RSD / %	Peak T / °C	Standard error / °C	RSD / %
A	290	± 1	< 1	398 - 610	± 1	< 1	610 – 890	± 2	< 1
B	288			395 - 608			608 – 884		
Average standard error: ± 1 °C									
Average RSD: < 1 %									

A5.7. OSC

The OSC of a Pd-CeO_2 sample was performed 3 times under the same conditions. The values and the standard error obtained from this can be found in Table A5-8:

Table A5-8: Calculation of OSC instrument standard error.

Temperature / °C	OSC_A / µmol g^{-1}	OSC_B / µmol g^{-1}	OSC_C / µmol g^{-1}	Standard error / µmol g^{-1}	RSD / %	Average standard error / µmol g^{-1}	Average RSD / %
100	0	0	0	0.0	0	± 7.9	11
150	34.6	28.6	43.5	4.3	21		
200	83.0	71.6	101.5	8.7	17		
250	124.5	100.2	130.5	9.3	13		
300	179.9	143.2	181.2	12.5	13		
350	228.3		217.5	5.4	3		
400	276.7		246.5	15.1	8		

A5.8. CO-SSITKA

For the reaction rate determination, each point measured during the CO-SSITKA was performed 3 times. The error was calculated for each measured point individually. An example of this calculation can be found below in Table A5-9:

Table A5-9: Calculation of reaction rate standard error.

Measurement	Reaction rate / µmol g^{-1} s^{-1}	Standard error / µmol g^{-1} s^{-1}	RSD / %
A	0.16	± 0.01	6
B	0.17		
C	0.15		

The E_a however was determined based on the slope of a regression line, where **x** was **1/T** and **y** was **ln(*k*)**. The standard deviation of the slope (S_b) is calculated using equation A5-5 [13]:

$$s_{y/x} = \sqrt{\frac{\sum_{i=1}^{N}(y_i - \hat{y}_i)^2}{n-2}} \qquad \text{A5-4}$$

$$s_b = \frac{s_{y/x}}{\sqrt{\sum_{i=1}^{N}(x_i - \bar{x})^2}} \qquad \text{A5-5}$$

Where
- $s_{y/x}$ standard deviation of the linear regression
- s_b standard deviation of the slope
- x_i measured value at the x-axes
- y_i measured value at the y-axes
- $\bar{x}$ average value
- $\hat{y}_i$ y-value based on the regression line equation
- N population

As an example, a regression line with equation x = 20.04 – 3255.90x and R^2 = 0.99 was obtained from the data shown below in Table A5-10. The standard deviation of the slope was calculated using the the A5-4 equation. In this case, the standard error of a sampling distribution corresponds to the standard error [13].

Table A5-10: Calculation of the standard deviation of the slope from a linear regression.

x = 1/T / K^{-1}	y = ln(*k*)	Standard deviation of slope
3.10E-03	9.93E+00	± 376.12
3.00E-03	1.03E+01	
2.92E-03	1.06E+01	
2.83E-03	1.08E+01	

Thus, the slope can be defined as -3255.90 ± 246.06 K. The E_a is determined from this slope (A5-5):

$$b = \frac{-E_a}{R} \qquad \text{A5-5}$$

Where b slope

E_a activation energy (J mol^{-1})

R universal gas constant (8.314 J mol^{-1} K^{-1})

Therefore

$$E_a = -(-3255.90\ K)(8.314\ J\ mol^{-1}\ K^{-1}) = 27056.53\ J\ mol^{-1}$$

And the error from this calculation can be calculated as

$$R\ Sb = (8.314\ J\ mol^{-1}\ K^{-1})(246.06\ K) = 2044.76\ J\ mol^{-1}$$

The E_a can be then expressed as:

$$E_a = 27056.53 \pm 2044.76\ J\ mol^{-1} \quad \text{or} \quad 27 \pm 2\ KJ\ mol^{-1}$$

A5.9. Activity Light-off

The light-off of a Pd-CeO_2 sample was performed twice under the same conditions. The values and the standard error obtained from this can be found in Table A5-11:

Table A5-11: Calculation of light-off instrument standard error, based on cold-start conditions (λ = 0.95).

Measurement	CO T50 / °C	Standard error / °C	RSD / %	NO_x T50 / °C	Standard error / °C	RSD / %	HC T50 / °C	Standard error / °C	RSD / %
A	230	± 4	3	253	± 2	1	325	± 1	< 1
B	239			257			326		
Average standard error: ± 2 °C									
Average RSD: 1 %									

A6. NM species during the co-precipitation preparation of NM-CeO_2 catalysts

In some cases, the co-precipitation method to prepare NM-CeO_2 catalysts led to precipitates that changed colour during the calcination. The changed in colour was associated to a change in the oxidation state of the metal. To demonstrate this, the dried and calcined powders of the NM-CeO_2 preparations (NM = Pd, Pt, Rh) were submitted for XPS. The results are detailed below:

A6.1. Effect of Ce-precursor in the co-precipitation of 0.5Pd-CeO_2 catalysts

A6.1.1. Ce^{3+} precursor ([0.5Pd+Ce^{3+}])

The preparation of 0.5Pd-CeO_2 using a Ce^{3+} precursor led to a dark grey precipitate that changed colour to bright yellow once calcined. The dark grey colour of the dried material suggested the presence of metallic Pd, and the change in colour to yellow after the calcination was a sign of the re-oxidation of the metallic Pd species to PdO.

These samples were submitted for XPS. The Pd3d profiles can be seen in Figure A6-1. Here it can be observed that the uncalcined material contained the presence of metallic Pd species (Pd3d bands at 335.1 and 341.6 eV) as well as Pd^{2+} (Pd3d bands at 337.4 and 342.7 eV). However, the calcined material did not contain

metallic Pd, only Pd^{2+} (Pd3d bands at 337.3 and 342.5 eV) and $Pd^{(2+\gamma)+}$ (Pd3d bands at 338.3 and 343.5 eV) species [14, 15].

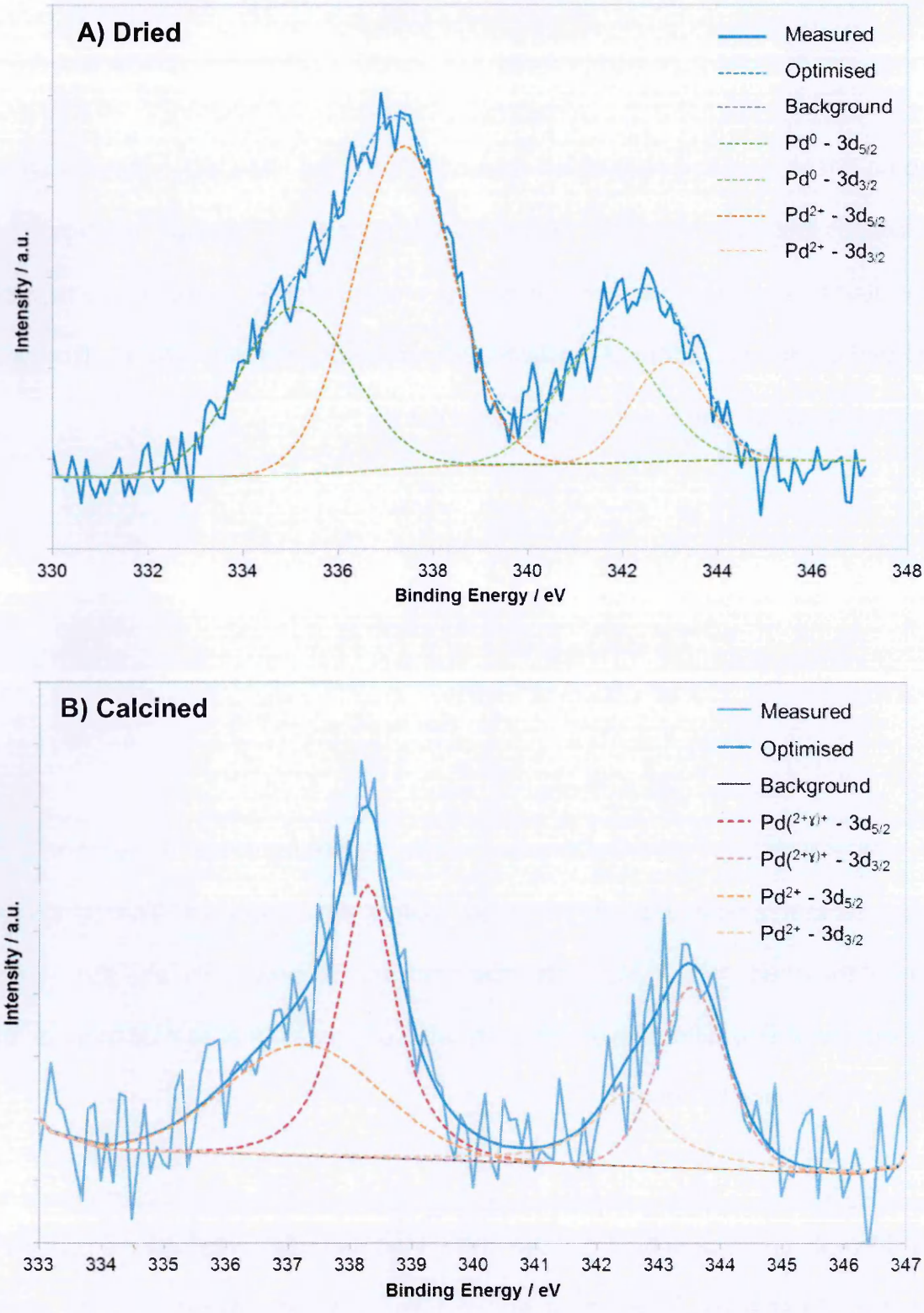

Figure A6-1: Deconvolution of Pd3d XPS peaks for 0.5Pd-CeO_2 samples prepared by co-precipitation with Ce^{3+} precursor. A) dried and B) calcined in air at 650 ºC for 2 hours.

It is interesting that not only metallic Pd species were found in the uncalcined material. Assuming that a completed redox reaction occurred between Pd^{2+} and Ce^{3+}, it is likely that the presence of air and the exposure to ~103 ºC (due to the basified solution being at boiling point) could have been responsible of the re-oxidation of some metallic Pd during the preparation.

A6.1.2. Ce^{4+} precursor ([0.5Pd+Ce^{4+}])

In the case of the co-precipitation of Pd^{2+} with Ce^{4+} precursors, the precipitate obtained was yellow in colour and did not change after the calcination. This suggested that all the Pd species present in this sample existed as PdO. To confirm this, these samples were also analysed by XPS.

In this case there was a significantly lower presence of Pd species in the near-surface, which affected the quality of the XPS signal. In Figure A6-2 it can be observed that no metallic Pd species were detected for either sample, confirming the initial hypothesis. For the uncalcined material the Pd3d bands appeared at 338.7 and 343.8 eV, related to $Pd^{(2+\gamma)+}$ species, whilst for the calcined material the same bands appeared shifted towards lower binding energies (at 337.7 and 343.6 eV) and were associated to Pd^{2+} [14, 15]. This suggests that there was a stronger interaction between Pd and Ce in the uncalcined material.

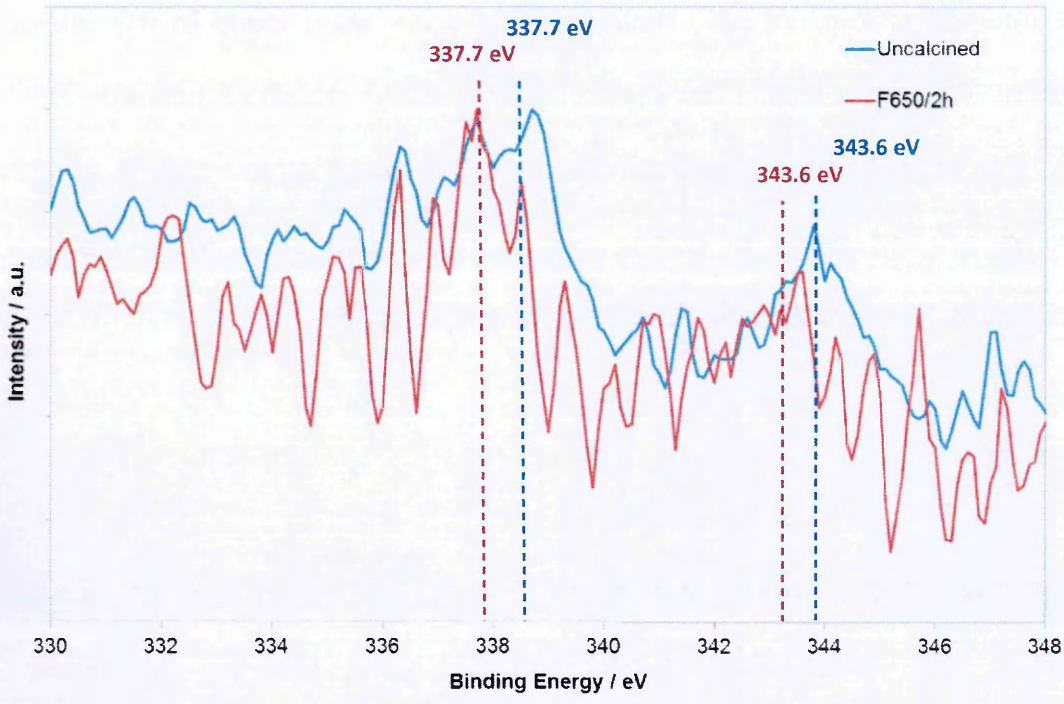

Figure A6-2: Pd3d XPS peaks for 0.5Pd-CeO_2 samples prepared by co-precipitation with Ce^{4+} precursor. Blue = dried; Red = calcined in air at 650 ºC for 2 hours.

A6.2. Pt-CeO_2 catalyst prepared with Ce^{3+} ([0.5Pt+Ce^{3+}])

Pt-CeO_2 catalysts prepared with Ce^{3+} precursor also suffered a change in colour, from grey when the precipitate was dried, to light brown after the calcination. The grey colour of the dried powder was associated with the presence of metallic Pt species. The light brown colour after the calcination was an indication of the re-oxidation of the metallic species to PtO_2.

The XPS Pt4f profiles for the dried and calcined [0.5Pt+Ce^{3+}] samples can be found in Figure A6-3. It can be seen that the dried precipitate contained metallic Pt (Pt4f bands at 73.0 and 76.4 eV) and Pt^{4+} (Pt4f bands at 71.2 and 74.6 eV) species, whilst the calcined material only contained Pt^{4+} species (Pt4f bands at 72.7 and 76.0 eV) [15, 16]. This confirms that a redox reaction exists between Pt^{4+} and Ce^{3+} during their co-precipitation.

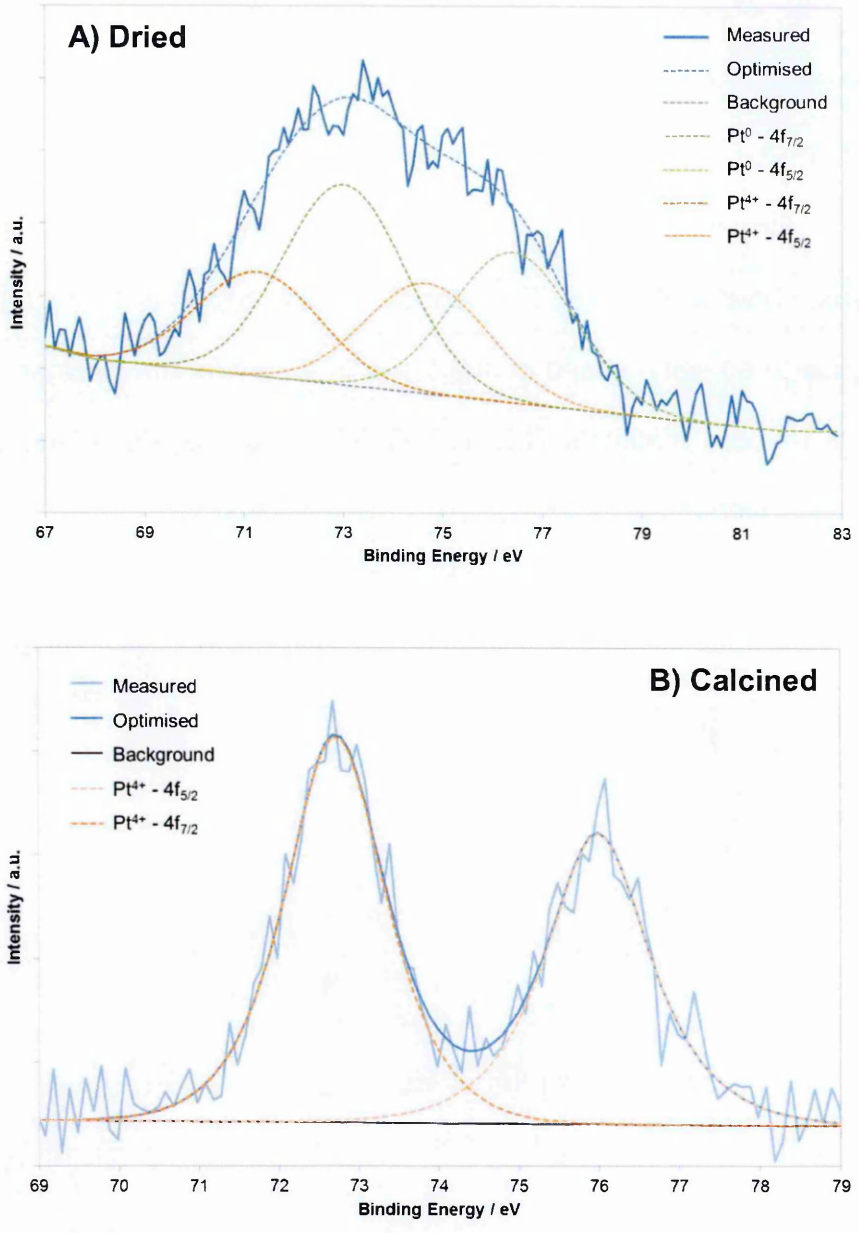

Figure A6-3: Deconvolution of Pt4f XPS peaks for 0.5Pt-CeO_2 samples prepared by co-precipitation with Ce^{3+} precursor. A) dried and B) calcined in air at 650 ºC for 2 hours.

Similar to the [Pd+Ce^{3+}] preparation, a combination of metallic Pt and Pt^{4+} species were found in the uncalcined material. Making similar assumptions, it is possible that the re-oxidation of some metallic species could have occurred in solution.

A6.3. Rh-CeO_2 catalyst prepared with Ce^{3+} ([0.5Rh+Ce^{3+}])

The co-precipitation of Rh^{3+} with Ce^{3+} was the only preparation that led to a brown precipitate that did not change colour during the calcination process. This suggested no further changes in the oxidation state of Rh. XPS analyses confirmed this, showing that only Rh^{3+} species (Rh3d bands at 309.3 and 314.0 eV for the uncalcined sample, and at 309.1 and 314.1 eV for the calcined sample) were present in both materials [15, 17]. Rh3d profiles of dried and calcined powders can be found in Figure A6-4:

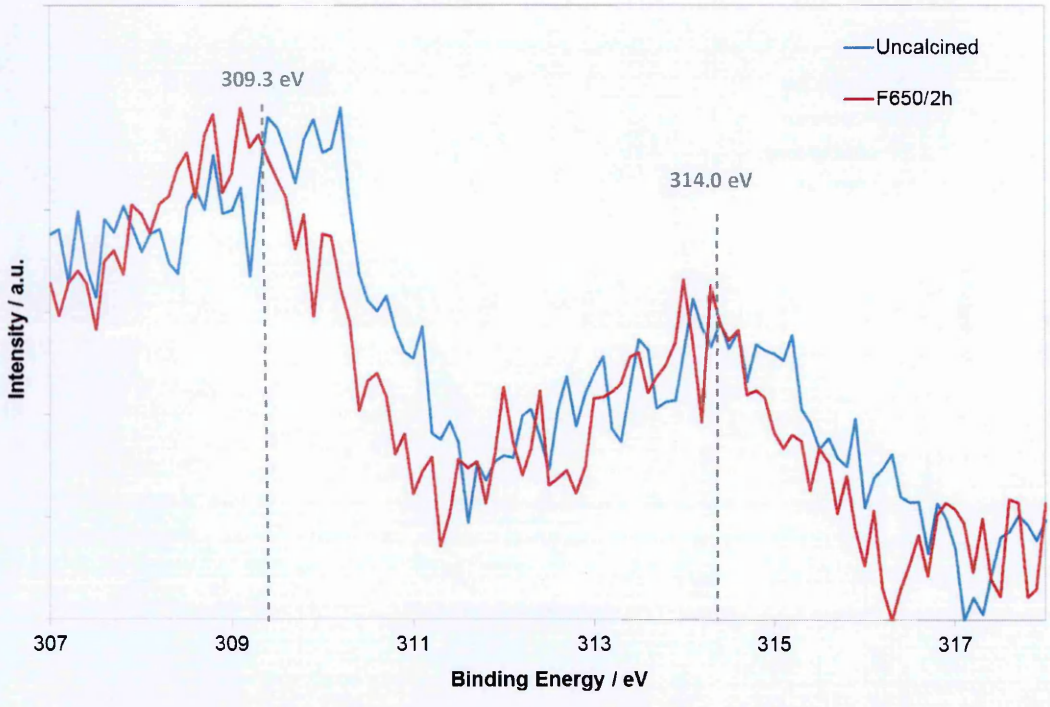

Figure A6-4: Rh3d XPS peaks for 0.5Rh-CeO_2 samples prepared by co-precipitation with Ce^{3+} precursor. Blue = dried; Red = calcined in air at 650 °C for 2 hours.

A6.4. Summary

The following table summarises the peak positions and assigned species found for the samples mentioned in the sections above:

Table A6-12: Summary of the peak positions and assigned species found for the NM-CeO_2 samples (NM = Pd, Pt, Rh) prepared by co-precipitation with Ce^{3+} precursor. Comparison of the species found before and after calcination in air at 650 °C for 2 hours.

Sample	Pd3d / eV		Pt4f / eV		Rh3d / eV	
	$3d_{5/2}$	$3d_{3/2}$	$4f_{7/2}$	$4f_{5/2}$	$3d_{5/2}$	$3d_{3/2}$
[0.5Pd+Ce^{3+}] dried	335.1 (Pd) 337.4 (Pd^{2+})	341.6 (Pd) 342.7 (Pd^{2+})	-	-	-	-
[0.5Pd+Ce^{3+}] calcined	337.3 (Pd^{2+}) 338.3 ($Pd^{(2+\gamma)+}$)	342.5 (Pd^{2+}) 343.5 ($Pd^{(2+\gamma)+}$)	-	-	-	-
[0.5Pt+Ce^{3+}] dried	-	-	73.0 (Pt) 71.2 (Pt^{4+})	76.4 (Pt) 74.6 (Pt^{4+})	-	-
[0.5Pt+Ce^{3+}] calcined	-	-	72.7 (Pt^{4+})	76.0 (Pt^{4+})	-	-
[0.5Rh+Ce^{3+}] dried	-	-	-	-	309.3 (Rh^{3+})	314.0 (Rh^{3+})
[0.5Rh+Ce^{3+}] calcined	-	-	-	-	309.1 (Rh^{3+})	314.1 (Rh^{3+})

References Appendix

[1] S. Lowel, J. E. Shields, M. A. Thomas and M. Thommes, *Characterisation of porous solids and powders: surface area, pore size and density*, Kluwer Academic Publisher, The Netherlands, 2004.

[2] S. Brunauer, P. H. Emmett and E. Teller, Journal of the American Chemical Society, 60 (1938) 309-319.

[3] C. Descorme, S. Bedrane and D. Duprez, Catalysis Today, 75 (2002) 401-405.

[4] H. S. Gandhi, G. W. Graham and R. W. McCabe, Journal of Catalysis, (2003) 433-442.

[5] M. Ozawa, Journal of Alloys and Compounds, 275-277 (1998) 886-890.

[6] J. Moore, C. Stanitski and P. Jurs, *Principles of Chemistry: The Molecular Science*, Cengage Learning, 2009.

[7] R. C. Weast, *Handbook of Chemistry and Physics, 64th edition*, CRC Press, Inc., 1983.

[8] A. Trovarelli, *Catalysis by Ceria and Related Materials*, Imperial College Press, 2002.

[9] S. L. Shannon and J. G. Goodwin, Chemical Reviews, 95 (1995) 677-695.

[10] P. Atkins and J. d. Paula, *Atkins' Physical Chemistry*, Oxford University Press, 2010.

[11] W. Masterton, C. Hurley and E. Neth, *Chemistry: Principles and Reactions*, Cengage Learning, 2011.

[12] F. Gravetter and L. Wallnau, *Essentials of Statistics for the Behavioral Sciences*, Cengage Learning, 2013.

[13] R. Johnson and P. Kuby, *Elementary Statistics*, Cengage Learning, 2007.

[14] A. I. Boronin, E. M. Slavinskaya, I. G. Danilova, R. V. Gulyaev, Y. I. Amosov, P. A. Kuznetsov, I. A. Polukhina, S. V. Koscheev, V. I. Zaikovskii and A. S. Noskov, Catalysis Today, 144 (2009) 201-211.

[15] A. V. Naumkin, A. Kraut-Vass, S. W. Gaarenstroom and C. J. Powell, *NIST X-ray Photoelectron Spectroscopy Database*, 2000.

[16] P. Bera, K. R. Priolkar, A. Gayen, P. R. Sarode, M. S. Hegde, S. Emura, R. Kumashiro, V. Jayaram and G. N. Subbanna, Chemistry of Materials, 15 (2003) 2049-2060.

[17] A. Gayen, K. R. Priolkar, P. R. Sarode, V. Jayaram, M. S. Hegde, G. N. Subbanna and S. Emura, Chemistry of Materials, 16 (2004) 2317-2328.